Year : 2022

Physical and biogeochemical processes regulating the dynamics of surface CO2 in a large and deep hardwater lake

Perolo Pascal

Perolo Pascal, 2022, Physical and biogeochemical processes regulating the dynamics of surface CO2 in a large and deep hardwater lake

Originally published at : Thesis, University of Lausanne

Posted at the University of Lausanne Open Archive http://serval.unil.ch
Document URN : urn:nbn:ch:serval-BIB_9DE85404D4541

UNIL | Université de Lausanne
Faculté des géosciences
et de l'environnement

FNSNF
Swiss National Science Foundation

Physical and biogeochemical processes regulating the dynamics of surface CO_2 in a large and deep hardwater lake

Thèse de Doctorat

Présenté à la

Faculté des Géosciences et de l'environnement de l'université de Lausanne

Pour l'obtention du grade de

Docteur en Sciences de l'environnement

par

Pascal Perolo

Directeur de thèse
Professeure Marie-Elodie Perga

Co-directeur de thèse
Professeur Damien Bouffard

Jury
Président du jury: Professeur Stuart Lane
Expert interne: Professeur Samuel Jaccard
Expert externe: Professeur Yves Prairie
Expert externe: Professeure Anne Ojala

Lausanne, Septembre 2022

UNIL | Université de Lausanne
Faculté des géosciences
et de l'environnement

FNSNF
Swiss National Science Foundation

Physical and biogeochemical processes regulating the dynamics of surface CO_2 in a large and deep hardwater lake

Thèse de Doctorat

Présenté à la

Faculté des Géosciences et de l'environnement de l'université de Lausanne

Pour l'obtention du grade de

Docteur en Sciences de l'environnement

par

Pascal Perolo

Directeur de thèse
Professeure Marie-Elodie Perga

Co-directeur de thèse
Professeur Damien Bouffard

Jury
Président du jury: Professeur Stuart Lane
Expert interne: Professeur Samuel Jaccard
Expert externe: Professeur Yves Prairie
Expert externe: Professeure Anne Ojala

Lausanne, Septembre 2022

IMPRIMATUR

Vu le rapport présenté par le jury d'examen, composé de

Président de la séance publique :	M. le Professeur Stuart Lane
Président du colloque :	M. le Professeur Stuart Lane
Directrice de thèse :	Mme la Professeure Marie-Elodie Perga
Co-directeur de thèse :	M. le Professeur Damien Bouffard
Expert interne :	M. le Professeur Samuel Jaccard
Expert externe :	M. le Professeur Yves Prairie
Experte externe :	Mme la Professeure Anne Ojala

Le Doyen de la Faculté des géosciences et de l'environnement autorise l'impression de la thèse de

Monsieur Pascal PEROLO

Titulaire d'un

Master of Science in geography, geomorphology, and management of mountain regions

de l'Université de Lausanne

intitulée

PHYSICAL AND BIOGEOCHEMICAL PROCESSES REGULATING THE DYNAMICS OF SURFACE CO2 IN A LARGE AND DEEP HARDWATER LAKE

Lausanne, le 08 septembre 2022

Pour le Doyen de la Faculté des géosciences et de l'environnement

Professeur Stuart Lane

Four years of dream…

… and nightmare

Cover photography

Lake Geneva and mouth of the Rhône River from Grammont (Perolo, 2019.07.20)

Acknowledgments

As a prelude to this doctoral thesis, I would like to express my most sincere thanks to the people who have given their support and their contribution to the accomplishment of this research, especially to:

- My thesis supervisor, Prof. Marie-Elodie Perga, and my co-supervisor, Dr Damien Bouffard, who accompanied me during these four years full of twists and turns. You have passed on to me your respective knowledge and your scientific rigor and have always supported and helped me in difficult times. I will never be able to forget you except major head trauma.

- Dr Nicolas Escoffier, Dr Thibault Lambert, Dr Gaël Many, Dr Gabriel Cotte, Isabel Herr, Dr Martiina Rantala, and Dr Janine Rüegg, colleagues, office friends for our great scientific discussions or not, our collaborations and all the good times spent in your company.

- Sébastien Lavanchy, technical manager of the LéXPLORE platform and Aurélien Ballu, field technician at IDYST, for their practical help.

- Sabrina Damiani and Carole Schröcker for their sympathy and help with administrative tasks, but also Laetitia Monbaron and Micaela Faria for their presence and helping with the laboratories.

- Dr Hannah Chmiel and Dr Bieito Fernández Castro for the scientific collaborations.

- Dr Alberto Borges and Dr Tonya DelSontro, experts during my two intermediate renderings.

- Prof Stuart Lane, Prof Samuel Jaccard, Prof Yves Prairie, and Dr Anne Ojala, for accepting to be members of my thesis jury.

- My family and my friends for their daily moral support.

- And to all the members of the IDYST that I was able to meet during my doctorate, but also previously in my master's and bachelor's degrees.

This thesis was supported by the CARBOGEN project (SNF 200021_175530), which is linked to the LéXPLORE project (SNF R'Equip, P157779) and the Primary Production Under Oligotrophication in Lakes project (SNF 200021_179123). I also acknowledge the five partner institutions involved with LéXPLORE: Eawag, EPFL, the University of Geneva, the University of Lausanne, and CARRTEL (INRAE-USMB).

Abstract

If inland waters have been acknowledged as significant CO_2 emitters and reactors of the global carbon cycle, light has been essentially shed on wetlands, permafrost, and humic lakes, under the overwhelming paradigm that lake supersaturation with CO_2 arises from metabolic processes. Within this picture, large and deep hardwater lakes such as Lake Geneva have been largely overlooked, considered neutral to the atmosphere. However, those conceptions rely on data that are poorly resolved in both time and space, leading to a deficient understanding of the fine-scale surface CO_2 dynamics in large, deep hardwater lakes and major uncertainties on their estimated annual lake-wide CO_2 emissions. Using Lake Geneva as a model for large, deep hardwater lake, the main objectives of this doctoral thesis are (i) to reach a high-resolution understanding of the surface CO_2 dynamics and fluxes at the lake, (ii) to untie the physical and biogeochemical processes controlling the CO_2 fluxes at the lake–atmosphere interface, and (iii) to derive methodological guidelines on the frequency at which the different components of the CO_2 fluxes should be monitored to reach representative estimates of annual CO_2 fluxes. The CO_2 fluxes at the surface of lakes operate through a net diffusive transport, obeying the first Fickian law often expressed as $F = k(C_w - C_{sat})$, where F is the CO_2 gas flux, k is the gas transfer velocity, C_w is the CO_2 concentration at the water surface, and C_{sat} is the CO_2 concentration at saturation with the atmosphere. The guideline of this work is the Fickian equation which is decomposed in its individual terms to quantify the role of physical and biogeochemical processes on their dynamics. In that objective, the temporal variation of the lake surface CO_2 and gas exchange velocity was measured at an hourly resolution while their spatial component was addressed by comparing the pelagic and littoral environments. This work benefited from the ongoing initiative of off-shore and in-shore stations for high-frequency monitoring: the LéXPLORE platform (110 m depth) and the Buchillon mast (4 m depth), representative of the two environments.

The first study is dedicated to the drivers of the gas transfer velocity (k). Direct and continuous measures of k are technically challenging, so that k values introduced within annual estimates of CO_2 fluxes for lakes are modelled. Insofar, k models in lakes accounted for the effect of wind shear (all lake sizes) and convection (small lakes). Unlike oceanographic studies, the effect of surface waves is typically not included in lake k models although those can occur in large lakes when the wind fetch is long enough. Herein, we demonstrate that accounting for surface waves generated during windy events (> 5 m s^{-1}) significantly improves the accuracy of k estimates in large lakes (i.e. fetch > 15 km). The computation of a new improved k model over a 1-year time period shows that episodic extreme events with surface waves can generate more than 20% of annual cumulative k and more than 25% of annual net CO_2 fluxes in Lake Geneva. Moreover, the integration of the spatial variability of k is proposed using spatial meteorological model.

Because all the terms of the flux equation are challenging to measure or parameterise at fine-time and space scale resolution over annual periods, few studies can simultaneously link the variabilities of CO_2 flux, water CO_2 and k. The aim of this second study is to assess the minimal sampling frequency of inputs data that is necessary to reach representative of estimates annual CO_2 fluxes at the surface of a large lake. Herein we show that representative estimates of CO_2 fluxes require high-frequency computations of k (hourly), all year round, to capture intense but short-lived turbulence events. Daily and weekly measurements of water CO_2 are necessary during shoulder periods, while the CO_2 sampling frequency can be loosened during periods of stability such as summer.

Besides, we show that littoral CO_2 fluxes, which are one order of magnitude greater than pelagic fluxes, contribute significantly to the total lake emissions even where they represent of very small share of the total lake surface. Finally, we propose solutions to improve these CO_2 gas exchange quantifications using currently available numerical tools such as spatial weather model, hydrodynamical model, and data reconstruction.

The last study is dedicated to the interaction between alkalinity and biological processes, in relation to surface CO_2 dynamics. In alkaline freshwater systems such as Lake Geneva, the apparent absence of carbon limitation to gross primary production (GPP) at low CO_2 concentrations suggests that bicarbonates can support GPP. However, the contribution of bicarbonates to GPP has never been quantified in lakes along the seasons. We can demonstrate for the first time that the available CO_2 at the lake surface is not sufficient to maintain GPP for two-thirds of the year in Lake Geneva. To support the high rate of O_2 production, aquatic primary producers withdraw bicarbonate from the alkalinity pool as a carbon supply for GPP. The neglected role of alkalinity in the freshwater carbon cycle is highlighted throughout an annual cycle. In addition, we show that bicarbonate-fixation by primary producers, far from being anecdotical, can be the dominant model for hardwater lakes.

Finally, all the results of these three studies coupled with the existing literature allow us to propose a conceptual carbon cycle for large and deep hardwater lakes. It highlights the complex interaction of physical and biogeochemical processes responsible for CO_2 emissions over an annual cycle and demonstrates that the lake can be considered as an active carbon transformer. To conclude, the limits and perspectives of this research are discussed with an emphasis on future estimates of CO_2 fluxes from lakes integrated in time and space using new numerical tools such as the coupling of physical and biogeochemical models, and Deep Learning.

Résumé

Si les eaux intérieures ont été reconnues comme d'importants émetteurs de CO_2 et réacteurs du cycle global du carbone, la lumière a été essentiellement faite sur les zones humides, le pergélisol et les lacs humiques, sous le paradigme selon lequel la sursaturation des lacs en CO_2 découle de processus métaboliques. Dans ce tableau, les grands lacs profonds, avec des duretés de l'eau élevées, tels que le lac Léman, ont été largement négligés, considérés comme neutres vis à vis de l'atmosphère. Cependant, ces conceptions reposent sur des données mal résolues dans le temps et dans l'espace, ce qui conduit à une compréhension déficiente de la dynamique du CO_2 de surface à petite échelle dans les grands lacs d'eau dure profonds et à des incertitudes majeures sur leurs émissions annuelles de CO_2 estimées à l'échelle du lac. En utilisant le lac Léman comme site modèle, les principaux objectifs de cette thèse de doctorat sont (i) d'obtenir une compréhension à haute résolution de la dynamique et des flux de CO_2 de surface au lac, (ii) de dénouer les liens physiques et processus biogéochimiques contrôlant les flux de CO_2 à l'interface lac-atmosphère, et (iii) de dériver des directives méthodologiques sur la fréquence à laquelle les différentes composantes des flux de CO_2 doivent être surveillées pour obtenir des estimations représentatives des flux annuels de CO_2. Les flux de CO_2 à la surface des lacs opèrent par un transport diffusif net, obéissant à la première loi de Fick, souvent exprimée comme $F = k(C_w - C_{sat})$, où F est le flux de gaz CO_2, k est la vitesse de transfert du gaz, C_w est la concentration de CO_2 à la surface de l'eau, et C_{sat} est la concentration de CO_2 à saturation avec l'atmosphère. La ligne directrice de ce travail est la décomposition des termes de l'équation Fickienne pour quantifier le rôle des processus physiques et biogéochimiques sur leur dynamique. Dans cet objectif, la variation temporelle du CO_2 de surface du lac et la vitesse d'échange de gaz a été mesurée à une résolution horaire tandis que leur composante spatiale a été abordée en comparant les environnements pélagiques et littoraux. Ces travaux ont bénéficié de l'initiative continue des stations off-shore et in-shore de surveillance haute fréquence : la plateforme LéXPLORE (profondeur 110 m) et le mât de Buchillon (profondeur 4 m), représentatifs des deux milieux.

La première étude est dédiée aux processus impliqués dans la vitesse de transfert du gaz (k). Les mesures directes et continues de k sont techniquement difficiles, de sorte que les valeurs de k introduites dans les estimations annuelles des flux de CO_2 pour les lacs sont modélisées plutôt que quantifiées sur le terrain. Jusqu'à présent, les modèles k dans les lacs ont tenu compte de l'effet du cisaillement du vent (toutes tailles de lacs) et de la convection (petits lacs). Contrairement aux études océanographiques, l'effet des vagues de surface, bien qu'occasionnellement présent dans les grands lacs lorsque le fetch du vent (distance de bord à bord d'un lac ou distance d'un bord à un point donnée sur le lac) est suffisamment long, n'est généralement pas inclus dans les modèles de k pour les lacs. Ici, nous démontrons que la prise en compte des vagues de surface générées lors d'événements venteux (> 5 m s^{-1}) améliore considérablement la précision des estimations de k dans les grands lacs (fetch > 15 km). L'application sur une période de 1 an du nouveau modèle k amélioré montre que des événements extrêmes épisodiques avec des vagues de surface peuvent générer plus de 20% du k cumulé annuel et plus de 25% des flux nets annuels de CO_2 dans le lac Léman. De plus, l'intégration de la variabilité spatiale du k est proposée à l'aide d'un modèle météorologique spatial.

Étant donné que tous les termes de l'équation de flux sont difficiles à mesurer ou à paramétrer à une résolution fine à l'échelle temporelle et spatiale sur des périodes annuelles, peu d'études peuvent relier simultanément les variabilités du flux de CO_2, du CO_2 de l'eau et de *k*. L'objectif de cette deuxième étude est d'évaluer la fréquence minimale d'échantillonnage des données d'entrée, nécessaire aux estimations représentatives des flux annuels de CO_2 à la surface d'un grand lac. Ici, nous montrons que des estimations représentatives des flux de CO_2 nécessitent des *k* modèles à haute fréquence (horaire), tout au long de l'année, pour capturer des événements de turbulence intense mais de courte durée. Des mesures quotidiennes et hebdomadaires du CO_2 de l'eau sont nécessaires pendant les périodes de transitions (printemps et automne), tandis que la fréquence d'échantillonnage du CO_2 peut être relâchée pendant les périodes de stabilité comme l'été. En outre, nous montrons que les flux de CO_2 littoraux, qui sont supérieurs d'un ordre de grandeur aux flux pélagiques, contribuent de manière significative aux émissions totales du lac même lorsque le littoral ne représente qu'une très petite part de la surface totale du lac. Enfin, nous proposons des solutions pour améliorer ces quantifications des échanges de gaz de CO_2 en utilisant des outils numériques actuels tels que les modèles météorologiques spatiaux, les modèles hydrodynamiques et la reconstruction de données.

La dernière étude est consacrée à l'interaction entre l'alcalinité et les processus biologiques, en relation avec les dynamiques de CO_2 de surface. Dans les systèmes d'eau douce alcalins tels que le lac Léman, l'apparente absence de limitation du carbone à la production primaire brute (GPP) à de faibles concentrations de CO_2 suggère que les bicarbonates peuvent soutenir la GPP. Cependant, la contribution des bicarbonates à la GPP n'a jamais été quantifiée dans les lacs au fil des saisons. Nous pouvons démontrer pour la première fois que le CO_2 disponible à la surface du lac n'est pas suffisant pour maintenir la GPP pendant les deux tiers de l'année dans le lac Léman. Pour soutenir le taux élevé de production d'O_2, les producteurs primaires aquatiques pompent les bicarbonates de l'alcalinité pour soutenir la GPP. Le rôle négligé de l'alcalinité dans le cycle du carbone de l'eau douce est mis en évidence tout au long d'un cycle annuel. De plus, nous montrons que la fixation des bicarbonates par les producteurs primaires, loin d'être anecdotique, peut être le modèle dominant pour les lacs d'eau dure.

Finalement, l'ensemble des résultats de ces trois études, couplé à la littérature existante, permet de proposer un cycle conceptuel du carbone pour les grands lacs alcalins profonds. Il met en évidence l'interaction complexe des processus physiques et biogéochimiques responsables des émissions de CO_2 sur un cycle annuel et démontre que le lac peut être considéré comme un transformateur de carbone actif. Pour conclure, les limites et les perspectives de cette recherche sont discutées en mettant l'accent sur les estimations futures des flux de CO_2 des lacs intégrés dans le temps et dans l'espace à l'aide de nouveaux outils numériques tels que le couplage de modèles physiques et biogéochimiques, et le Deep Learning.

Content

List of Figures

Chapter 1

Chapter 2

Chapter 3

Chapter 4

Chapter 5

List of Tables

Chapter 2

Chapter 4

Chapter 1

Introduction

1.1. State-of-the-art

1.1.1. Integrating lakes into the regional carbon cycle

The global carbon (C) cycle has long been depicted as two interacting, biogeochemically active compartments (land and ocean) connected through gas exchange with a third compartment, the atmosphere (Bolin 1981; Siegenthaler and Sarmiento 1993; IPCC, 2001). This conceptual vision of the global carbon cycle implicitly included inland waters as simple passive pipes, transporting carbon from the terrestrial compartment to the ocean (Degens et al., 1991; Schlesinger and Melack, 1981). This vision has been challenged by over three decades of research showing that surface waters are active carbon reactors, redistributing carbon pools and fluxes on their way from the land to the Ocean (Cole et al., 2007; Humborg et al., 2010; Weyhenmeyer et al., 2015). This paradigm shift has revealed our poor knowledge of carbon fluxes in continental waters, and especially in lakes, which underlying mechanisms have been poorly understood (Maberly et al., 2013; Finlay et al., 2015; Marcé et al., 2015; Perga et al., 2016).

At the European scale, the lateral C flux from soils to continental waters is of comparable magnitude to C accumulation in European forests (Ciais et al., 2008). Yet, ca. 50-70% is returned to the atmosphere as CO_2 before reaching the Ocean (Cole et al., 2007; Raymond et al., 2013; Wehrli, 2013). Most of these emissions arise from rivers and wetlands (Wehrli, 2013). However, lake contributions may be disproportionally relevant compared to the surface area they occupy on a global scale (Tranvik et al., 2009). Lakes and impoundments would emit 0.5 Pg C-CO_2 yr^{-1} (excluding methane) roughly equivalent to 20% of global fossil fuel CO_2 emissions (Del Sontro et al., 2018) , justifying their explicit inclusion in global carbon models (IPCC, 2014).

CO_2 fluxes at the surface of lakes operate through a net diffusive transport, obeying the first Fickian law commonly expressed for gas exchange as:

$$F = k(C_w - C_{sat}) , \quad (1\text{-}1)$$

where F is the CO_2 gas flux, k is the gas transfer velocity, C_w is the CO_2 concentration at the water surface, and C_{sat} is the CO_2 concentration at saturation with the atmosphere. Thereby, overall global lake CO_2 emissions is the consequences of lakes being mostly CO_2 supersaturated (e.g. Cole et al., 1994; Jonsson et al., 2003; Cole et al., 2007; Lapierre et al., 2013). The mechanisms responsible for this CO_2 supersaturation in lakes have motivated numerous research and studies over the last three decades. CO_2 concentrations in lakes have long been thought to be essentially controlled by lake metabolism. This long-standing paradigm arose from the combined observations that (i) most lakes are supersaturated with CO_2 (Cole et al. 1994), and (ii) that supersaturated lakes are heterotrophic (Del Giorgio et al., 1999) leading to the deduction that CO_2 supersaturation in lakes arises from respiration exceeding primary production as a result of inputs of allochthonous organic matter. From there, lakes have been acknowledged as active metabolic C reactors, respiring allochthonous organic carbon they receive from their catchment, and retrieving part of this C back to the atmosphere. Although lake metabolism undeniably plays a part in controlling lake CO_2, especially in humic, boreal lakes rich in dissolved organic carbon (Sobek et al., 2003), recent works have considerably challenged this paradigm. For instance, autotrophic, clearwater lakes can be CO_2 supersaturated (Stets et al., 2009), as a result of external inputs of inorganic carbon, due to inputs of CO_2-

supersaturated waters from soil respiration (Maberly et al., 2013) or alkalinity inputs from carbonate weathering (Marcé et al., 2015). Such contributions of hydrological inputs of inorganic carbon can also be significant in boreal humic lakes (Weyhenmeyer et al. 2015). Those recent research led to a conceptual revision of the role of lakes within regional carbon cycles (Engels et al., 2018).

In this concept, the role of lakes as reactors is further complexified by introducing geochemical processes by which alkalinity also controls CO_2 dynamics (i.e. geochemical reactors, Fig. 1-1) on top of metabolic processes. Alternatively, lakes could be seen as chimney or passive pipe within the hydrological continuum when they vent the dissolved CO_2 that they received from inflows and groundwaters (Fig. 1-1). Theoretically, the catchment settings, the hydrological characteristics, the size and trophic status of the lakes would determine where a given lake positions across this gradient (e.g. "function of lakes", Engels et al., 2018). Because the source of CO_2 in lakes different between chimneys (catchment-derived CO_2) and reactors (catchment-derived alkalinity or organic carbon), whether a lake functions as a chimney or an active reactor has large effect on their estimated role within global or regional transport of C from the land to the sea (Engels et al., 2018).

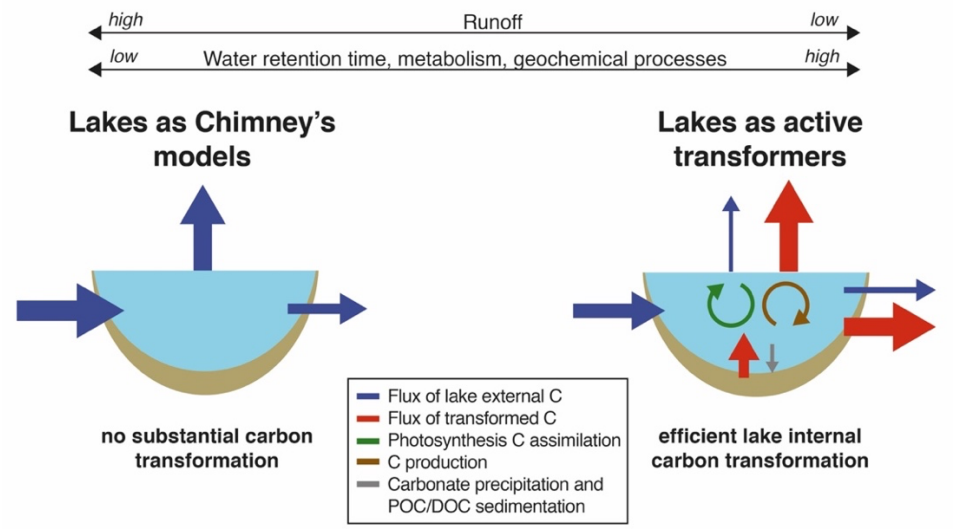

Fig. 1-1: Chimney's model vs Active transformer (adapted from Engel et al., 2018). Chimney's model considers only a passive exchange according to Fick's law, but without fundamental carbon transformation instead of the active transformer.

1.1.2 Can we anticipate the biogeochemical functions of Swiss, large peri-alpine lakes in the regional CO_2 cycle?

In Switzerland, lakes represent 36% of the total volume of available freshwaters (9% for rivers) and cover 5% of the entire territory. The vast majority of the lake surface of Switzerland (>95%) is represented by large (>10 km^2) and deep (>50 m) lakes, with moderate alkalinity (1-4 meq L^{-1}, Müller et al., 2016). Thereby, large, deep alkaline lakes are major components of the Swiss hydrological landscape, and their role in the transport, transformation and storage of C might then be of primary importance on the regional CO_2 fluxes. The state of knowledge yet does not allow to anticipate the magnitude of their CO_2 emissions to the atmosphere, nor to position them within the Engels et al. (2018) concept.

First, the long-standing paradigm that metabolism is the major driver of CO_2 supersaturation in lakes has led to a predominant attention on the study of CO_2 flux balance on small lakes (Del Sontro et al., 2018), or lakes rich in dissolved organic matter (Sobek et al., 2003). In this perspective, large, deep and clearwater lakes, with relatively low trophic status and low inputs of terrestrial DOC have been regarded as essentially neutral in terms of CO_2 exchange to the atmosphere (Del Sontro et al., 2018). On the other side, large perialpine lakes have relatively high alkalinity (> 1 meq L^{-1}), which according to the study by Marcé et al. (2015) shall make them significant sources of CO_2 to the atmosphere, although the underlying processes by which alkalinity gets transformed into CO_2 remain to be explicated (Khan et al., 2020). Their role as active biogeochemical transformers could be reinforced by their low runoff and long water residence times (Fig. 1-1).

Data on CO_2 concentrations and fluxes for large and deep lakes in Switzerland are scarce. Computing surface CO_2 from monthly alkalinity and pH data taken at the centre of 13 large lakes showed typical undersaturation in CO_2 in summer and supersaturation during spring mixing (Müller et al., 2016). Annual CO_2 concentrations and fluxes were yet not computed. A preliminary study on Lake Geneva concluded that the lake emitted 16 Gg C per year, from lowly resolved monitoring data. While results by Müller et al. (2016) also pointed to the role of alkalinity in supplying the CO_2 supersaturation in the lake, the mechanism tying alkalinity to CO_2 variability remain to be quantified.

So, virtually, CO_2 exchanges at the surface of large, clearwater lakes as those found in Switzerland remains virtually unknown, and this puzzle motivated by doctoral work. Using Lake Geneva as a model system, the overall purpose is to reach a representative estimate of the CO_2 fluxes at an annual scale, properly accounting for the spatial and temporal variability, and the underlying physical and biogeochemical processes.

1.2. Current state of knowledge in Lake Geneva

Lake Geneva was chosen as a study area for the carbon cycling processes because it is a model system that benefited from an exceptional wealth of data, modelling tools and monitoring structures since 1957. Furthermore, this lake is representative of large Swiss peri-alpine lakes. Its surface area (582 km^2) and its high depth (maximum of 309 m) make it the largest freshwater in Western Europe, with a volume of 89 km^3. Lake Geneva defines part of the Swiss French border, at 372 m above sea level (Fig. 1-2). The theoretical water retention time is 11.3 years. Its watershed covers an area of 7'999 km^2, of which 9.4% are glaciers. It covers Swiss and French territories with a relatively high average altitude of 1670 m (CIPEL report, 2015). In addition, most of these tributaries have glacio-nival or nivo-glacial hydrological regimes. These two most important water inflows come from the upper Rhône and the Dranse rivers, making up to 90%, while the outflows come out by the lower Rhône River. For decades, they have been monitored by the FOEN (CH) and the DREAL (FR). Dissolved inorganic carbon (DIC) and alkalinity (Alk) concentrations of the incoming waters are relatively high and very similar (1492 ± 237 µeq L^{-1} and 1515 ± 243 µmol L^{-1} respectively (mean ± standard deviation)) with an average calcium concentration of 43 ± 8 mg L^{-1}. DOC and phosphate concentrations are however very low (0.78 ± 0.34 mg L^{-1} and 0.079 ± 0.07 mg L^{-1} respectively) explaining by the low rate of forest and croplands in the catchment (only 25%).

Lake Geneva is a large, deep, alkaline hardwater lake and its water has been surveyed monthly or fortnightly since the late 1950s (OLA-IS, AnaEE-France, INRAE of Thonon-les-Bains, and CIPEL; Rimet et al., 2020). It is an oligomictic lake with complete deep mixing (309 m, latest in 2012) occurring every 7 years on average, while annual winter mixing average is ~150-200 m (Gaudard et al., 2017; Schwefel et al. 2016). The lake is stratified from spring to fall with a thermocline deepening from 3 to 30 m (Fig. 1-3). The surface alkalinity ranges from 1200 to 1700 µeq L^{-1} (Fig. 1-3 (c)) and the surface calcium concentration (Ca^{2+}) ranges from 38 to 46 mg L^{-1} (Fig. 1-3 (d)) according to the season and linked to calcite precipitation (Müller et al., 2016). Its trophic level is currently considered to be oligo-mesotrophic, but it had reach high level of eutrophication more than 40 years ago before drastic measures against anthropogenic phosphorus.

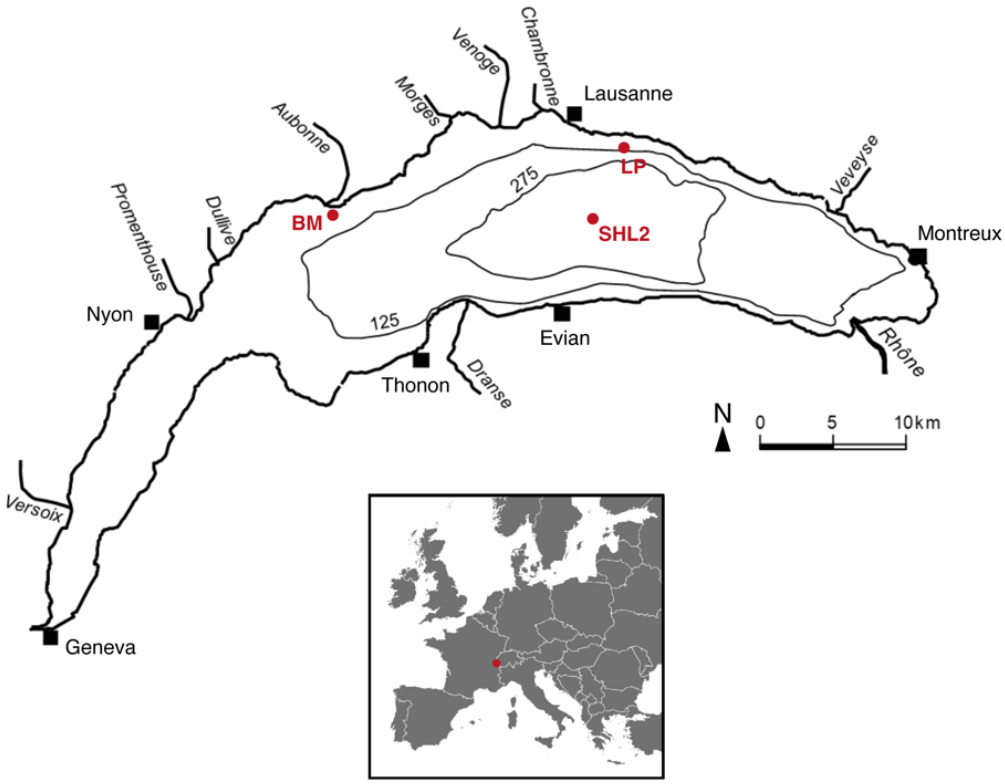

Fig. 1-2: Lake Geneva and its main hydrographic network **(top)**. SHL2 represents the sampling location point of the historical survey. LP (LéXPLORE platform) and BM (Buchillon mast) represent the location of the pelagic and littoral study sites of this PhD research where high frequency instrumentation has been done (more information in section 1.5.). Situation map of Lake Geneva in Europe **(down)**.

The surface CO_2 concentrations, as computed from the routine temperature, alkalinity, and pH measurements (Pierrot et al., 2006), show a typical seasonal cycle with high, supersaturated values during winter mixing (~800 ppm) and values below saturation during the stratified period (~200 ppm), while the oxygen concentration at the surface has the inverse dynamics (Fig. 1-3 (a-b)). Most of the inter-annual variability is due to winter concentrations and should therefore be linked to the depths of spring mixing. Surface CO_2 is yet only the tip of the iceberg and the range of variability of CO_2 over depth is even greater (~200-1,800 ppm). CO_2 redistribution within

the water column is tied to mixing/stratification dynamics, whilst deep respiration cannot explain most of the changes in hypolimnetic CO_2 concentration.

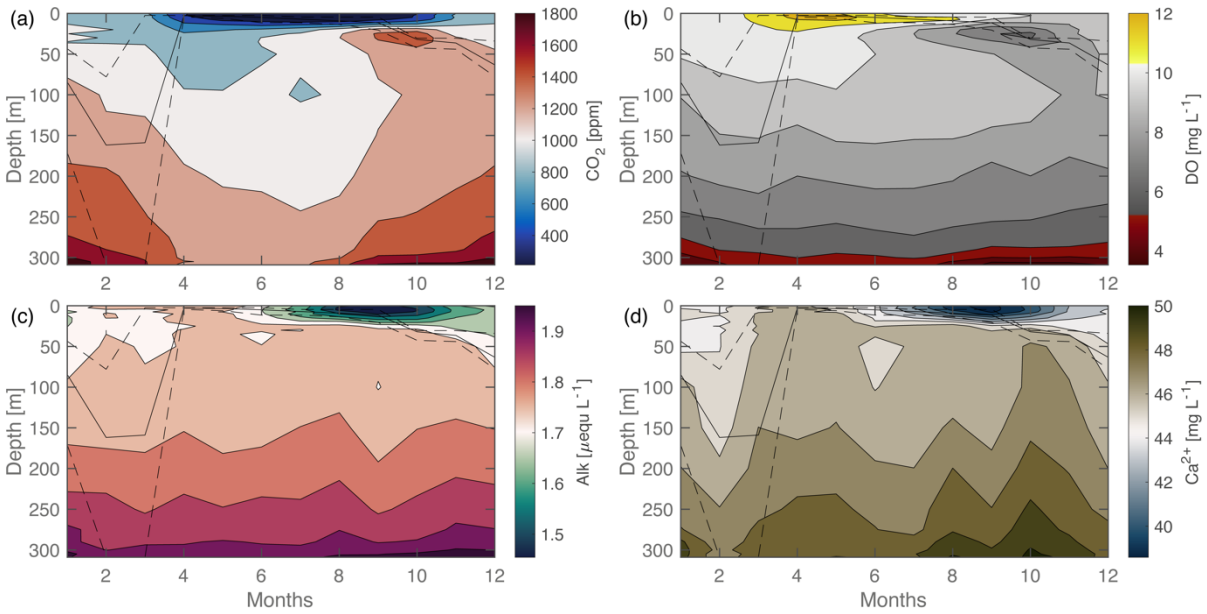

Fig. 1-3: Monthly mean (2006-2016) of: **(a)** CO_2 concentration, **(b)** dissolved oxygen, **(c)** alkalinity, and **(d)** calcium. Solid line is the mean of thermocline or winter mixing, and dash lines are their maximum and minimum on the temporal series. Data from Rimet et al. (2020) monthly data from the routine monitoring site SHL2. CO_2sys program (Pierrot et al., 2006) following Millero (1979).

Further, the drivers of CO_2 variability in Lake Geneva, such as the underlying mechanisms, appear to differ depending on the time and space scales of observations. A study by Perga et al. (2016), combining CO_2 reconstruction from a paleo-proxy and monitoring data revealed that CO_2 supersaturation was a by-product of its past eutrophication history. Before the early 1940s, the lake was most likely neutral to the atmosphere in summer. While changes in surface CO_2 over decades were attributed to variations in nutrient concentrations, the relationships between these two over time were non-linear. As a result, the underlying mechanisms are still unclear even though an interaction between metabolic processes and calcite precipitation is suspected. At this scale of observation, climate change was not identified as a significant driver. In addition, during a spring survey (May 2015, Bouffard and Perga, 2016), lake surface CO_2 varied by a factor of 2 over the Eastern part of Lake Geneva, as a likely consequence of spatial variation in primary production. These preliminary results highlight the necessity for a process-oriented approach to understand C-cycling in Lake Geneva, that fully integrates biogeochemistry and hydrodynamics.

1.3. The challenge of reaching representative CO_2 balance in large lakes

Surface water CO_2 (C_{wat}) and CO_2 gas exchange (Flux) from lakes can be sustained by several processes such as lake hydrodynamic, metabolism, watershed inputs and calcite reaction (see Fig. 1-4), through which CO_2 is either produced/consumed locally or transported from peripheral production sites (Vachon et al., 2017). Reaching

representative estimates of CO_2 fluxes over an annual mass balance requires to solve the Fiskian equation, acknowledging for the temporal and spatial variability of all three terms of the equation. Fig. 1-4 summarised all the reaction and transport processes likely to affect both surface CO_2 and the gas exchange velocity.

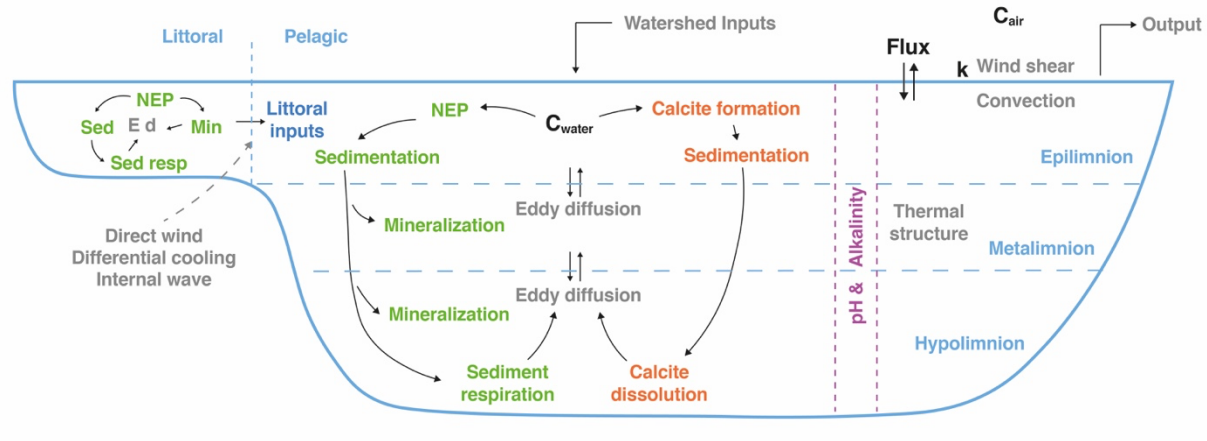

Fig. 1-4: Conceptual scheme of processes sustaining surface CO_2 dynamics: Variables linked to gas exchange (black), metabolism (green), calcite reaction (red), physical components (grey), chemical influence on processes (purple).

1.3.1. Hydrological components

The first physical process simply refers to river inflows and outflows of the lake system. These discharge variations are dependent on the natural hydrological regime of the watershed and how they are affected by human activities (e.g., hydroelectric construction, safety dam for large floods, regulation of lake water levels…). Besides, these hydrological regimes have evolved due to climate change, shifting peak flows earlier in the year in alpine regions (e.g. Zierl and Bugmann, 2005). Thus, all the tributaries imply variations of inputs and outputs throughout the year, which influence the variations of dissolved load and nutrient loading (e.g. DIC, P, Ca, Si, DOC, POC...), which both intervene directly or indirectly in the lake carbon cycle (Müller et al., 2016). Yet, Because of long-water residence time, the hydrological influence on the surface CO_2 of large lakes is expected to be limited, at least of seasonal and interannual time scales. Yet the seasonal variability of inflows can generate substantial spatial variability in lacustrine carbon processes, especially at lake-river estuaries (Escoffier et al, 2022).

1.3.2. Lake hydrodynamic

Lake's dynamic is primarily driven by heat and momentum exchanges with the atmosphere. At seasonal time scale, the evolution of thermal structure is a key parameter that regulates the surface CO_2 dynamics. This thermal structure results from a competition between heat flux and wind stress. During warm periods of the year, the thermal stratification creates a natural boundary between the surface and bottom waters (i.e. the thermocline), which has the effect of limiting the CO_2 vertical fluxes from the hypolimnion to the epilimnion. The wind action on this stratified system leads to basin scale internal waves that can locally increase vertical mixing and affects vertical fluxes (Wüest and Lorke 2003) and leads to short-term horizontal variability in the lake constituents.

1.3.3. Gas transfer velocity

Heat and momentum also modulate CO_2 gas exchanges. The gas transfer velocity or piston velocity, *k,* (Fig. 1-2; Vachon et al., 2010; Dugan et al., 2016) is a significant source of uncertainty in the flux estimates. *k* is inherently tied to turbulent mixing within the surface boundary layer, which enhances the diffusive gas exchange by renewing the surface mass content (Zappa et al., 2007). *k* is usually calculated as a function of wind speed, with wind stress viewed as a major source of near-surface turbulence (Cole and Caraco, 1998; Crusius and Wannikhof, 2003). The relationship linking *k* to wind has yet been inferred from a restricted number of studies (Vachon et al., 2010). In lake ecosystems influenced by low winds or more generally during periods of low winds, *k* depends also on the heat flux and especially on the surface cooling (Borges et al., 2004; MacIntyre et al., 2010; Read et al., 2012; Tedford et al., 2014). In the ocean, the contribution of surface waves as a source of turbulence is also included in *k* parameterisation while such contribution is traditionally neglected in lakes. *k* is inherently tied to the atmospheric conditions and can potentially vary from short (hourly-daily) to more seasonal time scales. Due to orographic wind or light shading, *k* could also significantly vary spatially, especially within large lakes, although this source of variability is rarely accounted for (e.g. Vachon and Prairie, 2013; Klaus and Vachon, 2020).

1.3.4. Metabolism

Metabolism is a fundamental ecological process that occurs at scales ranging from individual organisms to whole ecosystems (Brown et al., 2004). Whole-ecosystem metabolism cannot be measured directly but rather represents the balance between carbon fixation (gross primary production (GPP)) and biological carbon oxidation (ecosystem respiration (R)) in an ecosystem (Winslow et al., 2016). The difference between GPP and R is termed net ecosystem production (NEP) and is used to distinguish heterotrophic systems (negative NEP) from autotrophic systems (positive NEP). GPP varies with light availability and nutrient concentrations mainly, leading to a strong variability of surface CO_2 at hourly, daily and seasonal scales (Zwart and Brighenti, 2022). R varies with the concentrations of organic substrates and is usually strongly tied to GPP, as well as with ambient temperature, generating a similarly large range of temporal variability (Zwart and Brighenti, 2022).

However, metabolism has been shown to poorly explain the temporal (>daily) CO_2 variability in a number of lakes (Kelly et al. 2001, Finlay et al. 2009)*,* Because water clarity, nutrient concentrations and temperature are also spatially variable (see Fig. 1-5) , metabolism itself can generate a significant spatial variability in surface CO_2.

As littoral metabolism is usually greater than pelagic metabolism (e.g. Lauster et al., 2006; Sadro et al., 2011), CO_2 emissions have been observed to be greater in-shore as compared to off-shore in some lakes (e.g. Juutinen et al., 2003).

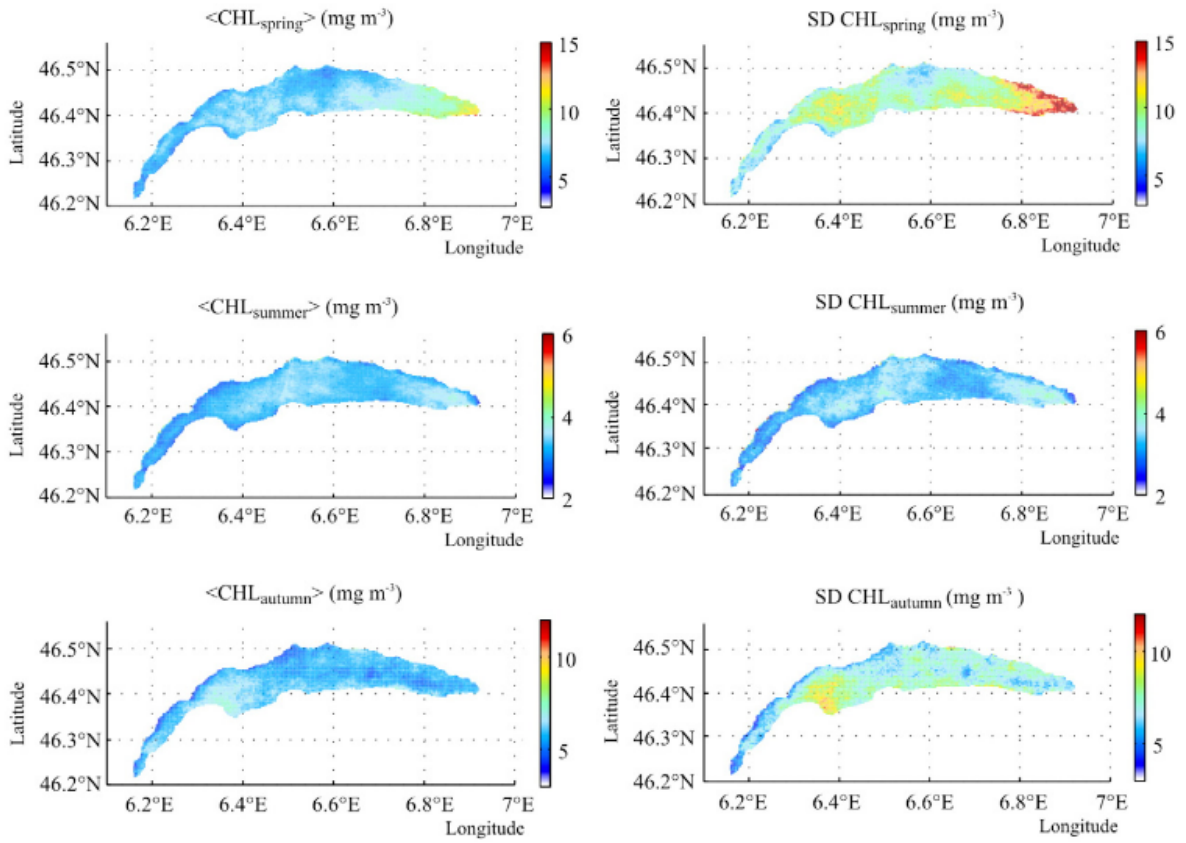

Fig. 1-5: Chlorophyll-a variability is represented as the mean (CHL, left) and the standard deviation (SD CHL, right) of the lognormal distribution of each pixel for spring **(top)**, summer **(middle)**, and autumn **(down)**. Consider the different colour scales for the two seasons, which better recognise the patterns (figure extracted from Kiefer et al., 2015).

1.3.5. Inorganic carbon chemistry and calcite reaction

Inorganic carbon chemistry is rarely explicated in lake CO_2 studies. I provide here a more detailed synthesis of the underlying mechanisms at the watershed and lake scale.

At first, the dissolution of atmospheric CO_2 into rainwaters (Fig. 1-6: Reaction 1) naturally acidifies the soil water (pH normally between 5 and 6, or smaller as a result of pollution). These acidic waters chemically alter the rock masses containing carbonates and silicates. The products of this alteration, once transferred to the lake basin by the rivers, influence the CO_2 sink capacity of the lakes. One of the most critical alteration products is calcium ion Ca^{2+}. This calcium is abundant in carbonates whose two main minerals are calcite $CaCO_3$ (calcium carbonate) and dolomite $CaMg(CO_3)_2$ (calcium and magnesium carbonate). Silicates also contain calcium in minerals such as plagioclase feldspaths, amphiboles or wollastonite (its simplest form: $CaSiO_3$), but to a lesser extent. When subjected to rains (acids), these two groups of minerals dissolve, carbonates being by far the most rapidly attacked. In both cases, calcium and bicarbonate ions are produced (Fig. 1-6: Reaction 2).

Calcium, bicarbonate, and silica are eroded from the soil, transported to the lakes by streams and subsequently contribute to the dissolved load. A portion of the Ca^{2+} and HCO_3^- ions abiotically form calcite ($CaCO_3$) by precipitation from the Ca^{2+} and HCO_3^- water in the lake, following the opposite reaction of reaction 2 (Figure 1-6: Reaction 3) (Stumm and Morgan, 1996). However, the pH must reach a relatively high threshold (> 8.2) for this reaction to occur. This threshold pertains to a decrease in dissolved CO_2, which can, for instance, be caused by the pumping of primary production. This has the effect of changing the carbonated balance towards an excess of CO_3^{2-} ions compared to HCO_3^- ions and, thus, allowing a supersaturation of calcite. However, this process must be accompanied by another trigger for the precipitation to occur, such as a change in temperature or biotic or abiotic nucleation, a mechanism that is still poorly understood (Stabel, 1986; Müller et al., 2016).

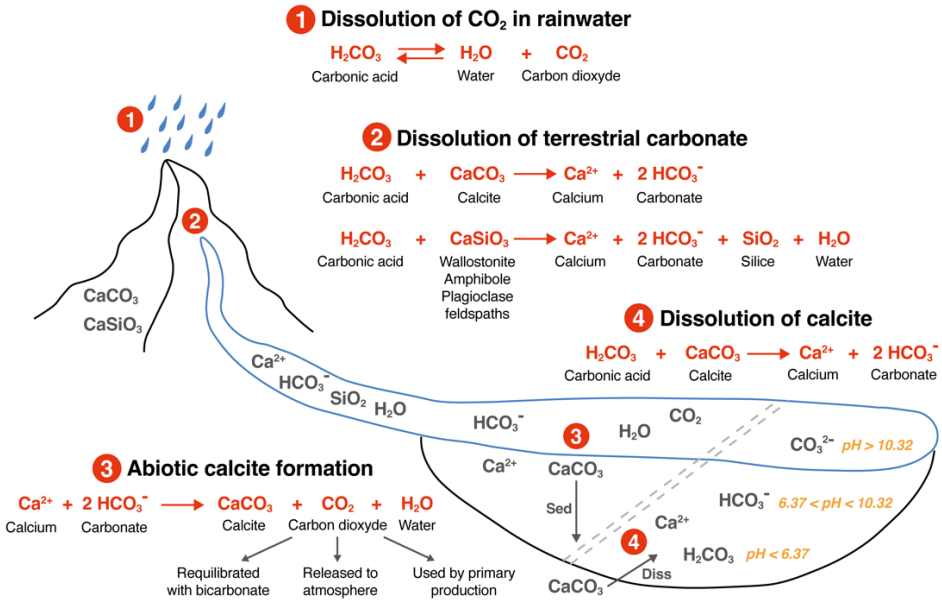

Fig. 1-6: Carbon and calcium cycling in the lake watershed such as Lake Geneva as well as the four main carbonate reaction involved.

In addition, the calcite formed by this reaction will sediment in the bottom of the lake in the form of inorganic carbon (IC) stock, transferring this IC from the epilimnion to the hypolimnion (Müller et al., 2016). Depending on the duration, this stock can either be buried for a very long time or be dissolved again in the water column, which recaptures some CO_2 (Fig. 1-6: Reaction 4) (Stumm and Morgan, 1996). Depending on water pH, calcium ions and carbonates or bicarbonates are released and play a crucial role in the set of reactions mentioned above.

Moreover, the solubility of CO_2 in gaseous form depends on the temperature and the pressure, which influences the pH variations of the water column (Stumm and Morgan, 1996). Not only the latter can vary due to the inputs discussed above, but it can also be affected by the effect of metabolism and by the mixing between different water layers of the lake. In addition, all of these chemical interactions on the carbon and calcium cycle can be temporally shifted and induce nonlinear feedback processes. For example, the CO_2 produced during calcite precipitation (Fig. 1-6: Reaction 3) can be directly degassed into the atmosphere but can also be used by a symbiotic alga, and its release into the atmosphere is delayed until the death of the algae or immediately requilibrate with bicarbonate.

The real contribution of calcite precipitation to the total carbon cycle of lakes is basically unquantified (e.g. Marcé et al., 2015).

1.3.6. Embedded scales of variability

All processed mentioned above vary in time and space at various scales. Their peak intensity can vary temporally over a few hours (gas exchange with the storm), a day-night (GPP), several days (calcite precipitation), several months (thermal stratification) or a year (sediment respiration, river inputs), depending on their characteristics (Fig. 1-7). Furthermore, spatial variations are significant, with greater change in epilimnion than in deep layers. Therefore, the question of when and where to sample and to observe the variations of these processes is of pivotal importance.

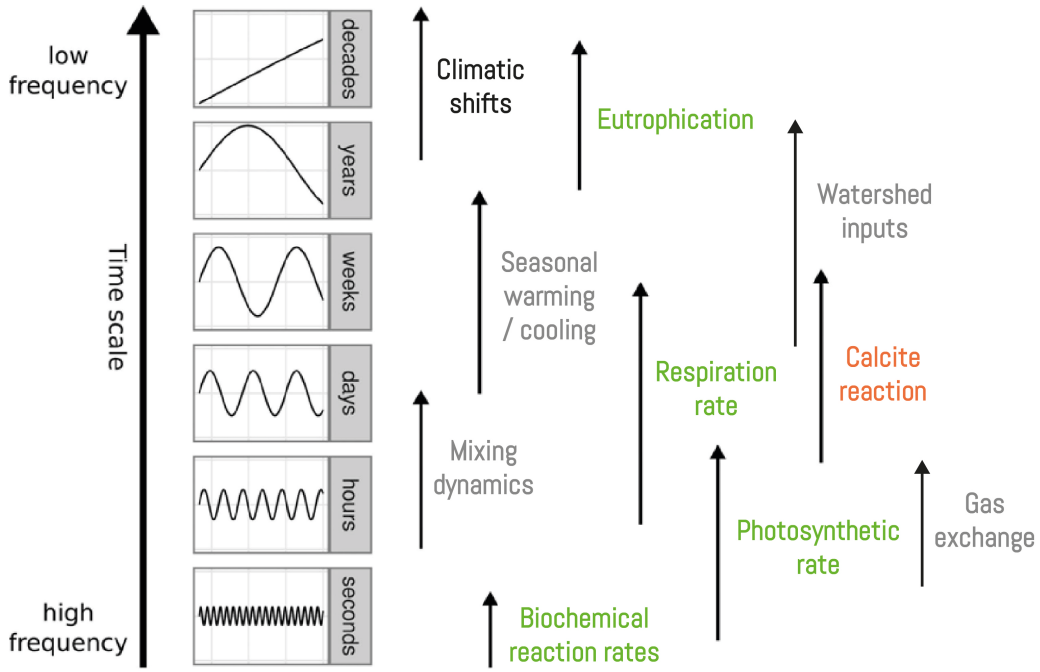

Fig. 1-7: Temporal scales of processes involved in surface CO_2 dynamics from high frequency to low frequency and their overlap.

A recent study regarding the changes in lake surface temperature clearly emphasised the need for in situ measurements at short intervals to avoid the production of inexact trends (Schmid, 2018), considering that a decrease in sampling frequency tends to decrease the observation of extreme values that may be disproportionately large over a fixed period. In addition, the CO_2 variations in Lake Geneva show that these variations can be of comparable magnitude at different time scales (Fig. 1-8). Therefore, it is necessary to study the CO_2 drivers in short- and long-term to successfully untie the mechanisms responsible for lake CO_2 emissions over a year.

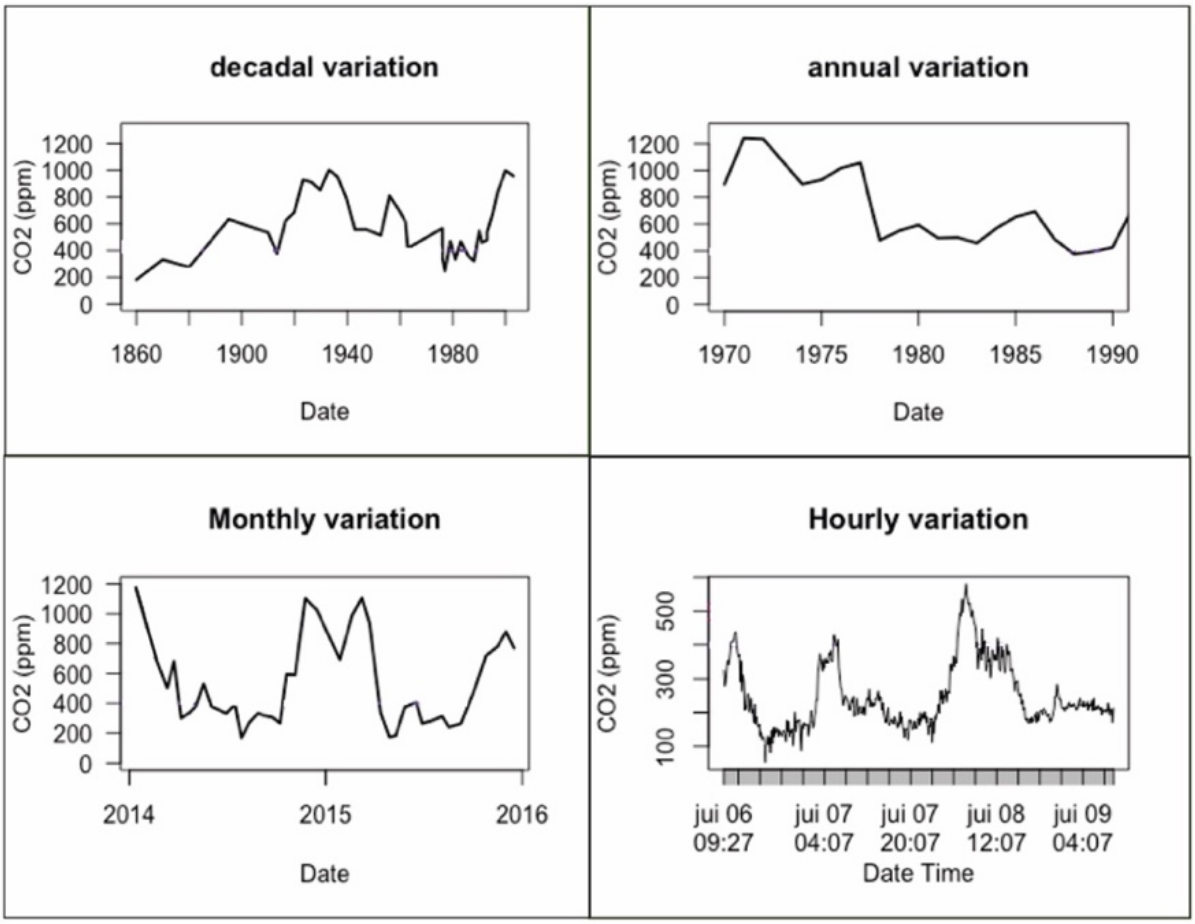

Fig. 1-8: Variabilities of surface CO_2 in Lake Geneva at different time scales. **(a)** From paleo reconstructions, **(b, c)** from monitoring data (data from Perga et al., 2016), and **(d)** personal data of Marie-Elodie Perga.

Consequently, there is a critical challenge in coupling single-point high-frequency measurement techniques with low-frequency but more extensive lake-based techniques to establish a realistic annual carbon budget so as to understand the interactions between physical and biogeochemical processes responsible for this cycle.

1.4. The doctoral research and its objectives

Using Lake Geneva as a model for large, deep hardwater lake, the main objectives of this doctoral thesis are (i) to reach a high-resolution understanding of the surface CO_2 dynamics and fluxes at the lake scale, (ii) to untie the physical and biogeochemical processes controlling the CO_2 fluxes at the lake-atmosphere interface, and (iii) to derive methodological guidelines on the frequency at which the different components of the CO_2 fluxes should be monitored to reach representative estimates of annual CO_2 fluxes. The guideline of this work is the Fickian equation which is decomposed in its individual terms (i.e. k, water CO_2, and atmospheric CO_2) to quantify the role of physical and biogeochemical processes on their dynamics. In that objective, the temporal variation of the lake surface CO_2 and gas exchange velocity was measured at an hourly resolution while their spatial component was addressed by comparing the pelagic and littoral environments.

The surface and atmospheric CO_2 concentrations can be relatively easily measured at high frequency using autonomous sensors. Yet, the *k* term of the equation is challenging to measure at high-frequency over continuous periods. The *k* term in gas flux estimates is modelled rather than measured. Accurate estimates of lake CO_2 fluxes requires that the *k* model used is parametrised for Lake Geneva. The first step of the work aims at resolving the temporal variability in the gas exchange velocity, addressing the relative contribution of wind shear, convection, and surface waves on the temporal variability of *k*, and deriving a *k* model adapted for Lake Geneva that could also solve the spatial variability.

High-frequency and year-round, spatially resolved measurements of the three terms of the Fiskian equation are data that are challenging to collect continuously and over multiple years. In a second step, we assess the minimal frequency at which data of the three terms have to be collected to reach reasonable estimates of annual CO_2 fluxes. We also test whether spatially resolved data (i.e. littoral and pelagic) are necessary in the case of Lake Geneva, where littoral habitats represent a very low share of the lake surface.

Alkalinity has been identified as a key-compartment of the CO_2 processes in alkaline lakes. In Swiss lakes, major drops in alkalinity occurs during the summer season when the lake is undersaturated in CO_2 (Müller et al., 2016). The third step investigates the relationships between alkalinity, CO_2, and GPP in the objective to delineate part of the processes by which alkalinity intervene in the lake carbon cycle.

1.5. Study sites and field instrumentation

This doctoral work benefited from the ongoing initiative of off-shore and in-shore stations for high frequency monitoring: the LéXPLORE platform (110 m depth; Wüest et al., 2021) and the Buchillon mast (4 m depth), representative of the pelagic and littoral environments, respectively (Figs. 1-2 and 1-9).

Monitoring was conducted at both sites over the years 2019, 2020 and 2021. The monitoring design was slightly lighter at the littoral station, but similar protocols conducted at one deep and one shallow site (Fig. 1-9) is one way by which we approach the role of depth on the surface and water column C processes. These stations were key to explore the short-time variability in surface CO_2 and its potential physical and biogeochemical drivers. I was the main person in charge of the fieldwork of these moorings and I took care of the temperature and CO_2 sensors in the pelagic site and in addition to the oxygen sensor in the littoral site during more than 25 maintenances between the two sites (see illustration in Fig 1-10). Dr Escoffier took care of the calibration of the pH and conductivity sensors in the pelagic and littoral sites while Dr Chmiel took care of the oxygen sensors in the pelagic site. A thermistor chain was set on the entire water column at LéXPLORE platform, a weather station is installed in both environments with an atmospheric CO_2 sensor in the pelagic (Fig. 1-9).

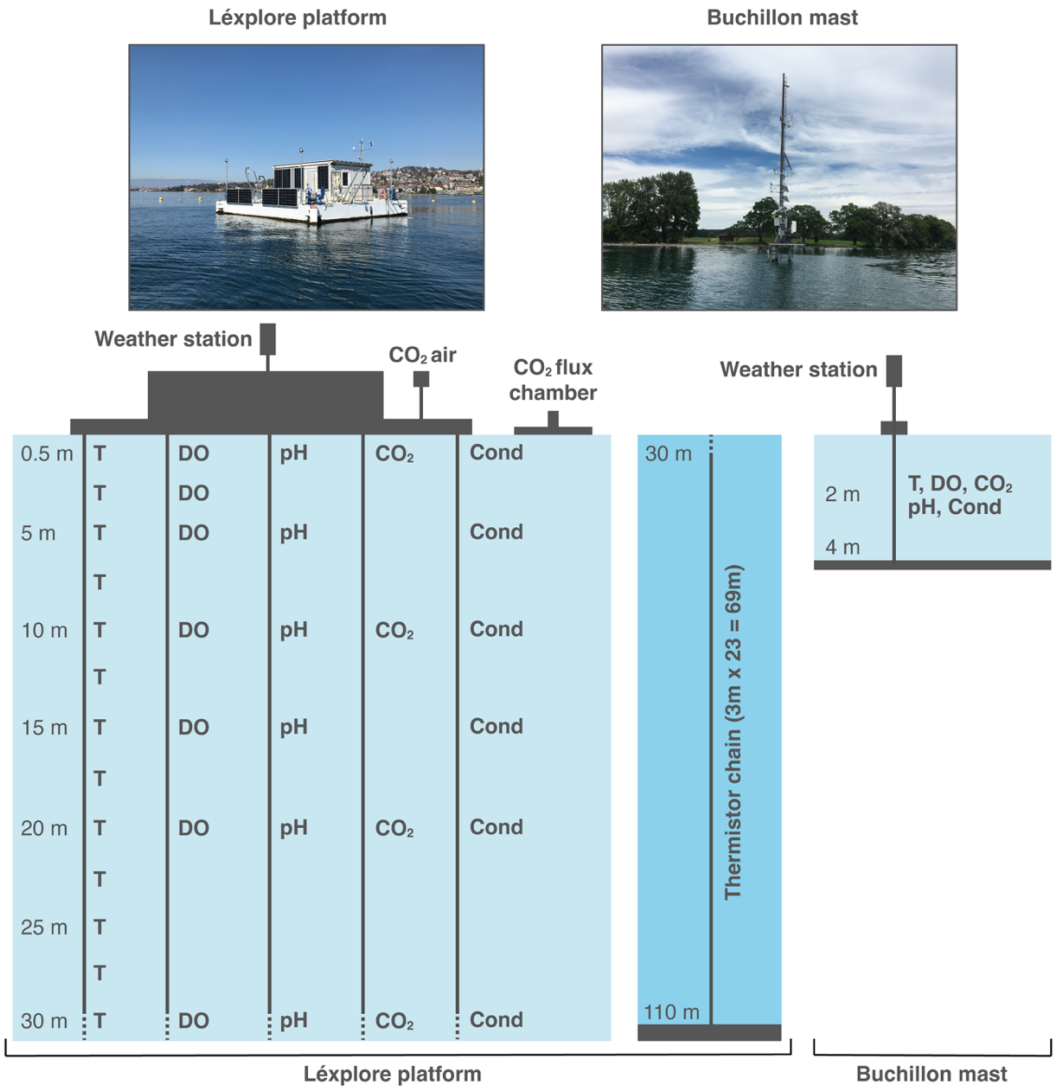

Fig. 1-9: Pictures of the two study sites investigated during this doctoral research: LéXPLORE platform **(left)** and Buchillon mast **(right)**. Shame of the main sensors used to accomplish this study in collaboration with Dr Escoffier and Dr Chmiel.

Specific protocol was conducted for the CO_2 sensors calibrated with two standard gases (0 and 2,000 ppm) and one control of atmospheric gas (~400 ppm) with a CO_2 gas analyser (Licor 830) every 4-6 weeks and corrected considering the drift if necessary. Unfortunately, during this study, we suffered various issues with all the sensors, especially CO_2 sensors, due to the natural environment of a large lake (e.g., strong storm, strong sunshine, use of ropes, loss or breakage of instruments…) and the reliability of the sensors (e.g., sensor drift, communication port…). Therefore, there are some gaps within the time-series.

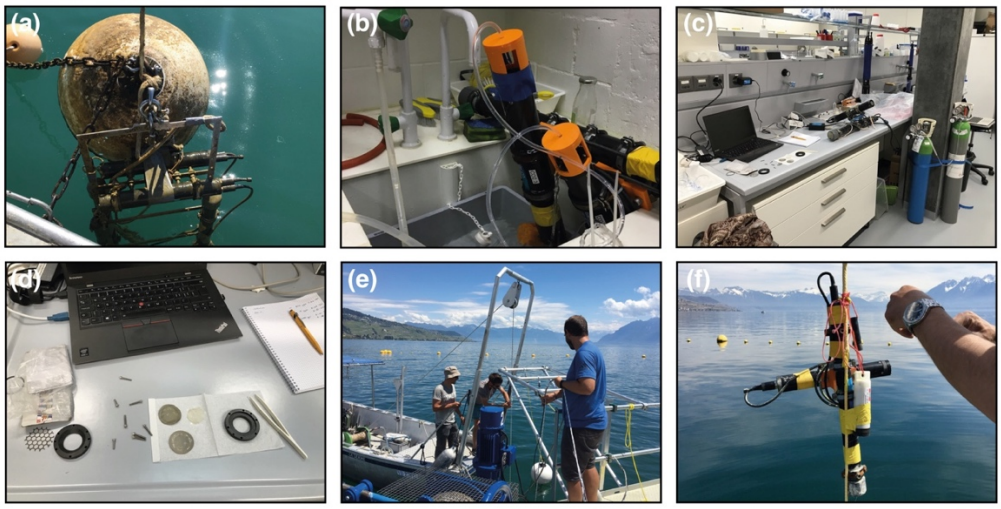

Fig. 1-10: Illustration of the type of work performed in the field and in the laboratory during maintenance. **(a)** Mooring recovery, **(b)** cleaning of sensors and membranes, **(c)** calibration check using two standard gases (0 and 2,000 ppm) and one control of atmospheric gas (~400 ppm) with a CO_2 gas analyser (Licor 830), **(d)** cleaning of membrane; **(e)** installation of the thermistor connected to the platform with live data visualisation, and **(f)** launching of the mooring after maintenance.

Furthermore, an automated (forced diffusion) CO_2 flux chamber derived from the soil study (Fig. 1-11; eosFD, Eosense; Risk et al. 2011; Spafford and Risk ,2018) was installed on the LéXPLORE platform to measure the CO_2 gas exchange. Before I could leave this flux chamber for several days or weeks at different times of the year on the lake, I had to go through various stages of construction and testing (Fig. 1-11). With advice from Eosense, I started by building a mini platform intended to support the instrument on the water and to test it in a river, then at LéXPLORE without electrical autonomy. After verification of proper operation, a solar panel and its battery were installed with a reinforcement of the buoyancy of the platform to let it operate autonomously.

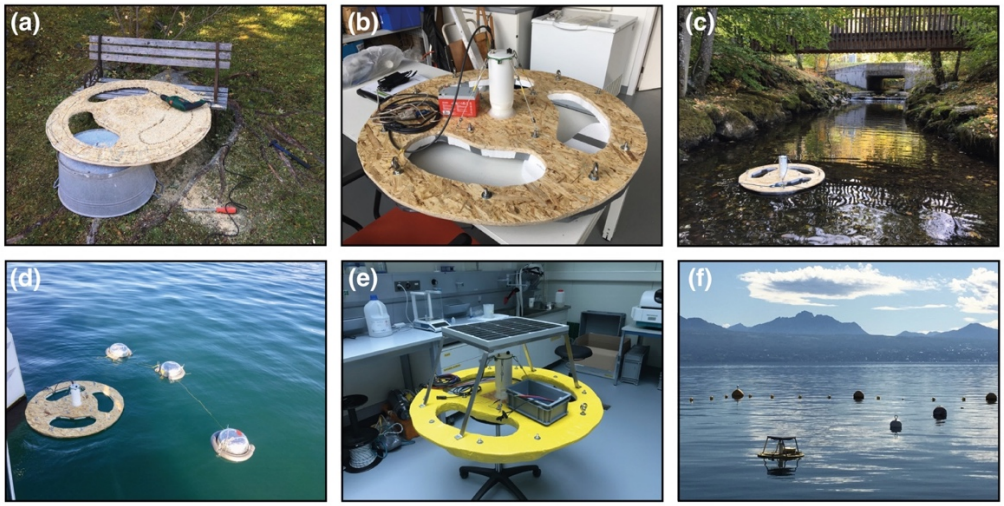

Fig. 1-11: Illustration of eosFD building and testing steps. **(a, b)** building the mini platform, **(c)** first test in a river, **(d)** comparison with manual and low-cost flux chamber at LéXPLORE, **(e)** finalisation of the power energy system and the buoyancy, and **(f)** autonomous data logging.

1.6. Structure

This doctoral thesis is structured into three chapters (2, 3 and 4), each corresponding to a separate article (accepted, submitted, or in preparation, respectively). The last chapter (5) synthesis the results of the three previous chapters as well as my collaboration (Fig. 1-12).

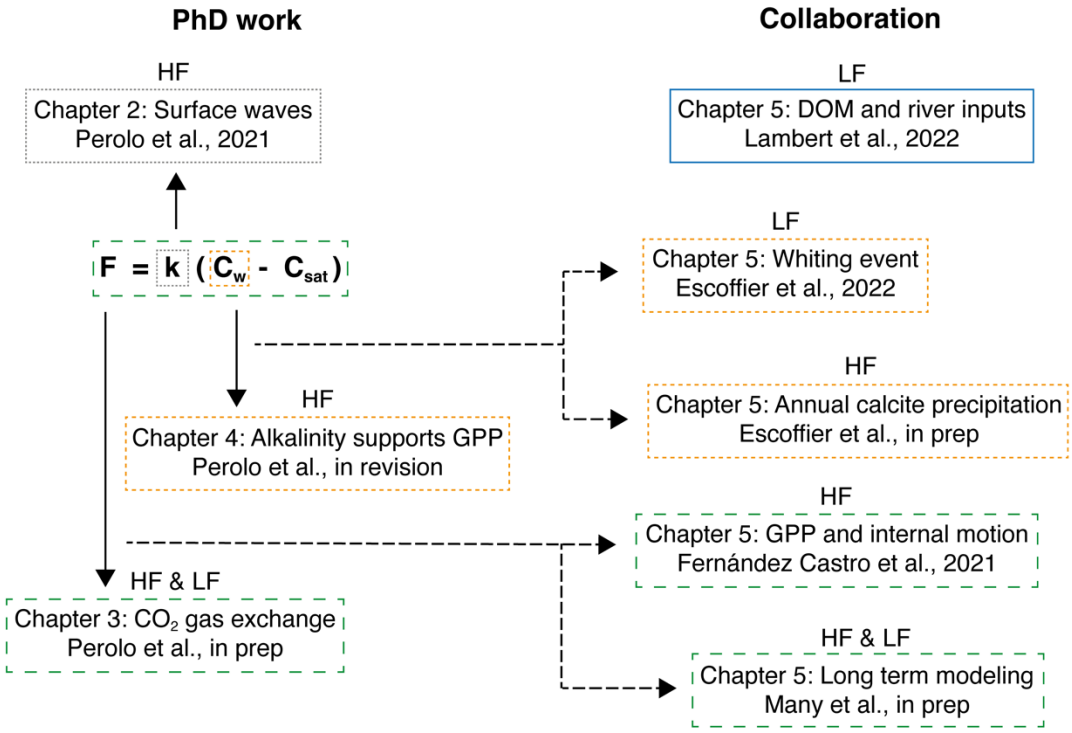

Fig. 1-12: Schematic structure of my workflow around the CO_2 flux equation as well as the collaborations done during the four years of my doctoral thesis linked to my topics.

Chapter 2 focuses on the physical processes generating turbulence near the air-water interface. It aims to identify the most adequate *k* model for a large lake to assess *k* values over a full annual cycle. For the first time, we measured enhanced gas exchanges by wind-induced waves at the surface of a large lake using a new generation of automated (forced diffusion) CO_2 flux chamber. We adapted an ocean-based model to account for the effect of surface waves on gas exchange in lakes. We finally show that intense wind events with surface waves contribute disproportionately to the annual CO_2 gas flux in a large lake.

Chapter 3 assesses the minimal sampling frequency of inputs data that is necessary to reach representative estimates annual CO_2 fluxes at the surface of a large lake. We combine at high frequency measurements of water and air pCO_2 and high-frequency computations of to estimate, at a fine-scale resolution, the CO_2 gas exchange over a complete annual cycle in the littoral and pelagic environments in a large and deep hardwater lake. We thereafter degrade the signal resolution and quantify errors in annual flux estimates resulting from the loss of information. We derive a sampling compromise that minimizes both the sampling frequency-sites and errors in CO_2 flux estimates over a complete annual cycle at the lake scale. Our temporal analyses highlight the importance of high-frequency data for the *k* and pCO_2 variables, but their impact on the flux estimation differs according to

the seasons and frequency. In terms of spatial variability, the yearly mean flux of the littoral environment is more than one order of magnitude greater than for the pelagic and should be integrated into the total lake fluxes. Finally, we propose solutions to improve these CO_2 gas exchange quantifications using currently available numerical tools such as spatial weather model, hydrodynamical model and data reconstruction.

Chapter 4 aims to study the physical and biogeochemical processes involved in the daily surface CO_2–O_2 dynamics in the littoral and pelagic environments. As gross primary production is considered as the main driver of these dynamics, CO_2 and O_2 should covary inversely accordingly to the stoichiometric ratio. However, in Lake Geneva, highest rates of O_2 production occur despite low CO_2 consumption suggesting that photosynthetic organisms can use an alternate carbon source, i.e. bicarbonate. Therefore, we detect the origin of the inorganic carbon maintaining GPP by analysing the daily stoichiometric ratios of CO_2–O_2 and Alkalinity–O_2. We relate the DIC source to the environmental conditions to estimate how much of the littoral and pelagic GPP are supported by bicarbonate use at an annual scale. Results show that bicarbonates are the dominant DIC source for GPP in Lake Geneva, with an even greater relevance in the pelagic as compared to the littoral habitats.

Chapter 5 highlights the key findings regulating the surface CO_2 dynamics and the CO_2 gas exchange of Lake Geneva using the main results of my doctoral research and of my collaborations. A conceptual carbon cycle for a deep hardwater lake is proposed to summarise the carbon fluxes transported and transformed over a year. Finally, the limits and perspectives of this research are discussed.

1.5. References

Bolin B. (1981). Carbon cycle modelling Scope Report no. 16. New York: Wiley.

Borges, A. V., Vanderborght, J.-P., Schiettecatte, L.-S., Gazeau, F., Ferron-Smith, S., Delille, B., & Frankignoulle, M. (2004). Variability of the gas transfer velocity of CO_2 in a macrotidal estuary (the Scheldt). Estuaries, 27 (Issue 4), 593–603.

Bouffard, D., & Perga, M.-E. (2016). Are flood-driven turbidity currents hot spots for priming effect in lakes? Biogeosciences, 13(12), 3573–3584. https://doi.org/10.5194/bg-13-3573-2016

Brown, J. H., Gillooly, J. F., Allen, A. P., Savage, V. M., & West, G. B. (2004). Toward a metabolic theory of ecology. Ecology, 85(7), 1771–1789. https://doi.org/10.1890/03-9000.

Ciais, P., Borges, A. V., Abril, G., Meybeck, M., Folberth, G., Hauglustaine, D., & Janssens, I. A. (2008). The impact of lateral carbon fluxes on the European carbon balance. Biogeosciences, 5, 1259-1271.

CIPEL (2015). Rapport de la Commission internationale pour la protection des eaux du Léman contre la pollution, Campagne 2014. https://www.cipel.org/wpcontent/uploads/2015/11/CIPEL_Rapport_scient_Camp2014.pdf

Cole, J. J., Prairie, Y. T., Caraco, N. F., McDowell, W. H., Tranvik, L. J., Striegl, R. G., Melack, J. (2007). Plumbing the Global Carbon Cycle: Integrating Inland Waters into the Terrestrial Carbon Budget. Ecosystems, 10(1), 172–185. https://doi.org/10.1007/s10021-006-9013-8.

Cole, J. J., & Caraco, N. F. (1998). Atmospheric exchange of carbon dioxide in a low-wind oligotrophic lake measured by the addition of SF_6. Limnology and Oceanography, 43 (4), 647–656. https://doi.org/10.4319/lo.1998.43.4.0647.

Cole, J. J., Caraco, N. F., Kling, G. W., & Kratz, T. K. (1994). Carbon Dioxide Supersaturation in the Surface Waters of Lakes. Science, New Series, 265 (5178), 1568–1570.

Crusius, J., & Wanninkhof, R. (2003). Gas transfer velocities measured at low wind speed over a lake. Limnology and Oceanography, 48 (3), 1010–1017. https://doi.org/10.4319/lo.2003.48.3.1010.

Degens E.T., Kempe S., Richey J.E. (1991). Chapter 15, summary: biogeochemistry of major world rivers. In: Degens E.T., Kempe S., Richey J.E., Eds. Biogeochemistry of major world river. Scope 42, New York: Wiley, pp 323–44.

Del Giorgio, P. A., Cole, J. J., Caraco, N. F., & Peters, R. H. (1999). Linking planktonic biomass and metabolism to net gas fluxes in northern temperate lakes. Ecology, 80(4), 1422–1431. https://doi.org/10.1890/0012-9658(1999)080[1422:LPBAMT]2.0.CO;2.

DelSontro, T., Beaulieu, J. J., & Downing, J. A. (2018). Greenhouse gas emissions from lakes and impoundments: Upscaling in the face of global change. Limnology and Oceanography Letters. https://doi.org/10.1002/lol2.10073

Dugan, H. A., Woolway, R. I., Santoso, A. B., Corman, J. R., Jaimes, A., Nodine, E. R., Weathers, K. C. (2016). Consequences of gas flux model choice on the interpretation of metabolic balance across 15 lakes. Inland Waters, 6 (4), 581–592. https://doi.org/10.1080/IW-6.4.836.

Engel, F., Farrell, K. J., McCullough, I. M., Scordo, F., Denfeld, B. A., Dugan, H. A., Weyhenmeyer, G. A. (2018). A lake classification concept for a more accurate global estimate of the dissolved inorganic carbon

export from terrestrial ecosystems to inland waters. The Science of Nature, 105(3–4). https://doi.org/10.1007/s00114-018-1547-z.

Escoffier, N., P. Perolo, T. Lambert, J. Rüegg, D. Odermatt, T. Adatte, T. Vennemann, and M.-E. Perga. 2022. Whiting events in a large peri-alpine lake: Evidence of a catchment-scale process. J. Geophys. Res.: Biogeosci.

Finlay, Kerri, Vogt, R. J., Bogard, M. J., Wissel, B., Tutolo, B. M., Simpson, G. L., & Leavitt, P. R. (2015). Decrease in CO2 efflux from northern hardwater lakes with increasing atmospheric warming. Nature, 519 (7542), 215–218. https://doi.org/10.1038/nature14172.

Finlay, K., Leavitt, P. R., Wissel, B., & Prairie, Y. T. (2009). Regulation of spatial and temporal variability of carbon flux in six hard-water lakes of the northern Great Plains. Limnology and Oceanography, 54 (6part2), 2553–2564. https://doi.org/10.4319/lo.2009.54.6_part_2.2553.

Gaudard, A., Schwefel, R., Vinnå, L. R., Schmid, M., Wüest, A., & Bouffard, D. (2017). Optimizing the parameterization of deep mixing and internal seiches in one-dimensional hydrodynamic models: A case study with Simstrat v1.3. Geoscientific Model Development, 10(9), 3411–3423. https://doi.org/10.5194/gmd-10-3411-2017

Goudsmit, G.-H., Burchard, H., Peeters, F., & Wüest, A. (2002). Application of k-ϵ turbulence models to enclosed basins: The role of internal seiches: Application of k-ϵ turbulence models. Journal of Geophysical Research: Oceans, 107 (C12), 23-1-23–13. https://doi.org/10.1029/2001JC000954.

Humborg, C., Mörth, C.-M., Sundbom, M., Borg, H., Blenckner, T., Giesler, R., & Ittekkot, V. (2010). CO_2 supersaturation along the aquatic conduit in Swedish watersheds as constrained by terrestrial respiration, aquatic respiration and weathering. Global Change Biology, 16(7), 1966–1978. https://doi.org/10.1111/j.1365-2486.2009.02092.x.

IPCC. (2001). Watson, R. T., Albritton, D. L., Intergovernmental Panel on Climate Change, Intergovernmental Panel on Climate Change, & Intergovernmental Panel on Climate Change (Eds.). (2001). Climate change 2001: synthesis report. Cambridge; New York: Cambridge University Press.

IPCC. (2014). Climate Change 2014: Impacts, Adaptation, and Vulnerability. Part A: Global and Sectoral Aspects. Contribution of Working Group II to the Fifth Assessment Report of the Intergovernmental Panel on Climate Change. Cambridge University Press, Cambridge, United Kingdom and New York, NY, USA.

Jonsson, A., Karlsson, J., & Jansson, M. (2003). Sources of Carbon Dioxide Supersaturation in Clearwater and Humic Lakes in Northern Sweden. Ecosystems, 6: 224-235, DOI: 10.1007/s10021-002-0200-y.

Juutinen, S., Alm, J., Larmola, T., Huttunen, J. T., Morero, M., Martikainen, P. J., & Silvola, J. (2003). Major implication of the littoral zone for methane release from boreal lakes. *Global Biogeochemical Cycles*, *17*(4). https://doi.org/10.1029/2003GB002105

Khan, H., Laas, A., Marcé, R., & Obrador, B. (2020). Major Effects of Alkalinity on the Relationship Between Metabolism and Dissolved Inorganic Carbon Dynamics in Lakes. *Ecosystems*, *23*(8), 1566–1580. https://doi.org/10.1007/s10021-020-00488-6

Kelly, C. A., Fee, E., Ramlal, P. S., Rudd, J. W. M., Hesslein, R. H., Anema, C., & Schindler, E. U. (2001). Natural variability of carbon dioxide and net epilimnetic production in the surface waters of boreal lakes of different sizes. Limnology and Oceanography, 46(5), 1054–1064. https://doi.org/10.4319/lo.2001.46.5.1054

Kiefer, I., Odermatt, D., Anneville, O., Wüest, A., & Bouffard, D. (2015). Application of remote sensing for the optimization of in-situ sampling for monitoring of phytoplankton abundance in a large lake. Science of The Total Environment, 527–528, 493–506. https://doi.org/10.1016/j.scitotenv.2015.05.011

Klaus, M. and Vachon, D. (2020). Challenges of predicting gas transfer velocity from wind measurements over global lakes, Aquat. Sci., 82, 53, https://doi.org/10.1007/s00027-020-00729-9

Lapierre, J.-F., Guillemette, F., Berggren, M., & del Giorgio, P. A. (2013). Increases in terrestrially derived carbon stimulate organic carbon processing and CO2 emissions in boreal aquatic ecosystems. Nature Communications, 4 (1), 2972. https://doi.org/10.1038/ncomms3972

Lauster, G. H., Hanson, P. C., & Kratz, T. K. (2006). Gross primary production and respiration differences among littoral and pelagic habitats in northern Wisconsin lakes. 63, 12.

Maberly, S. C., Barker, P. A., Stott, A. W., & De Ville, M. M. (2013). Catchment productivity controls CO2 emissions from lakes. Nature Climate Change, 3 (4), 391–394. https://doi.org/10.1038/nclimate1748

MacIntyre, S., Jonsson, A., Jansson, M., Aberg, J., Turney, D. E., & Miller, S. D. (2010). Buoyancy flux, turbulence, and the gas transfer coefficient in a stratified lake: Turbulence and gas evasion in lakes. Geophysical Research Letters, 37 (24). https://doi.org/10.1029/2010GL044164

Marcé, R., Obrador, B., Morguí, J.-A., Lluís Riera, J., López, P., & Armengol, J. (2015). Carbonate weathering as a driver of CO2 supersaturation in lakes. Nature Geoscience, 8 (2), 107–111. https://doi.org/10.1038/ngeo2341

Matzinger, A., Schmid, M., Veljanoska-Sarafiloska, E., Patceva, S., Guseska, D., Wagner, B., Wüest, A. (2007). Eutrophication of ancient Lake Ohrid: Global warming amplifies detrimental effects of increased nutrient inputs. Limnology and Oceanography, 52 (1), 338–353. https://doi.org/10.4319/lo.2007.52.1.0338

Millero, F. (1979). The thermodynamics of the carbonate system in seawater. *Geochemica et Cosmochemica Acta* 43:1651-1661.

Müller, B., Meyer, J. S., & Gächter, R. (2016). Alkalinity regulation in calcium carbonate-buffered lakes. Limnology and Oceanography, 61(1), 341–352. https://doi.org/10.1002/lno.10213

Perga, M.-E., Maberly, S. C., Jenny, J.-P., Alric, B., Pignol, C., & Naffrechoux, E. (2016). A century of human-driven changes in the carbon dioxide concentration of lakes. Global Biogeochemical Cycles, 30 (2), 93-104. https://doi.org/10.1002/2015GB005286

Pierrot, D., Lewis, E., and Wallace, D. W. R. (2006). MS Excel Program Developed for CO2 System Calculations, Tech. rep., Carbon Dioxide Inf. Anal. Cent., Oak Ridge Natl. Lab., US DOE, Oak Ridge, Tenn.

Raymond, P. A., Hartmann, J., Lauerwald, R., Sobek, S., McDonald, C., Hoover, M., Guth, P. (2013). Global carbon dioxide emissions from inland waters. Nature, 503 (7476), 355–359. https://doi.org/10.1038/nature12760

Read, J. S., Hamilton, D. P., Desai, A. R., Rose, K. C., MacIntyre, S., Lenters, J. D., Wu, C. H. (2012). Lake-size dependency of wind shear and convection as controls on gas exchange. Geophysical Research Letters, 39 (9). https://doi.org/10.1029/2012GL051886

Reiss, R. S., Lemmin, U., Cimatoribus, A. A., & Barry, D. A. (2020). Wintertime Coastal Upwelling in Lake Geneva: An Efficient Transport Process for Deepwater Renewal in a Large, Deep Lake. Journal of Geophysical Research: Oceans, 125(8). https://doi.org/10.1029/2020JC016095

Rimet, F., Anneville, O., Barbet, D., Chardon, C., Crépin, L., Domaizon, I., and Monet, G. (2020). The Observatory on LAkes (OLA) database: Sixty years of environmental data accessible to the public, J. Limnol., 78, 164–178. https://doi.org/10.4081/jlimnol.2020.1944

Risk, D., Nickerson, N., Creelman, C., McArthur, G., & Owens, J. (2011). Forced Diffusion soil flux: A new technique for continuous monitoring of soil gas efflux. Agricultural and Forest Meteorology, 151 (12), 1622–1631. https://doi.org/10.1016/j.agrformet.2011.06.020

Sadro, S., Melack, J. M., & MacIntyre, S. (2011). Spatial and Temporal Variability in the Ecosystem Metabolism of a High-elevation Lake: Integrating Benthic and Pelagic Habitats. Ecosystems, 14(7), 1123–1140. https://doi.org/10.1007/s10021-011-9471-5

Schlesinger WH, Melack JM. (1981). Transport of organic carbon in the world's rivers. Tellus 33:172–87.

Schmidt M. (2018) Is monthly sampling sufficient to reliably estimate trends in lake surface temperatures? Poster: Eawag – Swiss Federal Institute of Aquatic Science and Technology with contributions by the Global Lake Temperature Collaboration (GLTC).

Schwefel, R., Gaudard, A., Wüest, A., & Bouffard, D. (2016). Effects of climate change on deepwater oxygen and winter mixing in a deep lake (Lake Geneva): Comparing observational findings and modeling. Water Resources Research, 52 (11), 8811–8826. https://doi.org/10.1002/2016WR019194

Siegenthaler U., Sarmiento J.L. 1993. Atmospheric carbon dioxide and the ocean. Nature 365:119–25.

Sobek, S., Algesten, G., Bergstrom, A.-K., Jansson, M., & Tranvik, L. J. (2003). The catchment and climate regulation of pCO_2 in boreal lakes. Global Change Biology, 9 (4), 630–641. https://doi.org/10.1046/j.1365-2486.2003.00619.x

Spafford, L., & Risk, D. (2018). Spatiotemporal Variability in Lake-Atmosphere Net CO_2 Exchange in the Littoral Zone of an Oligotrophic Lake. Journal of Geophysical Research: Biogeosciences. https://doi.org/10.1002/2017JG004115

Stabel, H.-H. 1986. Calcite precipitation in Lake Constance: Chemical equilibrium, sedimentation, and nucleation by algae. Limnol. Oceanogr. 31: 1081–1093. doi:10.4319/lo.1986.31.5.1081

Stets, E. G., Striegl, R. G., Aiken, G. R., Rosenberry, D. O., & Winter, T. C. (2009). Hydrologic support of carbon dioxide flux revealed by whole-lake carbon budgets. Journal of Geophysical Research, 114(G1). https://doi.org/10.1029/2008JG000783

Stumm W, Morgan JJ. (1996). Aquatic chemistry, chemical equilibria and rates in natural waters. 3rd. ed. John Wiley & Sons, Inc., New York. 1022p p.

Tedford, E. W., MacIntyre, S., Miller, S. D., & Czikowsky, M. J. (2014). Similarity scaling of turbulence in a temperate lake during fall cooling. Journal of Geophysical Research: Oceans, 119(8), 4689–4713. https://doi.org/10.1002/2014JC010135

Tranvik, L. J., Downing, J. A., Cotner, J. B., Loiselle, S. A., Striegl, R. G., Ballatore, T. J., Weyhenmeyer, G. A. (2009). Lakes and reservoirs as regulators of carbon cycling and climate. Limnology and Oceanography, 54(6part2), 2298–2314. https://doi.org/10.4319/lo.2009.54.6_part_2.2298

Umlauf, L., & Lemmin, U. (2005). Interbasin exchange and mixing in the hypolimnion of a large lake: The role of long internal waves. Limnology and Oceanography, 50(5), 1601–1611. https://doi.org/10.4319/lo.2005.50.5.1601

Vachon, D., & Prairie, Y. T. (2013). The ecosystem size and shape dependence of gas transfer velocity versus wind speed relationships in lakes. Canadian Journal of Fisheries and Aquatic Sciences, 70(12), 1757–1764. https://doi.org/10.1139/cjfas-2013-0241

Vachon, D., Prairie, Y. T., & Cole, J. J. (2010). The relationship between near-surface turbulence and gas transfer velocity in freshwater systems and its implications for floating chamber measurements of gas exchange. Limnology and Oceanography, 55(4), 1723–1732. https://doi.org/10.4319/lo.2010.55.4.1723

Vachon, D., Solomon, C. T., del Giorgio, P. A. (2017). Reconstructing the seasonal dynamics and relative contribution of the major processes sustaining CO_2 emissions in northern lakes. Limnology and Oceanography, 62(2), 706–722. https://doi.org/10.1002/lno.10454

Wehrli, B. (2013). Conduits of the carbon cycle. 2. Nature: news and views research. Vol. 503

Weyhenmeyer, G. A., Kosten, S., Wallin, M. B., Tranvik, L. J., Jeppesen, E., & Roland, F. (2015). Significant fraction of CO_2 emissions from boreal lakes derived from hydrologic inorganic carbon inputs. Nature Geoscience, 8(12), 933–936. https://doi.org/10.1038/ngeo2582

Winslow, L. A., Zwart, J. A., Batt, R. D., Dugan, H. A., Woolway, R. I., Corman, J. R., Read, J. S. (2016). LakeMetabolizer: An R package for estimating lake metabolism from free-water oxygen using diverse statistical models. Inland Waters, 6(4), 622–636. https://doi.org/10.1080/IW-6.4.883

Wüest, A., Bouffard, D., Guillard, J., Ibelings, B. W., Lavanchy, S., Perga, M., & Pasche, N. (2021). LéXPLORE: A floating laboratory on Lake Geneva offering unique lake research opportunities. WIREs Water, 8(5). https://doi.org/10.1002/wat2.1544

Zappa, C. J., McGillis, W. R., Raymond, P. A., Edson, J. B., Hintsa, E. J., Zemmelink, H. J., Dacey, J. W. H., and Ho, D. T. (2007). Environmental turbulent mixing controls on air–water gas exchange in marine and aquatic systems, Geophys. Res. Lett., 34, L10601, https://doi.org/10.1029/2006GL028790

Zierl, B., and H. Bugmann (2005), Global change impacts on hydrological processes in Alpine catchments, Water Resour. Res., 41, W02028, doi:10.1029/2004WR003447.

Zwart J. and Brighenti, L.S. (in press) Measurement and Variability of Lake Metabolism. Encyclopedia of Inland Waters, 2nd edition. (T. Mehner and K. Tockner, eds).

Chapter 2

Accounting for surface wave improves gas flux estimation at high wind speed in a large lake

Pascal Perolo[1], Bieito Fernández Castro[2,3], Nicolas Escoffier[1], Thibault Lambert[1], Damien Bouffard[4], Marie-Elodie Perga[1]

[1]Institute of Earth Surface Dynamics, University of Lausanne, Lausanne, 1015, Switzerland

[2]Physics of Aquatic Systems Laboratory, Margareth Kamprad Chair, Swiss Federal Institute of Technology Lausanne, Lausanne, 1015, Switzerland

[3]Ocean and Earth Science, University of Southampton, National Oceanography Centre, Southampton, SO14 3ZH, United Kingdom

[4]Eawag, Swiss Federal Institute of Aquatic Science and Technology, Surface Waters – Research Management, Kastanienbaum, 6047, Switzerland

Earth System Dynamics – EGU

2.1. Abstract

The gas transfer velocity (k) is a major source of uncertainty when assessing the magnitude of lake gas exchange with the atmosphere. For the diversity of existing empirical and process-based k models, the transfer velocity increases with the level of turbulence near the air-water interface. However, predictions for k can vary by a factor of 2 among different models. Near-surface turbulence results from the action of wind shear, surface waves and buoyancy-driven convection. Wind shear has long been identified as a key driver, but recent lake studies have shifted the focus towards the role of convection, particularly in small lakes. In large lakes, wind fetch can, however, be long enough to generate surface waves and contribute to enhance gas transfer, as widely recognised in oceanographic studies. Here, field values for gas transfer velocity were computed in a large hard-water lake, Lake Geneva, from CO_2 fluxes measured with an automated (forced diffusion) flux chamber and CO_2 partial pressure measured with high-frequency sensors. k estimates were compared to a set of reference limnological and oceanic k models. Our analysis reveals that accounting for surface waves generated during windy events significantly improves the accuracy of k estimates in this large lake. The improved k model is then used to compute k over a 1-year time period. Results show that episodic extreme events with surface waves (6 % occurrence, significant wave height > 0.4 m) can generate more than 20 % of annual cumulative k and more than 25 % of annual net CO_2 fluxes in Lake Geneva. We conclude that for lakes whose fetch can exceed 15 km, k models need to integrate the effect of surface waves.

2.2. Introduction

Lakes are universally regarded as significant sources of CO_2 to the atmosphere; however, the accurate quantification of the magnitude of such emissions currently remains challenging (Cole et al., 2007; Tranvik et al., 2009; Raymond et al., 2013). CO_2 fluxes can be directly measured with floating chamber or eddy covariance systems (Vachon et al., 2010; Vesala et al., 2006). However, both approaches have their own constraints. The former suffers from limited time and space integration (from minutes to hours and from centimetres to metres respectively; Klaus and Vachon, 2020), whereas the latter remains technically difficult and can be influenced by non-local processes (entrainment from the shore or advection; Vachon et al., 2010; Esters et al., 2021). Thus, long-term direct flux measurements are there mostly restricted to small lakes (Huotari et al., 2011) and fluxes remain mostly estimated with models. CO_2 fluxes at the surface of lakes operate through a net diffusive transport, obeying the first Fickian law:

$$F = k\alpha\Delta pCO_2 \,, \qquad (2\text{-}1)$$

where F (mol m^{-2} s^{-1} but often expressed as μmol cm^{-2} h^{-1}) is the CO_2 gas flux, α is the CO_2 solubility coefficient (μmol cm^{-3} μatm^{-1}), ΔpCO_2 is the gradient of partial pressure of CO_2 (pCO_2) between the water and the atmosphere corrected for altitude (μatm), and k is the gas transfer velocity (cm h^{-1}).

Therefore, lake carbon emissions are primarily driven by the gradient of partial pressure of CO_2 between the surface lake water and the atmosphere, but the gas transfer velocity controls the rate of CO_2 exchange across the lake–atmosphere interface. Assessing the amount of lake CO_2 emissions to the atmosphere has been a major issue, starting with the Cole and Caraco (1998) seminal paper, with debates regarding both the representativeness of the measurements and the optimal conceptual model for air-water gas transfer (e.g. MacIntyre et al., 2001; Borges et al., 2004). As recent developments in sensor technologies allow continuous and accurate measurements of aqueous CO_2 concentrations, the gas transfer velocity currently remains the main source of uncertainties, which hinders attempts to achieve full carbon budgets (Dugan et al., 2016) or to quantify greenhouse gas emissions by lakes, at local, regional, or worldwide scales (Maberly et al., 2013; Raymond et al., 2013; Engel et al., 2018).

k is inherently tied to turbulent mixing within the surface boundary layer, which enhances the diffusive gas exchange by renewing the surface mass content (Zappa et al., 2007). At the lake–atmosphere interface, turbulent mixing is the product of wind shear (k_u), buoyancy flux (k_c), and wind-driven surface waves, whose effect can be split into wave action (k_w) and wave breaking (k_b or k_B), with the latter producing air bubble and water spray (Fig. 1; Wüest and Lorke, 2003, Soloviev et al., 2007). Regarding the prominent role of wind action on surface turbulence, first quantitative models have empirically scaled k to wind speed (referenced at a 10 m height; U_{10}), as a proxy for the level of wind-driven turbulence (Fig. 2-1; Cole and Caraco, 1998; Crusius and Wanninkhof, 2003). The parameterisations of the k–wind relationships vary between authors (e.g. Klaus and Vachon 2020), as a likely consequence of the local characteristics of the lakes used in the calibration datasets (Table 2-1). However, all studies suggested a polynomial relationship between U_{10} and k with an exponent larger than 1. Further development of empirical models integrated the lake surface area as a second parameter in the k–wind relationships, to account for the role of the fetch length for wind action (Vachon and Prairie, 2013). Generally, empirical wind-based models tend to underestimate fluxes, especially at low wind speed (e.g. Schubert et al., 2012;

Heiskanen et al., 2014; Mammarella et al., 2015) where turbulent mixing through buoyancy flux is expected to take over wind shear. Moreover, these empirical models require a proper calibration each time they are applied in a new system with different characteristics, i.e. a new set of lakes and/or meteorological conditions (Klaus and Vachon, 2020), thereby limiting their universal applicability.

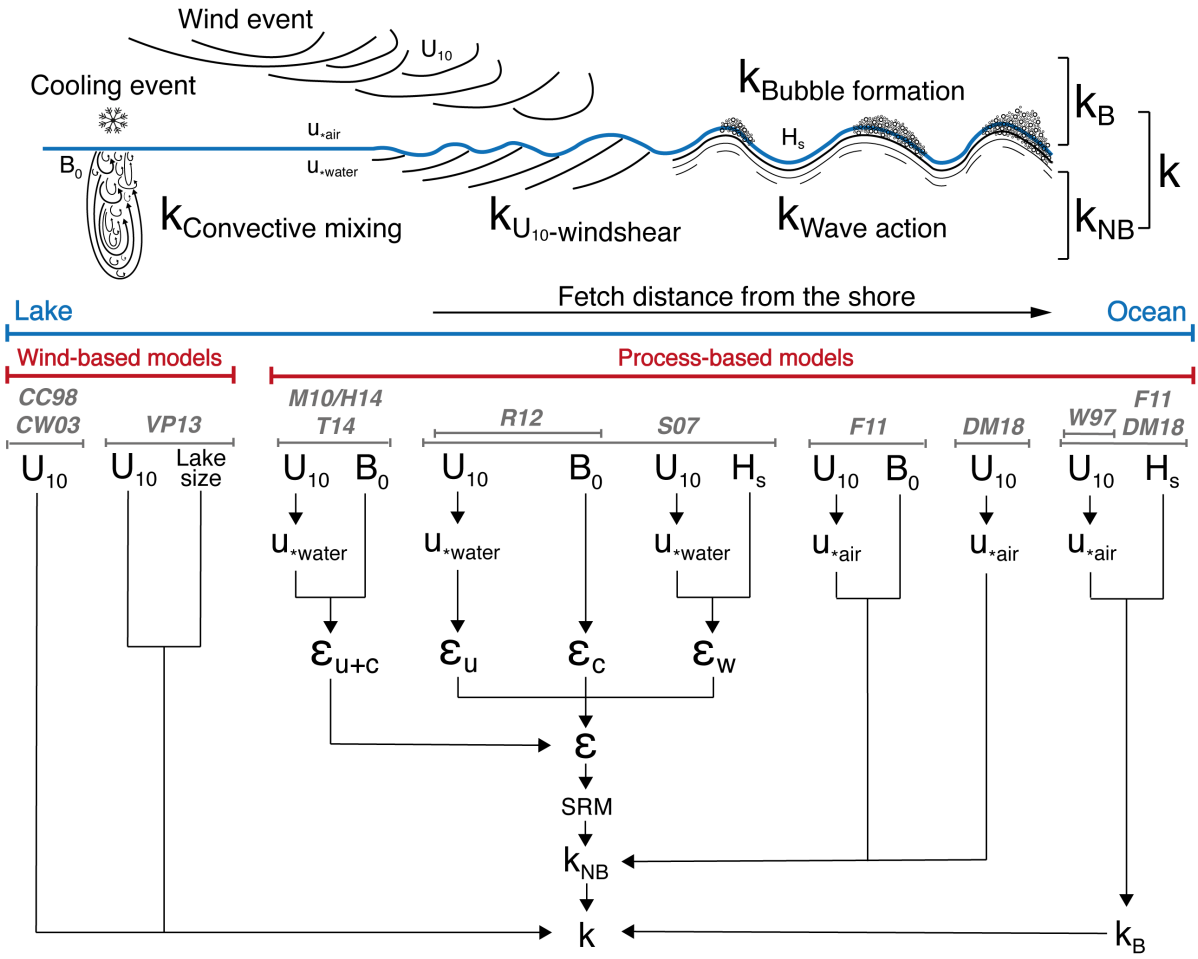

Fig. 2-1: Conceptual scheme of the four main processes driving gas transfer velocity (k) in a large lake induced by wind and cooling events. These four processes are split into two types of k: k-bubble for the bubble formation ($k_B = k_b$) and k-no bubble for the convective mixing, wind shear, and wave action term which are added ($k_{NB} = k_c + k_u + k_w$)**.** Below this scheme, a non-exhaustive review of the conceptual approaches of k models used in first Fickian law is given. From left to right, the increase in the complexity level of k models and their study site (limnological to oceanic case) is visible. All of these variables are described in Sect. 2.3.4. and Table 2-1.

In parallel to empirical wind-based models, process-based models attempt to link k directly to near-surface turbulence. The surface renewal model (SRM) is one of the first, and still most widely used, theories (Danckwerts 1951; Lamont and Scott, 1970) with k depending on the product of the turbulent kinetic energy dissipation rate (ε) and the kinematic viscosity of water (υ), both to a power of one-quarter as follows:

$$k = a_1(\varepsilon\upsilon)^{1/4}Sc^{-1/2}\,, \qquad (2\text{-}2)$$

where a_1 is a calibration constant parameter, and Sc is the Schmidt number. Recently, Lorke and Peeters (2006) and Katul and Liu (2017) demonstrated that this relationship, to which different approaches converge, can be seen

as a universal scaling. As opposed to the practical empirical models presented above, process-based models have the potential to predict *k* using the turbulent dissipation rate over a wide range of environmental conditions extending beyond those encountered in the calibration dataset (Zappa et al., 2007). As for lakes, SRM *k* models have so far considered the friction velocity at the water side ($u_{*,wat}$) and the turbulence created by thermal convection using the buoyancy flux at the surface (B_0) (Fig. 1; Eugster et al., 2003; MacIntyre et al., 2010; Read et al., 2012; Tedford et al., 2014; Heiskanen et al., 2014). It is noteworthy that the SRM approach leads to *k* being related to $u_{*,wat}$ (or U_{10}) to the first order (Wanninkhof, 1992; Lorke and Peeters 2006; see Sect. 2.3.), whereas the empirical models described above predict a higher-order polynomial relationship. This inconsistency is tentatively solved in oceanography by adding another source of gas exchange associated with wind-waves' whitecaps. Early gas flux parameterisation already accounted for wind and buoyancy-driven turbulence as well as surface waves (Fig. 1; Woolf et al., 1997; Soloviev et al., 2007; Fairall et al., 2011). However, the buoyancy-driven contribution can often be neglected in oceanography, and recent efforts have been dedicated to a better parameterisation of the bubble enhancement term (Fig. 1; Deike and Melville, 2018). In lakes, wind fetch can be long enough to generate surface waves (Wanninkhof, 1992; Frost and Upstill-Goddard, 2002; Borges et al., 2004; Guérin et al., 2007), implying that surface waves could be a significant driver of *k* and subsequent CO_2 fluxes (Schilder et al., 2013; Vachon and Prairie, 2013). Thus, the role of surface waves has been essentially empirically accounted for in lake *k* models, through the polynomial scaling to U_{10} in wind-based models, and most often neglected in studies using process-based parameterisations (mainly SRM) (e.g. Read et al., 2012). While this approximation may be appropriate for small-shielded lakes, it is likely to be insufficient in larger, long-fetched lakes.

Herein, we aim to identify the most adequate *k* model for Lake Geneva, a large, clear, hard-water lake in the Swiss Alps, to assess *k* values over a full annual cycle. We compare the performances of different models of gas transfer velocity, in their original or slightly modified published formulations from the limnological and oceanic literature. This set of models includes different levels of complexity, ranging from empirical models integrating wind speed and lake size to process-based models including wind shear, convection, and surface waves. Continuous ΔpCO_2 measurements by in situ automated sensors and CO_2 fluxes, obtained from a new generation of automated (forced diffusion) flux chamber, were collected during specific periods of intensive field survey covering a wide range of natural conditions. Empirical *k* values computed from chamber data are then compared to outputs from the different *k* models. Owing to the size of Lake Geneva, we anticipate that models accounting, implicitly or explicitly, for the four key exchange drivers (i.e., wind shear, convective mixing, wave action and bubble formation) will show the highest accuracy and precision in their estimation of *k* and that a precise integration of surface wave effects in such a large system should enhance model predictions. Thereafter, the relative distribution of these components is computed over a full year and analysed in the scope of the temporal variability of the gas transfer velocity. Finally, we expect that extreme wind and associated wave events should contribute disproportionately to accumulated *k* values over the year. In such a case, episodic weather events could generate large CO_2 fluxes over very short timescales that should be accounted for when computing annual CO_2 emission budgets.

2.3. Material and methods

2.3.1. Study site

Lake Geneva is a peri-Alpine Lake defining part of the Swiss–French border, at 372 m a.s.l. (metres above sea level) (46° 26' N, 6° 33' E). Its surface area (582 km^2) and its maximum depth (309 m) make it the largest freshwater body in western Europe, with a volume of 89 km^3 (Fig. 2-2). Lake Geneva is monomictic. The two prevailing winds are almost diametrically opposed and come from the southwest and northeast respectively (Fig. 2-2). The lake water has been surveyed monthly or fortnightly since the late 1950s (OLA-IS, AnaEE-France, INRAE of Thonon-les-Bains, and CIPEL; Rimet et al., 2020). The surface CO_2 concentrations, as computed from the routine temperature, alkalinity, and pH measurements (Stumm and Morgan, 1981), show a typical seasonal cycle with high, supersaturated values during winter mixing and values below saturation in summer (Perga et al., 2016).

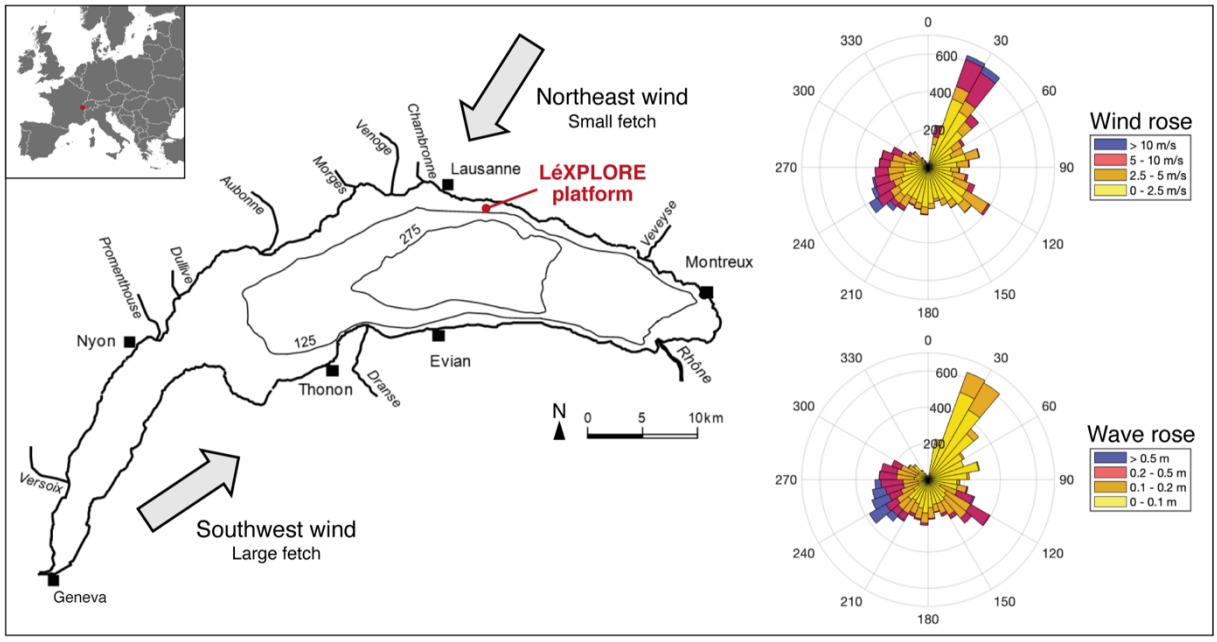

Fig. 2-2: Location and map of Lake Geneva with the two prevailing winds **(left)** also depicted by the wind rose **(top right)**. The wave rose highlights the highest wave field generated at the sampling location by the southwest wind with a larger fetch **(bottom right)**. Both the wind and wave roses are computed with annual data from 13th June 2019 to 12th June 2020 at LéXPLORE.

2.3.2. Field data at LéXPLORE

All field data were collected from the LéXPLORE platform, a 10 m by 10 m pontoon equipped with high-tech instrumentation and installed on Lake Geneva in 2019 (Wüest et al., 2021). LéXPLORE is moored at a 110 m depth, 570 m off the northern lake shore (Fig. 2-2).

On LéXPLORE, local weather conditions (air temperature, wind speed and direction, relative humidity, short-wave radiation, and atmospheric pressure) were continuously recorded (at 10 minutes intervals) by a Campbell Scientific automatic weather station. Lake surface temperature was measured every minute at 50 cm depth using a Minilog II-T (VEMCO, resolution 0.01° C). The partial pressure of water surface CO_2 (pCO_2) was also measured at 50 cm depth during specific surveys (see Sect 2.3.3.) using a mini CO_2 sensor (Pro-Oceanus Systems Inc.) with an accuracy of ± 30 ppm. Values of pCO_2 in parts per million (ppm) were converted into micro-atmospheres (µatm) following the basic equation correcting for altitude (Russell and Denn, 1972). Therefore, we assume that the concentration and the temperature are homogeneous over the first 50 centimetres.

Fetch distance (m) from LéXPLORE to the lake shores considering wind direction was computed using data from the Federal Office of Topography online portal (Swisstopo geoportal: geo.admin.ch). The position of LéXPLORE is particularly relevant for this study as the fetch ranges from ~0.5 km to ~30 km for the two prevailing winds. Significant wave height, H_s (in m), was computed after Hasselmann et al. (1973) according to the following equation:

$$H_s = 1.6 \cdot 10^{-3} \cdot U_{10} \cdot (Fetch/g)^{1/2} , \qquad (2\text{-}3)$$

where g is the gravitational constant. This variable H_s is defined as the average height of the highest one-third of the waves (crest to trough) corresponding to the thickness over which the wind can push laterally (Wüest and Lorke, 2003). This equation is equivalent to the formulation by Carter (1982) that is more widely used in the oceanic literature. Simon (1997) tested the model for significant wave heights in Lake Neuchâtel (a lake close to Lake Geneva) with a fetch distance of 9 km. These results showed that the significant wave height in this lake was consistent with this oceanic formulation. However, Simon (1997) highlighted that the Joint North Sea Wave Project (JONSWAP) wave breaking parametrisation did not hold for winds greater than 5 m s^{-1}, producing faster wave breaking and with a higher probability in the case of surface waves that were not fully developed. Such lake waves are characterised by steeper slopes that favour their wave breaking and wave action (Wüest and Lorke, 2003).

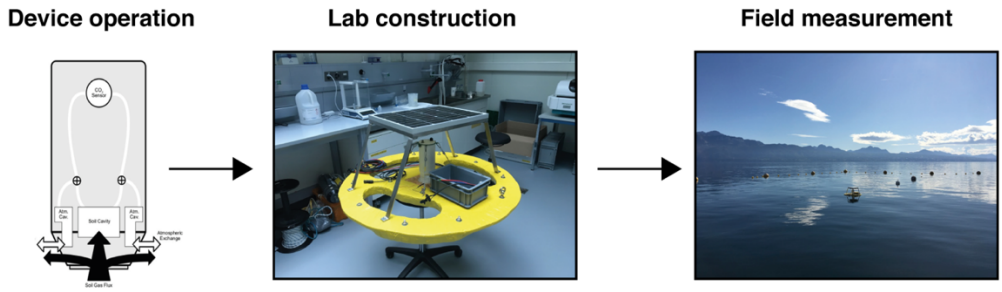

Fig. 2-3: Schematics of eosFD operation (https://eosense.com), its mini-platform construction, and its positioning for measurements in the field (Lake Geneva at LéXPLORE platform). The raft design also complies with recommendations to minimise artificial turbulence induced by the chamber's walls, with 10 cm long-edges entering the water (Vachon et al., 2010).

The net CO_2 flux at the lake–atmosphere interface, F, was directly measured with an automated (forced diffusion) floating CO_2 flux chamber (eosFD, Eosense: environmental gas monitoring; Fig. A1; Risk et al., 2011),

which was originally developed for soil flux studies. The flux chamber had a detection limit close to 0.05 µmol cm^{-2} h^{-1} and measured *F* every 15-minutes in summer and 30-minutes in winter for battery-saving purposes. The standard floating chambers require quiet surface conditions (e.g. Cole et al., 2010; Vachon et al., 2010; Bastviken et al., 2015), thereby limiting studies to low to moderate wind speed conditions. One typical problem with floating chambers arises from the possible atmospheric leakage under rough surface conditions (Fig. 2-4 (a)). To work around this problem, Vachon et al. (2010) recommend the creation of 10 cm long-edges entering the water (Fig. 2-4 (b)) and this design also reduces artificial turbulence generated by the chamber's walls at surface. A second typical issue with this method is potential flux enhancement by artificial (chamber-generated) turbulence. This was also studied by Vachon et al. (2010), who demonstrated that the overestimations due to this effect can be as high as 1000 % at low wind but less than 50 % when the wind speed exceeds 4 m s^{-1} in large lakes. At even higher wind speed, this overestimation should decrease further because the surface water turbulence becomes much greater than that produced by the floating chamber. Thus, our flux chamber was specifically conceived to increase stability under calm and windy conditions and to limit artificial turbulence, but we do not exclude a bias under low and moderate wind conditions (Fig. 2-3, Fig. 2-4 (c)).

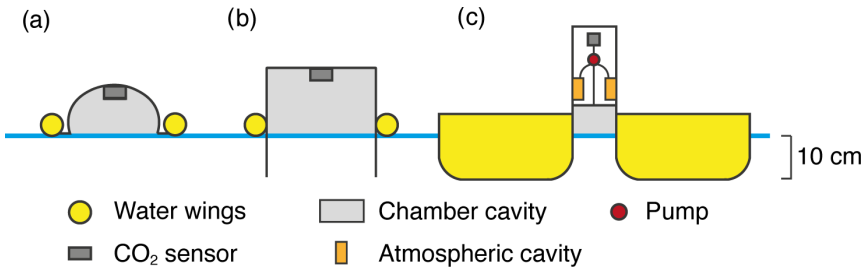

Fig. 2-4: (a) Classical floating chamber; **(b)** floating chamber with 10 cm long-edges; **(c)** platform design used in this study: 10 cm long-edges, rounded-edges, and flat and long water wings.

Regarding the operation of the eosFD, it has two independent cavities: one for the chamber and one for the atmosphere (Fig. 2-3). These are connected to the same CO_2 sensor by a pump which sends either the chamber gas or the air gas to the sensor at regular intervals (about 20 s) and then completely flushes the chamber cavity according to the programmed measurement time step (15-minutes or 30-minutes). Therefore, the advantage of this new instrument is to have a constant monitoring of the chamber's variation but also of the atmosphere. In addition, the use of the same CO_2 sensor for the two measurements limits the need for intercalibration between CO_2 sensors. We tested the performance of the floating chamber by comparing the standard deviation of the CO_2 concentrations of the atmosphere and in the chamber estimated from two separated cavities (Fig. 2-3; Risk et al., 2011). We did not observe any difference in the standard deviation between high and low wind conditions (Fig S2-1), suggesting that the measured fluxes remained reliable at high wind speed without leakage of the chamber.

We assessed the performances of our flux chamber during five specific periods over the annual cycle: 13th–14th June 2019, 27th–28th August 2019, 1st–5th October 2019, 18th–20th December 2019, and 20th–26th February 2020. To select the most robust dataset for comparison with *k* estimates derived from models, we discarded flux data that were below the detection limit as well as CO_2 gradients that ranged within the uncertainty of sensors (i.e. ± 20 ppm for air and ± 30 ppm for water, leading to ± 50 ppm) (Fig. 2-5). Accordingly, we were able to retain the

most robust data points during the following deployment periods: 18th–20th December 2019 and 20th–26th February 2020. Finally, all these field data were standardised at a 1 h time step.

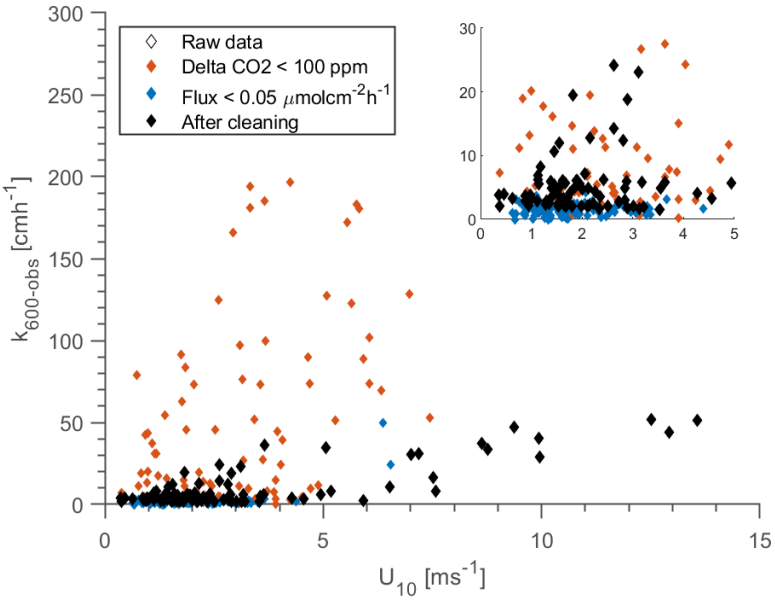

Fig. 2-5: Visualisation of 304 observed k_{600} values during the five periods of flux measurements: 13th–14th June 2019, 27th–28th August 2019, 1st–5th October 2019, 18th–20th December 2019, and 20th–26th February 2020.

2.3.3. Computed *k* values from field data

k values (cm h^{-1}) from field observations (k_{obs}) were computed from the gas transfer velocity equation:

$$k_{obs} = F/(\alpha \cdot \Delta pCO_2), \quad (2\text{-}4)$$

where F is the measured CO_2 flux (µmol cm^{-2} h^{-1}); α is the gas solubility coefficient (µmol cm^{-3} µatm^{-1}), which depends on the measured water temperature (Wanninkhof, 1992); and ΔpCO_2 is the differential of pCO_2 measured at 0.5 m below the surface ($pCO_{2\text{-water}}$) and pCO_2 at saturation ($pCO_{2\text{-sat}}$; in ppm) measured from the flux chamber corrected by altitude (µatm). It is noteworthy that the chemical enhancement factor (Wanninkhof and Knox, 1996) was not considered in this equation, as the fluxes retained corresponded to conditions of moderate pH (i.e. < 8). k_{obs} was then standardised in k_{600} using the dimensionless Schmidt number (Sc) of CO_2: $k_{600-obs} = k_{obs} \cdot (600/Sc)^{-1/2}$ (600 for freshwater standardised at 20° C).

2.3.4. Models for air–water gas transfer velocity

After years of debate, a consensus has begun to emerge on the relationship linking k, intensity of turbulence, and Sc (Eq. 2-2), even when starting from different physical assumptions (see Katul et al., 2018). In this study, we selected six parameterisations widely used in limnology and oceanography, combining specific calibration characteristics (Table 2-1). We first show that they can all be expressed following Eq. (2-2) for wind shear and convection, despite their different formulations. We then develop the effects of surface waves from oceanic models and adapt the wave action for a large lake. The final lake model integrating the wave effect is ultimately calibrated using our field data (Table 2-1).

Table 2-1: Summary of the characteristics of k_{Sc} models for predicting the air-water gas transfer velocity based on wind speed (*CC98 and CW03*) and lake size (*VP13*), surface renewal model (*T14, R12*, and *S07*), COARSE approach (*DM18*), and both adapted models, namely *SD21* and *SD21-fit*, from a combination of *S07* and *DM18*.

Model	Equation	Method	Site	Calibrated range
CC98	$k_{600} = 2.07 + 0.215 \cdot U_{10}^{1.7}$ $k_{Sc} = k_{600}\left(\frac{Sc}{600}\right)^{-1/2}$	Mass balance by gas tracer	Lake	Area (0.15-490 km^2) U_{10} (< 10 ms^{-1})
CW03	$k_{600} = 0.168 + 0.228 \cdot U_{10}^{2.2}$ $k_{Sc} = k_{600}\left(\frac{Sc}{600}\right)^{-1/2}$	Mass balance by gas tracer	Lake	Area (0.128 km^2) U_{10} (< 6 ms^{-1})
VP13	$k_{600} = 2.51 + (1.48 \cdot U_{10}) + (0.39 \cdot U_{10} \cdot log10(Lake\ size)$ $k_{Sc} = k_{600}\left(\frac{Sc}{600}\right)^{-1/2}$	Floating chamber	Lake	Area (0.2–602 km^2) U_{10} (< 6 ms^{-1})
T14	$k_{Sc} = a_1 \cdot (\varepsilon \cdot \upsilon)^{1/4} \cdot Sc^{-1/2}$ $\varepsilon = \varepsilon_{Wind\ shear\ +\ Convection}$	Microstructure profiling	Lake	Area (4 km^2) U_{10} (< 10 ms^{-1})
R12	$k_{Sc} = a_1 \cdot (\varepsilon \cdot \upsilon)^{1/4} \cdot Sc^{-1/2}$ $\varepsilon = \varepsilon_{Wind\ shear} + \varepsilon_{Convection}$	-	-	Following *S07*
S07	$k_{Sc} = k_{Sc-NB-S07} + k_{Sc-B-W97}$ $k_{Sc-NB} = a_1 \cdot (\varepsilon \cdot \upsilon)^{1/4} \cdot Sc^{-1/2}$ $\varepsilon = \varepsilon_{Wind\ shear} + \varepsilon_{Convection} + \varepsilon_{Wave\ action}$	Eddy covariance	Ocean	Area (>100'000 km^2) U_{10} (< 20 ms^{-1}) Wave (0–10 m)
DM18	$k_{Sc} = (k_{NB} + k_B) \cdot (Sc/600)^{-1/2}$ $k_{NB} = A_{NB} \cdot u_{*,atm}$ $k_B = (A_B / O_s) \cdot u_{*,atm}^{5/3} \cdot (g \cdot H_s)^{2/3}$	Eddy covariance	Ocean	Area (>100'000 km^2) U_{10} (< 30 ms^{-1}) Wave (1–10 m)
SD21	$k_{Sc} = k_{Sc-NB-S07*} + k_{Sc-B-DM18}$ *Adaptation of $\varepsilon_{Wave\ action}$ for large lake	Floating chamber	Lake	Area (582 km^2) U_{10} (< 16 ms^{-1}) Wave (0–1.2 m)
SD21-fit	$k_{Sc} = k_{Sc-NB-S07*} + k_{Sc-B-DM18}$ with a_1 from $k_{Sc-NB-S07*}$ and A_B from $k_{Sc-B-DM18}$ fitted to observations	-	-	-

CC98 Cole and Caraco (1998), *CW03* Crusius and Wanninkhof (2003), *VP13* Vachon and Prairie (2013), *T14* Tedford et al. (2014), *R12* Read et al. (2012), *S07* Soloviev et al. (2007), *DM18* Deike and Melville (2018).

Wind shear stress

We start with the case where near-surface dynamics are driven by a weak to moderate wind, in the absence of heat exchange. In this case, the contribution of surface waves can be neglected and the wind stress ($\tau_0 = \rho_{air} \cdot C_{10} \cdot {U_{10}}^2$, where ρ_{air} is air density and C_{10} is the drag coefficient at 10 m) is equal to the tangential shear stress

($\tau_t = \rho_{wat} \cdot {u_{*,wat}}^2$, where ρ_{wat} is water density). The relationship between ε and the sheared velocity on the water side, $u_{*,wat}$, is then derived from a law-of-the-wall scaling for the velocity profile: $\varepsilon = u_{*,wat}^3/(\kappa\, z(0))$, where κ is the von Kármán constant (= 0.41), and $z(0)$ is the thickness of the diffusive boundary layer. This relationship leads to

$$k_{NB} = a_1 \cdot \left(\nu\, u_{*,wat}^3/(\kappa z(0))\right)^{1/4} Sc^{-1/2}\,. \tag{2-5}$$

The challenge is then to define $z(0)$. Tedford et al. (2014) followed an ad hoc observational approach and chose $z(0)$= 0.15 m as the shallower depth where ε was measured. In contrast, theoretical studies have linked $z(0)$ to the thickness of the diffusive or viscous sublayer (~0.1–1 cm). In line with theory, we scale this layer as $z(0) = c\nu/u_{*,wat}$ (Wüest and Lorke, 2003; Lorke and Peeters, 2006) with *c* as a constant value. Taking *c* = 114 (Soloviev et al., 2007), the thickness of this layer typically ranges from 0.04 to 0.14 m under a wind regime of 10 to 1 m s^{-1}. Therefore, we modify Eq. (2-5) to compute the interfacial (no bubble, NB) exchange coefficient:

$$k_{NB} = a_1 u_{*,wat}(1/\kappa c)^{1/4} Sc^{-1/2}, \tag{2-6a}$$

or

$$k_{NB} = a_1(\rho_{air}/\rho_{wat}) C_{10} U_{10} (1/\kappa c)^{1/4} Sc^{-1/2}\,. \tag{2-6b}$$

These equations show that the SRM formulation (Table 2-1 and Fig. S2-2; Soloviev et al., 2007; Read et al., 2012) is analogous to the Coupled Ocean – Atmosphere Response Experiment Gas transfer algorithm (COAREG) flux algorithm (Fairall et al., 2011) and to the formulation used in Deike and Melville (2018) with the sheared velocity on the atmosphere side, $u_{*,atm}$ (Table 2-1: *DM18*). Indeed, when equating the expression by Deike and Melville (2018),

$$k_{NB} = A_{NB} u_{*,atm} (Sc/600)^{-1/2} = A_{NB} u_{*,wat} (\rho_{wat}/\rho_{atm})^{1/2} (Sc/600)^{-1/2}\,. \tag{7}$$

With Eq. (2-6a), we find that the coefficient a_1 = 0.29 in Soloviev et al. (2007) and Read et al. (2012) is essentially equivalent to the coefficient $A_{NB} = a_1(\kappa c)^{-1/4}(1/600)^{1/2}(\rho_{wat}/\rho_{air})^{-1/2} \approx 1.5 \times 10^{-4}$ in Deike and Melville (2018) (Fig. S2-2), which, in turn, was found to be equal to the coefficient of *A* = 1.5 in Fairall et al. (2011). These results agree with Lorke and Peeters (2006), who derived a unified relation for interfacial fluxes (air–water and water–sediment) through a linear relationship of $u_{*,wat}$ with *k*, especially at the bottom interface where shear is the only relevant process. Furthermore, Equation 2-6 has a similar (i.e. quasi-linear) *k*–wind relationship to the data-driven parameterisation from *VP13* but cannot explain the higher-order polynomial relationship reported in *CW03* and *CC98*.

Convection

A second source of dissipation at the surface is the convection (ε_c) resulting from surface cooling. In the SRM formulation, only the negative buoyancy flux is considered when this term directly enters into the turbulent kinetic equation as a production term. The combination of wind shear and free convection near a boundary is described by the Monin–Obukhov similarity theory (MOST) with a general form derived from a turbulent kinetic energy balance (Lombardo and Gregg, 1989; Tedford et al. 2014):

$$\varepsilon(z) = \varepsilon_u(z)\left(c_u + c_c\lfloor\frac{z}{L_{MO}}\rfloor\right), \tag{2-8}$$

where L_{MO} is the Monin–Obukhov length scale defined as $L_{MO} = u_{*,wat}^3/\kappa B_0$, including $\varepsilon(z) = c_u \cdot \varepsilon_u + c_c \cdot \varepsilon_c$ in Eq. (2-2). The latter expression can be rearranged as follows:

$$k_{NB} = a_1\left(\varepsilon_u(c_u + c_c \cdot B_0/\varepsilon_u)^{1/4}\right)Sc^{-1/2}\,, \tag{2-9}$$

where a_1 ranges in the literature from 0.2 to 1.2 (Soloviev et al., 2007; MacIntyre et al., 2010; Tedford et al., 2014; Heiskanen et al. 2014; Winslow et al., 2016), c_u ranges from 0.84 to 1 (Winslow et al., 2016) and c_c ranges from 0.37 to 2.5 (Wyngaard and Coté, 1971; Tedford et al., 2014). Hereafter, we use the following set of values: c_u = 1 and c_c = 1. Fairall et al. (2011) used an essentially equivalent approach but formulated in terms of a Richardson number to describe the partitioning between dissipation from convection and wind shear, expressing the wind shear in terms of the air-side friction velocity: $R_f = B_0\upsilon/u_{*,atm}^4$, which can be integrated into (2-9) as

$$k_{NB} = a_1\left(\frac{\rho_{atm}}{\rho_{wat}}\right)^{1/2} u_{*,atm}\left(\frac{c_u}{\kappa c}\left(1 + \frac{R_f}{R_{f,c}}\right)\right)^{1/4}\left(\frac{Sc}{600}\right)^{-1/2}\,, \tag{2-10}$$

where $R_{f,c} = \frac{c_u\rho_{atm}^2}{c_c\rho_{wat}^2\kappa c}$. The details of this demonstration can be seen in Soloviev and Schlüssel (1994).

Wave action

The effect of surface waves is commonly implemented in oceanography but barely considered in limnology. All process-based models rely on the same parameterisation of energy dissipation by wind shear and convection. However, they differ in how they parameterise energy dissipation by wave action and wave breaking.

The contribution of the wave action (ε_w) is, accordingly, added as a third source of turbulence (Fig. 2-1). In the presence of surface waves, the balance between τ_t and τ_0 no longer holds. Therefore, Soloviev and Schlüssel (1994) added a corrective factor, φ, using the Keulegan number ($Ke = u_{*,wat}^3/(g\nu)$), in order to decrease the component $\tau_t = \tau_0 \cdot \varphi$ (where $\varphi = 1/(1 + Ke/Ke_c)$), with the critical Keulegan number (Ke_c) defined in Soloviev and Lukas (2006). As a result, the equation for shear-driven dissipation $\varepsilon_u(z)$ is as follows:

$$\varepsilon_u(z) = \frac{u_{*,wat}^4}{\kappa c\upsilon} \cdot \varphi^2\,. \tag{2-11}$$

Following this step, the turbulent kinetic energy dissipation rate from wave action (ε_w) is added and defined with the Keulegan number by Soloviev et al. (2007) as follows:

$$\varepsilon_w = \alpha_W\left(\frac{3}{BS_q}\right)^{1/2}\frac{(Ke/Ke_c)^{3/2}}{(1+Ke/Ke_c)^{3/2}}\frac{u_{*,wat}g}{0.062\kappa C_T(2\pi A_w)^{3/2}}\frac{\rho_{atm}}{\rho_{wat}}\,, \tag{2-12}$$

where $C_T = (z_0/H_s)$. z_0 is the surface roughness scale from the water side and the C_T value is set as a constant at 0.6 (more details are given in Soloviev et al., 2007). This definition does not hold for closed basins because, in the case of incompletely developed waves, the dissipation of energy from wind shear transmitted to the waves is not fully redistributed in the water body (Simon, 1997). Hence, for the application in Lake Geneva, we followed Terray et al. (1996), who defined a varying C_T:

$$C_T = 1.38 \cdot 10^{-4}\left(\frac{U_{10}}{C_p}\right)^{2.66}\,, \tag{2-13}$$

where C_p is the peak speed of the wave spectrum defined in Deike and Melville (2018) according to Toba (1972, 1978). This leads to $C_T << 1$. This allows one to increase the effect of ε_w (inversely proportional to C_T in Eq. 2-12) on *k.* Here, we used this formulation to adapt the *S07* ocean model for a large lake (closed basin). Henceforth we refer to the adapted uncalibrated and calibrated models as *SD21* and *SD21-fit* respectively (Table 2-1). Finally, these three terms of ε (ε_u, ε_c, and ε_w) can be added before computing the SRM (Eq. 2) for determining *k*-no bubble (k_{NB}).

Bubble enhancement

Additional deviations from the linear relationship to U_{10} are explained by the gas transfer resulting from bubbles and sprays during wave breaking. This mechanism is accounted for by adding a *k*-bubble (k_B) term to the previously mentioned k_{NB}. Soloviev et al. (2007) used the empirical *k*-bubble parameterisation from Woolf et al. (1997):

$$k_B = W \frac{2450}{O_s\left(1+\frac{1}{(14 O_s Sc^{-0.5})^{1/1.2}}\right)^{1.2}}, \tag{2-14}$$

where W is the fractional whitecap coverage only expressed as a function of wind ($3.84 \cdot 10^{-6} \cdot U_{10}^{3.41}$), and O_s is the Ostwald gas solubility. This formulation does not take wave height into account (Fig. S2-2). Nevertheless, a recent study (Deike and Melville, 2018) performed a new numerical process-based parameterisation for gas transfer velocity from bubble enhancement considering H_s through the following equation:

$$k_B = \frac{A_B}{O_s} u_{*,atm}^{5/3} (g H_s)^{2/3} \left(\frac{Sc}{600}\right)^{-1/2}, \tag{2-15}$$

where A_B is an empirical factor with dimension (= 10^{-5} m^{-2} s^2), and O_s is defined by the ideal gas constant (R), the surface water temperature (T_0), and the CO_2 solubility coefficient in freshwater (α) (Reichl and Deike, 2020). The gas transfer velocity is the expressed as a sum of the no-bubble k_{NB} and bubble k_B components (Table 1: *S07*, *DM18*, *SD21, and SD21-fit*) following Keeling (1993) and Woolf et al. (1997, 2005). Our adapted model for lake includes a refined parametrisation of the wave action term ε_w from *S07* along with the bubble term from *DM18*. For these reasons, the model will be called *SD21* in the rest of the paper. In addition, for the appellation *SD21-fit*, the a_1 parameter of Eq. (2-2) and the A_B parameter of Eq. (2-15) were fitted to the k_{600} observations (a_1 = 0.33 and A_B = 3 10^{-5} m^{-2} s^2).

With this review of existing and adapting parameterisations, we show that (i) there is a discrepancy between an SRM-based model with shear stress as the only energy source and empirical parameterisations with a polynomial (order > 1) wind-based relationship. Such a discrepancy is tentatively resolved by adding the effect of convection and surface waves. (ii) We further highlight that most fitting parameters from the different SRM-based models are in good agreement. (iii) We finally recall that it is possible to provide a unifying parameterisation of *k* with an SRM model including wind shear, wind-induced waves, and convection with only a few input parameters such as U_{10}, B_0, and Fetch.

2.4. Results

2.4.1. Observed and predicted *k*

After quality check, our dataset contains 94 discrete CO_2 flux observations. We first assess the representativeness of our sampling by comparing the survey-specific and annual distributions of the three main inputs for *k* models: U_{10} (all models), B_0 during convective periods (*T14*, *S07*, *SD21,* and *SD21-fit*), and H_s (*S07*, *DM18*, *SD21,* and *SD21-fit*) (Fig. 2-6; the temporal evolution of these three terms is shown in Fig. S2-3). From 13th June 2019 to 12th June 2020, the average wind speed over Lake Geneva is 2.9 m s^{-1} with a mode at 2.5 m s^{-1}; very low wind speeds (< 1 m s^{-1}) are encountered 12 % of the year, whereas high (> 5 m s^{-1}) to very high (> 10 m s^{-1}) wind events represent 15 % and 2 % of the year respectively. The sampling surveys covered the full annual range of U_{10}. Average and modal values of B_0 over the year are close to 0.25 10^{-7} m^2 s^{-3}. However, the sampling covered only the lowest 50 % of the annual distribution and undersampled conditions of potentially strong convection. Considering that the dissipation by buoyancy flux, as parameterised in the process-based models, is already well known in the literature and that it is not the central point of our study, we posit that the undersampling of B_0 is not expected to significantly affect our analysis. The predicted modal H_s value is 0.15 m over the year. Events of high H_s (> 0.4 m) represent 6 % of the year, with a maximum H_s of 1.1 m. As for U_{10}, the surveys covered the full range of annual H_s.

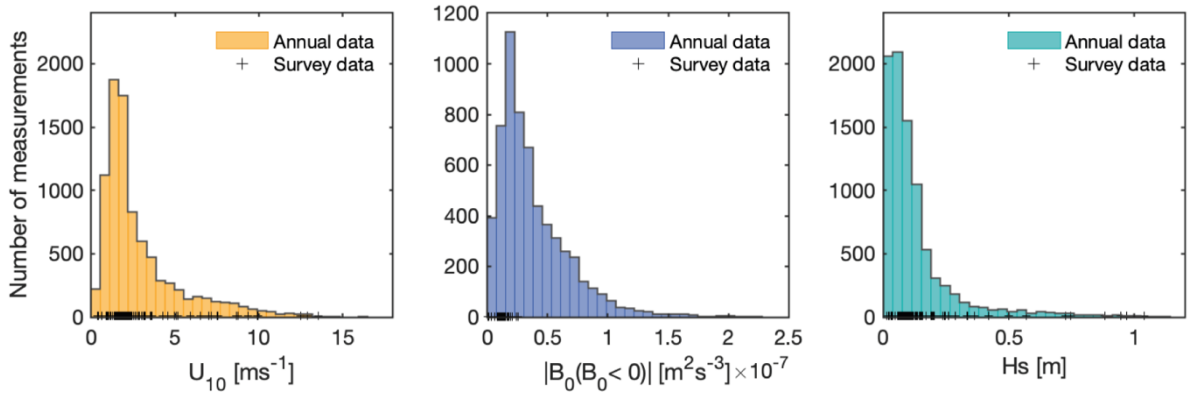

Fig. 2-6: The annual distribution of the three main components used to compute k_{600} models: wind speed at 10 m (orange); buoyancy flux at the surface during cooling (blue); significant wave height (turquoise). These survey data observed during CO_2 flux measurements after quality control (+) are also shown.

k_{600} values based on observations are shown in Fig. 2-7 (a) with their error bars corresponding to the uncertainties of the pCO_2 in air and in water (± 50 ppm). We notice that all of the measurements with a wave height > 0.4 m were observed for wind speeds > 5 m s^{-1}, and the corresponding k_{600} values are located above the linear function (i.e. from a linear regression against wind shear velocity; Fig. S2-2) scaling k_{600} to u_* (i.e. first-order relationship). We then compare the k_{600} observed during the specific surveys to the values computed with all k_{600} models throughout the annual cycle, in relation to U_{10} (Fig. 2-7 (b, c)). Table 2-2 provides the root-mean-square errors (RMSEs) for all model estimates compared to k_{obs} during the flux surveys, (i) for the full dataset (All Wind), and split (ii) for low wind (< 5 m s^{-1}, LW) and (iii) strong wind conditions (≥ 5 m s^{-1}, SW). The three empirical wind-based models only depend on wind (Fig. 2-7 (b)). Both *CC98* and *CW03* were originally calibrated

for small lakes, using a mass balance calibration method (Table 2-1). However, they lead to divergent gas transfer velocities, particularly above 5 m s^{-1}, illustrated by a RMSE for SW as high as 22.8 cm h^{-1} for *CC98*, whereas *CW03* performs better (RMSE SW = 12.8 cm h^{-1}). Furthermore, both models underestimate k_{600} at low wind (Fig. 2-7 (b)), with a higher deviation for *CW03* (Table 2-2). The *k* values predicted by *VP13* are closer to those of the process-based models that explicitly integrate wave actions (*S07* and *DM18*) (Fig. 2-7 (b, c)), demonstrating that lake size integration in the empirical model captures at least part of the wave action on *k*. Performances of *VP13* at strong winds (RMSE SW = 12.7 cm h^{-1}) were better than those of the ocean-derived models integrating surface waves (RMSE SW = 13–15.9 cm h^{-1}). However, *VP13* shows a positive offset during calm periods, along with the highest RMSE of the set of models at low wind speed (Fig. 2-7 (b); Table 2-2).

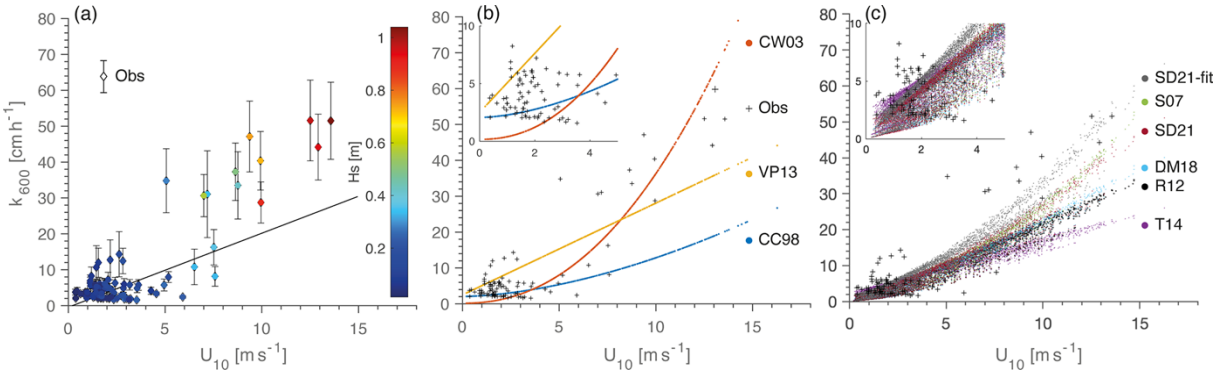

Fig. 2-7: (a) k_{600} observed as a function of U_{10} and coloured according to H_s (colour bar), showing the error bars produced by the uncertainty of ΔCO_2 ($\pm$ 50 ppm) as well as the $\boldsymbol{u}_*$–k_{600} linear regression (solid line; see also Fig. B1); **(b)** k_{600} wind-based models (*CC98*, *CW03,* and *VP13*); **(c)** k_{600} process-based models (*T14*, *S07*, *DM18*, *SD21*, and *SD21-fit*) computed with annual data. Observed k_{600} derived from CO_2 flux chamber measurements is shown using the "+" symbol.

The process-based models (Fig. 2-7 (c)) provide different k_{600} values for a given wind speed, owing to the integration of additional environmental components (i.e. the varying drag coefficient, the convective mixing in *R12* and *T14*, and the effect of waves in *S07*, *DM18*, *SD21*, and *SD21-fit)*. All process-based models are similar at low winds, as they share a common physical basis for parameterisation of wind shear and convection. Therefore, they lead to similar RMSEs (2.9–3.5 cm h^{-1}) under such conditions, where surface waves are negligible (Table 2-2). Divergences occur at higher wind speeds. *T14*, initially developed for small lakes with limited wind exposure, performed the worst (RMSE = 19.8 cm h^{-1}). This increased *k* underestimation at high winds can be attributed to (i) dissipation by wave action and bubble formation not being considered (in *R12* and *T14*) and (ii) to the use of a constant $z(0)$ = 0.15 m in the *T14* model (Eq. 2-5). This approximation of the diffusive layer is consistent with low wind speed but is almost 1 order of magnitude too large under strong wind speed. Other process-based models, designed for greater wind range (> 10 ms^{-1}), integrate surface waves and, as a result, lead to better estimates than *R12* and *T14* (RMSE = 10.4–15.9 cm h^{-1}). However, the ocean wave model of *DM18* shows lower performances at strong winds than *CW03* and *VP13* (Fig. 2-7 (b, c)). Finally, the specific fit parameterisation of the *SD21-fit* model improves the performance at high wind speeds by ~30 % (RMSE = 10.5 cm h^{-1}), outperforming all the other methods.

Table 2-2: RMSE of k_{600} models for all wind speed *(U_{10})*, $U_{10} < 5$ m s^{-1} (i.e. LW) and $U_{10} \geq 5$ m s^{-1} (i.e. SW).

RMSE	*CC98*	*CW03*	*VP13*	*T14*	*R12*	*S07*	*DM18*	*SD21*	*SD21-fit*
All U_{10}	9.8	6.5	6.7	8.6	7.5	6.2	7.3	6.2	5.2
$U_{10} < 5$ ms^{-1}	3.2	4.2	4.5	2.9	3.3	3.3	3.5	3.3	3.2
$U_{10} \geq 5$ ms^{-1}	22.8	12.8	12.7	19.8	16.6	13	15.9	13.1	10.5

2.4.2 Surface wave integration

Herein, we scrutinize how those varying parameterisations ultimately alter the shape of relationship between k_{600} and U_{10}. In *R12* (Fig. 2-8 (a)), wind is only included through wind shear, resulting in a linear relationship between k_{600} and U_{10}, as already anticipated. Adding the wave action (no bubble) through the *S07* parameterisation (Fig. 2-8 (b)) does not lead to any significant departure from the minimal *R12* model. Adapting wave action by decreasing C_T (for the no bubble term) leads to a departure from the wind shear linear relationship for $H_s > 0.4$ m (Fig. 2-8 (c)).

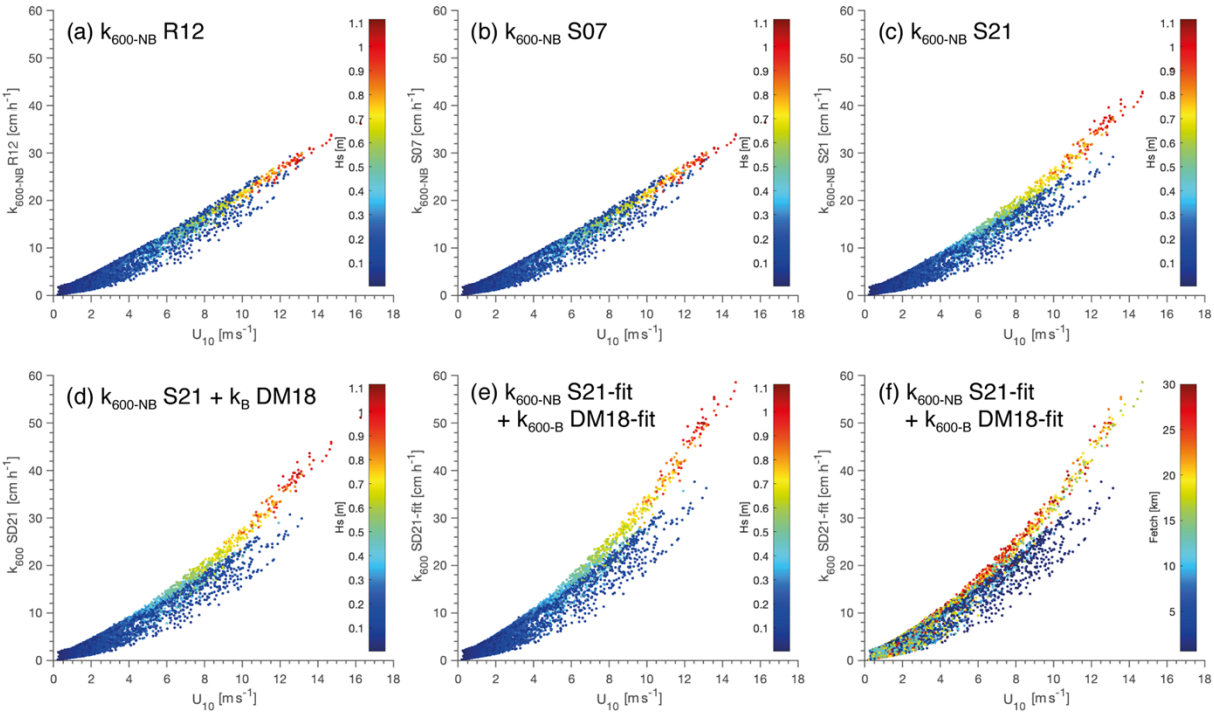

Fig. 2-8: The U_{10} vs k_{600} relationship modelled and coloured according to H_s (colour bar) in panels **(a)-(e)** as well as coloured according to fetch distance (colour bar) in panel **(f)**: **(a)** *R12* integrating wind shear and convection; **(b)** *S07* integrating wind shear, convection, and wave action for fully developed waves; **(c)** *S21* integrating wind shear, convection, and wave action for waves that are not fully developed; **(d)** *SD21* is similar to *S21* but the *k*-bubble term of *DM18* is added; **(e, f)** *SD21-fit* is similar to *SD21* but with a_1 and A_B fitted to observed *k*.

Adding the *k*-bubble term related to wave breaking of *DM18* further increases this deviation from the linear k_{600}-U_{10} relationship but also scatters k_{600} estimates for a given U_{10} (Fig. 2-8 (d)). Finally, the fitting with observationally based k_{600} improves the estimation for strong wind (Fig. 2-8 (e), Table 2-2). Given the range of

wind fetch from ~ 0.5 km to ~30 km, the contribution of waves varies for a given wind speed depending on the fetch, as evidenced by the scattering of the parameterised k_{600} for a given U_{10} (Fig. 2-8 (f)). A significant modification of k_{600} by wave action and wave breaking occurs for a fetch length > 15 km and U_{10} > 5 m s^{-1} (Fig. 2-8 (f)), in the case of Lake Geneva, generating wave of H_s > 0.4 m (Fig. 2-8 (e)).

Compared with k_{600} estimated by *R12* (Fig. 2-8 (a)), the *SD21* and *SD21-fit* models provide *k* estimates that are 20–50 % higher for U_{10} = 10 m s^{-1} respectively and 40–70 % higher for U_{10} = 15 m s^{-1} respectively. Therefore, adapting the surface waves, through the change in the wave action for incompletely developed waves and the fitting to observed data encountered in local lake conditions, leads to better performances of the *SD21* models. *SD21-fit* reached the lowest RMSE at all wind speeds and was thereafter used as a reference for the modelling of the annual gas transfer velocities.

2.4.3. Annual cumulative gas transfer velocity and the effect of extreme conditions

We show above that models accounting for surface waves better represent the non-linear increase in k_{600} at high winds. Because high-wind events remain rare, we test whether a better representation of k_{600} during rare, high-wind events affects the local estimates of k_{600} over a full year. To this end, cumulative sums of hourly k_{600} were computed over a full annual cycle (13th June 2019 – 12th June 2020) for all *k* models (Fig. 2-9). The annual dynamics, such as the annually averaged k_{600}, were compared using *SD21-fit* as a new reference model.

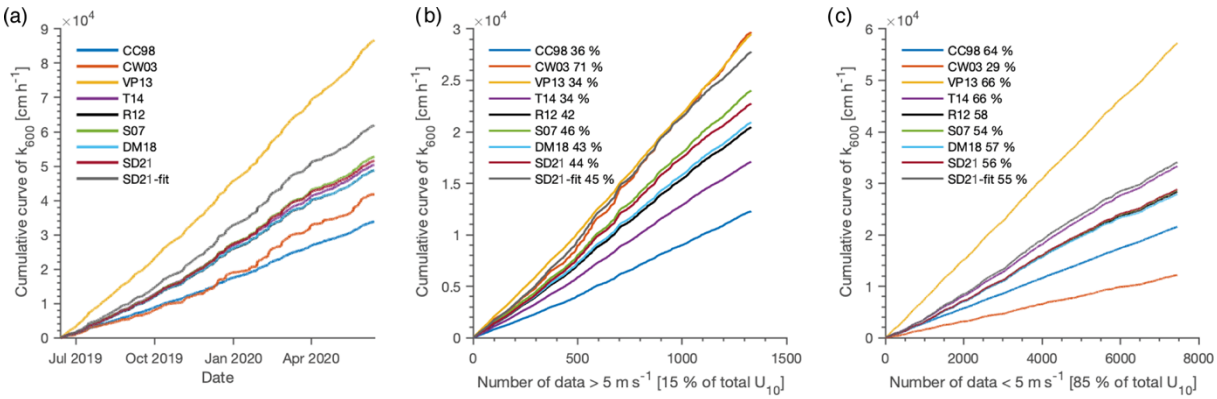

Fig. 2-9: (a) cumulative k_{600} modelled over an annual cycle; **(b)** cumulative k_{600} for wind > 5 m s^{-1}; **(c)** cumulative k_{600} for wind ≤ 5 m s^{-1}.

Cumulated k_{600} computed for *SD21-fit* shows some episodic steep increases between December and March, due to the winterly prevalence of high-wind events (the winter average wind speed, 3.25 m s^{-1}, was greater than the summer mean, 2.55 m s^{-1}, by 25 %) and greater significant wave height (the winter average wave height, 0.15 m, was greater than the summer value, 0.10 m, by 50 %) (Fig. S2-3). The average hourly k_{600} by the *SD21-fit* model is 7.3 ± 7.4 cm h^{-1} (mean ± SE, Fig. 2-9 (a)). Periods of high winds, although accounting for only 15 % of data points, contribute 44 % of annually cumulated k_{600} in the *SD21* and *SD21-fit* models (Fig. 2-9 (b)), whereas periods of high waves (H_s ≥ 0.4 m) accounting for only 6 % of data points, contribute to more than 20 % of annually cumulated k_{600}.The wind-based models are those for which cumulative k_{600} diverges the most from the

SD21-fit reference model, with the lowest annual averaged k_{600} for *CC98* and *CW03* (3.9 ± 2.7 and 4.8 ± 9.3 respectively) and the highest for *VP13* (9.9 ± 6.1). These divergences arise from the low performances of these models at low wind regimes (Fig. 2-7 (a), 2-9 (c); Table 2-2), which represent 85 % of data points. All of the other process-based models have relative dynamics of cumulative k_{600} similar to that of the *SD21-fit* model and end up with annually averaged k_{600} that are 15 % lower than for the *SD21-fit*. The representation of k_{600} at low wind speeds is similar for all process-based models, and the divergence arises from the representation of the rarer high-wind-speed episodes, which contribute to 43–46 % of annual cumulative k_{600} (Fig. 2-9 (b)).

2.5. Discussion

The history of *k* models, simulating the gas transfer velocity for surface waters, dates back from the early 1990s. *k* models have been developed and tested in small lakes sheltered from winds (e.g. Crusius and Wanninkhof, 2003; Tedford et al., 2014), large lakes under low to moderate wind speed (Vachon and Prairie, 2013), and oceans (e.g. Soloviev et al., 2007; Fairall et al., 2011; Esters et al., 2017; Deike and Melville, 2018). While the effects of surface waves on *k* can be neglected in small lakes, we question whether this assumption holds for large lakes such as Lake Geneva, in which surface waves are frequently observed (Fig. 2-2, S2-3). We evaluated the performance of different experimental-based and process-based models to estimate k_{600} in the large Lake Geneva. We show that integrating the effect of wave formation at high wind speeds and long fetch better represents the sharp increase in the k_{600} values during such episodic windy events.

2.5.1. Choice of *k* models

Wind-based models have long been known to misestimate k_{600} at low wind speeds (Eugster et al., 2003; MacIntyre et al., 2010; Erkkilä et al., 2018). Consistently, wind-based models showed the lowest performances for Lake Geneva, especially at low wind speeds (*CW03* and *VP13*), which resulted in large discrepancies in annually averaged and cumulative k_{600} over the full year. They are, however, easy to compute, require few inputs (only U_{10}), and remain by far the most used to estimate lakes' CO_2 emissions worldwide (e.g., Raymond et al. 2013). Another possibility is to broadly adopt process-based models. The presented process-based models require input data that are currently more easily accessible and are routinely acquired at high frequency in many lakes: wind speed, heat flux and wind fetch (i.e. distances from the shore). The development of R packages, such as Lake Metabolizer (Winslow et al., 2016), in which the calculations of process-based models are implemented also alleviates their computational difficulty. Both increased data availability and computational tools should foster the use of process-based *k* models, which hold great potential to obtain more accurate global k_{600} estimates.

The analysis of the models adapted from the existing literature to account for the effect of lake surface waves, *SD21* and *SD21-fit* (Fig. 2-8 (d, e, f)), showed that the wave contribution to *k* becomes significant for $H_s > 0.4$ m, corresponding, for Lake Geneva, to winds blowing at 5 m s^{-1} from the southwest where the fetch length is maximal (> 15 km) with respect to the measurement site. A significant contribution to the gas transfer velocity by surface waves is expected in lakes where $H_s > 0.4$ m is not infrequent. Wave heights beyond this threshold value of H_s are frequently encountered in lakes that are larger than or a similar size to Lake Geneva (6 % of annual time at the

LéXPLORE platform). In the Great Lakes of North America, Hubertz et al. (1991) showed that the mean wave heights of all of these lakes were > 0.4 m in summer and close to 1 m in winter with a maximum of up to 5 m. H_s > 0.4 m can also form over elongated lakes of smaller size, such as smaller Swiss lakes (e.g. Lake Neuchâtel and Lake Bienne) (Amini et al., 2017). As *SD21-fit* is a process-based model integrating the four main processes in a mathematically coherent way, we would expect that it can be applied to lakes experiencing H_s > 0.4 m and can improve the accuracy of *k* estimates. Because waves can physically damage inshore and offshore infra-structure, many large lakes benefit from wave forecasts. H_s data from those forecasting systems (e.g. National Data Buoy Centre – NOAA and Wave Atlas from SwissLakes.net; Amini et al., 2017) could allow one to test whether the *SD21-fit* models can be applied to those lakes and whether k_{NB} and k_B through a_1 and A_B need to be recalibrated or fitted to the local context if flux measurement data are available, as for this study. Energy dissipation during high-wave events increases the gas transfer velocity well beyond the linear relationship derived for wind shear alone. Therefore, we expect that computed gas fluxes at the air-water interface should be significantly improved by the integration of surface waves into the *k* models.

2.5.2. Implication of four components on the annual *k* estimation and the annual CO_2 flux

Seasonal and hourly distribution of k_{CO2}

Converting k_{600} to k_{CO2} using the Schmidt number (Wanninkhof, 1992) highlights the importance of water temperature in gas exchange dynamics. Indeed, the seasonal distribution of the cumulative k_{600} is ~20 % and ~30 % for the warm (spring and summer) and cold (fall and winter) seasons respectively. Once the temperature effect is accounted for, this distribution increases to 26.1 % for summer and decreases to 24.9 % for winter but remains unchanged for spring and fall. While *R12* only uses wind shear and convective terms, the selected process-based model (*SD21-fit*) allows a decomposition into the four main drivers of the gas transfer velocity, thereby paving the way to a better understanding of the implication of these processes throughout an annual cycle.

Wind shear remains the dominant component of the gas exchange velocity over the different seasons (Fig. 2-10 (a)). The annual contribution of surface waves (wave action and bubble formation) is limited to 9–10 % of the cumulative *k* in fall and winter. The contribution of the buoyancy flux at the surface to *k* is even smaller for both models (*R12* and *SD21-fit*) at this seasonal scale. However, both the buoyancy flux and the surface waves can significantly increase *k* during episodic events, during which they can contribute disproportionately to *k* at hourly (up to 80% for convection) and daily (up to 25 % for surface waves) timescales (Fig. 2-10 (b)). Several studies have emphasised the disproportionate contribution of episodic mixing events to the annual flux, bringing CO_2 back to lake surfaces such as after ice break in dimictic lakes (Karlsson et al., 2013; Finlay et al., 2019) or during fall mixing in a eutrophic deep lake (Reed et al., 2018). Process-based *k* models integrating both the buoyancy flux and the wind-induced waves offer the opportunity to mechanistically investigate how much these episodic events contribute to annual emissions through short-term modifications of the gas exchange velocity.

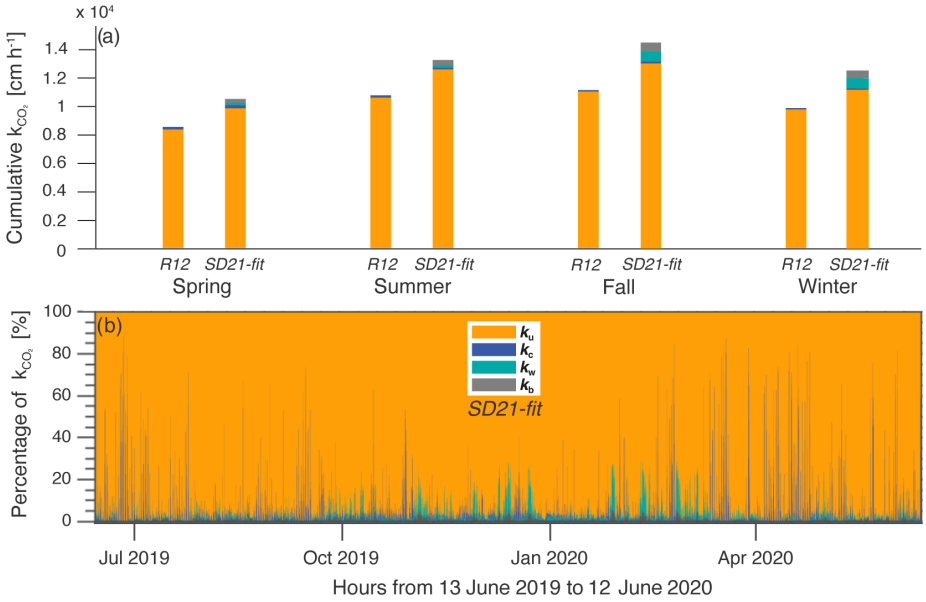

Fig. 2-10: (a) Distribution of k_{CO2} generated by two main processes (k_u and k_c) in *R12* and four main processes (k_u, k_c, k_w, and k_b) in *SD21-fit* for each season: spring (April–May–June), summer (July–August–September), fall (October–November–December), and winter (January–February–March). The height of the bar represents the cumulative k_{CO2} by season for both models (*R12* and *SD21-fit*). **(b)** Distribution of four *k* generated by wind shear, convection, wave action, and bubble enhancement (k_u, k_c, k_w, and k_b respectively) along the annual cycle. For the *SD21-fit* model, $\boldsymbol{k_u = SRM(\varepsilon_u)}$, $\boldsymbol{k_c = SRM(\varepsilon_u + \varepsilon_c + \varepsilon_w) - SRM(\varepsilon_u + \varepsilon_w)}$, $\boldsymbol{k_w = SRM(\varepsilon_u + \varepsilon_c + \varepsilon_w) - SRM(\varepsilon_u + \varepsilon_c)}$, and $\boldsymbol{k_b}$.

Consequence of the choice of k model on the seasonal to annual CO_2 flux estimation

We produced coarse estimates of monthly CO_2 fluxes with the objective of scaling the effects of wave integration at seasonal and annual scales. Monthly fluxes were computed based on *k* estimates at LéXPLORE from the different models at an hourly time step as well as the monthly average of water temperature and recorded pCO_2 at the lake surface (OLA-IS, AnaEE-France, INRAE of Thonon-les-Bains, CIPEL: Rimet et al., 2020; Perga et al., 2016) as well as a constant pCO_2 in the atmosphere (400 µatm). For months for which surface pH > 8.4, *k* values were computed with and without considering the chemical enhancement (CE; Wanninkhof and Knox, 1996) (Table 2-3). The dependency of the chemical enhancement factor on *k* (Wanninkhof and Knox, 1996) might generate a further uncertainty in estimated CO_2 fluxes (e.g. with a greater *k* value being related to a lower chemical enhancement factor).

As predicted by Fick's law, the highest outgassing fluxes occur in fall and winter, when water mixing brings CO_2 up to the lake surface, whereas low up-taking gas fluxes occur in spring and summer, when primary production depletes surface CO_2 below saturation. However, annual estimates of net CO_2 outgassing vary from 14.7 to 37.1 mmolC m^{-2} d^{-1} (Table 2-3) depending on the *k* model used for computation. Consistently, differences between model estimates are relatively low in summer, as both the ΔpCO_2 gradient (100-200 µatm) and wave occurrence are limited. Adding CE during the spring and summer months causes an increase in influx of the order of 5–128 % depending on the *k* model used. For example, using *CC98* in summer leads to a 93 % increase in the estimated influx (compared with fluxes without CE), whereas the increase is only 39 % for *SD21-fit*. This chemical

enhancement factor deserves more attention in future studies, especially for high pH lakes and summer seasons. However, the variability introduced by the CE at the annual scale remains low (~10 %) compared with that introduced by the choice of the *k* model. Estimated fluxes are also strongly dependent on the chosen *k* model in winter when both ΔpCO_2 (475 µatm) and surface wave occurrence are higher (Fig.2-10, Table 2-3). Therefore, while high-wave events represent only 6 % of the total surface wave occurrence (H_s > 0.4 m), an incomplete consideration and description of their contribution may lead to an annual flux underestimation of about 20–25 %.

Table 2-3: Seasonal to annual CO_2 flux estimation (mmol C m^{-2} d^{-1}) from *k* models (with, denoted "-CE", and without chemical enhancement), the monthly ΔCO_2 average (µatm), and the models' deviation from *SD21-fit*. CE was only considered for seasons when pH > 8.4.

Period	ΔCO_2	***CC98***	***CW03***	***VP13***	***T14***	***R12***	***S07***	***DM18***	***SD21***	***SD21-fit***
Spring	-51	-4.2	-5.9	-10.5	-5.5	-5.4	-6.2	-5.5	-5.6	-6.9
Spring-CE		*-5.9*	*-8.7*	*-11.1*	*-7.0*	*-7.2*	*7.9*	*-7.4*	*-7.4*	*-8.5*
Summer	-145	-9.0	-8.3	-23.7	-13.4	-12.8	-13.4	-12.8	-13.2	-16.3
Summer-CE		*-17.4*	*-18.9*	*-27.8*	*-20.1*	*-20.1*	*-20.7*	*-20.3*	*-20.4*	*-22.7*
Fall	350	29.0	41.2	74.8	47.6	47.9	52.2	48.4	52.1	64.5
Winter	475	43.1	63.1	108.1	65.7	64.5	71.1	64.1	69.7	86.0
Annual	157	14.7	22.5	37.1	23.6	23.4	25.9	23.5	25.7	31.8
Annual-CE		*12.2*	*19.2*	*36.0*	*21.6*	*21.3*	*23.7*	*21.2*	*23.5*	*29.8*
Annual $gCm^{-2}yr^{-1}$	-	64.6	98.8	163.1	103.6	102.8	113.9	103.3	113.0	139.7
Annual-CE $gCm^{-2}yr^{-1}$	-	*53.6*	*84.3*	*158.2*	*94.8*	*93.4*	*104.1*	*93.2*	*103.3*	*131.1*
Deviation from *SD21-fit*	-	-54 %	-29 %	+17 %	-26 %	-26 %	-18 %	-26 %	-19 %	-
Deviation-CE from SD21-fit		*-59 %*	*-36 %*	*+21 %*	*-28 %*	*-29 %*	*-21 %*	*-29 %*	*-21 %*	-

The weak contribution of convection is at odds with observations in small lakes, although not unexpected, as large lakes are exposed to stronger winds, such that wind-shear-driven ε_u often outpaces convectively driven ε_c (Read et al, 2012). However, the limited impact of the buoyancy flux on *k* does not rule out its contribution to CO_2 exchange. Indeed, convective mixing plays a central role in the deepening of the mixed layer allowing the export of the CO_2 stored in the hypolimnion towards the surface during the cold period and, thus, controlling the pCO_2 gradient (Zimmerman et al, 2019) and the observed wintertime outgassing. Altogether, both surface oversaturated CO_2 concentrations (as a result of convective mixing) and wind-induced waves are more relevant in fall and wintertime for the monomictic Lake Geneva, leading to most of the annual outgassing during this season (Table 2-3). As for many monomictic lakes, these seasons drive most of the annual CO_2 budget of Lake Geneva (Perga et al, 2016), whereas they usually correspond to those where direct measurements are the scarcest. An improved quantification of *k* values through SRM models including wind-induced waves should contribute to refining the overall estimation of large lakes' contribution to regional CO_2 emissions.

2.5.3. Wind and wave field on Lake Geneva and their impact on their spatial integration of k_{600}

SD21 and *SD21-fit* were built on the basis of a single measurement point on the lake, just as for most of the existing *k* models. Therefore, the question of the extrapolation of the model to the whole lake remains essential. Herein, we showcase two snapshot situations of high wind (i) to illustrate how process-based models could enable spatially resolved estimates of *k* values, and (ii) to exemplify how much *k* can vary as a result of the spatially variable wave and wind fields during a single episode. Two events of high and similar wind speed (11 m s^{-1}) but different directions (NE on 2020.03.30 at 08:00 and SW on 2020.02.10 at 06:00; Fig. 2-11 (a, b)) were extracted from the 0.01° hourly resolved numerical weather model of the Swiss Federal Office of Meteorology and Climatology (COSMO-1, MeteoSwiss). The two fetch distances from both prevailing wind directions (NE, SW) were then measured at each pixel of the grid (n = 583), from which the wave height field was mapped (Fig. 2-11 (c, d)) considering Equation (2-3) and the two wind grids. The maps were qualitatively consistent with previous studies on wind waves for Lake Geneva using the spectral wave model (SWAN) for wave height (Amini et al. 2016). Spatially resolved *k* values were computed from the fetch and wind grids, using the wind-based model *CC98*, the process-based model without lake wave implementation *R12* and the *SD21-fit* model containing the lake wave parametrisation.

Taking H_s > 0.4 m as a threshold for the significant effect of waves on *k*, the two prevailing winds show opposite wave responses, with long fetch and higher wave heights affecting either the northern or the southern shores for the SW and NE winds respectively. Under both conditions, more than 60 % of the full lake surface area experiences H_s values > 0.4 m, leading to *k* values as high as 68 cm h^{-1} as computed by *SD21-fit* (Fig. 2-11 (g)). The eastern part of lake experiences the lowest wind speeds and wave heights in both situations, as a consequence of the orographic effect of the Alps surrounding the Grand Lake.

Both the range and the mean of estimated *k* values increase with increasing model complexity. Accounting only for wind speed, through the wind-based model *CC98*, leads to a spatially integrated *k* value of 15.7 cm h^{-1} (range of 1–22 cm h^{-1}). *k* values computed from *R12*, accounting for both the wind shear and buoyancy flux, are on average 55 % greater (24.3 cm h^{-1}) with a moderate effect on the range of spatial variability. Finally, including surface waves results in a spatially averaged *k* value that is more than double the *k* value computed from wind speed only (35.5 cm h^{-1}), with a variability that is almost 3 times greater (range of 0–68 cm h^{-1}). It is noteworthy that the spatial average of the *k* values computed by the wind grids (Fig. 2-11 (g), diamonds) is equivalent to the average of *k* values computed from the spatial mean fetch (9.5 km for NE and 9.3 km for SW; Fig. 2-11 (g), crosses) under these specific weather conditions. Thus, the application of an average fetch would be relevant to estimate a spatially averaged *k*-value.

For all models, the integration of spatially resolved wind fields may improve the accuracy of *k* at the lake scale, but accounting for wind only would underestimate both the average gas piston velocity and its spatial variability. Therefore, a better understanding of wave behaviour in large lakes, using different approaches such as field and

laboratory measurements, new physical models, and technical development, would improve the accuracy of gas exchange estimates at the lake–water interface, at both temporal and spatial scales. Further estimates of lake-scale CO_2 fluxes would also require one to account for the spatial variability of CO_2. The question of the spatial variability of the ΔCO_2 is still open and remains difficult to analyse at high frequency in large lakes.

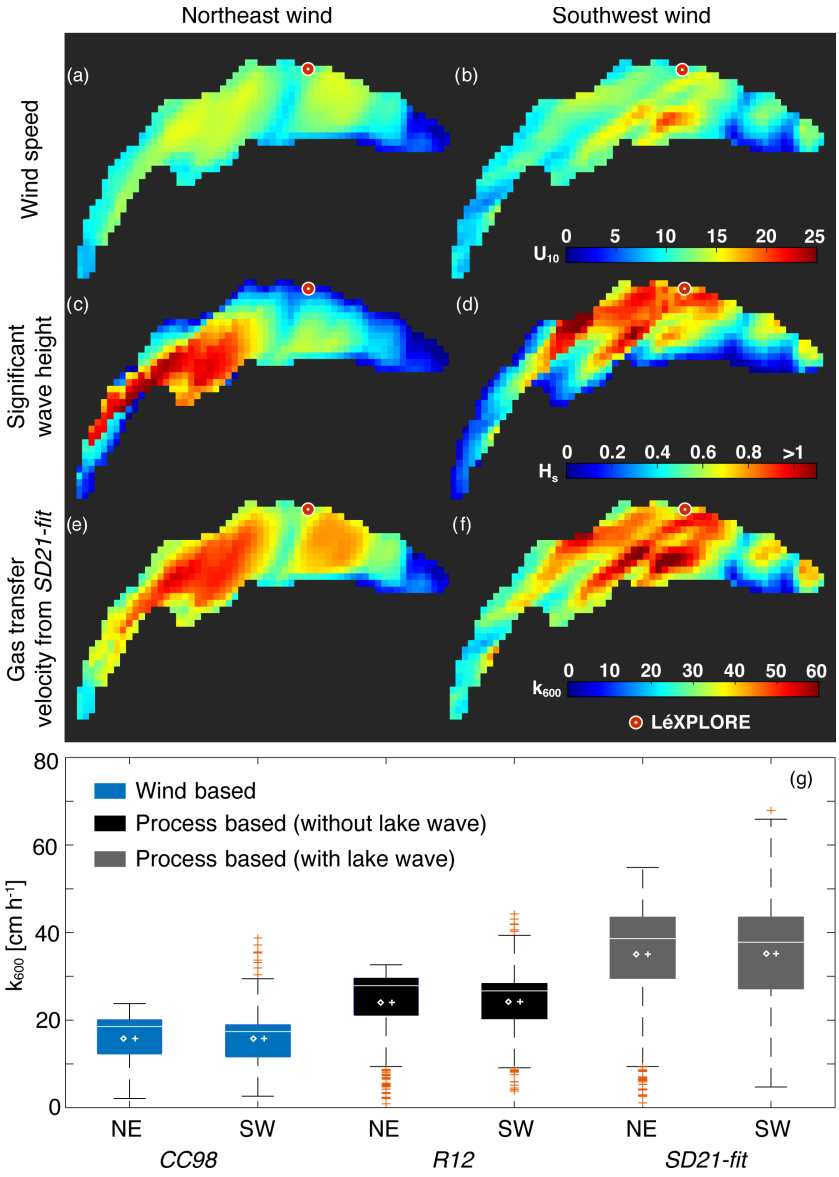

Fig. 2-11: (a, b) Wind fields from COSMO-1 for two episodes of northeast and southwest wind directions; **(c, d)** wave fields on Lake Geneva considering the two prevailing winds (northeast and southwest); **(e, f)** Gas transfer velocity from *SD21-fit*; **(g)** boxplots of the spatial variability, at the lake scale, of *k* values computed from *CC98*, *R12,* and *SD21-fit* under both meteorological conditions. Diamonds represents the spatial mean, and the cross (+) the *k* value computed from the averaged fetch distance (NE: 9.5 km; SW: 9.3 km).

2.6. Conclusion

Investigations of the four main processes generating the gas transfer velocity in the large Lake Geneva demonstrated the importance of considering surface waves during episodic windy events responsible for more than

44 % of annual cumulated k_{600}. The in-depth study of the behaviour of the process-based models has enabled us to underscore their consistent predictions under low and strong wind conditions, especially considering the new combination and adaptation model, *SD21-fit*. This last model significantly improves the estimation of the CO_2 flux when these three thresholds appear in the field, $U_{10} > 5$ ms^{-1}, Fetch > 15 km, and $H_s > 0.4$ m, making it applicable to a wide range of lake sizes. Furthermore, *SD21-fit* is assembled on solid theoretical bases coming from limnological and oceanic literature and allows one to analyse the distribution of these four main terms (k_u, k_c, k_w, and k_b) across a variety of timescales depending on the kind of study.

To conclude, the development of high-resolution gridded atmospheric models such as COSMO-1 is an asset for future estimates of the gas transfer velocity and the spatial heterogeneity of lake biogeochemical cycles. Moreover, this study sheds light on the complexity of large lakes located at the interface between small, sheltered lakes and the open oceans, experiencing a combination of processes relevant for both small and large systems. The possibility of using process-based models in a fairly simple way with few inputs to improve the precision of the gas transfer velocity and, therefore, the gas flux should be supported in future research. In addition, this approach is very promising with respect to uncovering long-term trends of CO_2 emissions from lakes as well as for finer estimation of fluxes during more intense episodic events.

2.7. Appendix

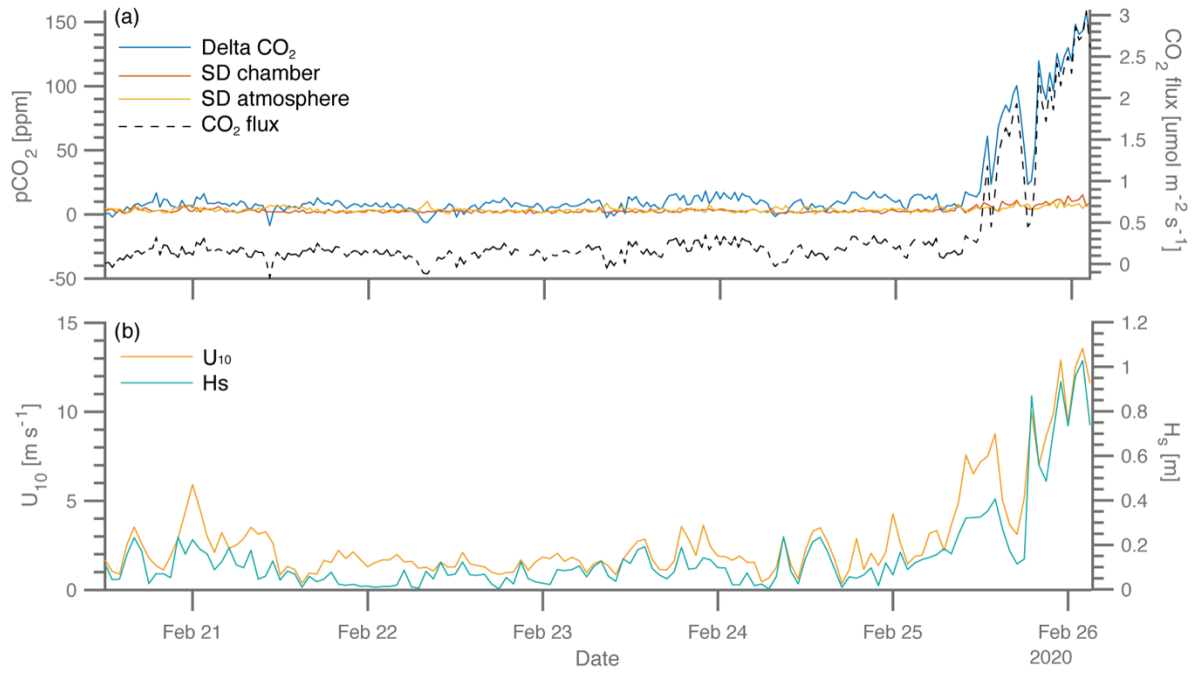

Fig. S2-1: (a) Raw outputs of the eosFD during one period of CO_2 flux measurements, showing ΔCO_2 between both cavities of measures (atmosphere cavity and chamber cavity) (blue line); the standard deviation of each cavity between two automated flushing events (30 minutes of interval), chamber cavity (red line), and atmosphere cavity (yellow line); and the CO_2 flux (black dash line). **(b)** Temporal evolution of U_{10} and H_s during the same period as the CO_2 flux measurements. The increase in flux on 25th February corresponds to the increase in wind speed and waves.

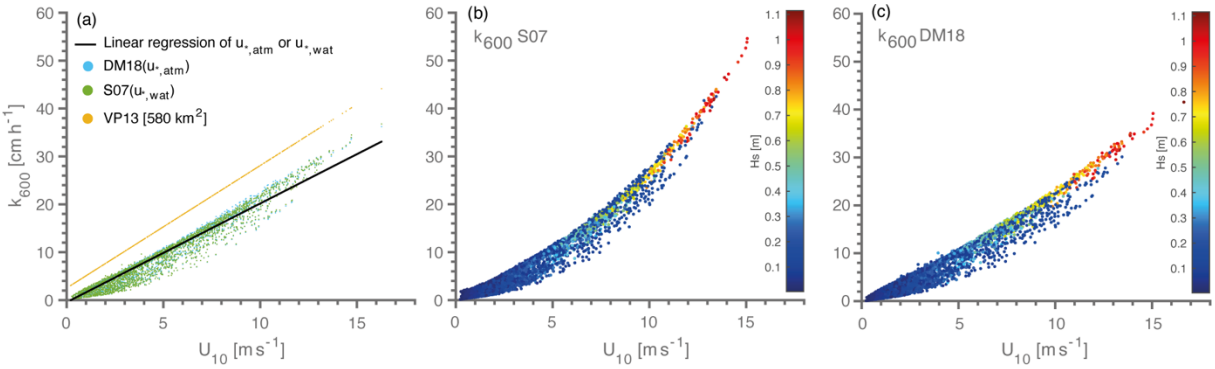

Fig. S2-2: Panel **(a)** shows the comparison of Soloviev et al. (2007) and Deike and Melville (2018) for the first-order function of friction velocity at the water side ($\boldsymbol{u_{*,wat}}$) (blue points) and at the atmosphere side ($\boldsymbol{u_{*,atm}}$) (green points) with their linear regression (black line), the linear function of Vachon and Prairie (2013) for a lake size of 582 km^2 (yellow points), and the linear regression from $\boldsymbol{u_{*,wat}}$ or $\boldsymbol{u_{*,atm}}$. Panel **(b)** is a visualisation of *S07* with empirical parameterisation of the bubble term (Woolf, 1997) regardless of wave height as a function of wind speed at 10 m. Panel **(c)** is a visualisation of *DM18* as a function of wind speed, only using the effect of the bubble term from 10 ms^{-1}.

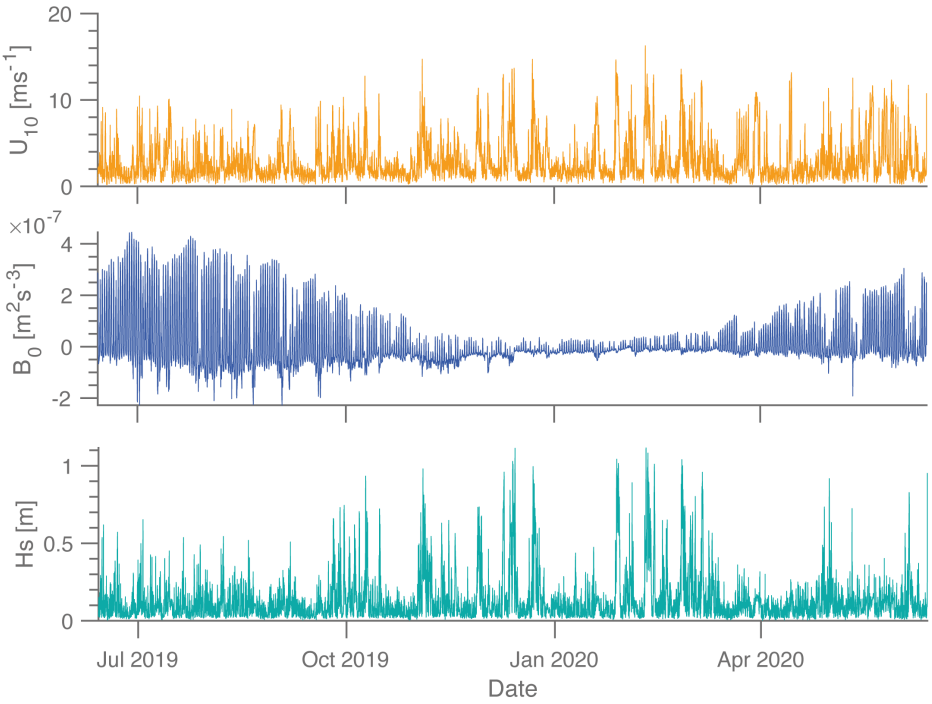

Fig. S2-3: Annual evolution of three main inputs of *k* models: wind speed at 10 m (U_{10}), buoyancy flux at surface ($\boldsymbol{B_0}$), and significant wave height (H_s).

2.8. References

Amini, A., Dhont, B., and Heller, P.: Wave atlas for Swiss lakes: modeling design waves in mountainous lakes, Journal of Applied Water Engineering and Research, 5, 103–113, https://doi.org/10.1080/23249676.2016.1171733, 2016.

Bastviken, D., Sundgren, I., Natchimuthu, S., Reyier, H., and Gålfalk, M.: Technical Note: Cost-efficient approaches to measure carbon dioxide (CO_2) fluxes and concentrations in terrestrial and aquatic environments using mini loggers, Biogeosciences, 12, 3849–3859, https://doi.org/10.5194/bg-12-3849-2015, 2015.

Borges, A. V., Vanderborght, J.-P., Schiettecatte, L.-S., Gazeau, F., Ferron-Smith, S., Delille, B., and Frankignoulle, M.: Variability of the gas transfer velocity of CO_2 in a macrotidal estuary (the Scheldt), Estuaries, 27, 593–603, https://doi.org/10.1007/BF02907647, 2004.

Bouffard, D., Sukys, J., Runnals, J., and Odermatt, D.: Datalakes: Heterogeneous data platform for operational modelling and forecasting of Swiss lakes, available at: https://www. datalakes-eawag.ch, last access: 23 February 2021.

Carter, D. J. T.: Prediction of wave height and period for a constant wind velocity using the JONSWAP results, Ocean Eng., 9, 17– 33, https://doi.org/10.1016/0029-8018(82)90042-7, 1982.

Cole, J. J. and Caraco, N. F.: Atmospheric exchange of carbon dioxide in a low-wind oligotrophic lake measured by the addition of SF_6, Limnol. Oceanogr., 43, 647–656, https://doi.org/10.4319/lo.1998.43.4.0647, 1998.

Cole, J. J., Prairie, Y. T., Caraco, N. F., McDowell, W. H., Tranvik, L. J., Striegl, R. G., Duarte, C. M., Kortelainen, P., Downing, J. A., Middelburg, J. J., and Melack, J.: Plumbing the Global carbon cycle: Integrating inland waters into the terrestrial carbon budget, Ecosystems, 10, 172–185, https://doi.org/10.1007/s10021- 006-9013-8, 2007.

Cole, J. J., Bade, D. L., Bastviken, D., Pace, M. L., and de Bogert, M. V.: Multiple approaches to estimating air–water gas exchange in small lakes, Limnol. Oceanogr. Meth., 8, 285—293, https://doi.org/10.4319/lom.2010.8.285, 2010.

Crusius, J. and Wanninkhof, R.: Gas transfer velocities measured at low wind speed over a lake, Limnol. Oceanogr., 48, 1010–1017, https://doi.org/10.4319/lo.2003.48.3.1010, 2003.

Danckwerts, P. V.: Significance of liquid-film coefficient in gas absorption, Ind. Eng. Chem., 43, 1460–1467, https://doi.org/10.1021/ie50498a055, 1951.

Deike, L. and Melville, W. K.: Gas transfer by break- ing waves, Geophys. Res. Lett., 45, 482–492, https://doi.org/10.1029/2018GL078758, 2018.

Dugan, H. A., Woolway, R. I., Santoso, A. B., Corman, J. R., Jaimes, A., Nodine, E. R., Patil, V. P., Zwart, J. A., Brentrup, J. A., Hetherington, A. L., Oliver, S. K., Read, J. S., Winters, K. M., Hanson, P. C., Read, E. K., Winslow, L. A., and Weathers, K. C.: Consequences of gas flux model choice on the interpretation of metabolic balance across 15 lakes, Inland Waters, 6, 581–592, https://doi.org/10.1080/IW-6.4.836, 2016.

Engel, F., Farrell, K. J., McCullough, I. M., Scordo, F., Denfeld, B. A., Dugan, H. A., de Eyto, E., Hanson, P. C., McClure, R. P., Nõges, P., Nõges, T., Ryder, E., Weathers, K. C., and Weyhenmeyer, G. A.: A lake classification concept for a more accurate global estimate of the dissolved inorganic carbon export from

terrestrial ecosystems to inland waters, Sci. Nat.-Heidelberg, 105, 25, https://doi.org/10.1007/s00114-018-1547-z, 2018.

Erkkilä, K.-M., Ojala, A., Bastviken, D., Biermann, T., Heiska- nen, J. J., Lindroth, A., Peltola, O., Rantakari, M., Vesala, T., and Mammarella, I.: Methane and carbon dioxide fluxes over a lake: comparison between eddy covariance, floating chambers and boundary layer method, Biogeosciences, 15, 429–445, https://doi.org/10.5194/bg-15-429-2018, 2018.

Esters, L., Landwehr, S., Sutherland, G., Bell, T. G., Christensen, K. H., Saltzman, E. S., Miller, S. D., and Ward, B.: Parameterizing air-sea gas transfer velocity with dissipation: Dissipation-based k-parametrization, J. Geophys. Res.-Oceans, 122, 3041–3056. https://doi.org/10.1002/2016JC012088, 2017.

Esters, L., Rutgersson, A., Nilsson, E., and Sahlée, E.: Non-local impacts on eddy-covariance air-lake CO_2 fluxes, Bound.-Lay. Meteorol., 178, 283–300, https://doi.org/10.1007/s10546-020- 00565-2, 2021.

Eugster, W., Kling, G. W., Jonas, T., McFadden, J. P., Wüest, A., MacIntyre, S., and Chapin, F. S.: CO_2 exchange between air and water in an Artic Alaskan and midlatitude Swiss lake: Importance of convective mixing, J. Geophys. Res., 108, D12, https://doi.org/10.1029/2002JD002653, 2003.

Fairall, C. W., Yang, M., Bariteau, L., Edson, J. B., Helmig, D., McGillis, W., Pezoa, S., Hare, J. E., Huebert, B., and Blomquist, B.: Implementation of the Coupled Ocean-Atmosphere Response Experiment flux algorithm with CO_2, dimethyl sulfide, and O_3, J. Geophys. Res., 116, C00F09, https://doi.org/10.1029/2010JC006884, 2011.

Finlay, K., Vogt, R. J., Simpson, G. L., and Leavitt, P. R.: Seasonality of pCO_2 in a hard-water lake of the northern Great Plains: The legacy effects of climate and limnological conditions over 36 years, Limnol. Oceanogr., 64, 118–129, https://doi.org/10.1002/lno.11113, 2019.

Frost, T. and Upstill-Goddard, R. C.: Meteorological controls of gas exchange at a small English lake, Limnol. Oceanogr., 47, 1165–1174, https://doi.org/10.4319/lo.2002.47.4.1165, 2002.

Guérin, F., Abril, G., Serça, D., Delon, C., Richard, S., Delmas, R., Tremblay, A., and Varfalvy, L.: Gas transfer velocities of CO_2 and CH_4 in a tropical reservoir and its river downstream, J. Marine Syst., 66, 161–172, https://doi.org/10.1016/j.jmarsys.2006.03.019, 2007.

Hasselmann K., Barnett T. P., Bouws, E., Carlson, H, Cartwright D. E., Enke, K., Ewing, J. A., Gienapp, H., Hasselmann, D. E., Kruseman, P., Meerburg, A., Müller, P., Olbers, D. J., Richter, K., Sell, W., and Walden, H.: Measurements of wind-wave growth and swell decay during the Joint North Sea Wave Project (JONSWAP), Dtsch. Hydrog. Z. Suppl. A, 8, 1–95, 1973.

Heiskanen, J. J., Mammarella, I., Haapanala, S., Pumpa- nen, J., Vesala, T., MacIntyre, S., and Ojala, A.: Effects of cooling and internal wave motions on gas transfer coefficients in a boreal lake, Tellus B, 66, 22827, https://doi.org/10.3402/tellusb.v66.22827, 2014.

Hubertz, J. M., Driver, D. B., and Reinhard, R. D.: Wind waves on the Great Lakes: A 32 year hindcast, J. Coastal Res., 7, 945–967, 1991.

Huotari, J., Ojala, A., Peltomaa, E., Nordbo, A., Launiainen, S., Pumpanen, J., Rasilo, T., Hari, P., and Vesala, T.: Long-term direct CO_2 flux measurements over a boreal lake: Five years of eddy covariance data, Geophys. Res. Lett., 38, L18401, https://doi.org/10.1029/2011GL048753, 2011.

Karlsson, J., Giesler, R., Persson, J., and Lundin, E.: High emission of carbon dioxide and methane during ice thaw in high latitude lakes, Geophys. Res. Lett., 40, 1123–1127, https://doi.org/10.1002/grl.50152, 2013.

Katul, G. and Liu, H.: Multiple mechanisms generate a universal scaling with dissipation for the air–water gas transfer velocity, Geophys. Res. Lett., 44, 1892–1898, https://doi.org/10.1002/2016GL072256, 2017.

Katul, G., Mammarella, I., Grönholm, T., and Vesala, T.: A structure function model recovers the many formulations for air–water gas transfer velocity, Water Resour. Res., 54, 5905–5920, https://doi.org/10.1029/2018WR022731, 2018.

Keeling, R. F., Najjar, R. P., Bender, M. L., and Tans, P. P.: What atmospheric oxygen measurements can tell us about the global carbon cycle, Global Biogeochem. Cy., 7, 37–67, https://doi.org/10.1029/92GB02733, 1993.

Klaus, M. and Vachon, D.: Challenges of predicting gas transfer velocity from wind measurements over global lakes, Aquat. Sci., 82, 53, https://doi.org/10.1007/s00027-020-00729-9, 2020.

Lamont, J. C. and Scott, D. S.: An eddy cell model of mass transfer into the surface of a turbulent liquid, AIChE J., 16, 513–519, https://doi.org/10.1002/aic.690160403, 1970.

Lombardo, C. P. and Gregg, M. C.: Similarity scaling of viscous and thermal dissipation in a convecting surface boundary layer. J. Geophys. Res., 94, 6273–6284, https://doi.org/10.1029/jc094ic05p06273, 1989.

Lorke, A. and Peeters, F.: Toward a unified scaling relation for interfacial fluxes, J. Phys. Oceanogr., 36, 955–961, https://doi.org/10.1175/JPO2903.1, 2006.

Maberly, S. C., Barker, P. A., Stott, A. W., and De Ville, M. M.: Catchment productivity controls CO_2 emissions from lakes, Nat. Clim. Change, 3, 391–394, https://doi.org/10.1038/nclimate1748, 2013.

MacIntyre, S., Eugster, W., and Kling, G. W.: The critical importance of buoyancy flux for gas flux across the air– water interface, in: Geophysical Monograph Series, edited by: Donelan, M. A., Drennan, W. M., Saltzman, E. S., and Wan- ninkhof, R., American Geophysical Union, Washington, DC, https://doi.org/10.1029/GM127p0135, pp. 135–139, 2001.

MacIntyre, S., Jonsson, A., Jansson, M., Aberg, J., Turney, D. E., and Miller, S. D.: Buoyancy flux, turbulence, and the gas transfer coefficient in a stratified lake: Turbulence and gas evasion in lakes, Geophys. Res. Lett., 37, L24604, https://doi.org/10.1029/2010GL044164, 2010.

Mammarella, I., Nordbo, A., Rannik, Ü., Haapanala, S., Levula, J., Laakso, H., Ojala, A., Peltola, O., Heiskanen, J., Pumpanen, J., and Vesala, T.: Carbon dioxide and energy fluxes over a small boreal lake in Southern Finland: CO_2 and Energy Fluxes Over Lake, J. Geophys. Res.-Biogeo., 120, 1296–1314, https://doi.org/10.1002/2014JG002873, 2015.

Perga, M.-E., Maberly, S. C., Jenny, J.-P., Alric, B., Pignol, C., and Naffrechoux, E.: A century of human-driven changes in the carbon dioxide concentration of lakes: 150 years of human impacts on lakes CO_2, Global Biogeochem. Cy., 30, 93–104, https://doi.org/10.1002/2015GB005286, 2016.

Perolo, P.: CO_2 flux measurements in Lake Geneva, Zenodo [dataset], https://doi.org/10.5281/zenodo.5679883, 2021.

Raymond, P. A., Hartmann, J., Lauerwald, R., Sobek, S., Mc- Donald, C., Hoover, M., Butman, D., Striegl, R., Mayorga, E., Humborg, C., Kortelainen, P., Dürr, H., Meybeck, M., Ciais, P., and Guth, P.: Global carbon dioxide emissions from inland waters, Nature, 503, 355–359, https://doi.org/10.1038/nature12760, 2013.

Read, J. S., Hamilton, D. P., Desai, A. R., Rose, K. C., Mac- Intyre, S., Lenters, J. D., Smyth, R. L., Hanson, P. C., Cole, J. J., Staehr, P. A., Rusak, J. A., Pierson, D. C., Brookes, J. D., Laas, A., and Wu, C. H.: Lake-size dependency of wind shear and convection as controls on gas exchange: Lake-size dependency of u_* and w_*, Geophys. Res. Lett., 39, L09405, https://doi.org/10.1029/2012GL051886, 2012.

Reed, D. E., Dugan, H. A., Flannery, A. L., and Desai, A. R.: Carbon sink and source dynamics of a eutrophic deep lake using multiple flux observations over multiple years: Carbon sink and source dynamics, Limnol. Oceanogr. Lett., 3, 285–292, https://doi.org/10.1002/lol2.10075, 2018.

Reichl, B. G. and Deike, L.: Contribution of sea-state dependent bubbles to air-sea carbon dioxide fluxes, Geophys. Res. Lett., 47, L087267, https://doi.org/10.1029/2020GL087267, 2020.

Rimet, F., Anneville, O., Barbet, D., Chardon, C., Crépin, L., Domaizon, I., and Monet, G.: The Observatory on LAkes (OLA) database: Sixty years of environmental data accessible to the public, J. Limnol., 78, 164–178. https://doi.org/10.4081/jlimnol.2020.1944, 2020.

Risk, D., Nickerson, N., Creelman, C., McArthur, G., and Owens, J.: Forced Diffusion soil flux: A new technique for continuous monitoring of soil gas efflux, Agr. Forest Meteorol., 151, 1622–1631, https://doi.org/10.1016/j.agrformet.2011.06.020, 2011.

Russell, T. W. F. and Denn, M. M.: Introduction to chemical engi- neering analysis, Wiley, New York, USA, 1972.

Schilder, J., Bastviken, D., van Hardenbroek, M., Kankaala, P., Rinta, P., Stötter, T., and Heiri, O.: Spatial heterogeneity and lake morphology affect diffusive greenhouse gas emission estimates of lakes: Spatial heterogeneity of diffusive flux, Geophys. Res. Lett., 40, 5752–5756, https://doi.org/10.1002/2013GL057669, 2013.

Schubert, M., Paschke, A., Lieberman, E., and Burnett, W. C.: Air– Water Partitioning of ^{222}Rn and its Dependence on Water Temperature and Salinity, Environ. Sci. Technol., 46, 3905–3911, https://doi.org/10.1021/es204680n, 2012.

Simon A.: Turbulent mixing in the surface boundary layer of lakes, PhD thesis no. 12,272, Swiss Fed. Inst. Technol. (ETH), Zurich, 1997.

Soloviev, A. and Lukas, R.: The Near-Surface Layer of the Ocean: Structure, Dynamics, and Applications, Springer, Dordrecht, NL, 572 pp., https://doi.org/10.1007/978-94-007-7621-0, 2006.

Soloviev, A. and Schlüssel P.: Parametrization of the cool skin of the ocean and of the air-ocean gas transfer on the basis of modeling surface renewal, J. Phys. Oceanogr., 24, 1339–1346, 1994.

Soloviev, A., Donelan, M., Graber, H., Haus, B., and Schlüssel, P.: An approach to estimation of near-surface turbulence and CO_2 transfer velocity from remote sensing data, J. Marine Syst., 66, 182–194, https://doi.org/10.1016/j.jmarsys.2006.03.023, 2007.

Stumm, W. and Morgan, J. J.: Aquatic Chemistry: An introduction emphasizing chemical equilibria in natural waters, 2nd edn., John Wiley and Sons Ltd, New York, USA, 1981.

Tedford, E. W., MacIntyre, S., Miller, S. D., and Czikowsky, M. J.: Similarity scaling of turbulence in a temperate lake dur- ing fall cooling, J. Geophys. Res.-Oceans, 119, 4689–4713, https://doi.org/10.1002/2014JC010135, 2014.

Terray, E. A., Donelan, M. A., Agrawal, Y. C., Drennan, W. M., Kahma, K. K., Williams III, A. J., Hwang, P. A., and Kitaigorodkii, S. A.: Estimates of kinetic energy dissipation under breaking waves, J. Phys. Oceanogr., 26, 792–807, 1996.

Toba, Y.: Local balance in the air-sea boundary processes, J. Oceanogr., 28, 109–120, https://doi.org/10.1007/BF02109772, 1972.

Toba, Y.: Stochastic form of the growth of wind waves in a single-parameter representation with physical implications, J. Phys. Oceanogr., 8, 494–507, https://doi.org/10.1175/1520-0485(1978)008<0494:SFOTGO>2.0.CO;2, 1978.

Tranvik, L. J., Downing, J. A., Cotner, J. B., Loiselle, S. A., Striegl, R. G., Ballatore, T. J., Dillon, P., Finlay, K., Fortino, K., Knoll, L. B., Kortelainen, P. L., Kutser, T., Larsen, Soren., Laurion, I., Leech, D. M., McCallister, S. L., McKnight, D. M., Melack, J. M., Overholt, E., Porter, J. A., Prairie, Y., Renwick, W. H., Roland, F., Sherman, B. S., Schindler, D. W., Sobek, S., Trem- blay, A., Vanni, M. J., Verschoor, A. M., von Wachenfeldt, E., and Weyhenmeyer, G. A.: Lakes and reservoirs as regulators of carbon cycling and climate, Limnol. Oceanogr., 54, 2298–2314, https://doi.org/10.4319/lo.2009.54.6_part_2.2298, 2009.

Vachon, D. and Prairie, Y. T.: The ecosystem size and shape dependence of gas transfer velocity versus wind speed relationships in lakes, Can. J. Fish. Aquat. Sci., 70, 1757–1764, https://doi.org/10.1139/cjfas-2013-0241, 2013.

Vachon, D., Prairie, Y. T., and Cole, J. J.: The relationship be- tween near-surface turbulence and gas transfer velocity in fresh- water systems and its implications for floating chamber measurements of gas exchange, Limnol. Oceanogr., 55, 1723–1732, https://doi.org/10.4319/lo.2010.55.4.1723, 2010.

Vesala, T., Huotari, J., Rannik, Ü., Suni, T., Smolander, S., Sogachev, A., Launiainen, S., and Ojala, A.: Eddy covariance measurements of carbon exchange and latent and sensible heat fluxes over a boreal lake for a full open-water period, J. Geophys. Res., 111, D11101, https://doi.org/10.1029/2005JD006365, 2006.

Wanninkhof, R.: Relationship between wind speed and gas ex- change over the ocean, J. Geophys. Res., 97, 7373–7382, https://doi.org/10.1029/92JC00188, 1992.

Wanninkhof, R. and Knox, M.: Chemical enhancement of CO_2 exchange in natural waters, Limnol. Oceanogr., 41, 689–697, https://doi.org/10.4319/lo.1996.41.4.0689, 1996.

Winslow, L. A., Zwart, J. A., Batt, R. D., Dugan, H. A., Woolway, R. I., Corman, J. R., Hanson, P. C., and Read, J. S.: LakeMetabolizer: An R package for estimating lake metabolism from free- water oxygen using diverse statistical models, Inland Waters, 6, 622–636, https://doi.org/10.1080/IW-6.4.883, 2016.

Woolf, D. K.: Bubbles and their role in gas exchange, in: The Sea Surface and Global Change, edited by: Liss, P. S. and Duce, R. A., Cambridge University Press, Cambridge, UK, https://doi.org/10.1017/CBO9780511525025.007, pp. 173–206, 1997.

Woolf, D. K.: Parametrization of gas transfer velocities and sea-state-dependent wave breaking, Tellus B, 57, 87–94, https://doi.org/10.3402/tellusb.v57i2.16783, 2005.

Wüest, A. and Lorke, A.: Small-scale hydrodynamics in lakes, Annu. Rev. Fluid Mech., 35, 373–412, https://doi.org/10.1146/annurev.fluid.35.101101.161220, 2003.

Wüest, A., Bouffard, D., Guillard, J., Ibelings, B. W., Lavanchy, S., Perga, M.-E., and Pasche, N.: LéXPLORE: A floating laboratory on Lake Geneva offering unique research opportunities, Wires Water, 8, e1544, https://doi.org/10.1002/wat2.1544, 2021.

Wyngaard, J. C. and Coté O. R.: The budgets of turbulent kinetic energy and temperature variance in the atmospheric surface layer, J. Atmos. Sci., 28, 190–201, 1971.

Zappa, C. J., McGillis, W. R., Raymond, P. A., Edson, J. B., Hintsa, E. J., Zemmelink, H. J., Dacey, J. W. H., and Ho, D. T.: Environmental turbulent mixing controls on air–water gas exchange in marine and aquatic systems, Geophys. Res. Lett., 34, L10601, https://doi.org/10.1029/2006GL028790, 2007.

Zimmermann, M., Mayr, M. J., Bouffard, D., Eugster, W., Steinsberger, T., Wehrli, B., Brand, A., and Bürgmann, H.: Lake overturn as a key driver for methan oxidation, CSH. Lab. bioRXiv, https://doi.org/10.1101/689182, 2019.

2.9. Acknowledgment

We would like to thank the entire team of the LéXPLORE platform for their administrative and technical support and the LéXPLORE core dataset. We also acknowledge the five partner institutions involved with LéXPLORE: Eawag, EPFL, the University of Geneva, the University of Lausanne, and CARRTEL (INRAE-USMB). This study was supported by the CARBOGEN project (SNF 200021_175530), which is linked to the LéXPLORE project (SNF R'Equip, P157779) and the Primary Production Under Oligotrophication in Lakes project (SNF 200021_179123). The authors thank Sébastien Lavanchy, the chief technical officer (APHYS-EPFL), and Aurélien Ballu, a member of the technical pool (IDYST-UNIL) of LéXPLORE platform, for their technical and field support.

2.10. Author contribution statement

PP, MEP, and DB designed the study. PP, BFC, NE, and TL collected field data and carried out data preprocessing. PP developed the model code and performed the simulation with contribution from DB. PP, MEP, and DB drafted the paper and all co-authors contributed to the final submitted article.

Chapter 3

From high to low frequency measurements: finding a compromise for CO_2 gas exchange estimation at the lake scale

Pascal Perolo[1], Gaël Many[1], Nicolas Escoffier[1], Damien Bouffard[2] and Marie-Elodie Perga[1]

[1]Institute of Earth Surface Dynamics, University of Lausanne, Quartier Mouline, CH-1015 Lausanne
[2]Eawag, Swiss Federal Institute of Aquatic Science and Technology, Surface Waters – Research and Management, Seestrasse 79, CH-6047 Kastanienbaum

In preparation…

3.1. Abstract

As lakes globally return some terrestrial carbon to the atmosphere, major efforts have been dedicated to increase the accuracy of estimated CO_2 emissions. The most common way to estimate CO_2 gas exchange consists in quantifying the product of the gas transfer velocity (k) and the CO_2 gas differential (ΔpCO_2), between the water concentration (pCO_2) and the saturation concentration. Yet, because all the terms of the equation are challenging to measure or parameterise at fine-time and space scale resolution over annual periods, few studies can simultaneously link the variabilities of CO_2 flux, pCO_2 and k. The aim of this study is to assess the minimal sampling frequency of inputs data that is necessary to reach representative estimates of annual CO_2 fluxes at the surface of a large lake. We combine high-frequency measurements of water and air pCO_2 with high-frequency computations of the gas exchange velocity, to estimate, at a fine-scale resolution, the CO_2 gas exchange over a complete annual cycle in the littoral and pelagic environments in a large and deep hardwater lake. We thereafter degrade the signal resolution and quantify errors in annual flux estimates resulting from the loss of information. We derive a sampling compromise that minimises both the data requirements (in sites and sampling frequency) and errors in CO_2 flux estimates over a complete annual cycle at the lake scale. We show that high frequency computations of k (hourly) are required all year round, in order to capture intense fluxes generated by episodic turbulence events. Daily and weekly measurements of pCO_2 is necessary during shoulder periods while the sampling frequency can be loosened during periods of stability such as summer. In terms of spatial variability, the yearly mean flux of the littoral environment is more than one order of magnitude greater than for the pelagic, with 26.8 and 1.92 g C m^{-2} $yr^{-1,}$ respectively. Moreover, we show that even if the littoral area represents a low share of the lake surface area (herein 2-8% of the total lake area for a max depth of the littoral of 4-12 m), the littoral CO_2 flux could contribute 25-50% of the entire lake flux, demonstrating the relevance of integrating littoral estimation for accurate flux balance. Finally, we propose solutions to improve these CO_2 gas exchange quantifications using currently available numerical tools such as spatial weather model, hydrodynamical model and data reconstruction.

3.2. Introduction

Lakes have been recognised, for more than three decades, as a source of CO_2 to the atmosphere due to their common supersaturation in CO_2 concentration (Cole et al., 1994; Cole et al., 2007). Flux measurement techniques at the air-water interface have been developed, since the 1990s, to better quantify CO_2 exchanges. However, these techniques such as mass balance (Cole and Caraco, 1998), manual flux chamber (Borges et al., 2004; Vachon et al., 2010), automated flux chamber (Duc et al., 2013; Spafford and Risk, 2018; Perolo et al., 2021), and eddy covariance systems (Vesala et al., 2006; Erkkilä et al., 2018) have their share of advantages and disadvantages (e.g. Vachon et al., 2010; Klaus and Vachon, 2020; Esters et al., 2021; Perolo et al., 2021). They often have shortcomings in terms of time and space integration or have measurement biases. Thus, the quantification of CO_2 gas exchange remains complex to achieve over long periods and at high frequency over a whole lake scale (Natchimuthu et al., 2017; Loken et al., 2019). To solve some of the issues, CO_2 fluxes at the surface of lakes are estimated using the first Fickian law operating through a net diffusive transport:

$$F = \propto k\ \alpha\ \Delta pCO_2\ , \qquad (3\text{-}1)$$

where F (mol m^{-2} s^{-1} but often expressed as µmol cm^{-2} h^{-1}) is the CO_2 gas flux, $\propto$ is the chemical enhancement (CE; dimensionless), k is the gas transfer velocity (cm h^{-1}), α is the CO_2 solubility coefficient (µmol cm^{-3} µatm^{-1}), and ΔpCO_2 is the gradient of partial pressure of CO_2 (pCO_2) between the water and the atmosphere corrected for altitude (µatm). With recent technological and theoretical developments, these variables had become easier to measure (pCO_2) or model (k). Yet all terms are expected to vary over time and space within a lake, so that sampling frequency and sites shall be accounted for when aiming for an annual CO_2 balance. Thus, the space and time integration of k and pCO_2 generates the spatiotemporal variability of the CO_2 gas exchange. The relative importance of these two variables on the CO_2 flux has been studied in small boreal lakes where a greater pCO_2 variability affects CO_2 flux from daily to weekly scale, while k variability drives variability in fluxes at shorter, hourly timescale (Natchimuthu et al. 2017). Moreover, a strong spatial CO_2 flux variability according to water depth has been highlighted in a small Canadian lake (Spafford and Risk, 2018) which can be explained by the strong differences in metabolism affecting pCO_2 between littoral and pelagic environments (Lauster et al., 2006; Sadro et al., 2011).

Water pCO_2 is perhaps the most complex to acquire at high frequency and fine scale resolution over long periods. It was first estimated using high-frequency pH and alkalinity sampling to reconstruct it using CO_2sys program (Pierrot et al, 2006) following Millero (1979). Still, computed pCO_2 estimates are reasonably accurate for lakes with low dissolved organic matter content but tend to overestimate CO_2 at high levels of dissolved organic matter (Abril et al., 2015). High-frequency CO_2 sensors have been developed for more than a decade, but records usually cover a few weeks up to a few months rather than complete annual cycles. Moreover, these sensors are expensive, require regular maintenance and calibration, and the installation of these instruments over the long term, particularly in pelagic environments, is complex. Therefore, boat sampling often monitors these data at a low frequency (weekly to monthly) and does not capture short-term variations.

The gas transfer velocity models, or k models, were first developed empirically based on wind speed, the prominent process generating surface turbulence (Cole and Caraco, 1998; Crusius and Wanninkhof, 2003), and

adding the lake size (Vachon and Prairie, 2013). Then, process-based models using the theories of the surface renewal model (Lamont and Scott, 1970) have been established considering the turbulent kinetic energy dissipation rate produced by wind shear and convection for small lakes (e.g. Eugster et al., 2003; MacIntyre et al., 2010; Read et al., 2012; Tedford et al., 2014; Heiskanen et al., 2014), and wind-driven surface waves for oceanic systems (Soloviev et al., 2007, Fairall et al., 2011; Deike and Melville, 2018) and large lakes (Perolo et al., 2021). Thus, these *k* models are calculated using mainly external input data such as meteorological data (air temperature, wind speed, wind direction, relative humidity, solar radiation, barometric pressure), which are obtained simply by the high-frequency weather stations or using spatial weather models such as COSMO-1 (Swissmeteo). In addition, the internal input data is the surface water temperature, which is also measured simply by high-frequency temperature sensors or can be estimated accurately by 1D hydrodynamic models (Flake, GLM, GOTM, Simstrat, MyLake) widely developed for several years and even 3D models (e.g. Deft-3D), which also requires external meteorological data to run.

Like the *k* model, the estimation of the solubility coefficient requires the surface water temperature for low saline lakes (Wanninkhof, 1992). Chemical enhancement is added to the flux equation in high bicarbonate (HCO_3^-) and high pH (>8.2) conditions during atmospheric CO_2 invasion (Wanninkhof and Knox, 1996). The carbonate buffering effect greatly enhances these inward fluxes, leading to fast hydration and deprotonation of incoming atmospheric CO_2 into HCO_3, with limited impact on pH and dissolved CO_2 concentrations (Bade & Cole, 2006) to keep high ΔpCO_2. The CE coefficient is estimated using the pH level and the surface water temperature. Atmospheric CO_2 is often fixed as a constant variable (e.g. ~400 ppm) but can vary by more than 20 ppm on an annual cycle (Dlugokencky et al., 2021) and even by more than 50 ppm on a daily scale (Higuchi et al., 2003). However, its effect on estimating CO_2 fluxes is still little studied. In addition, atmospheric CO_2 measures, as of meteorological variables, are mostly obtained from inland stations, at best from the lake shore, with potentially significant differences from values over the lake surface , especially for large systems.

The spatial variability of *k* was first linked to the lake size or fetch distance from the shore (Schilder et al., 2013; Vachon and Prairie, 2013). Further developments building on mechanistic *k* models include spatially resolved *k* estimates accounting for wave size induced by the wind according to the fetch, the lake shape, and the surrounding relief (Perolo et al., 2021). On the other hand, the spatial variability of water pCO_2 is related to biogeochemical and physical processes such as photosynthesis, respiration, proximity to sediment and macrophytes, river input, water stability, and water movement (e.g. mixing dynamic, internal wave, and upwelling) (e.g. Rudorff et al., 2011; Teodoru et al., 2011; Natchimuthu et al., 2017; Loken et al., 2019; Perolo et al., in preparation). In addition, these processes also have temporal variability throughout the year ranging from the day to the season.

Herein, we compute the CO_2 gas exchange using all the input variables of Eq. 4-1, recorded at high frequency over a complete annual cycle in littoral and pelagic environments in a large hardwater lake, Lake Geneva. Our objective is to determine the minimum temporal interval needed for each parameter that would allow a minimum loss in CO_2 fluxes estimate. The parametrisation and variability of k-models, as well as consequences on flux estimates, have been studied thoroughly in Perolo et al, 2021 (Chap 2). Herein, we assess the sensitivity of CO_2

flux estimates on the parametrisation of the chemical enhancement, on the value and sampling frequency of air pCO_2 and water pCO_2. Thereafter, we assess the relevance of taking measurements in the littoral environment in addition to the pelagic in estimating CO_2 fluxes at the global lake scale over a complete annual cycle. Finally, we discuss the results and propose appropriate solutions using currently available tools.

3.3. Material and methods

3.3.1. Study sites

Lake Geneva is a large, deep, alkaline hardwater lake defining part of the Swiss-French border, at 372 m a.s.l. (metres above sea level) (46° 26’ N, 6° 33’ E). Lake Geneva is an oligomictic lake with complete deep mixing (309 m) occurring every 7 years on average, while the annual winter mixing average is ~200 m (Gaudard et al., 2017; Schwefel et al. 2016). The lake water has been surveyed monthly or fortnightly since the late 1950s at the SHL2 point (Fig. 3-1; OLA-IS, AnaEE-France, INRAE of Thonon-les-Bains, and CIPEL; Rimet et al., 2020). Field datasets were collected from the LéXPLORE platform (110 m depth; Wüest et al., 2021; 46° 30’ 02’’ N, 6° 39’ 40’’ E) and the Buchillon mast (4 m depth; 46° 27’ 31’’ N, 6° 23’ 58’’ E) to cover pelagic and littoral environments over the years 2019, 2020 and 2021.

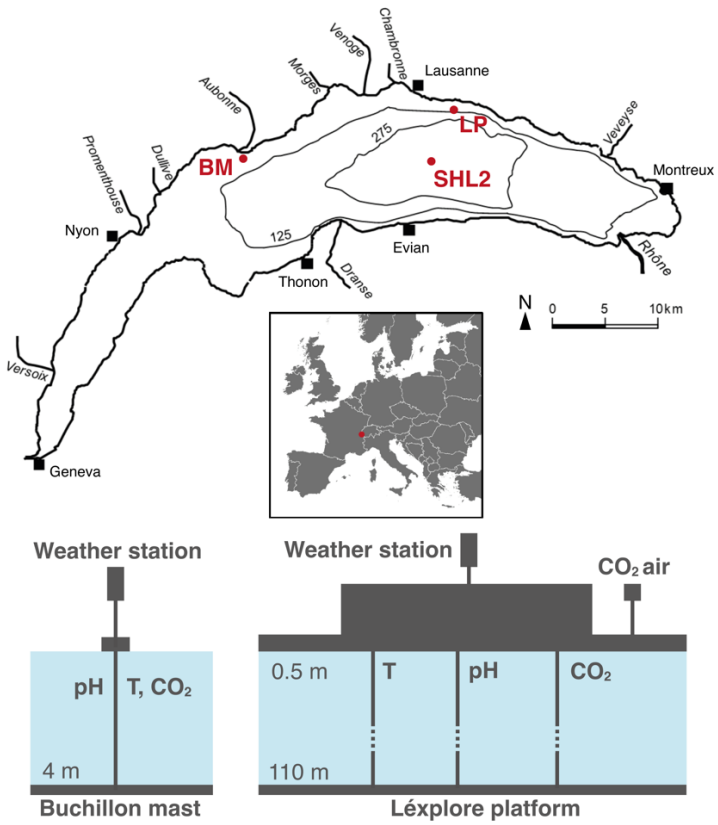

Fig. 3-1: The situation and map of Lake Geneva with the positions of the pelagic site, LéXPLORE platform (LP), the littoral site, Buchillon mast (BM), and of monthly or fortnightly sampling site (SHL2) since the late 1950s. The field instrumentation scheme shows the main measurements needed for this study: water temperature (T), pH, CO_2 concentration in water (CO_2), atmospheric CO_2 concentration (CO_2 air), and the weather station.

3.3.2. Field methods

Dissolved pCO_2 was measured every 30 min by miniCO_2 sensors (Pro-Oceanus System Inc.). These sensors have an accuracy of < 5% and a range of 0-2,000 ppm. They were calibrated with two standards (0 and 2,000 ppm) and one control of atmospheric gas (~400 ppm) with a CO_2 gas analyser (Licor 830) every 4-6 weeks and corrected considering the drift if necessary. pH was recorded every 15 min by HOBO sensors (HOBO). The calibration and the post-correction were performed following Escoffier et al. (In preparation). Water surface temperature was measured every minute at 50 cm depth using a Minilog II-T (VEMCO, resolution 0.01° C). On the LéXPLORE platform and the Buchillon mast, local weather conditions (air temperature, wind speed and direction, relative humidity, short-wave radiation, and atmospheric pressure) by a Campbell Scientific automatic weather station were continuously recorded at 10 minutes intervals, while only the LéXPLORE platform was equipped with an atmospheric CO_2 sensor connected to the weather. In the two study sites, fetch distance (m) with the lake shores was measured considering wind direction (Perolo et al., 2021) using data from the Federal Office of Topography online portal (Swisstopo geoportal: geo.admin.ch), allowing to compute significant wave height, H_s (m), according to Hasselmann et al. (1973). Finally, all variables were gridded at an hourly time step.

3.3.3. CO_2 gas exchange computing

To compute CO_2 gas exchange (Eq. 3-1), the gradient of partial pressure of CO_2 (ΔpCO_2) between the surface water and the saturation was corrected for altitude (µatm). The gas solubility coefficient, α (µmol cm^{-3} μatm^{-1}), depending on the measured water temperature, was estimated following Wanninkhof (1992). Regarding the gas transfer velocity, k (cm h^{-1}), three models were chosen considering different levels of complexity to compare their CO_2 flux estimation (i) when all the input variables were in high frequency and (ii) when the chemical enhancement was integrated into the inward fluxes. The first k model was an empirical wind-based model (*CC98*) from Cole and Caraco (1998), one of the most common in the literature, whose input variable is the wind speed at 10 m (U_{10}). The following two k models were process-based models that attempt to link k directly to near-surface turbulence using the surface renewal model (SRM). In the theories (Danckwerts 1951; Lamont and Scott, 1970), k depends on the product of the turbulent kinetic energy dissipation rate (ε) and the kinematic viscosity of water (υ), both to a power of one-quarter as follows:

$$k = a_1(\varepsilon\upsilon)^{1/4} Sc^{-1/2}\,, \qquad (3\text{-}2)$$

where a_1 is a constant calibration parameter, and Sc is the Schmidt number. Thus, the second k model (*R12*) is based on the turbulent kinetic energy dissipation rate generated by two components, wind shear and convection, mainly derived from U_{10} and buoyancy flux (B_0) (Read et al., 2012, following Soloviev et al., 2007). The third k model (*P21*) was explicitly developed in Lake Geneva for large lakes having high wind speed (> 5 m s^{-1}) and long fetch distance (> 15 km), accounting for surface waves. *P21* integrated wind-driven surface waves whose effect can be split into wave action and wave breaking, producing bubble formation. U_{10} and H_s are the main input variables (Perolo et al., 2021). These three k models are detailed with all the necessary variables in Perolo et al. (2021).

In alkaline hardwater lakes such as Lake Geneva, with typical pH values between 7.8 and 9, respectively in winter and summer), the DIC pool is mainly composed of bicarbonates (HCO_3^- > 95%; Stumm and Morgan, 1981). Therefore, in high pH and high HCO_3^-, chemical enhancement (CE) significantly increases atmospheric CO_2 invasion (Wanninkhof and Knox 1996). The CE calculation depends mainly on the pH value and the water temperature and on the choice of the *k* model used (e.g., a greater *k*-value related to a lower chemical enhancement factor). Thus, the three *k* models could generate different CEs and potentially different inward fluxes. The analysis is restricted to the six months during which pH values are high enough to induce CE (July-December).

3.3.4. Temporal analysis

The temporal analysis of this study is divided into three successive steps. The first step compares the CO_2 flux estimations considering the three *k* models previously selected over six months (July to December 2020), in order to evaluate how much the choice of the *k* model, through the computation of CE, affects estimates of inward and outward CO_2 fluxes. Once the *k* model and CE validated, the second step quantifies the temporal variability of atmospheric CO_2 and assesses errors in annual CO_2 fluxes due to the sampling frequencies (high frequency to annual mean) of atmospheric CO_2. Finally, the third step assesses the loss of information in the annual CO_2 gas exchange computation introduced by loosely time-resolved CO_2 concentration in water over the year comparable to those conducted by long-term observatories. For example, the pluri-decennial, routine monitoring survey of Lake Geneva has relied on monthly-fortnightly boat samplings (i.e. 15 and 20 times per year) at the same hour (close to 11:00 UTC) at the lake deepest point (SHL2; Fig. 3-1). Such samplings can only be carried out for low wind conditions. Therefore, we use the 2020 SHL2 monitoring dates to sample the pCO_2 values in our high-frequency dataset (annual cycle 2020 in the pelagic site) at 12:00 local time to evaluate the flux estimations. We also sample at 18:00, 00:00, and 06:00 local times to know if a specific time in the daily cycle would produce fewer errors. Then, we interpolate pCO_2 data along the annual cycle with Piecewise Cubic Hermite Interpolating Polynomial (PCHIP; Fritsch and Carlson, 1980) to compute CO_2 gas exchange and compare with the periods of high-frequency measurements.

3.3.5. Spatial variability

In Lake Geneva, which large and very deep, littoral areas represent only a minimal share of the lake surface. Considering an average euphotic depth of 10-15m over the last decade (CIPEL, 2020), the littoral habitat would represent in between 10% and 15% of the total lake surface area (based on bathymetric data, not shown). Yet, CO_2 fluxes can be greater and more temporally variable in littoral than in pelagic habitats (Larmola et al., 2004; Paranaíba et al., 2018; Loken et al., 2019) and we question whether littoral fluxes would matter within the total lake budget. We use the most complete annual data-series from both the pelagic and littoral habitats : from January to December 2020 at the Lexplore site (pelagic; Fig. S3-1) and from August 2019 to July 2020 at Buchillon (littoral; Fig. S3-2). The CO_2 gas exchange is computed from all the high-frequency variables except for atmospheric CO_2, where the results of step 2 are introduced. The distributions of the inward, outward, and balance fluxes are then analysed on a seasonal and annual scale with those of the *k* integrating the CE and the ΔpCO_2 to highlight the variable generating the most significant difference between the two study sites and at which season.

Finally, we conceptualise an extrapolation of the results from the two study sites to the lake scale by considering their spatial distribution according to depth, from which we estimate a total flux balance at the annual scale.

3.4. Results

3.4.1. Effect of chemical enhancement on CO_2 gas exchange

Fig. 3-2 present fluxes estimated from the three *k* models, excluding or including estimates for chemical enhancement. The six months of computation (from July to December) cover major lakes conditions, i.e. (summer) stratification, (fall) transition period and (winter) cooling convective phase.

Time series of CO_2 fluxes at the air-water interface including CE are illustrated in Fig. 3-2 (a). Notwithstanding the *k* model used, computed CO_2 fluxes are inward from July to mid-October before they shift outward. Inward flux (~1 mmol m^{-2} h^{-1}) is twice higher than outward flux (~0.5 mmol m^{-2} h^{-1}), but the flux peaks are much more pronounced during the outward flux. Estimates of inward or outward fluxes at low wind speed (LW < 5 m s^{-1}) are very similar regardless of the selected *k* model (Figure 3-2 (c) (Inward -LW, Outward-LW, and Balance-LW). However, estimated CO_2 fluxes differ significantly during high wind events (HW ≥ 5 m s^{-1}; Fig. 3-2 (a) and (b): Inward-HW, Outward-HW, and Balance HW). *P21* simulates the strongest fluxes by integrating the four components producing turbulence (wind shear, convection, wave action, and bubble formation), while simulated fluxes are 25% and 50% lower with *R12* and *CC98* respectively.

Including CE has only significant effect of estimated inward fluxes at low wind (i.e. doubling inward fluxes at low wind, Fig. 3-2 (b) and Fig. 3-2 (c): Inward-LW). However, the magnitude of the CE effect is similar between *k* models during inward flux (for CC98 2.0 ± 0.8, R12 2.1 ± 2.8 and *P21* 1.8 ± 2.2) and outward flux (for all models 1.1 ± 0.1) so that the integration of CE in the CO_2 flux computation leads to similar results (0.2-1.3 mmol m^{-2} h^{-1}) regardless of the *k* models chosen (Fig. 3-2 (b)). Even though the CE effect is limited to inward flux (0.5-1.4 mmol m^{-2} h^{-1}), and is greater at low than high windspeed, including or excluding CE changes the direction of estimated CO_2 flux (Fig. 3-2 (c): Balance-CE and -no CE); the lake being a source over the 6 months of computation when CE is neglected, and becoming a sink when CE is included. In the following sections, fluxes will be computed using *P21* as *k* model and always accounting for CE.

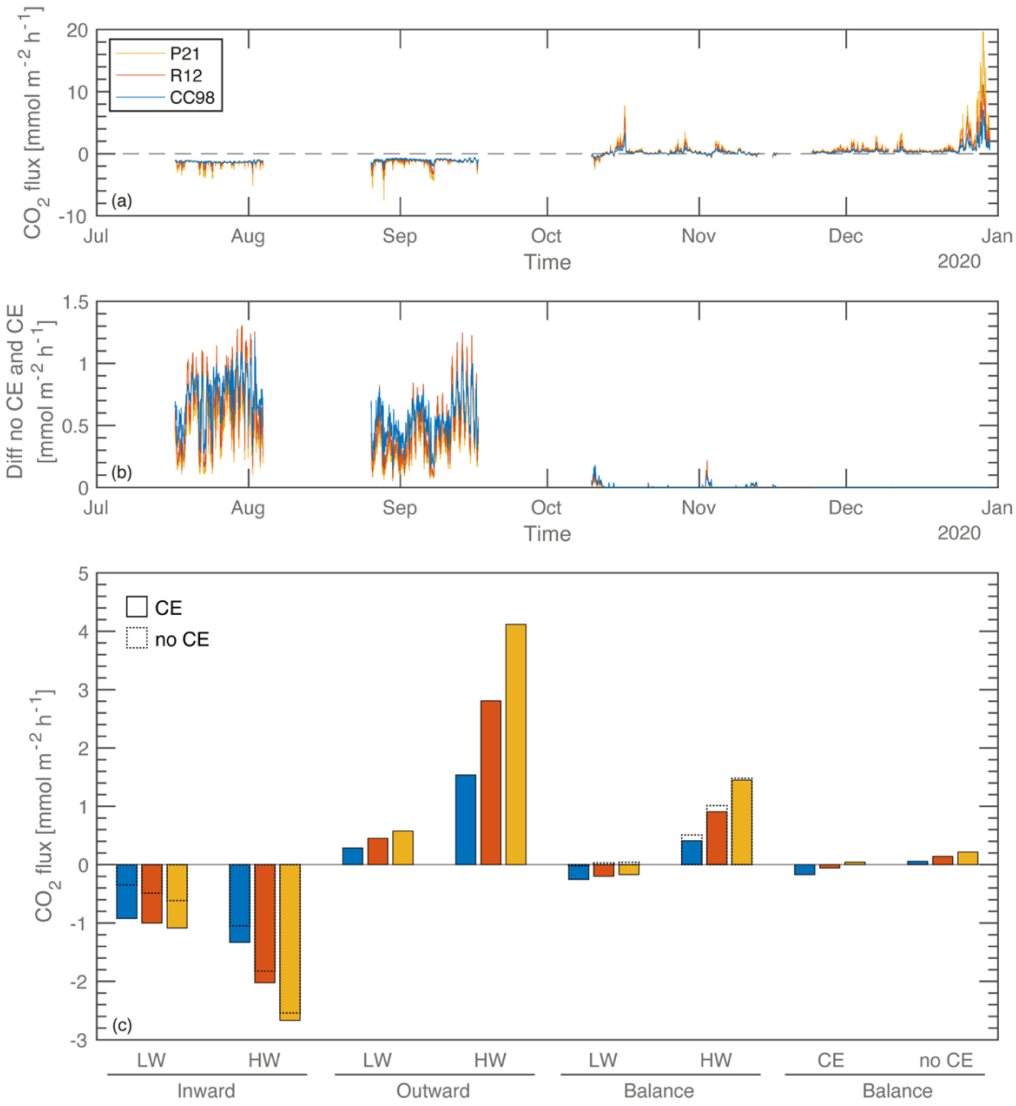

Fig. 3-2: (a) Time series of CO_2 flux (mmol m^{-2} h^{-1}) computed with three *k*-models (*P21*, *R12*, and *CC98*) and the chemical enhancement (CE) where all input data are in high frequency (1-hour timestep). **(b)** Difference of CO_2 flux between the computation with CE and without CE. **(c)** Mean CO_2 flux value considering the different categorisations: inward and outward fluxes at low wind (LW; < 5 m s^{-1}) and strong wind (SW; ≥ 5 m s^{-1}); Balance between inward and outward flux at low and strong wind; Balance between inward and outward fluxes with and without CE.

3.4.2. Atmospheric CO_2

Over a full annual cycle (July 2020 to April 2021), atmospheric CO_2 ranges from 380 ppm up to 500 ppm, for an average value of 405 ppm ± 19 ppm. There is no clear seasonal dynamics of the atmospheric CO_2 measured above the lake, neither from hourly data (Fig 3-3 (a)), nor from monthly averages (Fig. S3-3). However, atmospheric CO_2 was tied to windspeed, with narrower range of variation and lower average values for atmospheric CO_2 at greater windspeeds (i.e. range: 120 ppm for 1 m s^{-1} and 30 ppm for 10 m s^{-1} (Fig. 3-3 (b)). Fig. 3-3 (c) highlights this effect of high wind on the dynamics of atmospheric CO_2 with an average of 390 ppm ± 10 ppm, while at low wind, this average rises to 410 ppm ± 19 ppm.

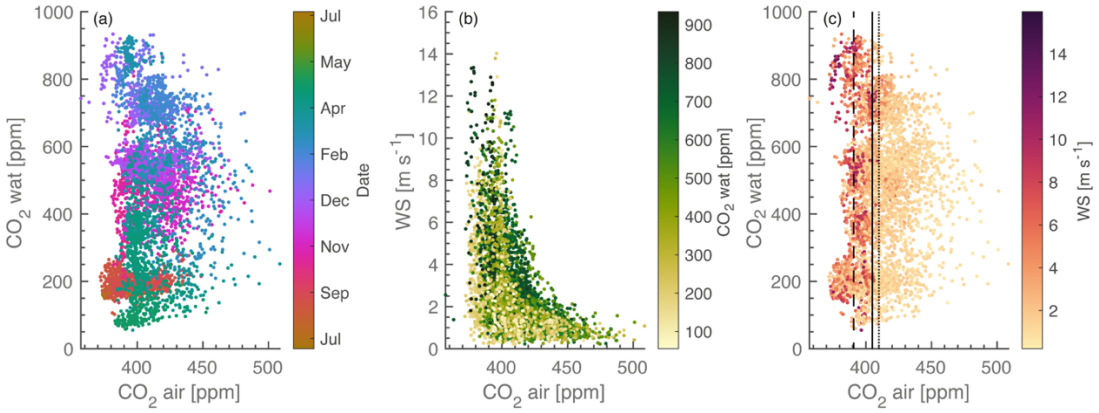

Fig. 3-3: (a) Relation between CO_2 air and CO_2 wat coloured according to the months of the year; (b) relation between CO_2 air and wind speed coloured according to the CO_2 wat; (c) relation between CO_2 air and CO_2 wat coloured according to wind speed. The solid black line is the annual mean of CO_2 air; the black dash line is the mean of CO_2 air for wind speed ≥ 5 m s^{-1}, and the dotted black line is the mean of CO_2 air for wind speed < 5 m s^{-1}.

For the same six-month period, we compute the CO_2 gas exchange by fixing only the atmospheric CO_2 to its annual average (405 ppm), to the monthly averages, and to a wind-dependent value, i.e. 390 ppm at high wind speed (≥ 5 m s^{-1}) and at its monthly average for at low windspeed. Overall, there is a very limited impact of the frequency of the atmospheric CO_2 data on estimated fluxes (Fig. 3-4). For low wind speed, all estimates are identical to high frequency (0.16 mmol m^{-2} h^{-1}). For high wind speed, estimated values decrease along with the sampling frequency, but the effect remains minor (19% for the annual average, 18% for the monthly averages, and only 3% for the addition of the wind condition). As the variability of the atmospheric CO_2 is 20 times smaller than the change in water CO_2, it is of second order within final estimates of CO_2 fluxes and does not require to be measured at high frequency. The last method which combined monthly averages and wind-dependent conditions leads to final fluxes estimates that are the closest to the high-frequency reference estimates, while remaining a straightforward method to apply. This is the method that was applied in the following sections.

Fig. 3-4: Mean CO_2 flux value for low wind (LW; < 5 m s^{-1}) and strong wind (SW; ≥ 5 m s^{-1}) considering different atmospheric CO_2 data used in the computing: **(left to right)** annual average (405 ppm), monthly averages, wind-dependent values, i.e. monthly averages except at wind speed ≥ 5 m s^{-1} (i.e. 390 ppm), and high-frequency data.

3.4.3. High to low frequency of water CO_2 concentration

To evaluate the loss of information when water CO_2 concentrations are sampled at a low frequency over a year, as in the case of long-term monitoring in Lake Geneva, we perform the analysis on the annual cycle of 2020 in the pelagic environment. The CO_2 high-frequency data series is resampled according to the actual dates at which the long-term monitoring survey was performed at SHL2 in 2020 (Fig. 3-5 (a) and Fig. S3-4). The average wind speed at the sampling dates is ~1.5 m s^{-1}, while the annual average wind speed is twice higher (~2.9 m s^{-1}), confirming that field sampling on large lakes reflect specific, calm weather conditions.

The interpolations of water CO_2 sampling dates at different day hours (0:00, 06:00, 12:00, and 18:00) are presented in Fig. 3-5 (a). The longest gaps between sampling dates occur during the shoulder periods (in March, October, and November) and during the intense events in winter. Both undersampled periods coincide with the time-periods of the greatest water CO_2 variability. In summer, the water CO_2 variability being low, these interpolations overlap well with high-frequency data. These differences generated by the low sampling frequency are reflected in the cumulative CO_2 flux, i.e. the deviation of high-frequency estimate (black line) compared to low frequency (coloured lines; Fig. 3-5 (c)). The differences between the high-frequency CO_2 fluxes (Fig. 3-5 (b)) and those carried out at low frequency and at different times of the day are also greater in March, October, and November (see Fig. S3-5 (a-d)), leading to an underestimation of the outward fluxes. On the other hand, few errors are produced during the inward flux (Fig. 3-5 (c)) except for the sampling carried out at midnight (Fig. S3-5 (d)).

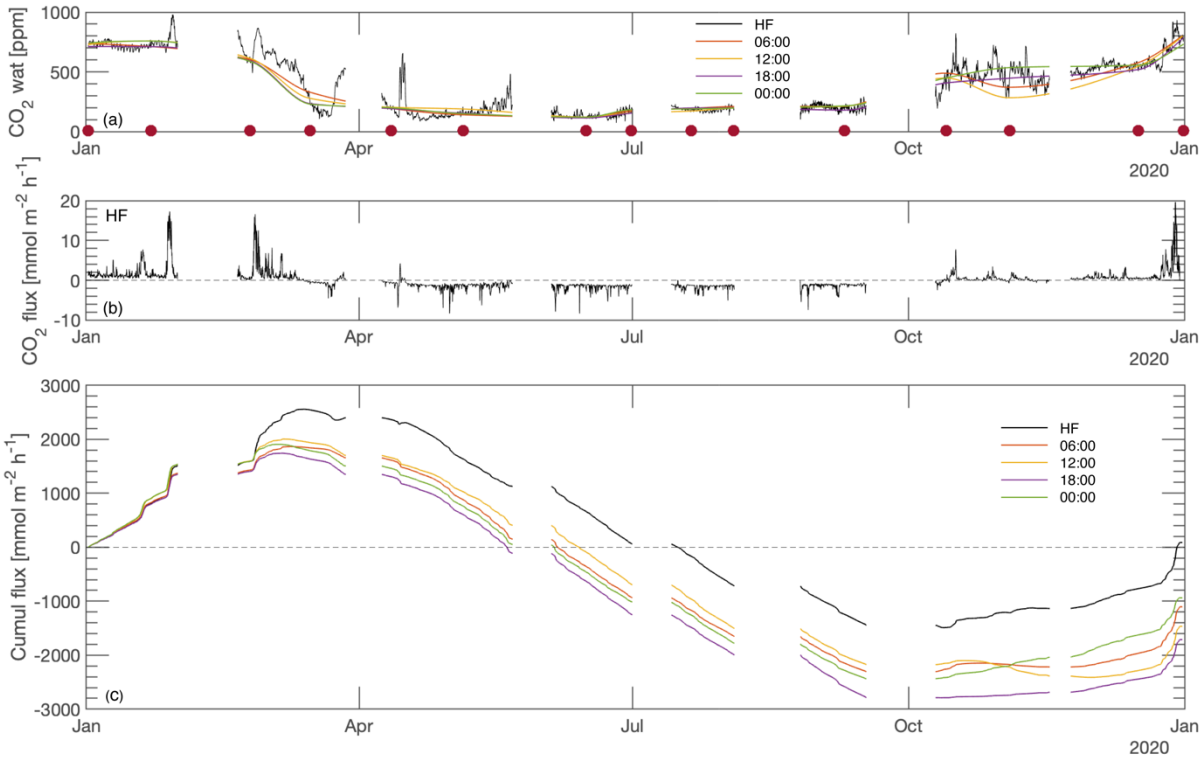

Fig. 3-5: (a) Time series of CO_2 wat (ppm) along an annual cycle with the punctual sampling days and the interpolation of these days regarding the sampling hour done (06:00, 12:00, 18:00, and 00:00); **(b)** CO_2 flux (mmol m^{-2} h^{-1}) computed using high-frequency CO_2 wat and the *P21* model for the gas transfer velocity; **(c)** Cumulative CO_2 fluxes regarding the five computations.

In summary, CO_2 flux estimates computed from water CO_2 measured at a frequency mimicking that of the monitoring survey of Lake Geneva underestimate outward flux over the whole year. While the reference, high-frequency dataset leads to a slightly outward flux balance, i.e. Lake Geneva as a carbon source, low-frequency data would conclude to an inward flux balance, a carbon sink. Note that this first annual approximation in the pelagic environment is based on 70% of the complete cycle.

3.4.4. CO_2 gas exchange in the pelagic and littoral areas

Here, we scrutinise the spatiotemporal variability of the CO_2 gas exchange, assessing the sensitivity of estimates to k and ΔpCO_2 throughout the seasons (Fig. 3-6).

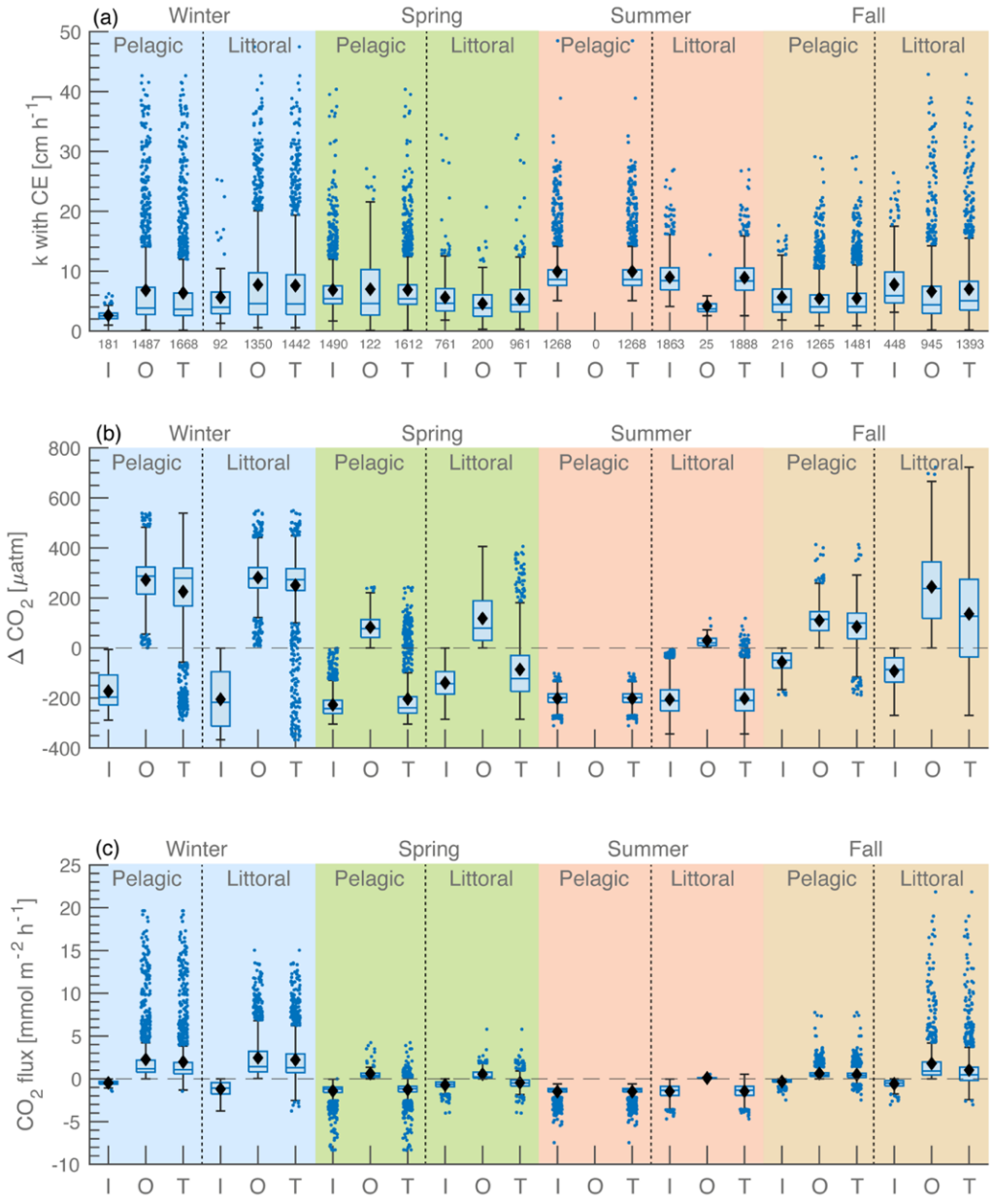

Fig. 3-6: Boxplots and mean values (black diamond) of: **(a)** *P21 k* model, **(b)** ΔpCO_2, and **(c)** CO_2 flux categorised according to the season as well as their flux directions (I: inward, O: outward) and their total (T).

The spatial variability of k shows similar results in the pelagic and littoral environments for spring and summer (Fig. 3-6 (a)). In contrast, the k values are slightly higher in the littoral environment during fall and winter. The temporal variability of k changes over these seasons, with greater values in winter, due to the intense wind events occurring more regularly in this season, and in summer due to the increase in k through chemical enhancement. On the other hand, the spatiotemporal variability of ΔpCO_2 is more heterogeneous (Fig. 3-7 (b)). The winter season provides identical distributions of ΔpCO_2 in both environments. However, the CO_2 differentials differ significantly during the shoulder periods, with a negative differential that is twice as high in the pelagic site in spring and, conversely, a positive differential 50% greater in the littoral area in fall. In summer, the mean distributions of ΔpCO_2 between both sites are similar, but the range of values is twice larger in the littoral as compared to the pelagic (300 µatm and 150 µatm respectively).

Therefore, the spatiotemporal variability in both k and ΔpCO_2 affects the CO_2 flux estimates (Fig. 3-6 (c)). In winter, outward fluxes are the strongest of the year in both environments. These average fluxes are 10% higher in the littoral than in the pelagic (2.2 and 2 mmol m^{-2} h^{-1} respectively), which can be explained by slightly stronger k in the littoral. Conversely, fluxes go inward both the littoral and pelagic in spring, but the inward pelagic fluxes are more than twice higher (-1.25 mmol m^{-2} h^{-1} for -0.45 mmol m^{-2} h^{-1} in the littoral). CO_2 fluxes are similar during the summer season despite the more pronounced daily variations of ΔpCO_2 for the littoral site (Fig. S3-1 and S3-2). Fall fluxes go outward but are twice greater in the littoral than the pelagic (1 and 0.49 mmol m^{-2} h^{-1}, respectively). From spring to fall, differences in fluxes intensity between the littoral and pelagic sites are caused by their different ΔpCO_2, rather than any spatial variability in k. Finally, we can highlight three distinct dynamics of CO_2 gas exchange throughout the year in Lake Geneva composed of a first period of high outward flux (winter), a second of inward flux (summer), and a third of alternating inward and outward fluxes (spring and fall).

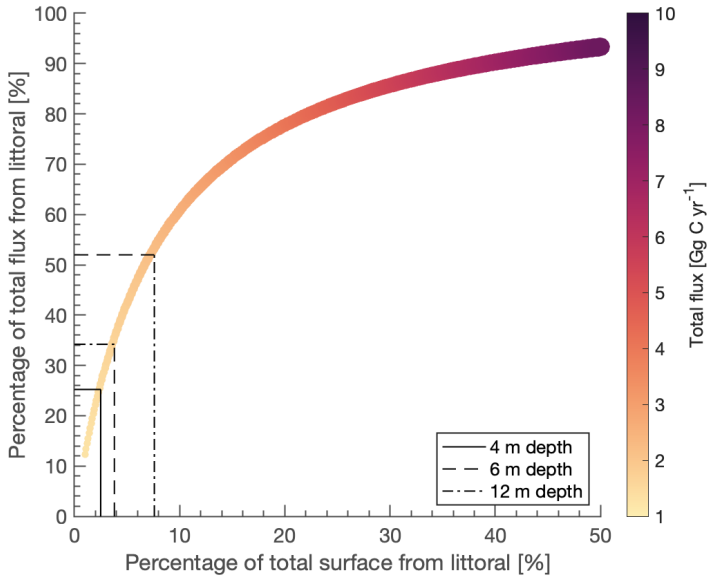

Fig. 3-7: Total annual flux estimation on Lake Geneva integrating the littoral flux to the pelagic flux considering to a change in the proportion of the littoral area (0-50% of the total area of Lake Geneva). Four depths (4 m, 6 m, and 12 m) are added on the figure to highlight the proportion of littoral surface and flux that could generate regarding the depth limit defining the littoral area.

From the high-frequency times series from both monitoring sites (~70% of the whole year), annual CO_2 fluxes are estimated at 1.92 g C m^{-2} yr^{-1} for the pelagic site, more than an order of magnitude greater in the littoral with 26.8 g C m^{-2} yr^{-1} . The annual difference in fluxes comes from the lower inward mean flux in spring and greater outward mean flux in the fall for the littoral (Fig. 4-5). When extrapolated to the whole lake, considering four depth limits for littoral areas (4 m, 6 m, and 12 m) from which the lake's littoral surface area could be computed (Fig. 3-7), littoral fluxes could generate 25-50% of the total flux of the lake, while representing only 2-8% of the lake surface area. Accounting for littoral areas would increase the overall estimate for CO_2 flux to the atmosphere from 1 Gg C yr^{-1} to 3 Gg C yr^{-1}. This conceptual extrapolation nevertheless suggests that littoral flux should be included in total flux estimates even for large and deep lakes where littoral areas represent a very low share of the whole surface.

3.5. Discussion

3.5.1. Relevant variables and their frequency

The terms of the CO_2 flux equation have significant temporal and spatial variability at the lake scale. High-frequency measurements are a significant asset for better understanding the processes involving these variations and quantifying these gas exchanges with a greater accuracy. However, this study shows that it is unnecessary to get all the variables on an hourly scale to reach a reliable estimate of the annual flux balance (Fig. 3-8).

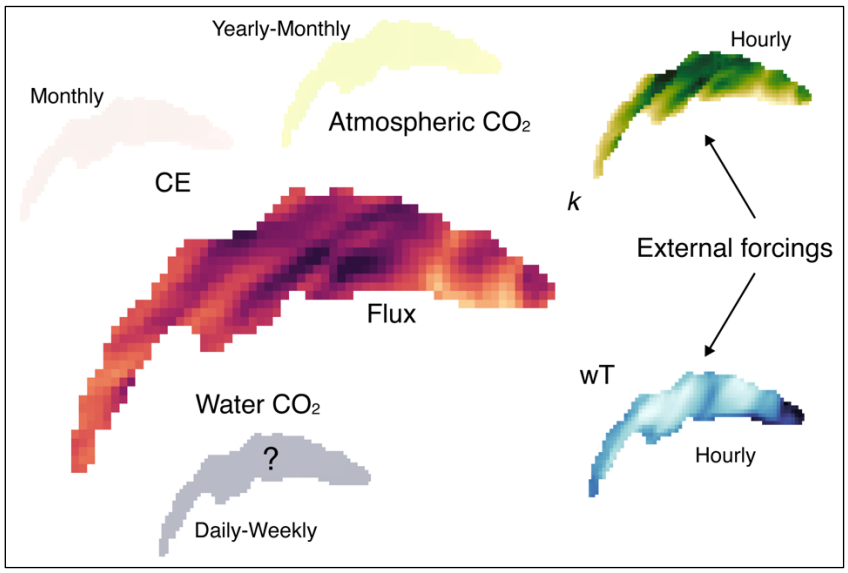

Fig. 3-8: Scheme of different frequency (time and space) proposed for each variable of the CO_2 flux equation considering the study results and literature.

The study of *k* models shows the importance of high-frequency data to capture intense meteorological events occurring over a short period, since those can strongly impact the annual flux estimates (Fig. 3-2). The need to account for surface waves in large lakes has already been shown in Perolo et al. (2021). Accurate estimates of annual CO_2 flux require high-frequency estimates of *k*, which get nevertheless easier to obtain. Most *k* models have been implemented in user-friendly packages (e.g. R Lake Metabolizer; Winslow et al., 2016). Besides, input data to *k* models can be acquired simply at high frequency by meteorological stations and water temperature

sensors or by spatial weather models and 1D or 3D hydrodynamic models allowing a representation of spatial variability of the gas transfer velocity (Perolo et al., 2021; Fig. 3-8).

On the other hand, although the calculation of the CE depends on the choice of the *k* model, it generates little difference in terms of computed inward flux. Actually, in between k-models, the value for *k* differs mostly at high wind, while the CE has little effect in these conditions (Wanninkhof and Knox, 1996). The addition of CE in pH conditions encountered in Lake Geneva (8.4-9) is significant because it doubles the inward flux during the warm period of high CO_2 undersaturation and can change the annual balance (Fig. 3-2). This result is similar to the estimate made using monthly and seasonal CE data in Perolo et al. (2021), demonstrating that the necessary pH value can be integrated at low frequency (monthly) into flux estimates (Fig. 3-8).

The decrease in the frequency of atmospheric CO_2 data until an annual average generates little difference in the average estimate of the CO_2 fluxes, especially for the inward fluxes (Fig. 3-4). The integration of monthly averages slightly improves outward flux estimates. In addition, strong windspeeds (> 5 m s^{-1}) significantly affect the dynamics of atmospheric CO_2 leading to a baseline of 390 ppm (Fig. 3-3), which is explained by a mixing of the air column and homogenisation of the air concentration. Adding this simple condition to the computation during high wind also increase the outward flux estimates keeping a higher ΔpCO_2 (Fig. 3-4). The temporal analysis of the atmospheric CO_2 variability deserves in-depth studies concerning its impact on the CO_2 flux estimates at the intraday scale.

The use of low-frequency data (biweekly or monthly) for water pCO_2, i.e. typical frequency of the long-term monitoring of Lake Geneva leads to substantial underestimates of the outward flux compared to the high-frequency reference estimates (Fig. 3-5), due to the loss of intense events in terms of water conditions (mixing dynamics). In addition, these underestimations change the annual balance from a carbon source lake to a carbon sink lake (Fig. 3-5 (g)). The loss of information occurs mainly during fall and spring when the inter-daily variability of CO_2 is greatest between a succession of days favouring GPP that decreases the concentration at surface and intense wind events mixing the water column and remobilising CO_2 from the bottom to the surface. Yet, the fact that samplings are done during daytime minimally affect final estimates. Thus, variations of water column stability and metabolism rate influence the surface CO_2 dynamics of Lake Geneva during the shoulder period, as demonstrated in Perolo et al. (in review, chapter 4). In addition, the maintenances of high-frequency sensors produce gaps in the annual cycle of up to a few weeks for various technical, logistical, and weather conditions reasons. As a result, only 70% of the year is monitored, and the remaining 30% could also lead to discrepancies in the annual balance.

Therefore, the water pCO_2 is the most challenging variable of the flux equation to acquire at a high frequency over a long period and can produce the greatest error when estimating the gas exchange over a year if it is poorly monitored. Different solutions can be applied depending on the study's objectives, available resources, and prior knowledge of the system studied. In the case of low-frequency sampling, the substantial variations of pCO_2 are linked in many studies to the mixing dynamics (e.g. MacIntyre and Melack, 2009; Åberg et al., 2010; Ojala et al., 2011). These specific periods should be more intensely monitored to capture the daily or weekly changes better. However, weather-dependent boat sampling will always be biased.

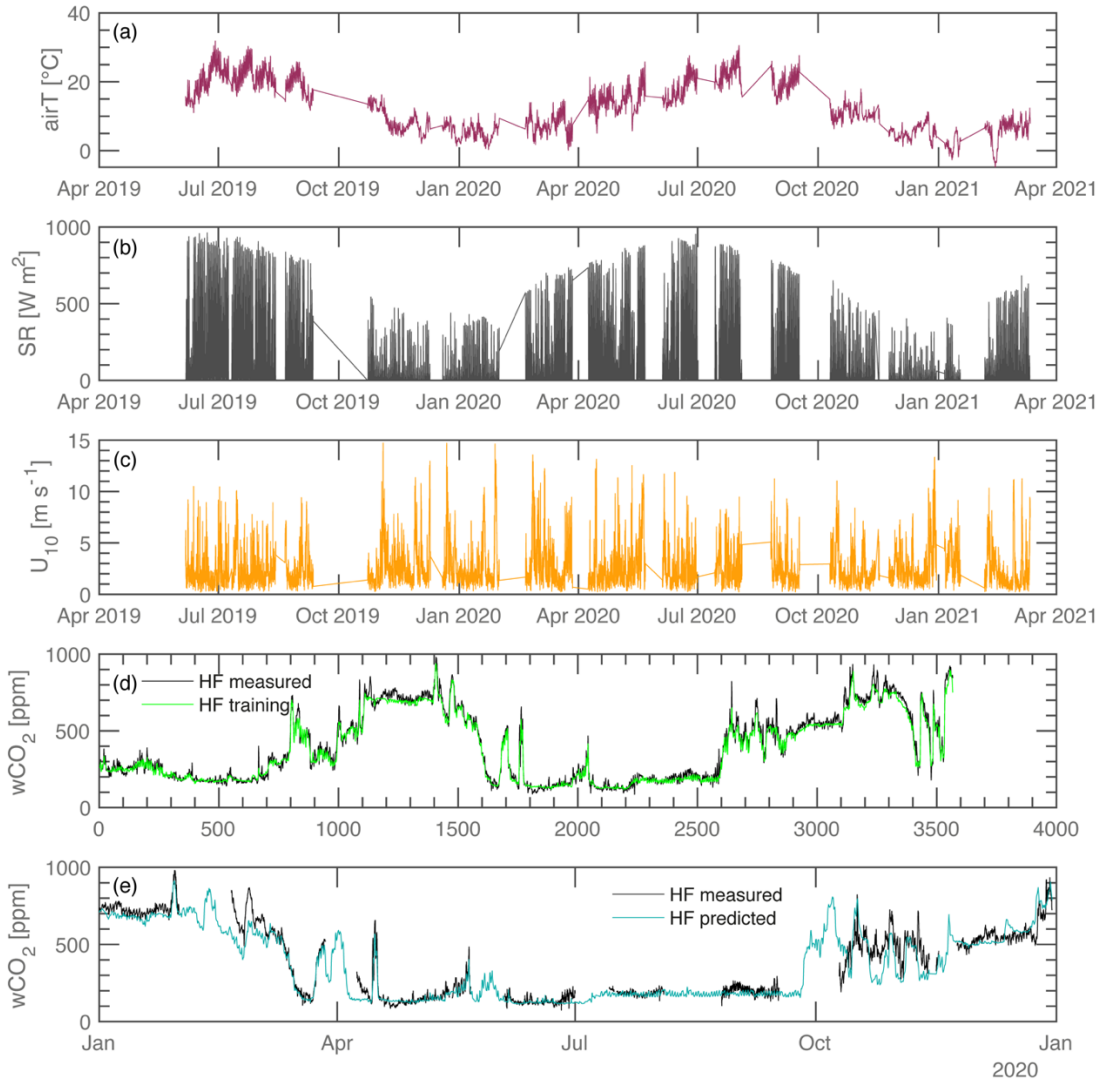

Fig. 3-9: (a-c) Three inputs of the prediction model to generate water CO_2 after training, validation, and test (details in Fig. S3-6, S3-7, S3-8); **(d)** High-frequency CO_2 measured and trained dataset generated by the prediction model; **(e)** Water CO_2 concentration recorded in the pelagic environment of Lake Geneva in 2020 (black line) and water CO_2 concentration predicted using air temperature, solar radiation, and wind speed in 2020 (blue line). This preliminary result gives a good accuracy all year (model behaviour) but still a low precision, especially during the transition period.

Here, as a proof of concept, we propose a solution to reconstruct the missing CO_2 data produced by the maintenances of high-frequency sensors. This approach uses a digital deep learning tool, Long Short-Term Memory (LSTM) Networks (Hochreiter et al., 1997), a type of recurrent neural network (RNN). The goal is to create a data-driven model for filling in the gaps in the 2020 annual cycle in the pelagic environment using external variables (predictors, here: air temperature, solar radiation, and wind speed; Fig. 3-9 (a-c)) that have been collected continuously over the entire year (Fig. S3-1). The LSTM model trains on the periods when the predictors and the CO_2 were recorded simultaneously (Fig. 3-9 (d)). Above all, we must define the training, validation, and testing

period of the model before the simulations. Three different fractionations were performed (see details in Fig. S3-6, S3-7, and S3-8).

The model, trained, tested, and validated, is applied to the 2020 annual cycle. The best preliminary result is shown in Fig. 3-9 (e). The predicted CO_2 dynamics give a good accuracy throughout the year (model behaviour) with yet a low precision, especially during the transition period. The root mean square error between the recorded and reconstructed data is ~40 ppm. This reconstruction of the missing data could initially allow us to know whether or not it is essential to cover the entire annual cycle or whether, as in our case, 70% of the year is fairly representative. In a second step, this technique could estimate the water CO_2 over a more extended period using external data and better estimate the CO_2 flux. However, it would be necessary to deploy high-frequency sensors over at least for several one week-session, spread over the year, to capture the different dynamics to train and validate the model in each new studied system. In addition, other predictors should be added for interannual reconstruction, such as water temperature, water stability, and others, to better account for the different dynamics between years.

3.5.2. Spatiotemporal variability

This study highlights the great spatiotemporal variability of the CO_2 gas exchange of a large hardwater lake throughout the year. These variations of fluxes between the littoral and pelagic sites arise mostly from the water pCO_2, caused by mixing dynamics and metabolism (Perolo et al., in review, chapter 4), and to a lower extent by the variability in *k*. However, these two variables do not necessarily impact CO_2 fluxes on the same temporal scale. Indeed, we show that the *k* must be used at high frequency (hourly data) to represent its short time variability properly. At the same time, the pCO_2 could be integrated at a medium frequency (daily to weekly data) to keep a reasonable estimate of the CO_2 flux. These results agree with those of Natchimuthu et al. (2017), demonstrating that the variability of pCO_2 is greater and affects CO_2 flux more than *k* over long periods.

Three main flux dynamics are distinguished in the littoral and pelagic environments annually. First, the winter outward flux period has the strongest flux of the year. They are induced by the greatest absolute ΔpCO_2 of the four seasons (Fig. 3-6 (b)) produced by deep winter mixing bringing CO_2-rich bottom water to the surface. The highest *k* values further reinforce these high fluxes during winter's more frequent wind and waves events. Second, the summer inward flux period is relatively stable throughout the season. Only the daily cycles of ΔpCO_2 differ between the two study areas without generating any deviation from the summer average. The establishment of a strong stratification can explain the stability of the signal during the warm period isolating the surface layer from the CO_2 diffusion coming from the deep layers. In addition, the high levels of GPP encountered in summer (Fernández et al., 2021; Perolo et al., in review, chapter 4) lead to constant undersaturation on the surface of Lake Geneva. Third, the transition periods or shoulder periods (spring and fall) are alternated by inward and outward fluxes implied by the variations of pCO_2, which are generated by the same processes governing the winter and summer patterns. Nevertheless, these processes are of lower intensity and alternate more quickly over time. In the pelagic, slight stratification can be created in a few days of good weather, increasing GPP decreasing pCO_2 and producing inward flux. Then, following this period of calm, wind events destroy the weak stratification and

replenish surface CO_2, implying a change in flux direction towards the atmosphere. These rapid changes are, therefore, the most challenging to capture temporally. On the other hand, the littoral pCO_2 remained higher than in the pelagic because the shallow depth does not generate stratification and the surface layer remains in contact with the CO_2 flux from sediment.

As for the temporal variability of fluxes over long periods, the spatial variability is also generated more by the pCO_2 variable between the littoral and the pelagic, leading to an estimate of the littoral fluxes higher by an order of magnitude than in the pelagic. However, this result is to be discussed through the relevance of the two measurement points chosen on Lake Geneva. Indeed, this study shows that there is very little difference in terms of *k* between the two environments studied, but both sites are in the northern part of the lake. They, therefore, have the same wind and wave characteristics throughout the year, while the spatial study of *k* at the lake scale has shown strong heterogeneity during high wind (Perolo et al., 2021). The measured pCO_2 may not also represent a hotspot such as a river mouth (Paranaíba et al., 2018) or the involvement of anthropized coastline in CO_2 conditions. In addition, estimating the proportion of littoral flux over the entire lake (Fig 3-7) show the difficulty of defining the littoral surface, while the choice of this size can double the annual flux. Consequently, we believe that the spatial integration of fluxes must pass in future studies through a coupling of high-frequency measurements, 3D hydrodynamical model and data prediction tools.

3.6. Conclusion

The CO_2 gas exchange study of Lake Geneva demonstrates a high spatiotemporal variability throughout the year. The intensity of flux and their seasonal dynamics are very marked, and the littoral flux average was ten times greater than the pelagic. The CO_2 flux quantification integrated into time and space at the lake scale is still complex to perform accurately. However, high-frequency instruments are major tools for understanding flux dynamics and better estimating them temporally. The variables necessary for estimating CO_2 fluxes are relatively easily accessible at high frequency and even at a spatial level for regions equipped with spatial weather models and 3D hydrodynamic models. However, one of the most critical variables, water pCO_2, is still currently challenging to acquire, and its spatial modelling is not achieved. The democratisation of high-frequency CO_2 measurements in water systems may improve flux estimates and allow better monitoring in understudied systems. In addition, the coupling of these instruments with physical and biogeochemical models and new learning and prediction tools could provide a better spatial representation of these fluxes.

4.7. Supplementary

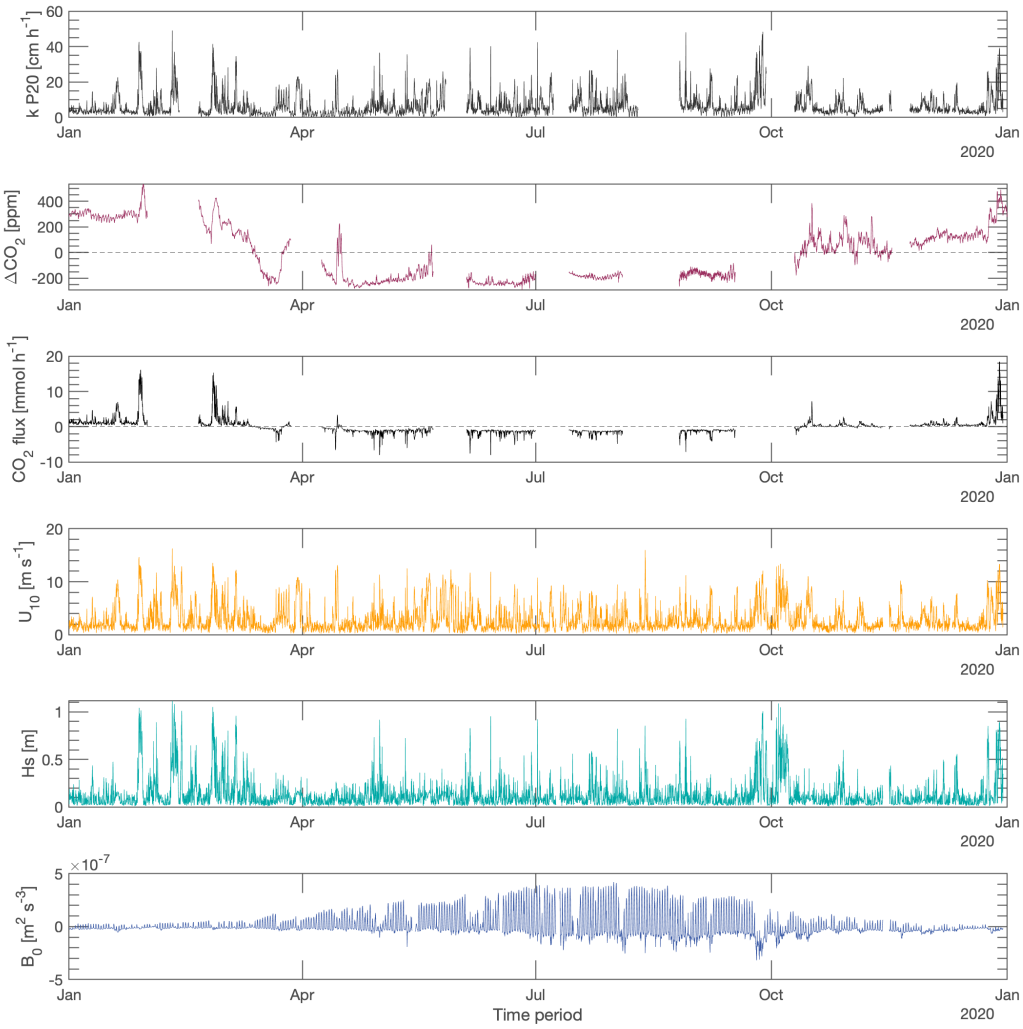

Fig. S3-1: Annual time series of the main variables used to compute CO_2 gas exchange and *k* model in the pelagic environment. **(Top to down)** *k P21* model; ΔpCO_2 , CO_2 gas exchange; three main inputs of *k* model: wind speed at 10 m (U_{10}), significant wave height (H_s), and buoyancy flux at surface ($\boldsymbol{B_0}$), and).

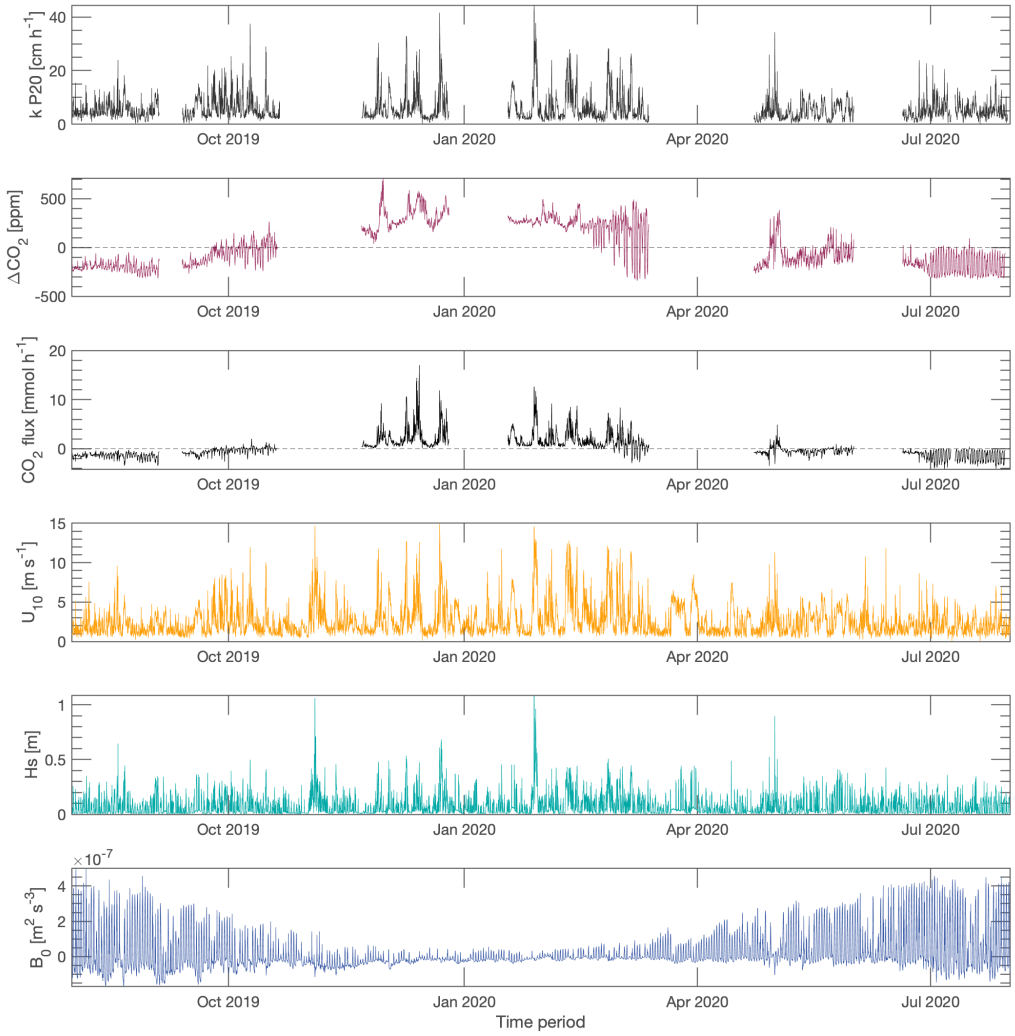

Fig. S3-2: Annual time series of the main variables used to compute CO_2 gas exchange and *k* model in the littoral environment. **(Top to down)** *k P21* model; ΔpCO_2 , CO_2 gas exchange; three main inputs of *k* model: wind speed at 10 m (U_{10}), significant wave height (H_s), and buoyancy flux at surface ($\boldsymbol{B_0}$), and).

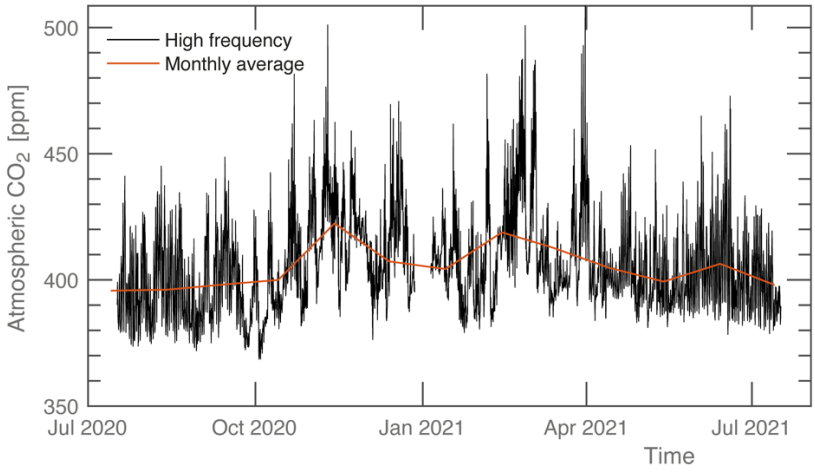

Fig. S3- 3: Time series of atmospheric CO_2 (1-hour timestep) and the monthly average.

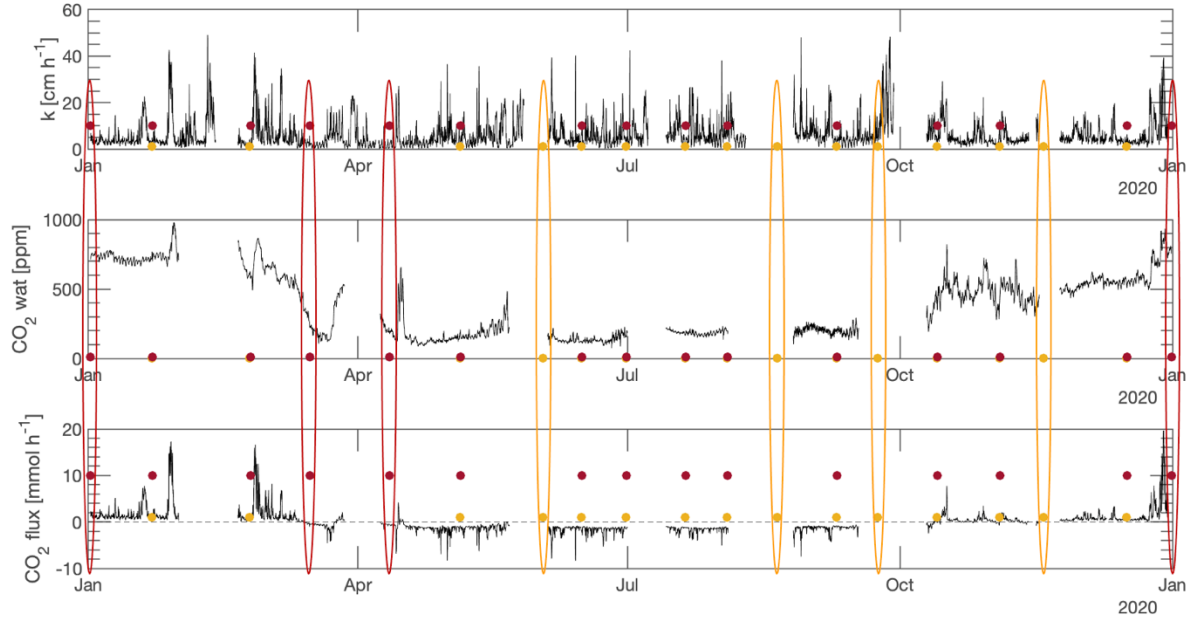

Fig. S3-4: (Top to down) Representation of annual time series of *k P21* model, CO_2 in water, and CO_2 flux. Orange points are the exact dates of SHL2 water sampling done by CIPEL in 2020 (15 dates). Orange ellipses are the SHL2 dates which do not correspond to the periods of high-frequency measurements. Red points are the dates used in the analysis of the section 3.4.3 (15 dates). Red ellipses are the dates added at the beginning and the end of the year for the technical reasons of interpolation as well as two dates added in March and April when samplings could not be done due to the COVID lockdown.

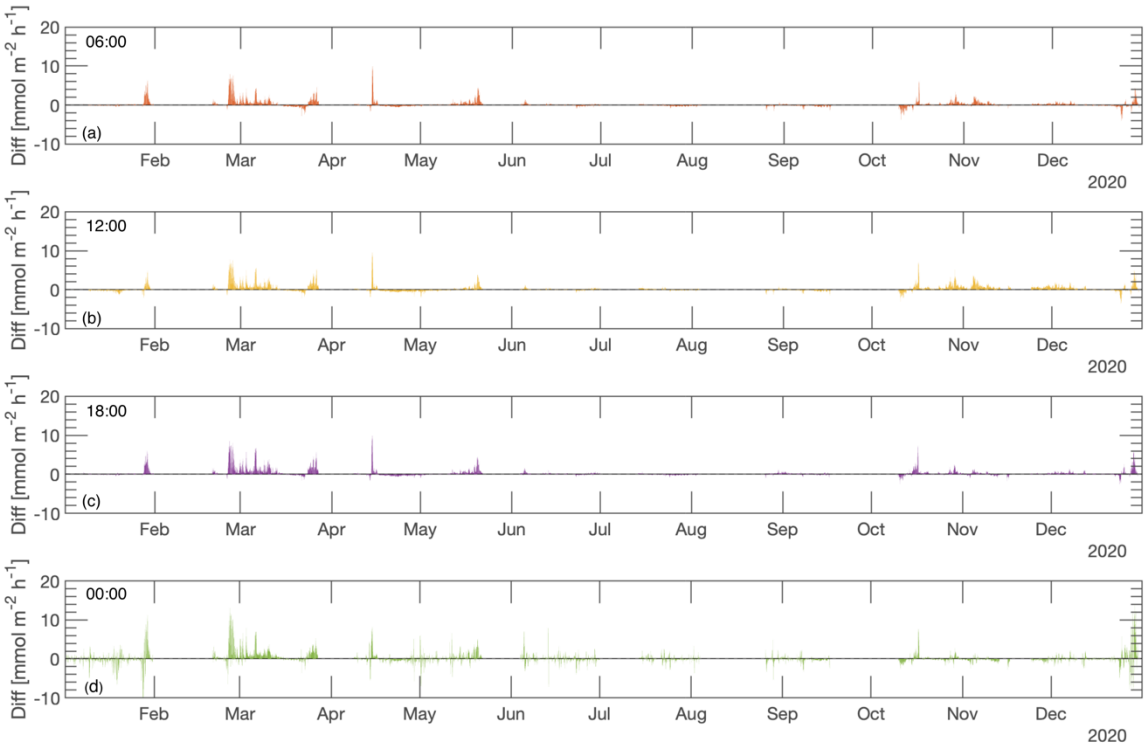

Fig. S3-5: (a-d) Difference of CO_2 flux between the computation done with high-frequency CO_2 wat and the computation done with low frequency regarding the sampling hour done during the day: 6:00, 12:00, 18:00, and 00:00 respectively (positive values are underestimation and negative values are overestimation).

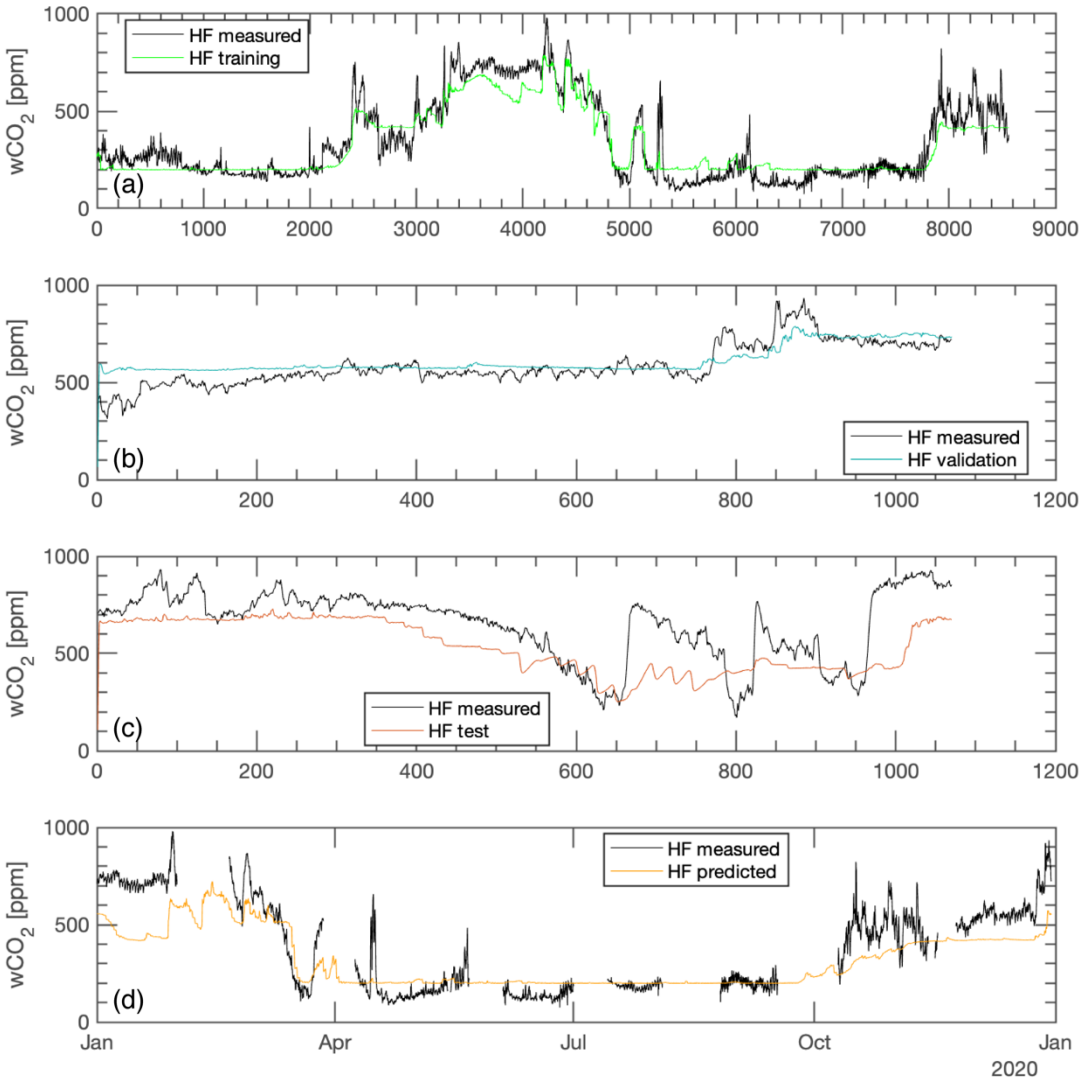

Fig. S3-6: LSTM configuration of the three-dataset needed to generate the predicted model for water CO_2 using three inputs variables (air temperature, solar radiation, and wind speed). **(a)** High frequency CO_2 measured and trained data corresponding to 80% of the whole dataset used; **(b)** High frequency CO_2 measured and validated data corresponding to 10% of the whole dataset used; **(c)** High frequency CO_2 measured and tested data corresponding to 10% of the whole dataset used; **(d)** High frequency CO_2 measured in 2020 and data predicted by the model generated by the training and validation dataset.

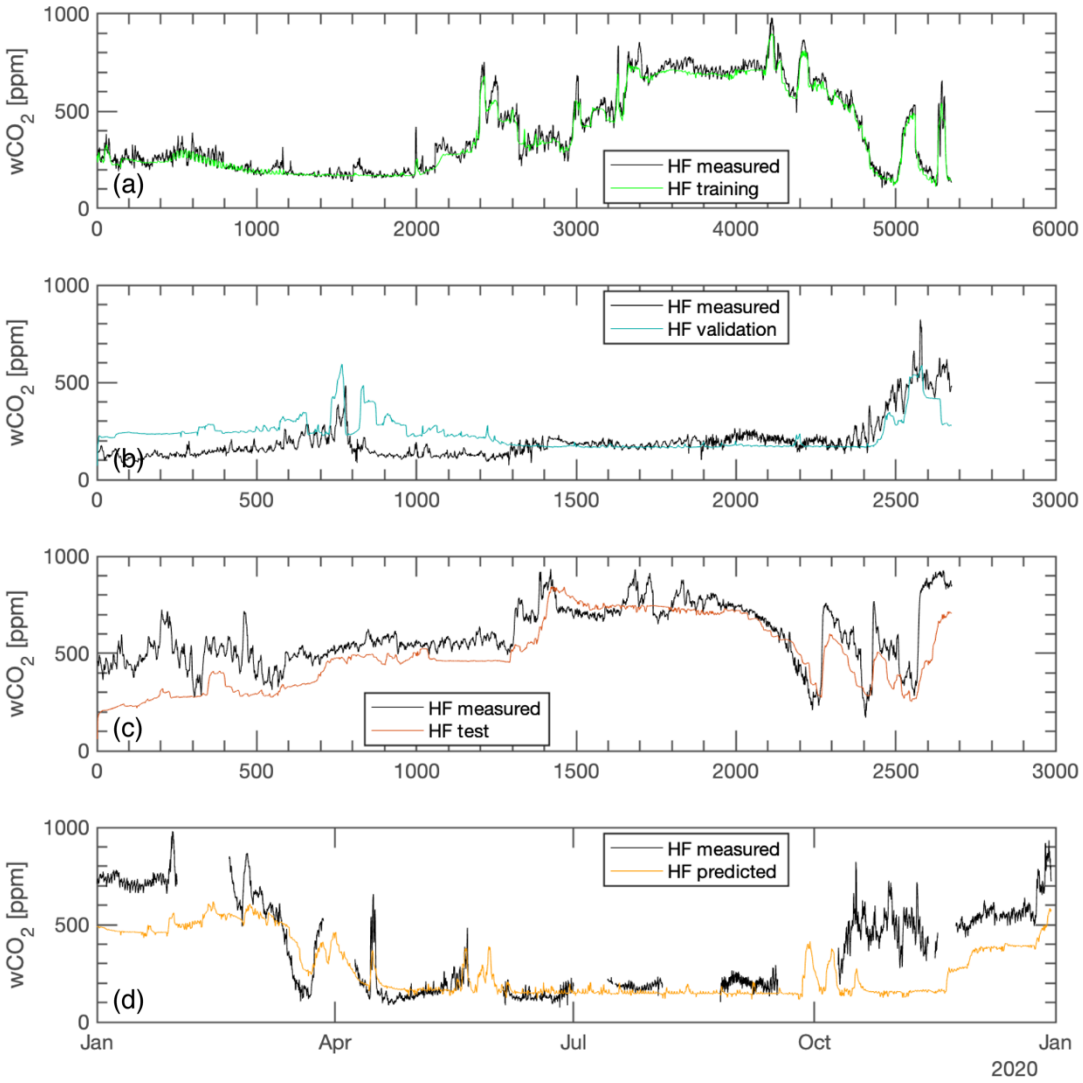

Fig. S3-7: LSTM configuration of the three-dataset needed to generate the predicted model for water CO_2 using three inputs variables (air temperature, solar radiation, and wind speed). **(a)** High frequency CO_2 measured and trained data corresponding to 50% of the whole dataset used; **(b)** High frequency CO_2 measured and validated data corresponding to 25% of the whole dataset used; **(c)** High frequency CO_2 measured and tested data corresponding to 25% of the whole dataset used; **(d)** High frequency CO_2 measured in 2020 and data predicted by the model generated by the training and validation dataset.

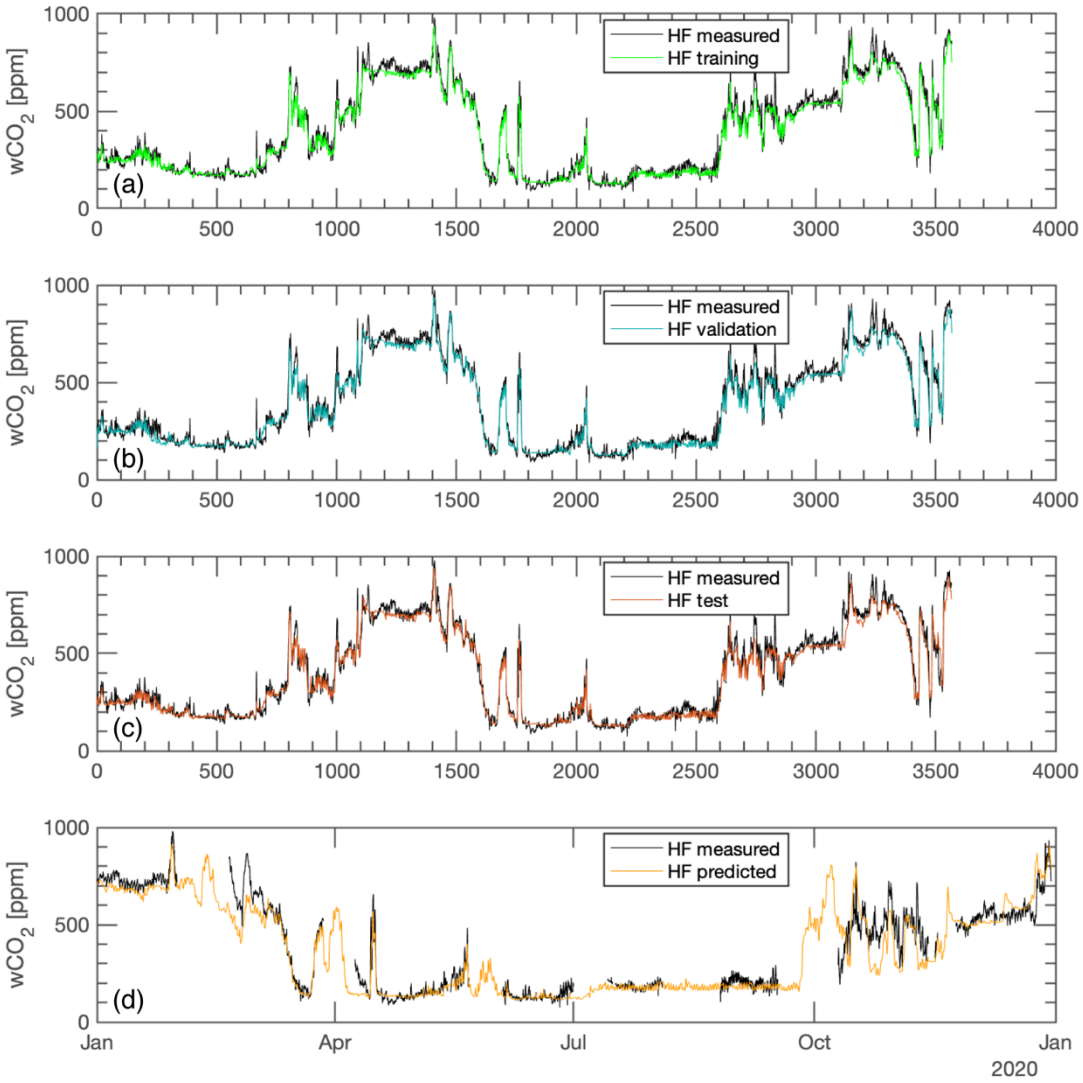

Fig. S3-8: LSTM configuration of the three-dataset needed to generate the predicted model for water CO_2 using three inputs variables (air temperature, solar radiation, and wind speed). **(a)** High frequency CO_2 measured and trained data corresponding to 1 value out of 3 taken in the whole dataset used; **(b)** High frequency CO_2 measured and validated data corresponding to 1 value out of 3 taken in the whole dataset used; **(c)** High frequency CO_2 measured and tested data corresponding to 1 value out of 3 taken in the whole dataset used; **(d)** High frequency CO_2 measured in 2020 and data predicted by the model generated by the training and validation dataset.

3.8. References

Åberg, J., M. Jansson, and A. Jonsson (2010), Importance of water temperature and thermal stratification dynamics for temporal variation of surface water CO2 in a boreal lake, J. Geophys. Res., 115, G02024, doi:10.1029/2009JG001085.

Abril, G., Bouillon, S., Darchambeau, F., Teodoru, C. R., Marwick, T. R., Tamooh, F., Ochieng Omengo, F., Geeraert, N., Deirmendjian, L., Polsenaere, P., & Borges, A. V. (2015). Technical Note: Large overestimation of <i>p</i>CO₂ calculated from pH and alkalinity in acidic, organic-rich freshwaters. *Biogeosciences*, *12*(1), 67–78. https://doi.org/10.5194/bg-12-67-2015

Bade, D. L., & Cole, J. J. (2006). Impact of chemically enhanced diffusion on dissolved inorganic carbon stable isotopes in a fertilized lake. *Journal of Geophysical Research*, *111*(C1), C01014. https://doi.org/10.1029/2004JC002684

Borges, A. V., Vanderborght, J.-P., Schiettecatte, L.-S., Gazeau, F., Ferron-Smith, S., Delille, B., & Frankignoulle, M. (2004). Variability of the gas transfer velocity of CO2 in a macrotidal estuary (the Scheldt. *Estuaries*, *27*(Issue 4), 593–603.

Cole, J. J., & Caraco, N. F. (1998). Atmospheric exchange of carbon dioxide in a low-wind oligotrophic lake measured by the addition of SF $_6$. *Limnology and Oceanography*, *43*(4), 647–656. https://doi.org/10.4319/lo.1998.43.4.0647

Cole, J. J., Caraco, N. F., Kling, G. W., & Kratz, T. K. (1994). Carbon Dioxide Supersaturation in the Surface Waters of Lakes. *Science, New Series*, *265*(5178), 1568–1570.

Cole, J. J., Prairie, Y. T., Caraco, N. F., McDowell, W. H., Tranvik, L. J., Striegl, R. G., Duarte, C. M., Kortelainen, P., Downing, J. A., Middelburg, J. J., & Melack, J. (2007). Plumbing the Global Carbon Cycle: Integrating Inland Waters into the Terrestrial Carbon Budget. *Ecosystems*, *10*(1), 172–185. https://doi.org/10.1007/s10021-006-9013-8

Crusius, J., & Wanninkhof, R. (2003). Gas transfer velocities measured at low wind speed over a lake. *Limnology and Oceanography*, *48*(3), 1010–1017. https://doi.org/10.4319/lo.2003.48.3.1010

Danckwerts, P. V. (1951). Significance of liquid-film coefficient in gas absorption. *Industrial and Engineering Chemistry*, *43*(6), 1460–1467.

Deike, L., & Melville, W. K. (2018). Gas Transfer by Breaking Waves. *Geophysical Research Letters*, *45*(19), 10,482-10,492. https://doi.org/10.1029/2018GL078758

Dlugokencky, E. J., Mund, J. W., Crotwell, A. M., Crotwell, M. J., and Thoning, K. W. (2021) Atmospheric Carbon Dioxide Dry Air Mole Fractions from the NOAA GML Carbon Cycle Cooperative Global Air Sampling Network, 1968–2020, Version: 2021-07-30, NOAA Global Monitoring Laboratory Data Repository [dataset], https://doi.org/10.15138/wkgj-f215

Duc, N. T., Silverstein, S., Lundmark, L., Reyier, H., Crill, P., & Bastviken, D. (2013). Automated Flux Chamber for Investigating Gas Flux at Water–Air Interfaces. *Environmental Science & Technology*, *47*(2), 968–975. https://doi.org/10.1021/es303848x

Erkkilä, K.-M., Ojala, A., Bastviken, D., Biermann, T., Heiskanen, J. J., Lindroth, A., Peltola, O., Rantakari, M., Vesala, T., & Mammarella, I. (2018). Methane and carbon dioxide fluxes over a lake: Comparison between

eddy covariance, floating chambers and boundary layer method. *Biogeosciences*, *15*(2), 429–445. https://doi.org/10.5194/bg-15-429-2018

Esters, L., Rutgersson, A., Nilsson, E., & Sahlée, E. (2021). Non-local Impacts on Eddy-Covariance Air–Lake $$\hbox {CO}_2$$ Fluxes. *Boundary-Layer Meteorology*, *178*(2), 283–300. https://doi.org/10.1007/s10546-020-00565-2

Eugster, W., Kling, G. W., Jonas, T., McFadden, J. P., Wüest, A., MacIntyre, S., & Chapin, F. S. (2003). Co2 exchange between air and water in an Artic Alaskan and midlatitude Swiss lake: Importance of convective mixing. *Journal of Geophysical Research*, *108*(D12). https://doi.org/10.1029/2002JD002653

Fairall, C. W., Yang, M., Bariteau, L., Edson, J. B., Helmig, D., McGillis, W., Pezoa, S., Hare, J. E., Huebert, B., & Blomquist, B. (2011). Implementation of the Coupled Ocean-Atmosphere Response Experiment flux algorithm with CO_2, dimethyl sulfide, and O_3. *Journal of Geophysical Research*, *116*, C00F09. https://doi.org/10.1029/2010JC006884

Fernández Castro, B., H. E. Chmiel, C. Minaudo, S. Krishna, P. Perolo, S. Rasconi, and A. Wüest. 2021. Primary and Net Ecosystem Production in a Large Lake Diagnosed from High-Resolution Oxygen Measurements. Water Resour. Res. 57(5), doi:10.1029/2020WR029283

Fritsch, F. N. &. Carlson R. E. (1980). Monotone Piecewise Cubic Interpolation. *SIAM Journal on Numerical Analysis*. Vol. 17, 1980, pp.238–246.

Gaudard, A., Schwefel, R., Vinnå, L. R., Schmid, M., Wüest, A., & Bouffard, D. (2017). Optimizing the parameterization of deep mixing and internal seiches in one-dimensional hydrodynamic models: A case study with Simstrat v1.3. *Geoscientific Model Development*, *10*(9), 3411–3423. https://doi.org/10.5194/gmd-10-3411-2017

Hasselmann K., Barnett T. P., Bouws, E., Carlson, H, Cartwright D. E., Enke, K., Ewing, J. A., Gienapp, H., Hasselmann, D. E., Kruseman, P., Meerburg, A., Müller, P., Olbers, D. J., Richter, K., Sell, W., and Walden, H.: Measurements of wind-wave growth and swell decay during the Joint North Sea Wave Project (JONSWAP), Dtsch. Hydrog. Z. Suppl. A, 8, 1–95, 1973.

Heiskanen, J. J., Mammarella, I., Haapanala, S., Pumpanen, J., Vesala, T., MacIntyre, S., & Ojala, A. (2014). Effects of cooling and internal wave motions on gas transfer coefficients in a boreal lake. *Tellus B: Chemical and Physical Meteorology*, *66*(1), 22827. https://doi.org/10.3402/tellusb.v66.22827

Higuchi, K., Worthy, D., Chan, D., & A. Shashkov (2003). Regional source/sink impact on the diurnal, seasonal and inter-annual variations in atmospheric CO2 at a boreal forest site in Canada, Tellus B: Chemical and Physical Meteorology, 55:2, 115-125, https://doi.org/10.3402/tellusb.v55i2.16752

Hochreiter, S., and J. Schmidhuber. "Long short-term memory." *Neural computation*. Vol. 9, Number 8, 1997, pp.1735–1780.

Klaus, M., & Vachon, D. (2020). Challenges of predicting gas transfer velocity from wind measurements over global lakes. *Aquatic Sciences*, *82*(3), 53. https://doi.org/10.1007/s00027-020-00729-9

Lamont, J. C., & Scott, D. S. (1970). An eddy cell model of mass transfer into the surface of a turbulent liquid. *AIChE Journal*, *16*(4), 513–519. https://doi.org/10.1002/aic.690160403

Lauster, G. H., Hanson, P. C., & Kratz, T. K. (2006). Gross primary production and respiration differences among littoral and pelagic habitats in northern Wisconsin lakes. *Canadian Journal of Fisheries and Aquatic Sciences,* 63, 12.

Larmola, T. (2004). Contribution of vegetated littoral zone to winter fluxes of carbon dioxide and methane from boreal lakes. *Journal of Geophysical Research*, *109*(D19), D19102. https://doi.org/10.1029/2004JD004875

Loken, L. C., Crawford, J. T., Schramm, P. J., Stadler, P., Desai, A. R., & Stanley, E. H. (2019). Large Spatial and Temporal Variability of Carbon Dioxide and Methane in a Eutrophic Lake. *Journal of Geophysical Research: Biogeosciences*, *124*(7), 2248–2266. https://doi.org/10.1029/2019JG005186

MacIntyre, S., and J. M. Melack (2009), Mixing dynamics in lakes across climatic zones, in Encyclopedia of Inland Waters, edited by G. E. Likens, pp. 603–612 , Academic Press, Oxford.

MacIntyre, S., Jonsson, A., Jansson, M., Aberg, J., Turney, D. E., & Miller, S. D. (2010). Buoyancy flux, turbulence, and the gas transfer coefficient in a stratified lake: TURBULENCE AND GAS EVASION IN LAKES. *Geophysical Research Letters*, *37*(24), n/a-n/a. https://doi.org/10.1029/2010GL044164

Millero, F. (1979). The thermodynamics of the carbonate system in seawater. *Geochemica et Cosmochemica Acta* 43:1651-1661.

Natchimuthu, S., Sundgren, I., Gålfalk, M., Klemedtsson, L., & Bastviken, D. (2017). Spatiotemporal variability of lake pCO $_2$ and CO $_2$ fluxes in a hemiboreal catchment: SPATIOTEMPORAL VARIABILITY OF LAKE CO $_2$. *Journal of Geophysical Research: Biogeosciences*, *122*(1), 30–49. https://doi.org/10.1002/2016JG003449

Ojala, A., J. López Bellido, T. Tulonen, P. Kankaala, and J. Huotari (2011), Carbon gas fluxes from a brown-water and a clear-water lake in the boreal zone during a summer with extreme rain events, Limnol. Oceanogr., 56(1), 61–76, doi:10.4319/lo.2011.56.1.0061

Paranaíba, J. R., Barros, N., Mendonça, R., Linkhorst, A., Isidorova, A., Roland, F., Almeida, R. M., & Sobek, S. (2018). Spatially Resolved Measurements of CO $_2$ and CH $_4$ Concentration and Gas-Exchange Velocity Highly Influence Carbon-Emission Estimates of Reservoirs. *Environmental Science & Technology*, *52*(2), 607–615. https://doi.org/10.1021/acs.est.7b05138

Perolo, P., Fernández Castro, B., Escoffier, N., Lambert, T., Bouffard, D., & Perga, M.-E. (2021). Accounting for surface waves improves gas flux estimation at high wind speed in a large lake. *Earth System Dynamics*, *12*(4), 1169–1189. https://doi.org/10.5194/esd-12-1169-2021

Pierrot, D., Lewis, E., and Wallace, D. W. R. (2006). MS Excel Program Developed for CO2 System Calculations, Tech. rep., Carbon Dioxide Inf. Anal. Cent., Oak Ridge Natl. Lab., US DOE, Oak Ridge, Tenn.

Read, J. S., Hamilton, D. P., Desai, A. R., Rose, K. C., MacIntyre, S., Lenters, J. D., Smyth, R. L., Hanson, P. C., Cole, J. J., Staehr, P. A., Rusak, J. A., Pierson, D. C., Brookes, J. D., Laas, A., & Wu, C. H. (2012). Lake-size dependency of wind shear and convection as controls on gas exchange: LAKE-SIZE DEPENDENCY OF u_* AND w_*. *Geophysical Research Letters*, *39*(9), n/a-n/a. https://doi.org/10.1029/2012GL051886

Rimet, F., Anneville, O., Barbet, D., Chardon, C., Crépin, L., Domaizon, I., Dorioz, J.-M., Espinat, L., Frossard, V., Guillard, J., Goulon, C., Hamelet, V., Hustache, J.-C., Jacquet, S., Lainé, L., Montuelle, B., Perney, P., Quetin, P., Rasconi, S., Monet, G. (2020). The Observatory on LAkes (OLA) database: Sixty years of environmental data accessible to the public: The Observatory on LAkes (OLA) database. *Journal of Limnology*, *79*(2). https://doi.org/10.4081/jlimnol.2020.1944

Rudorff, C. M., Melack, J. M., MacIntyre, S., Barbosa, C. C. F., & Novo, E. M. L. M. (2011). Seasonal and spatial variability of CO_2 emission from a large floodplain lake in the lower Amazon. *Journal of Geophysical Research*, *116*(G4), G04007. https://doi.org/10.1029/2011JG001699

Sadro, S., Melack, J. M., & MacIntyre, S. (2011). Spatial and Temporal Variability in the Ecosystem Metabolism of a High-elevation Lake: Integrating Benthic and Pelagic Habitats. Ecosystems, 14(7), 1123–1140. https://doi.org/10.1007/s10021-011-9471-5

Schilder, J., Bastviken, D., van Hardenbroek, M., Kankaala, P., Rinta, P., Stötter, T., & Heiri, O. (2013). Spatial heterogeneity and lake morphology affect diffusive greenhouse gas emission estimates of lakes: SPATIAL HETEROGENEITY OF DIFFUSIVE FLUX. *Geophysical Research Letters*, *40*(21), 5752–5756. https://doi.org/10.1002/2013GL057669

Schwefel, R., Gaudard, A., Wüest, A., & Bouffard, D. (2016). Effects of climate change on deepwater oxygen and winter mixing in a deep lake (Lake Geneva): Comparing observational findings and modeling: CLIMATE CHANGE EFFECTS IN A DEEP LAKE. *Water Resources Research*, *52*(11), 8811–8826. https://doi.org/10.1002/2016WR019194

Soloviev, A., Donelan, M., Graber, H., Haus, B., & Schlüssel, P. (2007). An approach to estimation of near-surface turbulence and CO2 transfer velocity from remote sensing data. *Journal of Marine Systems*, *66*(1–4), 182–194. https://doi.org/10.1016/j.jmarsys.2006.03.023

Spafford, L., & Risk, D. (2018). Spatiotemporal Variability in Lake-Atmosphere Net CO_2 Exchange in the Littoral Zone of an Oligotrophic Lake. *Journal of Geophysical Research: Biogeosciences*. https://doi.org/10.1002/2017JG004115

Tedford, E. W., MacIntyre, S., Miller, S. D., & Czikowsky, M. J. (2014). Similarity scaling of turbulence in a temperate lake during fall cooling. *Journal of Geophysical Research: Oceans*, *119*(8), 4689–4713. https://doi.org/10.1002/2014JC010135

Teodoru, C. R., Prairie, Y. T., & del Giorgio, P. A. (2011). Spatial Heterogeneity of Surface CO2 Fluxes in a Newly Created Eastmain-1 Reservoir in Northern Quebec, Canada. *Ecosystems*, *14*(1), 28–46. https://doi.org/10.1007/s10021-010-9393-7

Vachon, D., & Prairie, Y. T. (2013). The ecosystem size and shape dependence of gas transfer velocity versus wind speed relationships in lakes. *Canadian Journal of Fisheries and Aquatic Sciences*, *70*(12), 1757–1764. https://doi.org/10.1139/cjfas-2013-0241

Vachon, D., Prairie, Y. T., & Cole, J. J. (2010). The relationship between near-surface turbulence and gas transfer velocity in freshwater systems and its implications for floating chamber measurements of gas exchange. *Limnology and Oceanography*, *55*(4), 1723–1732. https://doi.org/10.4319/lo.2010.55.4.1723

Vesala, T., Huotari, J., Rannik, Ü., Suni, T., Smolander, S., Sogachev, A., Launiainen, S., & Ojala, A. (2006). Eddy covariance measurements of carbon exchange and latent and sensible heat fluxes over a boreal lake for a full open-water period. *Journal of Geophysical Research*, *111*(D11). https://doi.org/10.1029/2005JD006365

Wanninkhof, R. (1992). Relationship between wind speed and gas exchange over the ocean. *Journal of Geophysical Research*, *97*(C5), 7373. https://doi.org/10.1029/92JC00188

Wanninkhof, R., & Knox, M. (1996). Chemical enhancement of CO2 exchange in natural waters. *Limnology and Oceanography*, *41*(4), 689–697. https://doi.org/10.4319/lo.1996.41.4.0689

Winslow, L. A., Zwart, J. A., Batt, R. D., Dugan, H. A., Woolway, R. I., Corman, J. R., Read, J. S. (2016). LakeMetabolizer: An R package for estimating lake metabolism from free-water oxygen using diverse statistical models. Inland Waters, 6(4), 622–636. https://doi.org/10.1080/IW-6.4.883

Wüest, A., Bouffard, D., Guillard, J., Ibelings, B. W., Lavanchy, S., Perga, M., & Pasche, N. (2021). LéXPLORE: A floating laboratory on Lake Geneva offering unique lake research opportunities. *WIREs Water*, *8*(5). https://doi.org/10.1002/wat2.1544

Chapter 4

Alkalinity as the dominant carbon source for gross primary production in a deep stratified hardwater lake

Pascal Perolo[1], Nicolas Escoffier[1], Hannah E. Chmiel[2], Gaël Many[1], Damien Bouffard[3] and Marie-Elodie Perga[1]

[1]Institute of Earth Surface Dynamics, University of Lausanne, Quartier Mouline, CH-1015 Lausanne

[2]Physics of Aquatic Systems Laboratory, Margareth Kamprad Chair, Swiss Federal Institute of Technology Lausanne, Station 2, CH-1015 Lausanne

[3]Eawag, Swiss Federal Institute of Aquatic Science and Technology, Surface Waters – Research and Management, Seestrasse 79, CH-6047 Kastanienbaum

In revision for *Limnology and Oceanography Letters*

4.1. Scientific Significance Statement

If CO_2 is the main carbon-substrate for photosynthesis, how can gross primary production carry on when CO_2 gets very limiting? In Lake Geneva, gross primary production can reach its highest rates despite low CO_2 concentrations at the surface. This suggests that photosynthetic organisms could heavily use an alternate carbon source, i.e. bicarbonates, that is abundant in hardwater lakes. We could demonstrate for the first time that bicarbonates support the gross primary production for two-thirds of the year. In the littoral and pelagic environments, we estimated that between 40-80% of the annual primary production was ultimately provided by bicarbonate fixation. We showed that bicarbonate-fixation by primary producers, far from being anecdotical, can be the dominant model for hardwater lakes.

4.2. Abstract

In alkaline freshwater systems, the apparent absence of carbon limitation to gross primary production (GPP) at low CO_2 concentrations suggests that bicarbonates can support GPP. However, the contribution of bicarbonates to GPP has never been quantified in lakes along the seasons. To detect the origin of the inorganic carbon maintaining GPP, we analyse the daily stoichiometric ratios of CO_2–O_2 and Alkalinity–O_2 in a deep hardwater lake. Results show that aquatic primary production withdraw bicarbonates from the alkalinity pool for two-thirds of the year. Alkalinity rather than CO_2 is the dominant inorganic carbon source to gross primary production throughout the stratified period in both the littoral and pelagic environments. This study sheds light on the neglected role of alkalinity in the freshwater carbon cycle throughout an annual cycle.

4.3. Introduction

In aquatic ecosystems, gross primary production (GPP) converts dissolved inorganic carbon (DIC = CO_2 + HCO_3^- + CO_3^{2-}) into organic matter (OM). Nutrients (nitrogen and phosphorus) and light are the main limiting factors of GPP (Schindler et al., 1973; Dillon & Rigler, 1974; Krause-Jensen & Sand-Jensen, 1998; Karlsson et al., 2009). Because additions of inorganic carbon (IC) to lakes were not sufficient to increase GPP levels (Schindler, 1971, 1974), IC limitation of GPP has been regarded as unlikely, especially since most inland waters are supersaturated with CO_2 (Cole et al., 1994). This statement has been questioned in cases of near-surface CO_2 undersaturation when GPP demand surpasses inward atmospheric CO_2 fluxes (Schindler et al., 1972; Finlay et al., 1999; Zhang et al., 2017; Zagarese et al., 2021). Under such conditions, the GPP in low-alkaline soft water lakes has been proven to be carbon-limited (Kragh and Sand-Jensen, 2018).

Kragh and Sand-Jensen (2018), however, reported in the same study similarly low near-surface CO_2 concentrations in high-alkaline hardwater lakes without any carbon limitation of GPP. The absence of carbon limitation was therein attributed to the high DIC stocks. However, at pH values typical for moderate hardwater lakes (7.8-9), the DIC pool is mainly composed of bicarbonates (HCO_3^- > 95%; Stumm and Morgan, 1981) that cannot be readily fixed by most primary producers. Besides, while at high HCO_3^- concentrations and high pH, atmospheric CO_2 invasion is greatly enhanced by chemical enhancement (Wanninkhof and Knox 1996), the carbonate buffering effect leads to fast hydration and deprotonation of incoming atmospheric CO_2 into HCO_3^- with limited effect on pH and dissolved CO_2 concentrations (Bade & Cole, 2006). Thus, the chemical enhancement of atmospheric inward fluxes in alkaline lakes cannot directly supply CO_2 to primary producers. Thereby, the lack of carbon limitation of GPP in alkaline hardwater lakes despite low CO_2 concentrations suggests that alkalinity (Alk) itself can deliver IC to primary producers (Li et al., 2018) but at probably higher cost for organisms leading to a lower GPP in an absolute term.

Primary producers, inhabiting environments with low CO_2, high HCO_3^-, and high light levels (Maberly & Gontero, 2017) have evolved complex strategies to use bicarbonates for maintaining GPP (e.g. Steeman Nielsen, 1946; Thomas & Tregunna, 1968; Price et al., 2008; Maberly & Gontero, 2017; Iversen et al. 2019). At low CO_2 concentrations, certain microalgae and cyanobacteria can mobilise active bicarbonate uptake systems and transport HCO_3^- to certain cell compartments where specific enzymes concentrate and convert HCO_3^- into CO_2 (CO_2-concentrating mechanism (CCM); e.g. carbon anhydrase; Colman et al. 2002; Li et al. 2018). For active bicarbonate uptake, one mole of alkalinity is lost for one mole of inorganic carbon fixed within photosynthesis. Additionally, many algae and macrophytes capture the CO_2 released during calcite precipitation (CP) that can occur close to their membranes (CP: 2 HCO_3^- + Ca^{2+} ⇄ $CaCO_3$ + CO_2 + H_2O), ensuring carbon supply for GPP (Kelts & Hsü, 1978; Larsson & Axelsson, 1999; Pełechaty et al., 2013; Müller et al., 2016). For indirect bicarbonate use through CP, two moles of alkalinity are lost for one mole of inorganic carbon fixed within photosynthesis, the remaining mole being precipitated as calcite.

Alkalinity was shown to be the main IC source to macrophytes in a downstream reach of a river in the South of France (Maberly et al., 2015). A recent study of GPP in five US rivers (Aho et al., 2021) estimated that bicarbonates could support up to 30% of the annual GPP in one large and sunny reach of the Connecticut River.

The contribution of bicarbonates in supporting GPP in lakes remains to be quantified, and its implications for the carbon cycle of hardwater lakes to be understood.

Lake Geneva is a moderately hardwater lake with surface CO_2 concentrations below saturation for the stratified period. Herein, we aim at detecting the origin of the dominant IC supporting GPP in both the pelagic and littoral environments of Lake Geneva on a daily scale. By combining hourly measurements of CO_2, O_2, and alkalinity over a complete annual cycle, we categorise the dominant daily source of DIC (CO_2 or HCO_3^-) to GPP based on the stoichiometric changes of CO_2–O_2 and Alk–O_2. We relate the DIC source to the environmental conditions to estimate the importance of bicarbonate use for the littoral and pelagic at an annual scale.

4.4. Material and methods

4.4.1. Study sites

Lake Geneva is a large, deep, alkaline hardwater lake with surface alkalinity ranging from 1200 to 1700 µeq L^{-1}, a surface calcium concentration (Ca^{2+}) ranging from 38 to 46 mg L^{-1} and a salinity level of ~ 0.2 ‰. The lake is stratified from April to September with a thermocline deepening from 3 to 30 m. Calcite precipitation has been reported during the stratification period (Müller et al., 2016). Two study sites (Fig. S4-1 (a-c)), the LéXPLORE platform (110 m depth; Wüest et al., 2021) and the Buchillon mast (4 m depth), representative of the pelagic and littoral environments, were investigated over the years 2019 and 2020.

4.4.2. Field methods

Dissolved oxygen and water temperature were measured every 5 min by miniDOT sensors (PME). The calibration and the post-correction were performed as in Fernández Castro et al. (2021). Dissolved pCO_2 was measured every 30 min by miniCO_2 sensors (Pro-Oceanus System Inc., accuracy <5%, range of 0-2,000 ppm). Sensors were calibrated with two standards (0 and 2,000 ppm) and one control of atmospheric gas (~400 ppm) with a CO_2 gas analyser (Licor 830) every 4-6 weeks and corrected considering the drift if necessary.

Alkalinity is strongly correlated to the specific conductance over the whole year in Lake Geneva (R^2 = 0.95; Supplementary Methods). The sub-daily dynamics of alkalinity are thereby estimated using a conductivity logger (HOBO U24-001, Onset) every 15 min with a range of 0-1,000 µS cm^{-1}. Sensors were placed at 0.7 m depth ± 0.2 m and 2 m depth ± 0.2 in pelagic and littoral areas, respectively.

Local weather conditions were continuously recorded at a 10 min interval by a Campbell Scientific automatic weather station at each site. Water temperatures were measured every minute from 0.7 to 30 m with 2.5 m of interval depth using Minilog II-T (VEMCO, resolution 0.01°C) in the pelagic area (unstratified littoral). These temperatures were used to compute the Schmidt stability (Idso, 1973) and the mixed layer depth (Imberger, 1985). Finally, all variables were gridded at an hourly time step.

4.4.3. Data analysis and modelling

The CO_2 and O_2 concentrations at the lake surface were expressed in terms of departure from atmospheric equilibrium in µmol L^{-1} as in Vachon et al. (2020). Given the pH of Lake Geneva's surface waters (7.8-9; see Fig. S4-2), we assumed the Alk variations is equal to the HCO_3^- variations (Groleau et al., 2000) because bicarbonates represent > 95 % of the Alk and carbonate (CO_3^{2-}) cannot be used by GPP. The origin of the DIC supporting GPP was detected from the analysis of paired CO_2–O_2 and Alk–O_2 dynamics (Aho et al., 2021; Stets et al., 2017), following an approach inspired but expanded from Vachon et al. (2020) (Fig. S4-3).

Briefly, the slopes of the daily point clouds of CO_2–O_2 (α) and Alk–O_2 (β; 95 % of confident interval) were used to categorise the dominant source of DIC supporting GPP based on the following stoichiometric ratios. The photosynthesis from CO_2 uptake leads to daily molar ratios for CO_2–O_2 between 1:1 to 1:1.4 (Lefèvre & Merlivat, 2012). Daily point clouds of CO_2–O_2 with α slopes equivalent to –1 and –1.4 were categorised as days of CO_2 uptake. α < –1.4 indicates O_2 production for limited changes of CO_2 but demonstrating the use of an alternative IC source also requires evidence of alkalinity consumption. For cases with α < –1.4, coupled Alk–O_2 changes were scrutinized, to check whether daily alkalinity consumption matched O_2 production (Fig. S4-8). Direct bicarbonate use for CCM generates a molar Alk–O_2 ratio of 1:1 to 1:1.4, while for IC uptake from calcite precipitation, the molar Alk–O_2 ratio is expected to be lower (1:0.5 to 1:1). Daily point clouds of Alk–O_2 with β slopes between –0.5 and –1.4 were categorised as days of HCO_3^- use. Only days with significant linear correlations between CO_2–O_2 and Alk–O_2 were retained for the analysis (i.e. p-value < 0.05 and R^2 > 0.66). The remaining days, not attributed to any category, are, in most cases, either days where the daily signal was too weak or days with a noisy daily signal because of significant transport resulting from short-lived events such as internal waves or upwelling (Fernández Castro et al., 2021) produced by wind events (> 5 m s^{-1}; Fig. S4-5).

Noteworthily, the daily Alk–O_2 analyse was primordial to obtain this categorisation, because the daily CO_2-O_2 alone does not provide unambiguous evidence for HCO_3^- use even with very steep α slopes. Indeed, in alkaline and hardwater lakes, the bicarbonate buffer system, influenced by the water temperature and the alkalinity level, generates a non-linear relationship between the CO_2 and O_2 departures as illustrated in Fig. 4-1. We simulated a theoretical model of consumption or production of CO_2 related to O_2 variation in different conditions (fixed alkalinity and temperature variation, fixed temperature and alkalinity variation and a variety of conditions encountered in Lake Geneva) assuming no flux with the atmosphere (see details in Supplementary Method). In summary, in alkaline systems, CO_2 consumption by photosynthesis shifts the bicarbonate chemical equilibrium to the left, regenerating CO_2 from the HCO_3^-+CO_3^{2-} pool to CO_2. Yet, because the loss of HCO_3^-+CO_3^2 is compensated by the loss of H^+, the buffering effect from the carbonate system does not lead to noticeable changes in alkalinity. Thus, the analysis of the β slopes is necessary to determine the HCO_3^- use by CCM and CP.

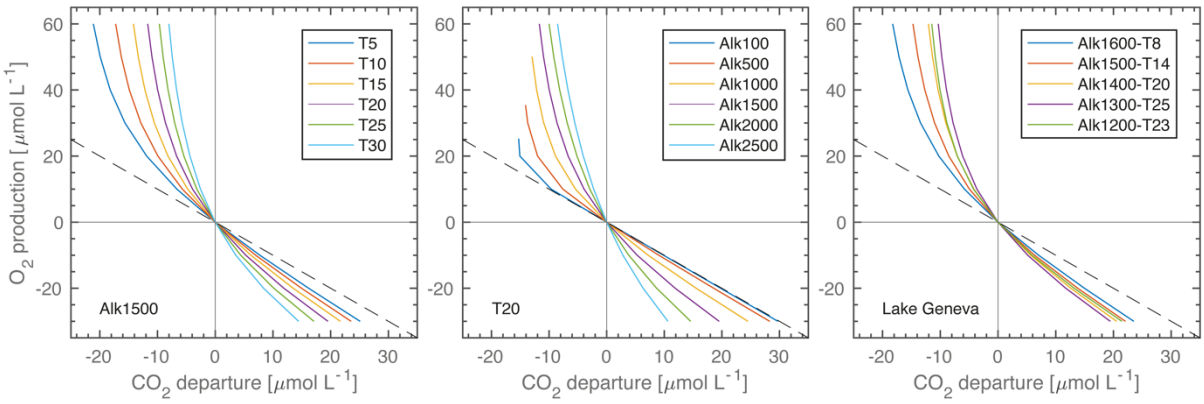

Fig. 4-1: Three panels show the theoretical effect of the bicarbonate buffer system in the non-linearity of the CO_2–O_2 stoichiometry through different conditions of temperature and alkalinity level to demonstrate the importance of the alkalinity measurements to justify the bicarbonate use in this kind of study. Panel **(left side)** shows different conditions of water temperature with a fixed alkalinity level at 1500 µeq L^{-1}. Panel **(middle)** shows different level of alkalinity with a fixed water temperature at 20 °C. Panel **(right side)** shows different conditions encountered in Lake Geneva in winter, early spring, late spring, summer, and late summer, respectively. Note that a warmer temperature with less alkalinity can give the same results (e.g. T20 and Alk1400 is equal to T23 and Alk1200). The dashed line represents the –1 slope.

Daily rates of GPP (µmol O_2 L^{-1} d^{-1}) were computed using a Bayesian Lake Metabolism model provided in the LakeMetabolizer R package (Winslow et al., 2016; Read et al., 2011; Supplementary Method). We tested whether the dominant origins of IC supporting GPP could be predicted from the four (littoral) and five (pelagic) daily averaged selected environmental variables (GPP rate, CO_2 departure, wind speed, solar radiation, and Schmidt stability) using classification trees (Supplementary Method). The best models were used to reconstruct the dominant daily DIC sources of GPP for the not-classified days for which GPP could be computed.

4.5. Results

4.5.1. Spatiotemporal variability

The annual CO_2–O_2 dynamics of the littoral and pelagic environments are illustrated at an hourly resolution in Fig. 4-2 (Time series in Fig. S4-6). Two distinct periods are observed in the littoral and pelagic environments (Fig. 4-2 (a) and (b)): a cold period (September to March) corresponding to the first windy event in fall until the end of the winter mixing and a warm period (April to August) corresponding to the highest levels of solar radiation and stratification strength.

During the cold period, the conditions are mainly undersaturated in O_2 and oversaturated in CO_2 (right lower most quadrant of the diagram). The slope of the CO_2–O_2 dynamics remains close to –1, reflecting the classical stoichiometry of photosynthesis (i.e. use of CO_2). The range of CO_2 departures is similar for the littoral and pelagic sites, while the O_2 departures are, on average, ~30 µmol L^{-1} lower in the littoral as compared to the pelagic site.

These conditions shift to an O_2 oversaturation and a CO_2 undersaturation during the stratified period (left uppermost quadrant of the diagram). Over these months, the slope of the CO_2–O_2 dynamic strongly deviates from –1 and becomes much steeper. This high production of O_2 and low consumption of CO_2 sheds light on the potential CO_2 limitation in this system, especially in the pelagic environment suggesting another contribution from the DIC pool.

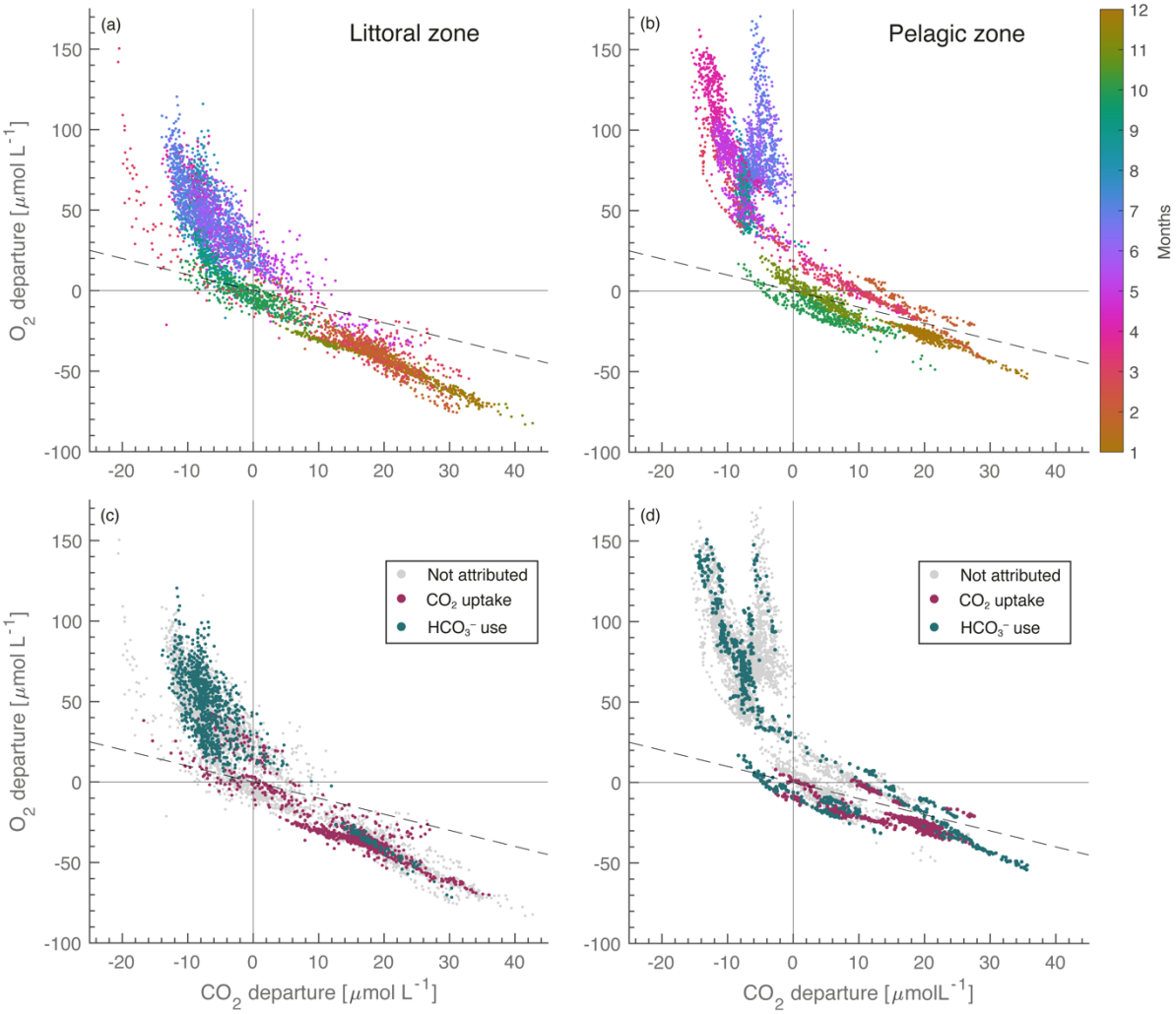

Fig. 4-2: Panels **(a, b)** show the annual dynamic of CO_2 departure vs O_2 departure (µmol L^{-1}) in littoral and pelagic environments coloured according to the months of the year. The two annual cycles present more than 65% of the days of the year distributed over all months (See also Fig. S4-4). Panels **(c, d)** highlight the two categorisations of CO_2 uptake (***α*** slopes from –1 to –1.4: red points) and HCO_3^- use (***β*** slopes from –0.5 to –1.4: green points) as well as the not attributed days (grey points). The dashed line represents the –1 slope.

The data distribution within the CO_2-O_2 diagram is more scattered for the shoulder seasons (March-April and September-October, Fig. S4-4), especially for the littoral site. For those shoulder months, the CO_2–O_2 variability within a single day can be almost as wide as the monthly and annual CO_2-O_2 variability (Fig. S4-7).

Figs 4-2 (c) and (d) show the results of the two processes including CO_2 uptake or HCO_3^- use for GPP. More examples are provided in Fig. S4-7. The distribution of IC sources is broadly partitioned depending on O_2–CO_2 departures, with most days of CO_2 uptake at CO_2 supersaturated and O_2 undersaturated daily conditions (right lower most quadrant) and HCO_3^- use at CO_2 undersaturated and O_2 oversaturated conditions (left uppermost quadrant). However, GPP could rely on HCO_3^- use even on days with supersaturated daily averaged CO_2 values, especially in the pelagic site.

4.5.2. Influence of chemical and physical conditions

Fig. 4-2 presents the relationships between the CO_2 uptake and HCO_3^- use of GPP and the daily chemical and physical conditions.

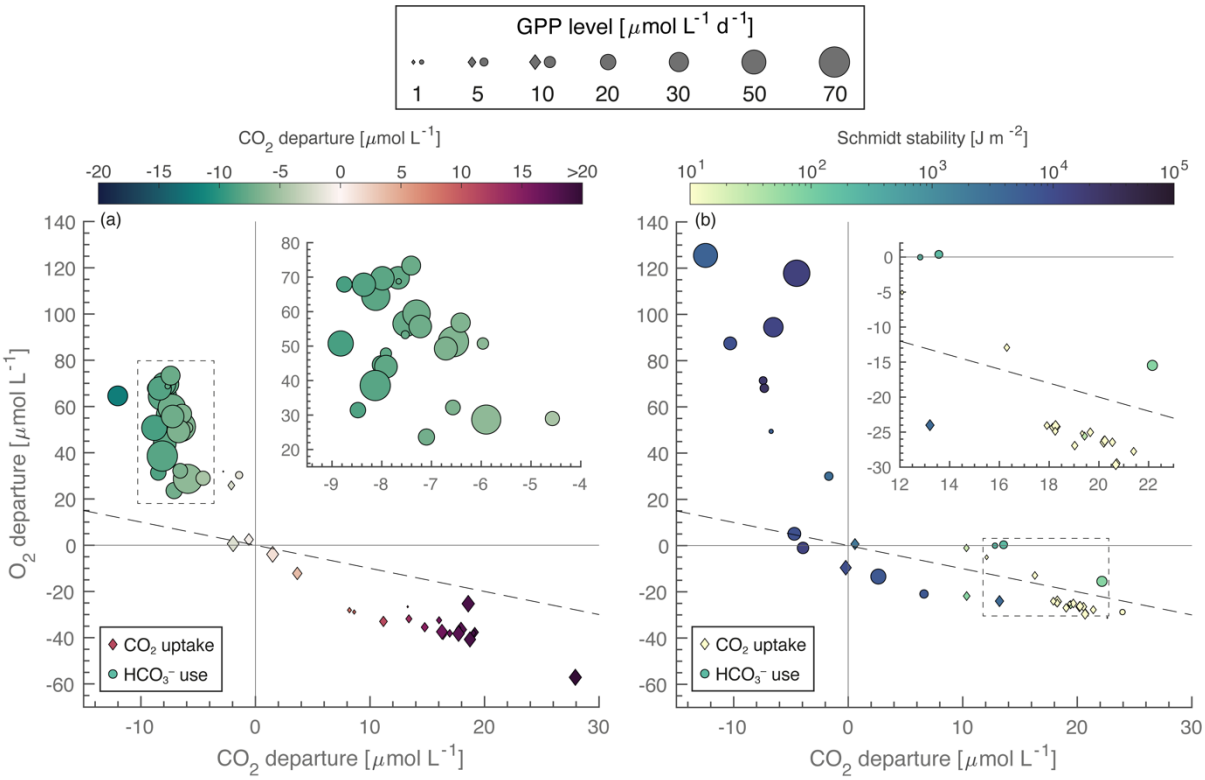

Fig. 4-3: Panels **(a, b)** show daily GPP level (size of symbol, µmol O_2 L^{-1} d^{-1}) matching categorised days for CO_2 uptake (diamond) or HCO_3^- use (circle). Panel **(a)** is coloured according to the daily average of CO_2 departure (µmol L^{-1}) in the littoral environment. Panel **(b)** is coloured according to the daily Schmidt stability (J m^{-2}) in the pelagic environment. The dashed line represents the –1 slope. Dash rectangles are the specific zooms created in the small frames in the upper right corners.

In the littoral site, Fig. 4-3 (a) shows a clear partition of IC source according to GPP and average daily CO_2 departures with HCO_3^- use for CO_2 departures <–4.4 µmol L^{-1} and GPP >16 µmol O_2 L^{-1} d^{-1} (classification tree of the littoral in Table S4-1). The physical conditions, such as wind speed, have limited impact on DIC use (Fig. S4-9). In the pelagic site, the water column stability is the main driver of DIC use, followed by the GPP level, with HCO_3^- use for a Schmidt stability >116 J m^{-2} and a GPP >5 µmol O_2 L^{-1} d^{-1} (Fig. 4-3 (b) and classification tree of the pelagic in Table S4-2). Moreover, for the highest GPP level >50 µmol O_2 L^{-1} d^{-1}, the slopes of CO_2–O_2

ratio tend to infinity, while the slopes of Alk–O_2 ratio align to the 1:–1 involving an assimilation > 95% of HCO_3^- to maintain these GPP levels (Fig. S4-8).

4.5.3. DIC pool contribution to GPP along the year

The predictions accuracies for the classification trees are > 80% and reveal the strong predictive power of some specific drivers (i.e. CO_2 departure and GPP for the littoral environment, Stability and GPP for the pelagic environment; Tables S4-1 and S4-2). Trained classification models are thereafter used to reconstruct the dominant DIC use for days that could not be categorised from their stoichiometric relationships (approx. two-thirds of the datasets). The distributions of GPP within DIC use categories were very similar between the training dataset and the predictions (see violin plots Before | After in Fig. 4-4).

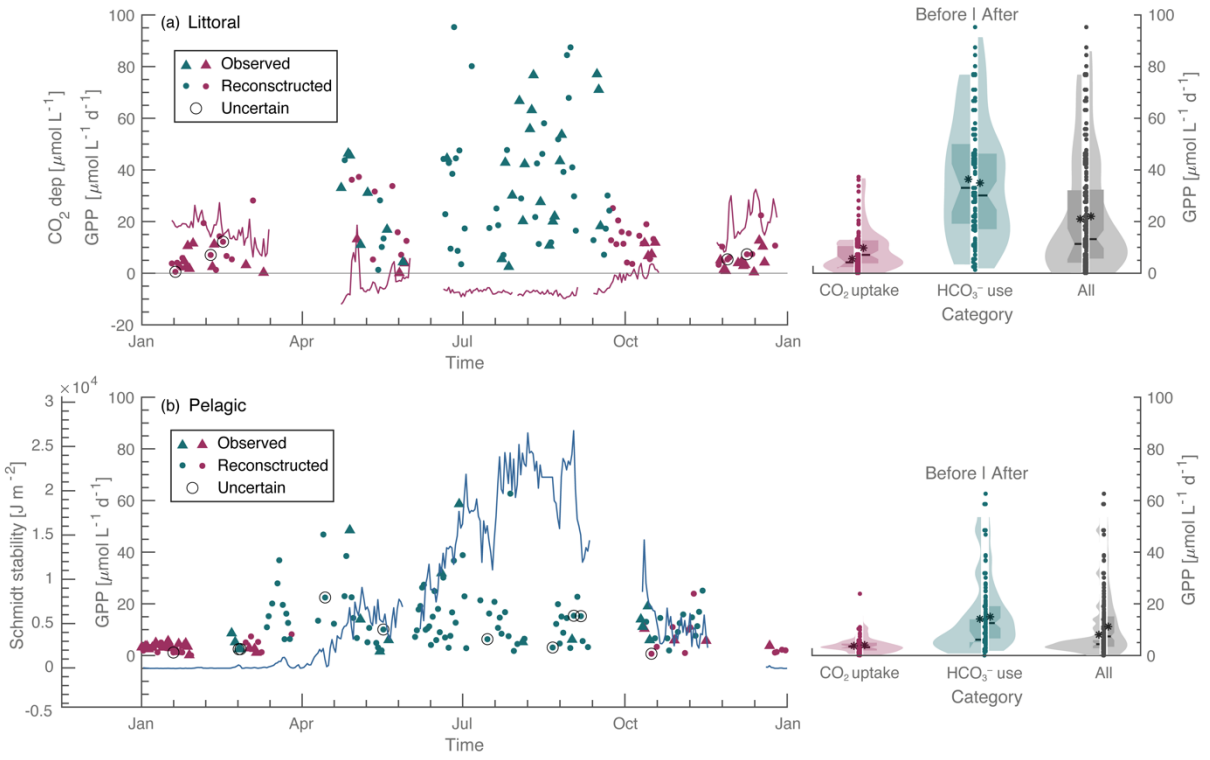

Fig. 4-4: Panels **(a, b)** show the temporal evolution of estimated GPP levels (µmol O_2 L^{-1} d^{-1}) along the year (left side) coloured according to categorisations of the dominant DIC source: CO_2 uptake (red) and HCO_3^- use (green). Panel **(a)** adds the temporal evolution of the CO_2 departure (µmol L^{-1}) as the best predictor of the littoral environment as well as the atmospheric equilibrium (black line). Panel **(b)** adds the temporal evolution of the Schmidt stability (J m^{-2}) as the best predictor of the pelagic environment. The distributions and the boxplots (violin plots) of GPP levels are shown on the right side of panels **(a, b)** for both DIC categories and the whole GPP levels before and after the reconstruction by the classification tree.

In the littoral site, GPP was exclusively supported by CO_2 uptake in winter and late fall, while HCO_3^- use was the dominant source for GPP in summer (June-August), when the highest GPP rates were recorded. From March to May, GPP was alternatively supported by HCO_3^- and CO_2 because of strong daily fluctuations in CO_2 (Fig. 4-4 (a)). Overall, we estimated that 75% of the total annual littoral GPP (sum of GPP with a dominant bicarbonate

source divided by sum of total GPP; from data in Fig. 4-4) is supported by > 50% of HCO_3^- use and that 100% of the summer GPP (June to August) is supported by > 50% of HCO_3^- during the highest GPP rate.

DIC use was more seasonally partitioned for the pelagic site (Fig. 4-4 (b)), with exclusive CO_2 uptake limited to winter (December-March). The dominance of HCO_3^- use started in March and remained the main source supporting GPP for over 8 months, until October coinciding to the stratified period. The DIC source for GPP alternated in early fall, as the water column stability fluctuated around 2000 J m^{-2}. Because bicarbonate use dominates during the most productive season, we estimated that almost all of GPP during the stratification period is supported by > 50% of HCO_3^- and that 82% of the total annual pelagic GPP is supported by > 50% of HCO_3^-.

4.6. Discussion

The high-frequency data coupling of CO_2, O_2, and alkalinity provides meaningful ecosystem function information (e.g. Stets et al., 2017; Vachon et al., 2020). The analyses of both stoichiometric ratios allowed to detect the origin of the dominant DIC supporting GPP and proved to be an interesting and easily reproducible approach for semi-quantitative estimations. Moreover, the daily Alk–O_2 analyse (β slope) was essential to perform the categorisation of the DIC source to avoid misinterpretations generated by the non-linear relationship between the CO_2 and O_2 departures (α slope) in alkaline and hardwater lake such as Lake Geneva (Fig. 4-1 (c)). In addition, the categorisation according to the daily CO_2–O_2 and Alk–O_2 is, yet, limited by the robustness of the selected slopes, which excluded some days, as well as by their uncertainties, which prevented to distinguish some processes (i.e. precise CO_2–HCO_3^- co-fixation, CCM and CP) and therefore to accurately quantify the intraday consumption of CO_2 and HCO_3^-. However, in term of semi-quantification, this approach is well complemented by the classification tree method that allows consistent predictions through training datasets.

This study provides a semi-quantification of DIC pool contribution to GPP along an annual cycle in both the littoral and pelagic environments of a moderate alkaline and hardwater lake. The results show that GPP is not limited by carbon availability throughout the year, even during CO_2 depletion, as demonstrated in other freshwater systems (Maberly et al., 2015; Kragh and Sand-Jensen, 2018; Li et al., 2018; Aho et al., 2021). To support the high rate of O_2 production, GPP relies on HCO_3^- withdrawal from the water to subsidise the missing CO_2 (Fig. S4-7), resulting in a depleted alkalinity pool, especially in the pelagic environment (Fig. S4-6). Both lake environments are auspicious for CCM with specific conditions such as CO_2 depletion, high HCO_3^- availability and high levels of solar radiation (Maberly & Gontero, 2017). Pico- and nanoplankton are known to use CCM (e.g. Maberly & Gontero, 2017; Mishra et al., 2018), and they have been documented in relatively high abundances in Lake Geneva from spring to fall, when they can contribute up to 76% of the pelagic biomass of primary producers (Parvathi et al., 2014). In addition, authigenic CP has previously been reported in the pelagic area (Escoffier et al., 2022; Müller et al., 2015; Fig. S4-1 (g)) as well as directly observed on the leaves of macrophytes from the littoral site (*Characea* and *Potamogeton perfoliatus*; Fig. S4-1 (d-f)) in accordance with the monitoring of macrophytes in Lake Geneva (CIPEL; Labat & Blanchard, 2020).

Exploring the temporal and spatial variabilities also offers interesting insights into macro and micro patterns at different resolutions. At the seasonal scale, an evident temporal variability is observed between cold (CO_2 uptake) and warm periods (HCO_3^- use), with heterogeneity in IC source during shoulder periods (Figs 4-1 and 4-2). At the annual scale, the dominant source of bicarbonate (> 50%) supporting the total GPP is relatively similar in the two environments (i.e. 75% for the littoral environment and 82% for the pelagic environment). However, this dominant consumption of HCO_3^- in the littoral environment only occurred for 3 to 4 months (middle June to middle September) while in the pelagic environment it was spread over 8 months (March to October). This annual similarity comes from the fact that summer littoral GPP rates are almost twice as high in this environment compared to the pelagic environment. The faster CO_2 depletion in the pelagic domain can be explained by the thermal stratification isolating the epilimnion from CO_2 fluxes coming from the hypolimnion and bottom sediments. In contrast, the shallower depth in the littoral area allows for greater proximity with sediment-derived CO_2 fluxes all year round and explains that CO_2 depletion appears later when GPP levels become higher. The daily observations support such dynamics in the littoral domain with changes in slopes between morning (lower) and afternoon (steeper), illustrating the cycling of different IC sources. In contrast, the pelagic slopes stay linear and steeper all day (Fig. S4-4 and S4-8). These daily patterns also highlight a greater dynamic from the littoral environment during the shoulder period with a constant return to early morning conditions (Fig. S4-4 and S4-8), while the pelagic has greater inertia, as observed in March, where the daily cycle of the littoral is the same as the monthly cycle in the pelagic (Fig. S4-7), linked to an increase in the Schmidt stability (Fig. 4-3).

To conclude, this study, as several recent studies (Maberly et al., 2015; Kragh & Sand-Jensen, 2018; Stets et al., 2017; Khan et al., 2020; Aho et al., 2021), sheds light on the overlooked role of alkalinity in the freshwater carbon cycle and how it contributes to GPP. Aquatic primary producers of Lake Geneva are thus not limited in inorganic carbon despite CO_2 depletion. The spatial study also underlines that the main identified drivers of IC sources differ in the pelagic and littoral environments of the lake. On a Swiss scale, the vast majority of lake surfaces (~90 %; Müller et al., 2016) have the same characteristics, i.e. large (>10 km^2) and deep (>50 m) with moderate alkalinity (1-4 meq L^{-1}) while globally about 50% of lakes are considered alkaline (>1 meq L^{-1}; Marcé et al., 2015) demonstrating the potential importance of biogeochemical processes linked to strong bicarbonate concentration in freshwater carbon cycle. Moreover, future trends suggest an increasing stratification period (Schwefel et al., 2016) and thus faster CO_2 depletion enhanced by shallower winter mixing (Gaudard et al., 2017), and finally decreased surface replenishment. Therefore, less CO_2 at the surface could lead to a potential increase in HCO_3^- use and a shift in species communities capable of such an assimilation.

4.7. Supplementary Figures

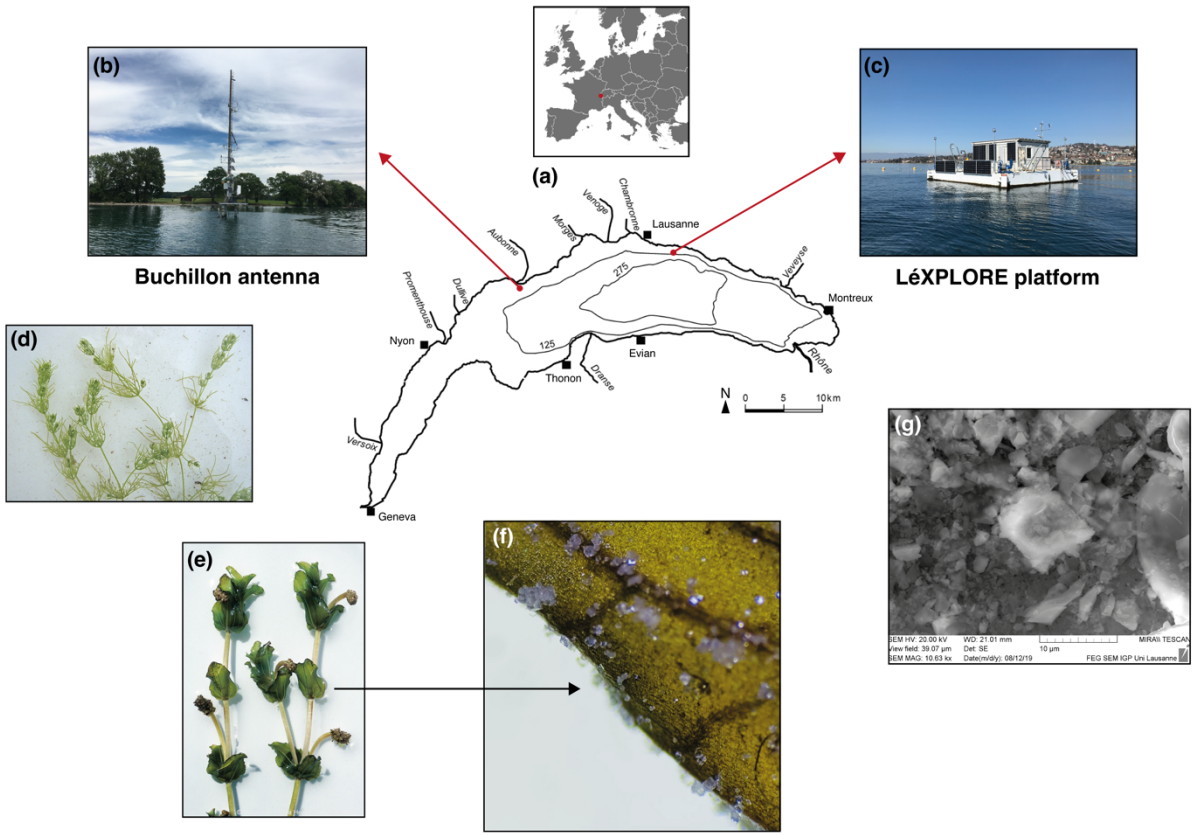

Fig. S4-1: Panels **(a-c)** show the situation and the map of Lake Geneva with the two study sites, Buchillon antenna for the littoral zone and LéXPLORE platform for the pelagic zone. Panels **(d-g)** show the different calcite precipitation indices observed on the field. **(d, e)** Specific macrophytes in the littoral environment: **(d)** *Characea* (Latin name; Inflora website: https://www.infoflora.ch/fr/flore/chara-vulgaris.html, last access 25 November 2021), and **(e)** *Potamogeton perfoliatus* (Latin name; Inflora website: https://www.infoflora.ch/fr/flore/potamogeton-perfoliatus.html, last access 25 November 2021), **(f)** Picture of calcite crystal on a macrophyte leaf sampled at Buchillon. **(g)** Picture of calcite crystal from LéXPLORE platform in the water column.

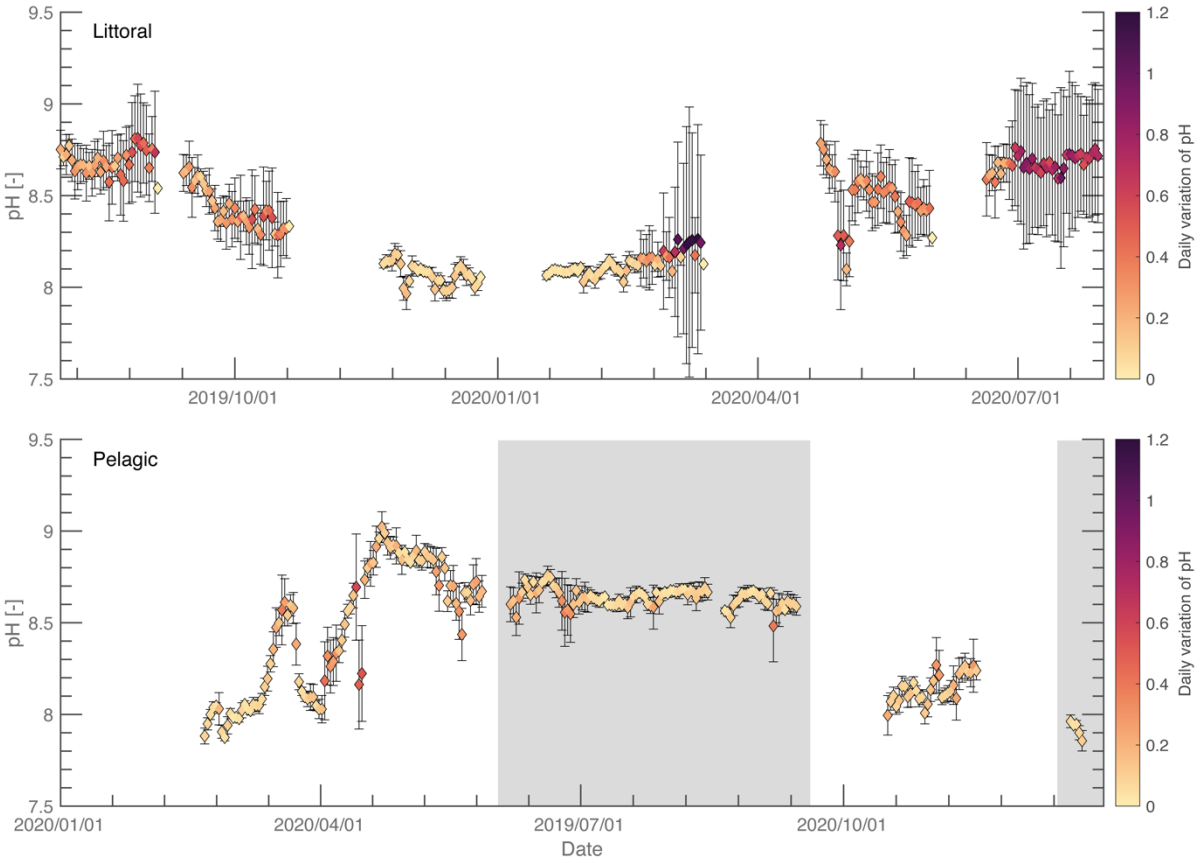

Fig. S4-2: Time series of pH variables for the littoral **(top)** and the pelagic **(down)** sites. The grey rectangles show that these measurement periods were recorded in 2019, while the remaining data were recorded in 2020 due to different issues concerning the sensors in the pelagic environment.

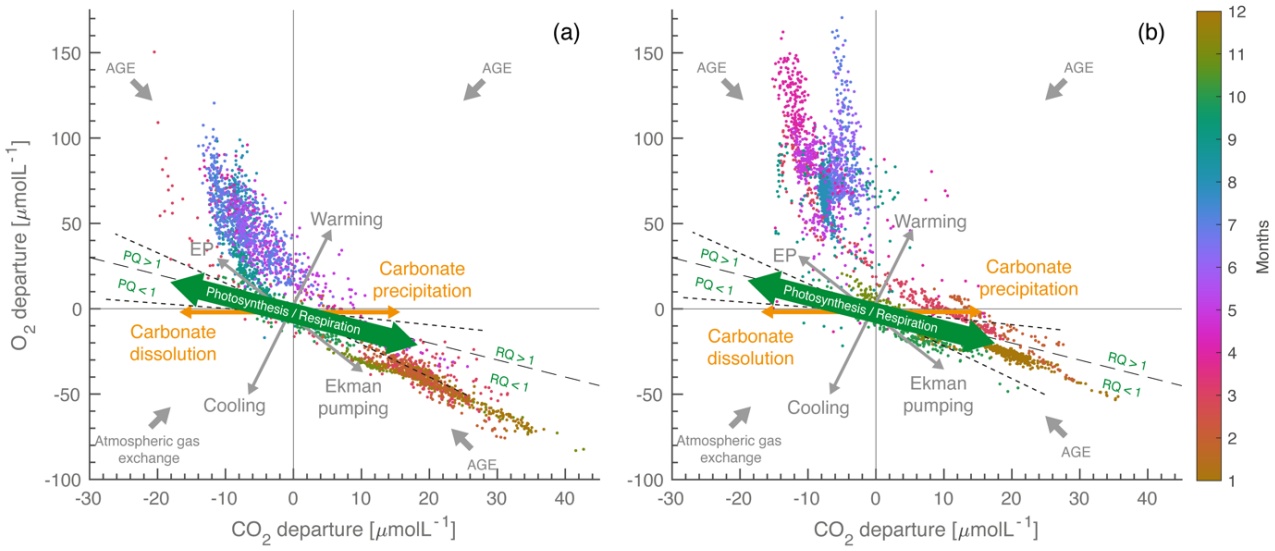

Fig. S4-3: Panels (a, b) present the physical and biogeochemical processes involved in the dynamics of CO_2 and O_2 departure from atmospheric equilibrium along a year, respectively, for the littoral and pelagic environments in Lake Geneva (inspired by Vachon et al., 2020). Briefly, each arrow represents a type of process influencing these dynamics alone or in combination at different time scales. These arrows are not static on the point of atmospheric equilibrium (0;0) but can move in the different quadrants like the geometric vectors. Green arrows represent biological processes. Grey arrows represent physical processes. Orange arrows represent chemical processes linked to carbonate system (here precipitation and dissolution of calcite, but there is also CCM and carbonate buffering system).

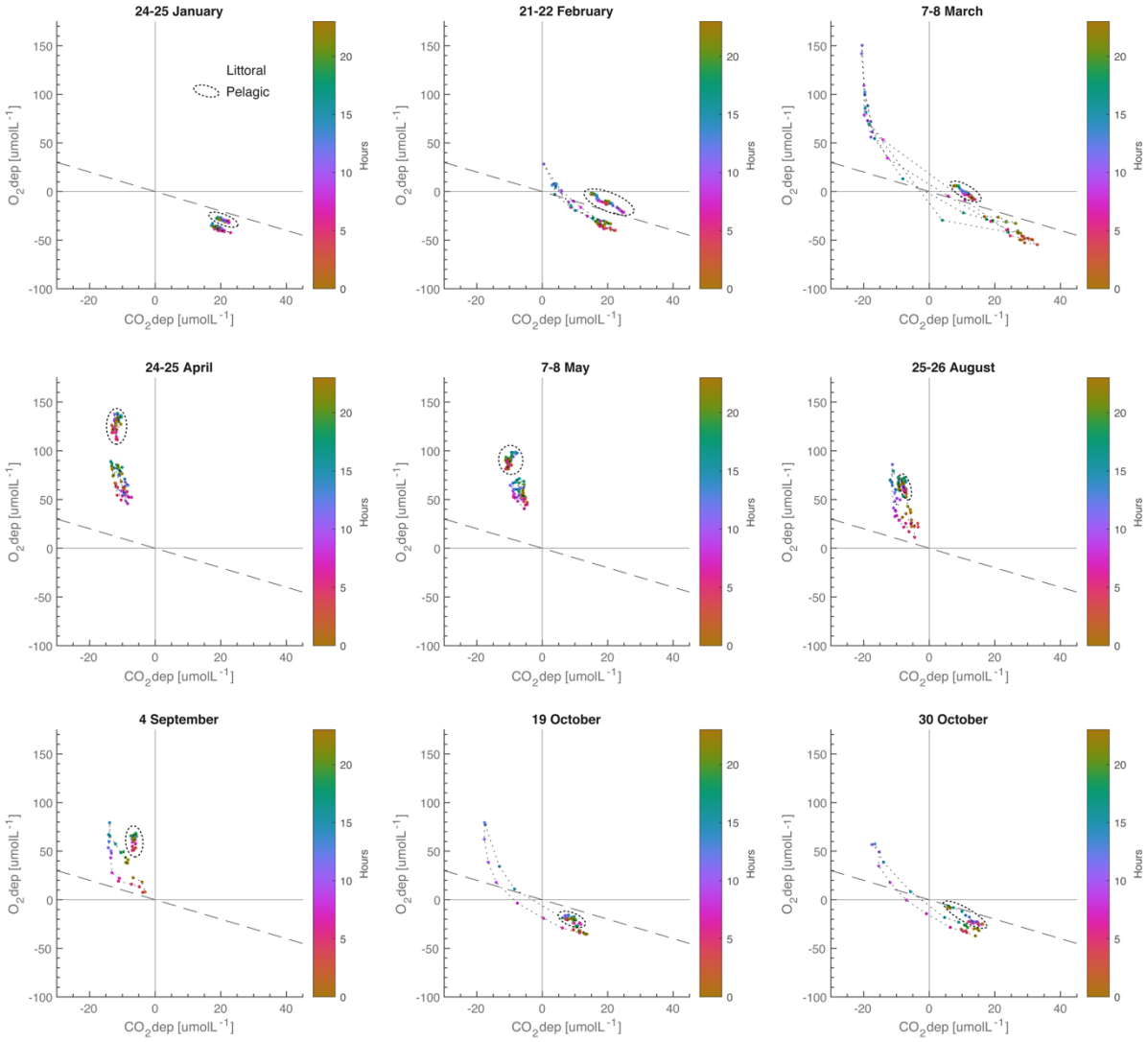

Fig. S4-4: Temporal evolution of daily CO_2–O_2 dynamics along the year (from January to October) for sunny and calm days. The dotted ellipses surrounding the point clouds are used to differentiate the dynamics of the pelagic from that of the littoral.

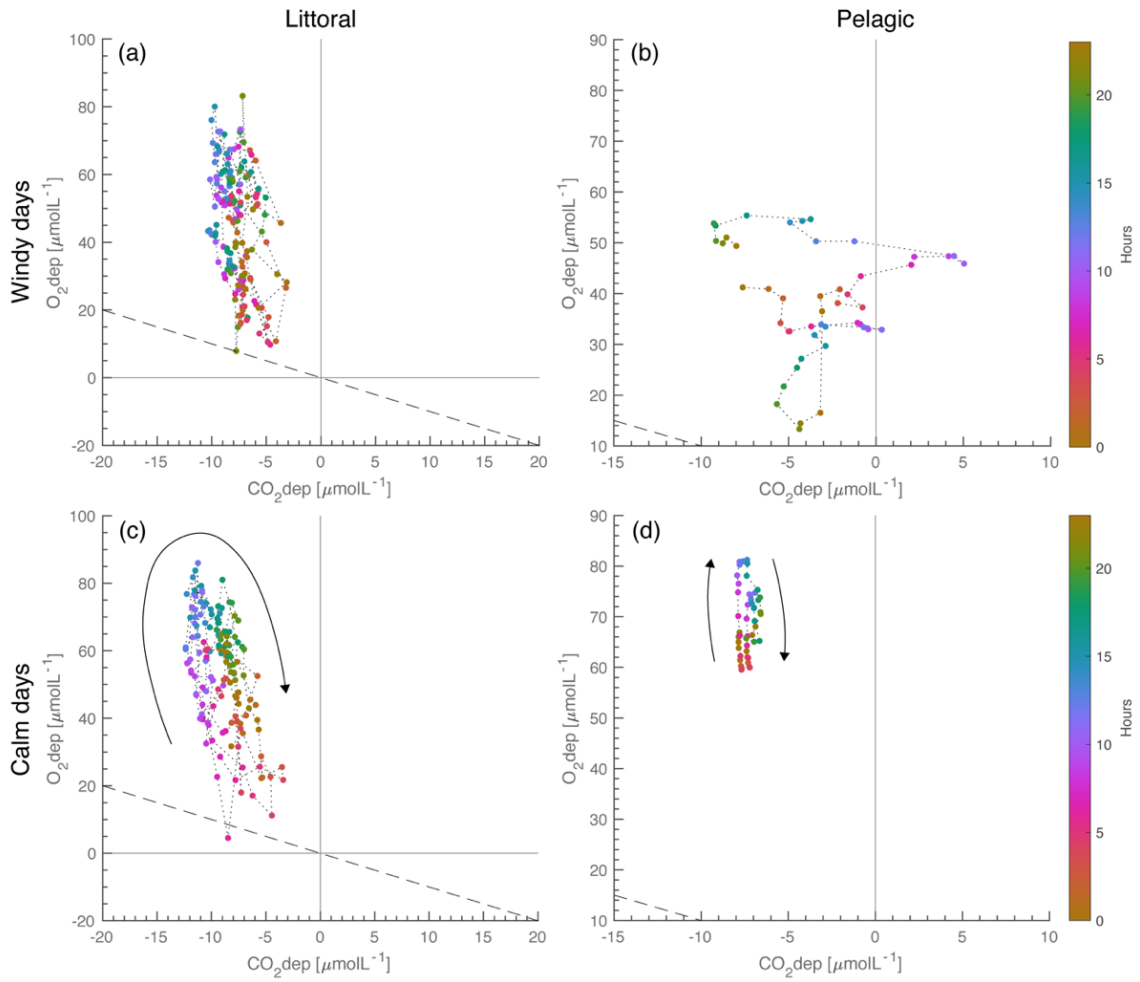

Fig. S4-5: Examples of **(a)** noisy daily signal impacted by wind (> 5 m s^{-1}) in littoral (15-21 August), **(b)** no metabolism signal impacted by strong wind (> 10 m s^{-1}) and Ekman pumping effect (19-21 May), **(c)** clear daily signal during calm and sunny days in littoral site (25-30 August), and **(d)** clear daily signal during calm and sunny days in pelagic site (3-4 August).

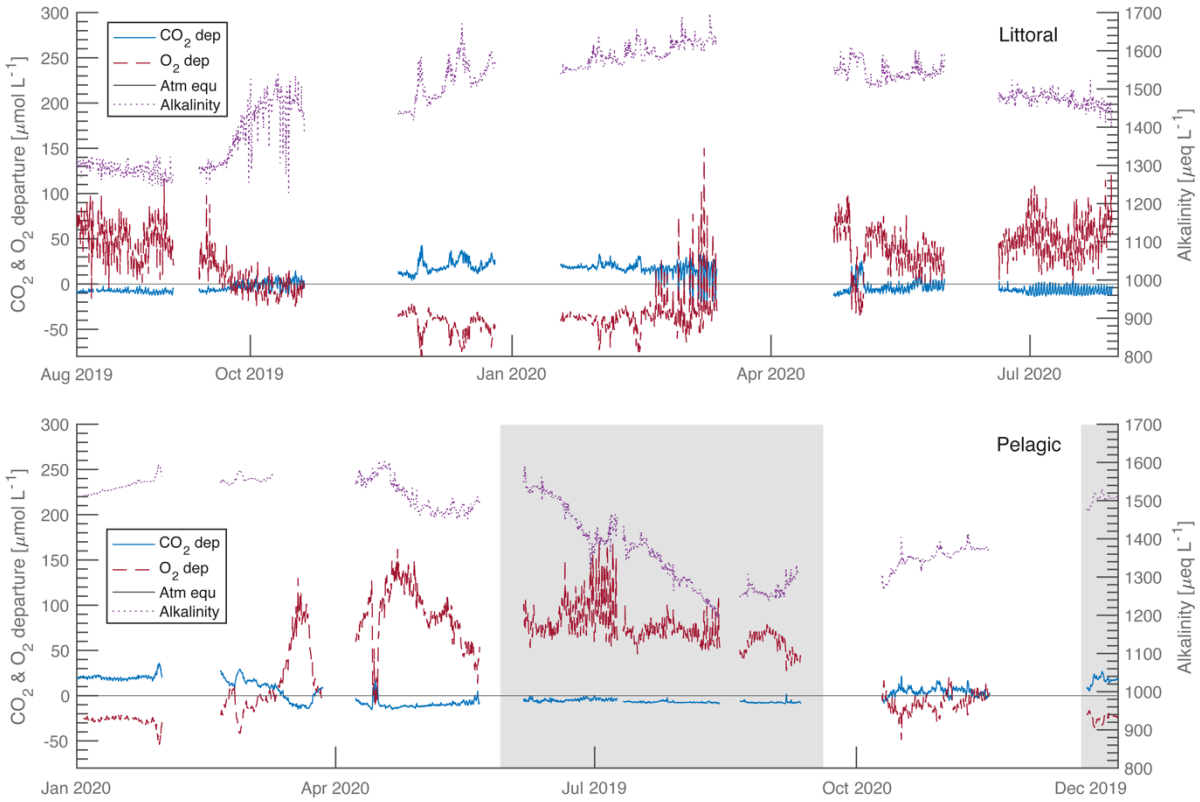

Fig. S4-6: Time series of three main variables used in this study for the littoral **(top)** and the pelagic **(down)** sites: CO_2 departure, O_2 departure, and alkalinity. The grey rectangles show that these measurement periods were recorded in 2019, while the remaining data were recorded in 2020 due to different issues concerning the sensors in the pelagic environment.

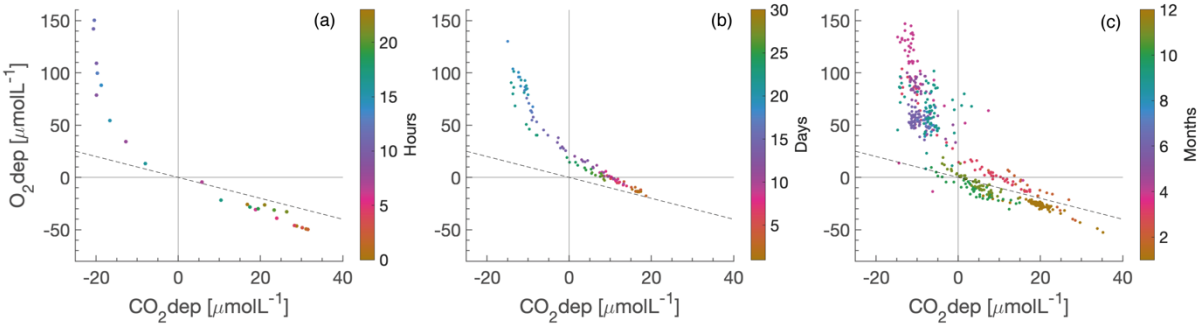

Fig. S4-7: Three observations of similar dynamics of O_2–CO_2 departures at different time scales from daily to annual scale. **(a)** The daily cycle of 7 March 2020 in littoral at 1h-time step, **(b)** monthly cycle of March 2020 in pelagic at 6h-timestep, **(c)** annual cycle of 2020 in pelagic at 12h-time step.

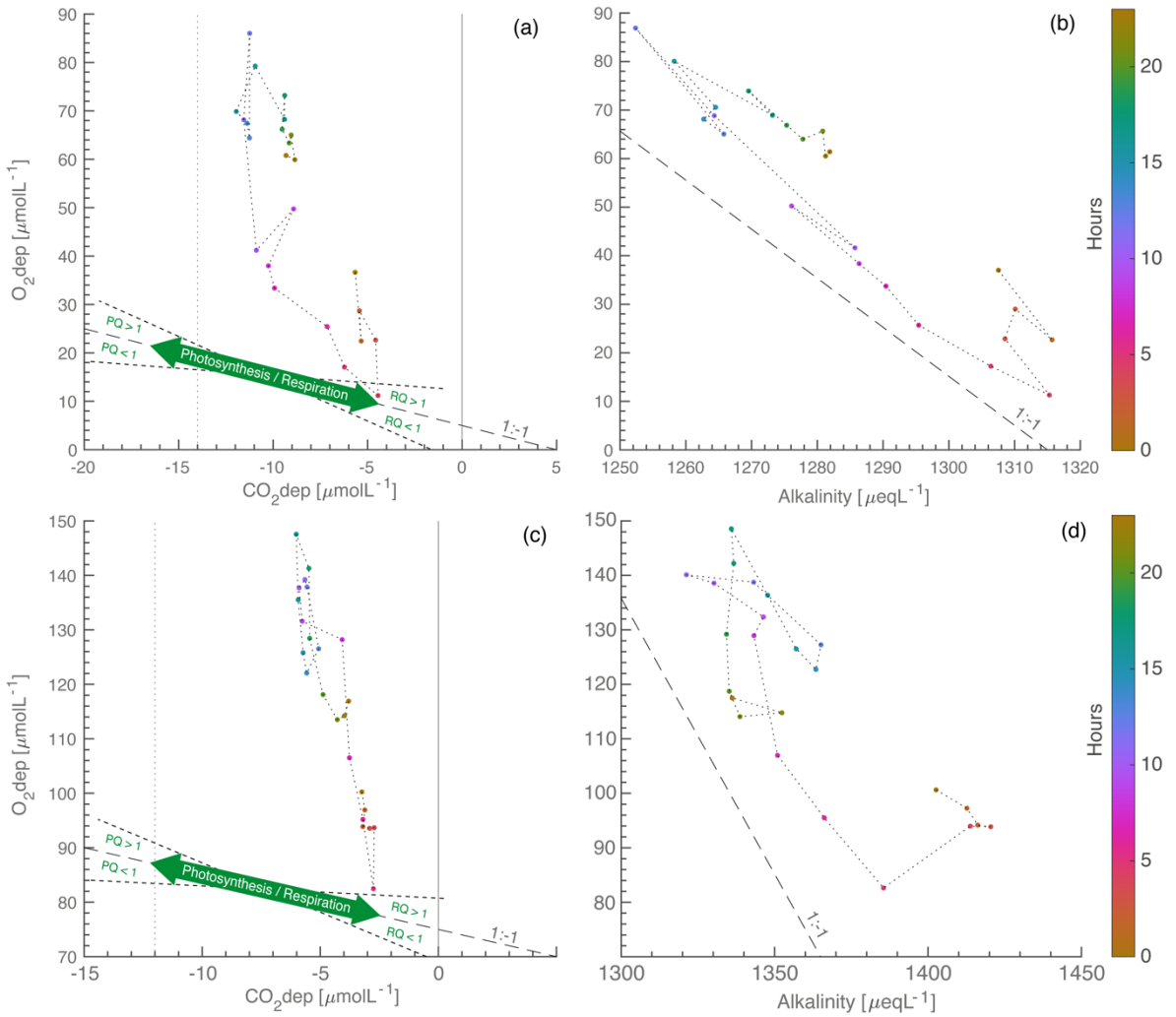

Fig. S4-8: Daily CO_2dep vs O_2dep in littoral **(a)** and pelagic **(c)** environments and present one day (26 August 2019 in littoral and 29 June 2019 in pelagic) of high GPP rate (53.6 µmol O_2 L^{-1} d^{-1} and 58.6 µmol O_2 L^{-1} d^{-1} respectively) with the representation of the metabolic stoichiometry in a molar ratio of 1 to 1.4 (photosynthesis and respiration; green arrow). The vertical dotted line is the theoretical threshold of the complete CO_2 depletion considering water temperature. Alkalinity vs O_2dep during the same days for both environments **(b, d)**. The dashed lines represent the –1 slope.

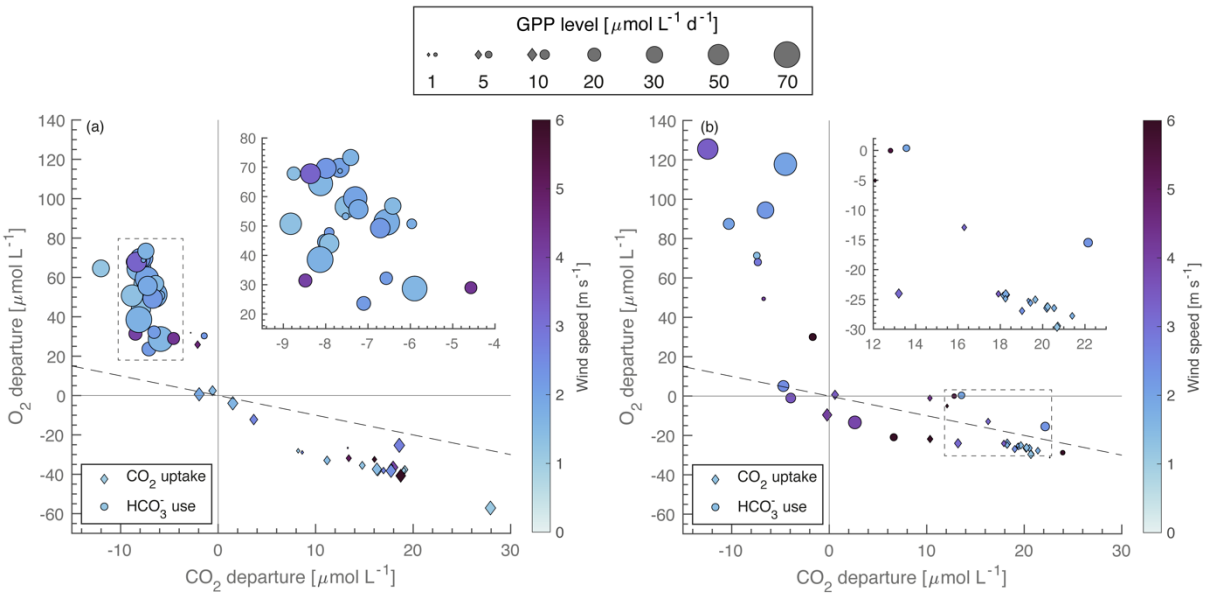

Fig. S4-9: Daily GPP level (size of symbol, µmol O_2 L^{-1} d^{-1}) matching categorised days for CO_2 uptake (diamond) or HCO_3^- use (circle) **(a, b)**. Panels **(a, b)** are coloured according to the daily average of wind speed (m s^{-1}) in the littoral **(right side)** and pelagic **(left side)** sites. The dashed lines represent the –1 slope. Dash rectangles are the specific zooms created in the small frames.

4.8. Supplementary Tables

Table S4-1: Presentation of the different combinations of the classification trees tested with accuracy (for a test dataset of 50% of the total dataset) and the thresholds found for the two best predictors in the littoral environment. The green gradient shows the relative importance of four predictors used to reconstruct the IC sources to GPP (µmol O_2 L^{-1} d^{-1}). SR and WS correspond to solar radiation and wind speed, respectively. CO_2dep is in µmol C L^{-1}.

Test	Significant variables							Accuracy
1	CO_2dep	>	GPP	~	SR	>	WS	1
2			GPP	~	SR	>	WS	0.85
3			GPP	~	SR			0.85
4			GPP					0.96
Thresholds	–4.4		16					

Table S4-2: Presentation of the different combinations of the classification trees tested with their accuracy (for a test dataset of 50% of the total dataset) and the thresholds found for the two best predictors in the pelagic environment. The green gradient shows the relative importance of four predictors used to reconstruct the IC sources to GPP (µmol O_2 L^{-1} d^{-1}). SR and WS correspond to solar radiation and wind speed, respectively. Stability is the Schmidt stability in J m^{-2}.

Test	Significant variables									Accuracy
1	CO_2dep	>	Stability	>	GPP	~	SR	>	WS	0.7
2	CO_2dep	>			GPP	~	SR	>	WS	0.7
3			Stability	>	GPP	~	SR	>	WS	0.8
4			Stability	>	GPP	~	SR			0.8
5			Stability	>	GPP					0.8
Thresholds			116		5					

4.9. Supplementary Methods

Alkalinity data

Raw conductivity was transformed in specific conductance at 25° C using water temperature (APHA, 1989). For the determination of alkalinity (Alk), raw water samplings were filtered through 0.22 µm pore size polyethersulfone (PES) syringe filters (Minisart, Sartorius AG, Goettingen, Germany). Samples were then stored at 4 °C in the dark in pre-rinsed pre-acid washed or sterile polypropylene tubes (Greiner Bio-One) until analyses within two weeks. The alkalinity was assessed by colorimetric titration using a SmartChem 200 analyser (AMS Alliance, France) following Escoffier et al. (2022). For Alk, the methyl-orange titration to a final pH of 3.2 was used, achieving a precision of 2 % on externally prepared standards. Finally, linear regression between alkalinity measured and specific conductance was performed, giving a clear relationship across the entire range of Lake Geneva ($R^2 = 0.95$; Escoffier et al., in preparation).

Model of bicarbonate buffering system

The theoretical experiment of the model of bicarbonate buffering system carried out here demonstrated the importance of alkalinity measurements to justify a consumption of bicarbonate supporting GPP through CP and CCM. At the beginning of the simulation, we supposed a water in perfect equilibrium with the atmosphere with a high alkalinity (like Lake Geneva, annual average of 1500 µeq L^{-1}) and a water temperature at 10°C (Fig. 4-1). Further, we assumed that alkalinity never changes during the experiment. In the first case, the system was net heterotrophic and CO_2 build up. The level to which the CO_2 will eventually accumulate will depend on the atmospheric exchange coefficient, but this is not important in this theoretical demonstration because we could think that the lake is sealed at the surface. So as more CO_2 was building up in the water, we will shift the equilibrium slightly to the right, but the chemistry of the equilibrium will dictate that the vast majority of the added CO_2 will remain as CO_2. Only very little amount of CO_2 will be moved to the HCO_3^-+CO_3^{2-} pool. As an example, increasing CO_2 to a level corresponding to a concentration increase of 264 µmol L^{-1} will move only about 4 µmol L^{-1} in the HCO_3^-+CO_3^{2-} pool. So, in conditions of oversaturation, the dynamics of CO_2 essentially reflected the dynamics of the total DIC pool.

However, the same is not true when the system is undersaturated in CO_2. If we began our experiment again at equilibrium but now CO_2 was consuming for photosynthesis such that we removed only 15 µmol L^{-1} of CO_2, the chemical equilibrium will have shifted about 140 µmol L^{-1} from the HCO_3^-+CO_3^{2-} pool to the CO_2 pool. This extra 140 µmol L^{-1} is what is being used to fuel the photosynthesis and O_2 production. Thus, there is a large non-linearity between the CO_2 and O_2 departures from equilibrium especially in autotrophic conditions. This exercise was then repeated for different conditions of water temperature and alkalinity level to produce Fig. 4-1 and to highlight their important role in the carbonate system equilibrium. Therefore, care must take in interpreting these CO_2–O_2 dynamic analyses when alkalinity data are not available.

Lake metabolism from oxygen data

Bayesian model for estimating lake metabolism from free oxygen (LakeMetabolizer; Winslow et al., 2016) was used to compute GPP. The mixed layer depth (Imberger, 1985; Read et al., 2011) was calculated using the thermistor chain (0-30 m) in the pelagic zone, while it was fixed at 4 m depth in the littoral zone throughout the year, assuming a constant homogeneity of the water column. We tested two gas transfer velocities (Read et al., 2012; Soloviev et al., 2007) to compute the gas exchange. Therefore, no significant difference was observed, and we used the first, including the wind shear and the buoyancy-driven convection terms. It should also be noted that most of the days of high winds (daily average wind >5 m s^{-1}) could not be estimated because of too noisy daily signals as in the analysis of the slopes (α and β).

Classification Trees

We tested whether the origins of IC supporting GPP could be predicted from the four (littoral) and five (pelagic) day-averaged selected environmental variables (GPP level, CO_2, wind speed, solar radiation, and Schmidt stability) using classification trees. The absence of normality and the collinearity between the environmental predictors justified the choice to apply a classification tree model (R package "rpart"; Therneau & Atkinson, 2022; R version 3.6.2). Two training-test dataset sizes were tested (50%–50% or 80%–20%) which led to similar results. The best models with four predictors (Table S4-1 and S4-2) were used in each environment to reconstruct the IC sources to GPP for the not-classified days for which GPP could be computed.

4.10. References

APHA. 1989. Standard Methods for the Examination of Water and Wastewater, 17th ed. APHA, AWWA, WPCF, Washington, DC.

Aho, K. S., J. D. Hosen, L. A. Logozzo, W. R. McGillis, and P. A. Raymond. 2021. Highest rates of gross primary productivity maintained despite CO2 depletion in a temperate river network. Limnol. Oceanogr. Lett. lol2.10195, doi:10.1002/lol2.10195

Bade, D. L., and J. J. Cole. 2006. Impact of chemically enhanced diffusion on dissolved inorganic carbon stable isotopes in a fertilised lake. J. Geophys. Res. 111(C1), C01014, doi:10.1029/2004JC002684

Cole, J. J., N. F. Caraco, G. W.Kling and, T. K. Kratz. 1994. Carbon Dioxide Supersaturation in the Surface Waters of Lakes. Science, New Series, 265(5178), 1568–1570. Doi:10.1126/science.265.5178.1568

Colman, B., I. E. Huertas, S. Bhatti and J. S. Dason. 2002. The diversity of inorganic carbon acquisition mechanisms in eukaryotic microalgae. Funct. Plant Biol. 29(3), 261, doi:10.1071/PP01184

Dillon, P. J., and F. H. Rigler. 1974. The phosphorus-chlorophyll relationship in lakes. Limnol. Oceanogr. 19(5), 767–773, doi:10.4319/lo.1974.19.5.0767

Escoffier, N., P. Perolo, T. Lambert, J. Rüegg, D. Odermatt, T. Adatte, T. Vennemann, and M.-E. Perga. 2022. Whiting events in a large peri-alpine lake: Evidence of a catchment-scale process. J. Geophys. Res.: Biogeosci.

Fernández Castro, B., H. E. Chmiel, C. Minaudo, S. Krishna, P. Perolo, S. Rasconi, and A. Wüest. 2021. Primary and Net Ecosystem Production in a Large Lake Diagnosed from High-Resolution Oxygen Measurements. Water Resour. Res. 57(5), doi:10.1029/2020WR029283

Finlay, K. 1999. Effect of water velocity on algal carbon isotope ratios: Implications for river food web studies.

Gaudard, A., R. Schwefel, L. R. Vinnå, M. Schmid, A. Wüest, and D. Bouffard. 2017. Optimising the parameterisation of deep mixing and internal seiches in one-dimensional hydrodynamic models: A case study with Simstrat v1.3. Geosci. Model Dev. 10(9), 3411–3423, doi:10.5194/gmd-10-3411-2017

Groleau, A., G. Sarazin, B. Vinçon-Leite, B. Tassin, and C. Quiblier-Llobéras. 2000. Tracing calcite precipitation with specific conductance in a hard water alpine lake (Lake Bourget). Water Res. 34(17), 4151–4160, doi:10.1016/S0043-1354(00)00191-3

Idso, SB 1973. On the concept of lake stability. Limnol. Oceanogr. 18, 681–683, doi:10.4319/lo.1973.18.4.0681

Imberger, J. 1985. The diurnal mixed layer. Limnol. Oceanogr. 30, 737–770, doi:10.4319/lo.1985.30.4.0737

Iversen, L. L., A. Winkel, L. Baastrup-Spohr, A. B. Hinke, J. Alahuhta, A. Baattrup-Pedersen, S. Birk, P. Brodersen, P. A. Chambers, F. Ecke, T. Feldmann, D. Gebler, J. Heino, T. S. Jespersen, S. J. Moe, T. Riis, L. Sass, O. Vestergaard, S. C. Maberly, and O. Pedersen. 2019. Catchment properties and the photosynthetic trait composition of freshwater plant communities. Science, 366(6467), 878–881, doi:10.1126/science.aay5945

Karlsson, J., P. Byström, J. Ask, P. Ask, L. Persson, and M. Jansson. 2009. Light limitation of nutrient-poor lake ecosystems. Nature, 460(7254), 506–509, doi:10.1038/nature08179

Kelts, K., and K. J. Hsü. 1978. Freshwater Carbonate Sedimentation. In A. Lerman (Ed.), Lakes (pp. 295–323). Springer New York, doi:10.1007/978-1-4757-1152-3_9

Khan, H., A. Laas, R. Marcé, and B. Obrador. 2020. Major Effects of Alkalinity on the Relationship Between Metabolism and Dissolved Inorganic Carbon Dynamics in Lakes. Ecosystems, 23(8), 1566–1580, doi:10.1007/s10021-020-00488-6

Kragh, T., and K. Sand-Jensen. 2018. Carbon limitation of lake productivity. Proc. R. Soc., Ser. B, 285(1891), 20181415, doi:10.1098/rspb.2018.1415

Krause-Jensen, D., and K. Sand-Jensen. 1998. Light attenuation and photosynthesis of aquatic plant communities. Limnol. Oceanogr. 43(3), 396–407, doi:10.4319/lo.1998.43.3.0396

Labat, F., and M. Blanchard. 2020. CIPEL: Etude de la végétation macrophytique de lac Léman, Suivi 2019. 1–208.

Larsson, C., and L. Axelsson. 1999. Bicarbonate uptake and utilization in marine macroalgae. Eur. J. Phycol. 34(1), 79-86, doi:10.1080/09670269910001736112

Lefèvre, N., and L. Merlivat. 2012. Carbon and oxygen net community production in the eastern tropical Atlantic estimated from a moored buoy: NCP IN THE EASTERN TROPICAL ATLANTIC. Global Biogeochem. Cycles, 26(1), doi:10.1029/2010GB004018

Li, H., Y. Wu, and L. Zhao. 2018. Effects of carbon anhydrase on utilisation of bicarbonate in microalgae: A case study in Lake Hongfeng. Acta Geochim. 37(4), 519–525, doi:10.1007/s11631-018-0277-4

Maberly, S. C., and B. Gontero. 2017. Ecological imperatives for aquatic CO2-concentrating mechanisms. J. Exp. Bot., 68(14), 3797–3814, doi:10.1093/jxb/erx201

Maberly, S. C., S. A. Berthelot, A. W. Stott, and B. Gontero. 2015. Adaptation by macrophytes to inorganic carbon down a river with naturally variable concentrations of CO2. J. Plant Physiol. 172, 120–127, doi:10.1016/j.jplph.2014.07.025

Mishra, S., B. Joshi, P. Dey, H. Pathak, and A. Kohra. 2018. CCM in photosynthetic bacteria and marine alga. J. Pharmacogn. Phytochem. 7(6), 928-937.

Müller, B., J. S. Meyer, and R. Gächter. 2016. Alkalinity regulation in calcium carbonate-buffered lakes. Limnol. Oceanogr. 61(1), 341–352, doi:10.1002/lno.10213

Parvathi, A., X. Zhong, A. S. Pradeep Ram, and S. Jacquet. 2014. Dynamics of auto- and heterotrophic picoplankton and associated viruses in Lake Geneva. Hydrol. Earth Syst. Sci. 18(3), 1073–1087, doi:10.5194/hess-18-1073-2014

Pełechaty, M., A. Pukacz, K. Apolinarska, A. Pełechata, and M. Siepak. 2013. The significance of Chara vegetation in the precipitation of lacustrine calcium carbonate. Sedimentology, 60(4), 1017–1035, doi:10.1111/sed.12020

Price, G. D., M. R. Badger, F. J. Woodger, and B. M. Long. 2008. Advances in understanding the cyanobacterial CO2-concentrating-mechanism (CCM): Functional components, Ci transporters, diversity, genetic regulation and prospects for engineering into plants. J. Exp. Bot. 59(7), 1441–1461, doi:10.1093/jxb/erm112

Read, J. S., D. P. Hamilton,I. D. Jones, K. Muraoka, L. A. Winslow, R. Kroiss, C. H. Wu, and E. Gaiser. 2011. Derivation of lake mixing and stratification indices from high-resolution lake buoy data. Environ. Modell. Softw. 26(11), 1325–1336, doi:10.1016/j.envsoft.2011.05.006

Read, J. S., D. P. Hamilton, A. R. Desai, K. C. Rose, S. MacIntyre, J. D. Lenters, R. L. Smyth, P. C. Hanson, J. J. Cole, P. A. Staehr, J. A. Rusak, D. C. Pierson, J. D. Brookes, A. Laas, and C. H. Wu. 2012. Lake-size

dependency of wind shear and convection as controls on gas exchange. Geophys. Res. Lett. 39(9), 1325–1336, doi:10.1029/2012GL051886

Schindler, D., W. 1971. Carbon, Nitrogen, and Phosphorus and the eutrophication of freshwater lakes. J. Phycol. 7, 321-329, doi:10.1111/j.1529-8817.1971.tb01527.x

Schindler, D. W., G. Brunskill, S. Emerson, W. Broecker, and T.-H. Peng. 1972. Atmospheric carbon dioxide: Its role in maintaining phytoplankton standing crops. Science, 177, 1192–1194, doi:10.1126/science.177.4055.1192

Schindler, D. W., H. Kling, R. V. Schmidt, J. Prokopowich, V. E. Frost, R. A. Reid, and M. Capel. 1973. Eutrophication of Lake 227 by Addition of Phosphate and Nitrate: The Second, Third, and Fourth Years of Enrichment, 1970, 1971, and 1972. J. Fish. Res. Board Can. 30(10), 1415–1440, doi:10.1139/f73-233

Schindler, D. W. 1974. Eutrophication and Recovery in Experimental Lakes: Implications for Lake Management. Science, 184(4139), 897–899, doi:10.1126/science.184.4139.897

Schwefel, R., A. Gaudard, A. Wüest, and D. Bouffard. 2016. Effects of climate change on deepwater oxygen and winter mixing in a deep lake (Lake Geneva): Comparing observational findings and modeling. Water Resour. Res. 52(11), 8811–8826, doi:10.1002/2016WR019194

Soloviev, A., M. Donelan, H. Graber, B. Haus, and P. Schlüssel. 2007. An approach to estimation of near-surface turbulence and CO2 transfer velocity from remote sensing data, J. Marine Syst., 66, 182–194, doi:10.1016/j.jmarsys.2006.03.023

Steemann Nielsen, E. S. 1946. Carbon sources in the photosynthesis of aquatic plants. Nature, 158, 594–596, doi:10.1038/158594a0

Stets, E. G., D. Butman, C. P. McDonald, S. M. Stackpoole, M. D. DeGrandpre, and R. G. Striegl. 2017. Carbonate buffering and metabolic controls on carbon dioxide in rivers: Controls on CO2 in Rivers. Global Biogeochem. Cycles, 31(4), 663–677, doi:10.1002/2016GB005578

Stumm, W., and J. J. Morgan. 1981. Aquatic Chemistry: An introduction emphasising chemical equilibria in natural waters, 2nd ed.Wiley.

Therneau, T., and B. Atkinson. 2022. Recursive Partitioning and Regression Trees: Package “rpart”. https://github.com/bethatkinson/rpart

Thomas, E. A., and E. B. Tregunna. 1968. Bicarbonate ion assimilation in photosynthesis by Sargassum muticum. Can. J. Bot. 46(4), 411–415, doi:10.1139/b68-063

Vachon, D., S. Sadro, M. J. Bogard, J. Lapierre, H. M. Baulch, J. A. Rusak, B. A. Denfeld, A. Laas, M. Klaus, J. Karlsson, G. A. Weyhenmeyer, and P. A. Giorgio. (2020). Paired O2–CO2 measurements provide emergent insights into aquatic ecosystem function. Limnol. Oceanogr. Lett. 5(4), 287–294, doi:10.1002/lol2.10135

Wanninkhof, R., and M. Knox. 1996. Chemical enhancement of CO2 exchange in natural waters. Limnol. Oceanogr. 41(4), 689–697, doi:10.4319/lo.1996.41.4.0689

Winslow, L. A., J. A. Zwart, R. D. Batt, H. A. Dugan, R. I. Woolway, J. R. Corman, P. C. Hanson, and J. S. Read. 2016. LakeMetabolizer: An R package for estimating lake metabolism from free-water oxygen using diverse statistical models. Inland Waters, 6(4), 622–636, doi:10.1080/IW-6.4.883

Wüest, A., D. Bouffard, J. Guillard, B. W. Ibelings, S. Lavanchy, M.-E. Perga, and N. Pasche. 2021. LéXPLORE: A floating laboratory on Lake Geneva offering unique lake research opportunities. WIREs Water, 8(5), doi:10.1002/wat2.1544

Zagarese, H. E., M. Sagrario, G. de los Á, D. Wolf-Gladrow, P. Nõges, T. Nõges, K. Kangur, S.-I. S. Matsuzaki, A. Kohzu, M. J. Vanni, D. Özkundakci, S. A. Echaniz, A. Vignatti, F. Grosman, P. Sanzano, B. Van Dam, and L. B. Knoll. 2021. Patterns of CO2 concentration and inorganic carbon limitation of phytoplankton biomass in agriculturally eutrophic lakes. Water Res. 190, 116715, doi:10.1016/j.watres.2020.116715

Zhang, T., J. Li, J. Pu, J. B. Martin, M. B. Khadka, F. Wu, L. Li, F. Jiang, S. Huang, and D. Yuan. 2017. River sequesters atmospheric carbon and limits the CO2 degassing in karst area, southwest China. Sci. Total Environ. 609, 92–101, doi:10.1016/j.scitotenv.2017.07.143

4.11. Acknowledgment

We would like to thank the entire team of the LéXPLORE platform for their administrative and technical support and the LéXPLORE core dataset. We also acknowledge the five partner institutions involved with LéXPLORE: Eawag, EPFL, the University of Geneva, the University of Lausanne, and CARRTEL (INRAE-USMB). This study was supported by the CARBOGEN project (SNF 200021_175530), which is linked to the LéXPLORE project (SNF R'Equip, P157779) and the Primary Production Under Oligotrophication in Lakes project (SNF 200021_179123). The authors thank Sébastien Lavanchy, the chief technical officer (APHYS-EPFL), and Aurélien Ballu, a member of the technical pool (IDYST-UNIL) of LéXPLORE platform, for their technical and field support.

4.12. Author contribution statement

PP, MEP, and DB conceived the study design. PP, NE, and HC collected field data and carried out data pre-processing. PP and MEP performed data analysis and modelling. PP, MEP, and DB drafted the manuscript with inputs from all authors.

Chapter 5

Synthesis

5.1. Relevant physical and biogeochemical processes regulating the surface CO_2 dynamics in Lake Geneva

In this doctoral thesis, I aimed at untying and understanding the physical and biogeochemical processes regulating the dynamics of surface CO_2 at different spatiotemporal scales in a large and deep hardwater lake through the decomposition of the CO_2 flux equation at the air-water interface. This work led me to the main results of chapters 2, 3, and 4 but also to scientific collaborations in terms of understanding the connection between alkalinity and the carbonate cycle at the catchment scale (Escoffier et al., 2022) and the link between CO_2 variations in the epilimnion and the internal dynamics of water mass movements (Fernández et al., 2021). In the two following subsections, I emphasise how **the key findings** of my doctoral work that for me, contributed within two main aspects. The first contribution revolves around how the quantification of the underlying (mainly physical) processes can improve gas flux estimates at the lake scale. The second contribution is a first step toward a mechanistic integration of alkalinity within CO_2 processes in lakes through GPP. From these two types of key findings, I derive a conceptual framework of "GPP-alkalinity pump", which could explain why Lake Geneva is overall a CO2 source to the atmosphere.

5.1.1. The role of the different terms of the equation in the spatiotemporal CO_2 fluxes

Concerning the drivers of **gas transfer velocity**, we have seen that the limnological community has focused on the effect of wind (Cole et Caraco, 1998; Crusius and Wanninkhof, 2003) and convection (e.g. MacIntyre et al., 2010; Read et al., 2012; Tedford et al., 2014) and that there were premises on the effect of lake size and fetch distance (Vachon et al., 2013). I show that for a large lake like Lake Geneva, it is necessary to introduce **wind-induced waves** for wind speed >5 m s^{-1} and fetch distance >15 km to compute gas transfer velocity. These intense episodic events can generate more than **20% of annual cumulative *k*** and more than 25% of net yearly CO_2 fluxes in Lake Geneva.

The role of **chemical enhancement** on the inward CO_2 flux in high alkaline and pH conditions is well established (Wanninkhof and Knox, 1996; Bade and Cole, 2006). However, its dependence on the choice of *k* model and its contribution to the net annual CO_2 flux balance are rarely studied. My results show that its integration at high or low frequency doubles the inward fluxes during the warm period and that, depending on the choice of *k* model, the **net annual CO_2 flux balance** can be **opposed**.

A constant value is often set for **atmospheric CO_2** used in the gas exchange computation. The study of its integration at high frequency shows that the effect is not very substantial. Average monthly data produce estimates very close to high frequencies for annual estimates, but its impact on flux estimates at hourly scale could be relevant. In addition, I highlight the **effect of strong wind on its variability,** which maintains a constant concentration close to 390 ppm, allowing a higher ΔpCO_2 during outward flux, but with a **negligible effect** on an annual scale.

The **relevance of high-frequency** data for the *k* and water pCO_2 variables is highlighted in my temporal analyses. Still, their impact on the flux estimation differs according to the seasons and frequency, as demonstrated by Natchimuthu et al. (2017). High-frequency computations of ***k*** (**hourly**) are relevant all year round and capture intense turbulence events generating an increase in fluxes on an hourly and daily scale. On the other hand, **daily** and **weekly** measurements of **pCO_2** are necessary during shoulder periods, while the sampling frequency can be loosened during periods of stability such as summer. Finally, we propose solutions to improve these CO_2 gas exchange quantifications using currently available numerical tools such as spatial weather model, hydrodynamical model, and data reconstruction.

In terms of **spatial variability**, the yearly mean flux of the **littoral** environment is more than **one order of magnitude greater** than for the **pelagic**, with 26.8 and 1.92 g C m^{-2} $yr^{-1,}$ respectively. This significant difference is mainly due to the spatial variability of pCO_2, which I assimilate to the proximity of sediment producing CO_2. Moreover, I show that even if the littoral area represents a low share of the lake surface area (herein 2.2% of the total lake area for a max depth of the littoral of 4 m), **littoral CO_2 flux** already contributes **25%** of the total lake flux, demonstrating the relevance of integrating littoral estimation for accurate flux balance.

My results also allow me to propose a new way to **integrate the gas exchange at the lake scale**. Indeed, the **gas transfer velocity** can be modelled at **high frequency** in **time** and **space** using a 2-3D meteorological model (e.g. COSMO-1; Swissmeteo). The atmospheric CO_2 can be assumed to be homogenous on the lake, and its value is integrated at a low frequency (monthly to yearly). The effect of strong wind can even be implemented spatially through a meteorological model. However, the **pCO_2 remains very challenging** to acquire at high frequency without expensive sensors and even more spatially due to the great physical dynamics of the lake at different periods of the year (e.g. shoulder periods). This limit and these future perspectives are more substantiated in section 5.3.

My collaboration with Dr Fernández and Dr Chmiel (Fernández et al., 2021) allowed me to understand the wind effect on this stratified layer, which leads to complex motions, ranging from direct circulation to internal waves making it difficult to estimate the integrated metabolism of the water column. Indeed, these **internal motions** cause regular **thermocline depth variations** throughout the day, influencing the recorded **DO and CO_2 signal** in a non-biological way. Thus, they applied DO signal **filtering methods** using temperature change to correct the DO signal influenced by physical processes to improve the metabolic estimates at the scale of a large lake. Nevertheless, the signal deviation is mainly localised around the thermocline between 10 and 20 m depending on the period but has **little influence on the surface signal** (0-5 m).

My collaboration with Dr Escoffier (Escoffier et al., 2022) taught me that the **coupling** of specific **river conditions** (due to catchment processes) and **lake conditions** produce punctually in spring and summer **whiting events**, a particular event of massive calcium carbonate precipitation at the lake surface manifested by a turquoise colour. This process influences the regulation of surface CO_2 by producing one mole of CO_2 during the precipitation reaction and therefore leads to **spatial variability** according to water movements such as gyres.

5.1.2. Tying alkalinity, GPP, and CO_2

The two main biological processes influencing surface CO_2 variations are GPP, consuming CO_2, and respiration, producing CO_2 and inversely for O_2 leading to a theoretical molar ratio of ~1.2. CO_2–O_2 departure coupling method (Vachon et al., 2020) shows high O_2 production rates despite CO_2 depletion during the stratification period in Lake Geneva. Therefore, **GPP** relies on **HCO_3^- withdrawal** from the water to subsidise the missing CO_2 for **two-thirds of the year**, resulting in a depleted alkalinity pool in the littoral and pelagic environments, as recently demonstrated in the Connecticut River (Aho et al., 2021). Indirect or direct mechanisms are associated with this HCO_3^- uptake, **calcite precipitation** (CP) and **CO_2-concentrating mechanis**m (CCM), respectively. Moreover, daily CO_2 variations are more pronounced in the littoral environment, which is related to the proximity of sedimentary respiration, implying **spatial differences** in surface CO_2 dynamics.

5.2. Conceptual carbon cycle for a deep hardwater lake and CO_2 emission: the GPP-alkalinity pump

The pooling of all the findings presented in this work, coupled with many studies done on Lake Geneva during the CARBOGEN project, allows us to propose a conceptual carbon cycle for a deep hardwater lake with low allochthonous organic matter but with a high contribution of alkalinity and calcium coming from the watershed (Fig. 5-1). Through this conceptual scheme, we try to highlight (i) why Lake Geneva is a source of CO_2 to the atmosphere on an annual scale and (ii) why these CO_2 fluxes can be considered as transformed carbon according to the concept of lake transformer (Engel et al., 2018; Cole et al. 2007). As several recent studies on freshwater systems (Kragh & Sand-Jensen, 2018; Stets et al., 2017; Khan et al., 2020; Aho et al., 2021), the relevant role of alkalinity in the aquatic carbon cycle and its close links with aquatic ecosystems are primordial to understand better the processes regulating the surface CO_2 dynamics. According to past studies (e.g. Stets et al., 2017; Marcé et al., 2015), calcite precipitation is responsible for CO_2 supersaturation of hardwater and alkaline freshwater systems, causing CO_2 emissions to the atmosphere. However, processes linking alkalinity and outward CO_2 fluxes are not specified in their research, and Kahn et al. (2020) showed that CP generates little surface CO_2.

Our results show that CO_2 depletion necessary to reach the conditions of CP does not allow a positive differential between the water and the atmosphere. Moreover, this produced CO_2 by CP had to be directly consumed by GPP to maintain the production of O_2 observed and transformed into organic carbon (CH_2O). Thus, this mechanism transfers C from the surface alkalinity to the bottom lake in the forms of calcite and organic carbon. Thus, this mechanism transfers C from the surface alkalinity to the lake bottom in the form of calcite and organic carbon. Then, we assume that this C is transformed back into CO_2 in the hypolimnion and that it will be reinjected towards the surface to support winter supersaturation during deep mixing. Therefore, we could have an autotrophic lake source of CO_2, in absence of significant CO_2 inputs by inflows or groundwaters. This hypothesis is detailed along an annual cycle (from spring to winter) in the following paragraphers.

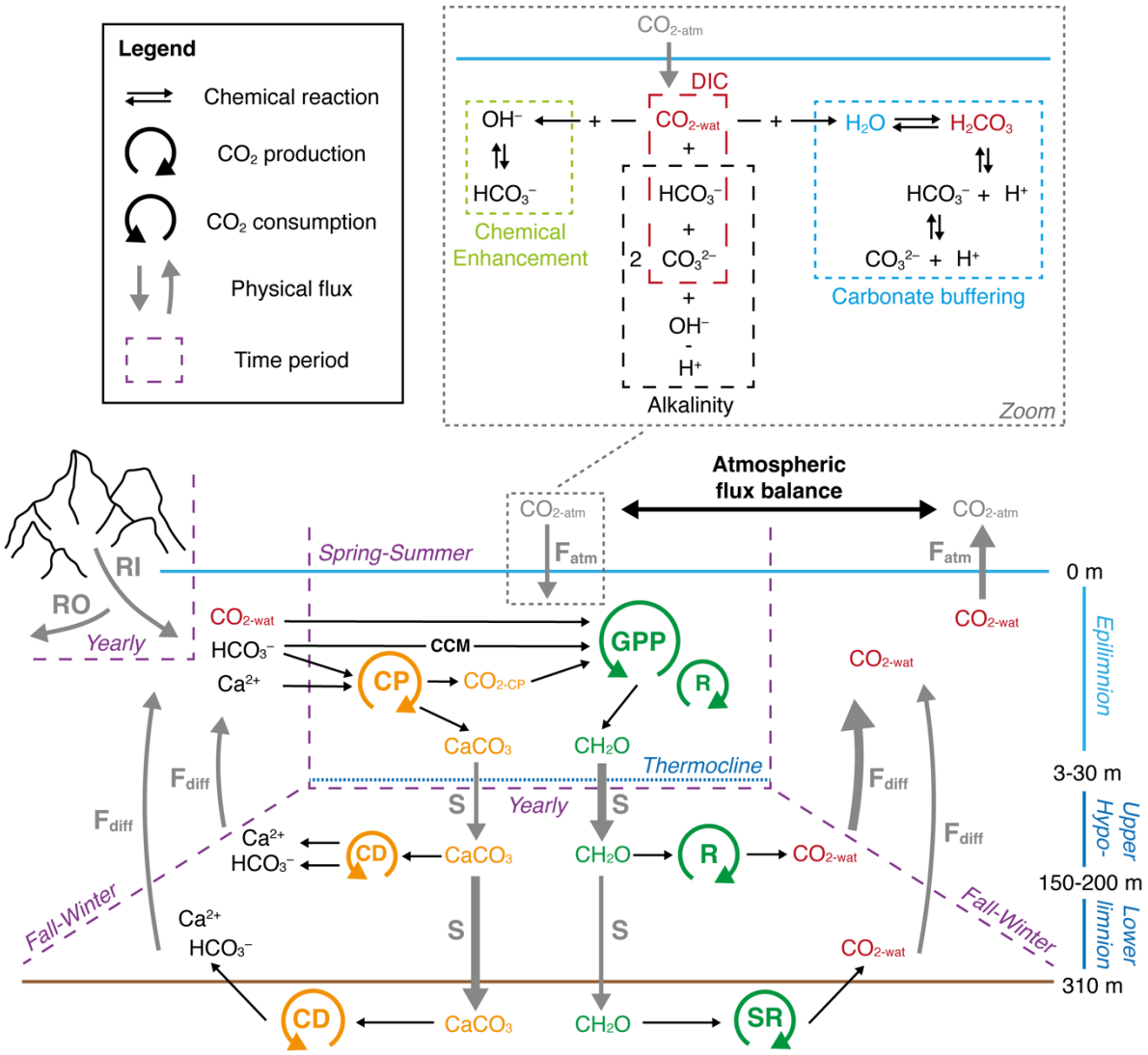

Fig. 5-1: Conceptual scheme of carbon model for Lake Geneva. Physical fluxes are represented in grey for river input (RI), river output (RO), sedimentation of calcite and organic matter (S), diffusion flux (F_{diff}), and atmospheric flux (F_{atm}). Carbonate's chemical reactions are represented in orange for calcite precipitation (CP) and calcite dissolution (CD). Biological processes are described in green for gross primary production (GPP), respiration (R), and sediment respiration (SR). Zoom box focuses on the air-water interface during CO_2 invasion with two possible reactions: chemical enhancement and carbonate buffering.

The connection between watershed and lake is primordial because river inputs (RI) drive alkalinity, calcium, and DIC in lakes (Müller et al., 2016; Weyhenmeyer et al., 2015). After winter mixing, the nutrients are homogenised over the water column or at least a large part. GPP is slightly limited by light and water temperature. In these conditions, a few days to a few weeks of good weather allows early spring bloom leading to undersaturated CO_2 concentration influenced by the beginning of the stratified layer. However, the stratification is still weak, and the first wind event remixes the surface layers and restores them to their initially homogeneous state with supersaturated CO_2 concentration. Thus, this period is alternated by outward and inward CO_2 fluxes on a daily and weekly scale.

From mid-spring, GPP rates increase, and CO_2 depletion starts to be pronounced all day at the lake surface, reinforced by the consistent implementation of the thermal stratification limiting the CO_2 diffuse flux coming from the hypolimnion. In these specific conditions, the CO_2 inward flux from the atmosphere is increased by the chemical enhancement, but the incoming CO_2 is directly transformed into HCO_3^- not allowing basic GPP support. During the same time, the conditions are conducive for the calcite precipitation, and this process occurs until the beginning of fall as high GPP level. Therefore, most of the carbon needed to maintain GPP levels is supported by HCO_3^- uptake either direct by CCM or indirect by CP. All these inorganic carbon (CO_2 and HCO_3^-) are transformed into organic matter (CH_2O) during the warm period.

The sedimentation (S; Fig. 5-1) of calcite ($CaCO_3$) and organic matter (CH_2O) occurs annually from surface to bottom. However, the thermocline layer, during the stratification period, is not stable due to internal motions (Bouffard and Lemmin, 2013) and should decrease the sedimentation more particularly for organic matter than calcite crystal because the calcite is denser (2.71 and 1.25 kg m^{-3}, respectively) and its shape is more compact. Thus, this organic matter could remain longer between 20 and 50 m and be highly respired/mineralised at the end of summer and in fall, as seen in the long-term data from CIPEL by the formation of CO_2 patch and high consumption of O_2 (Fig. 1-8 (a), (b) in the introduction). On the other hand, calcite sedimentation could occur faster, and this dissolution starts deeper regarding specific conditions since no observation of patch in alkalinity and calcium are done (Fig. 1-8 (c), (d)). Nevertheless, the dissolution is more efficient at the bottom due to sediment respiration (SR) and high CO_2 concentration. Moreover, this opposite effect of sedimentation could be accentuated by the current climate change. Indeed, warmer water temperatures should improve the mineralisation of organic matter and lead to less organic carbon burial (Gudasz et al., 2010). On the other hand, increasing the stratification period could lead to more calcite precipitation, and warmer water at the bottom lake could dissolve less.

In fall, three physical processes (F_{diff}), seiche, upwelling, and water exchange between small and large basins (Umlauf et Lemmin, 2005), can bring the rich CO_2 from the upper hypolimnion to the surface to be released to the atmosphere depending on the intensity and the frequency. These events produce intense outward flux, but for a short period. In contrast, winter mixing (F_{diff}) takes place over a more extended period due to the gradual decrease in air temperature and the succession of more frequent wind events in this season (Perolo et al., 2021), causing deep convection (Schwefel et al., 2016; Gaudard et al., 2017) up to 309 m during very severe winter (most recent in winter 2012). Moreover, a recent study highlighted a wintertime coastal upwelling as an efficient transport process for deep-water renewal up to 200 m without strong convection (Reiss et al., 2020). This winter remobilisation of CO_2 on the water surface allows strong degassing reinforced by the surface wave more present than in summer (Perolo et al., 2021).

Lake Geneva, therefore, has a positive annual atmospheric flux balance according to our most detailed estimates (~2-4 Gg C yr^{-1}; Chpt 4). This source of CO_2 to the atmosphere can be explained by a higher absolute ΔpCO_2 in winter than in summer despite a longer period of undersaturation and higher production of turbulence, k, during the cold period produced by wind and wind-induced waves that are more frequent and intense.

Finally, this conceptual carbon cycle for a deep hardwater lake is in accord with the recent paradigm of lakes as active carbon transformers (Engel et al., 2018; Cole et al., 2007) and that they act as CO_2 reactor through different pathways allowing to release more atmospheric evasion than invasion in this kind of system. The assimilation of HCO_3^- by the CP and CCM through organic matter generates a kind of battery from which alkalinity is converted to organic matter at the surface, then to CO_2 at depth by respiration, with a time and space lag between the physical and biogeochemical processes. Alkalinity can therefore be considered as the core of the carbon cycle of Lake Geneva and has a significant role in the regulation of the CO_2 surface dynamics.

5.3. Limits and perspectives

This doctoral thesis is the first attempt to understand the physical and biogeochemical processes regulating surface CO_2 dynamics in a large and deep hardwater lake on an hourly scale throughout annual cycles. The results presented can already improve the quantification of these processes and reveal their spatial and temporal influence but do not yet allow the quantification of a complete carbon budget. Gaps in the knowledge of each process studied have yet to be filled, mainly at the spatial lake scale. This last section discusses the limits and perspectives of these results to improve future research.

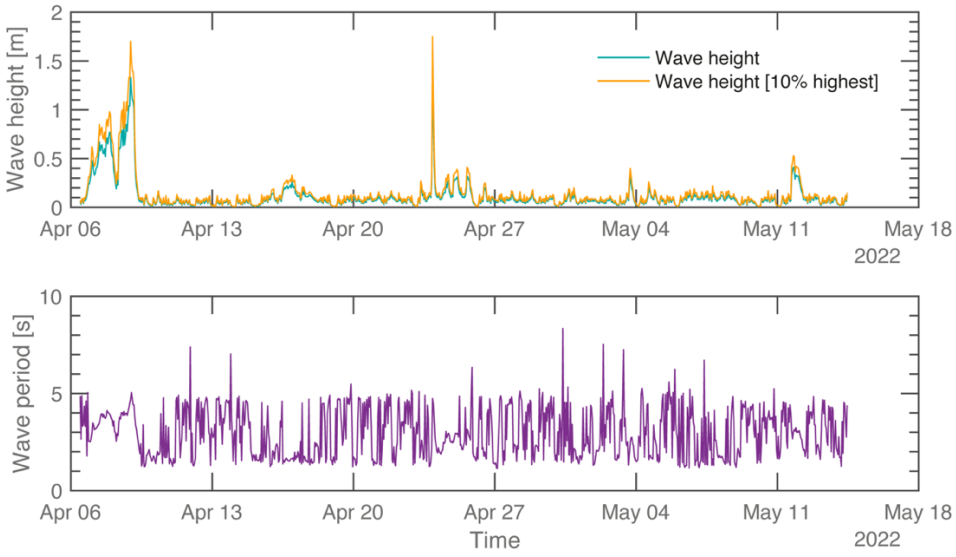

Fig. 5-2: Wave buoy measurement at LéXPLORE platform; **(top)** Temporal series of wave height and 10% highest wave; **(down)** Temporal series of wave period.

Chapter 2 showed the relevance of accounting for surface waves in the parameterisation of the gas transfer velocity and that it could be modelled at high frequency in time and space. However, the wave height estimation has only been estimated using the formula of Hasselmann et al. (1973). The formation of the waves and their behaviour in a lacustrine environment has still little been studied. Therefore, their direct measurement in the field would be important to refine this input variable of the *k* model and provide new knowledge on the lake wave dynamic. The wave buoy system has been recently installed on the LéXPLORE platform since April 2022 with live data visualisation on the Datalakes portal (Fig. 5-2). In addition, an intriguing question has come to us

concerning the true lake surface in wave conditions since the fluxes are always related to a unit area. So, would an oily lake condition compared to a severe wave condition lead to significant true surface differences?

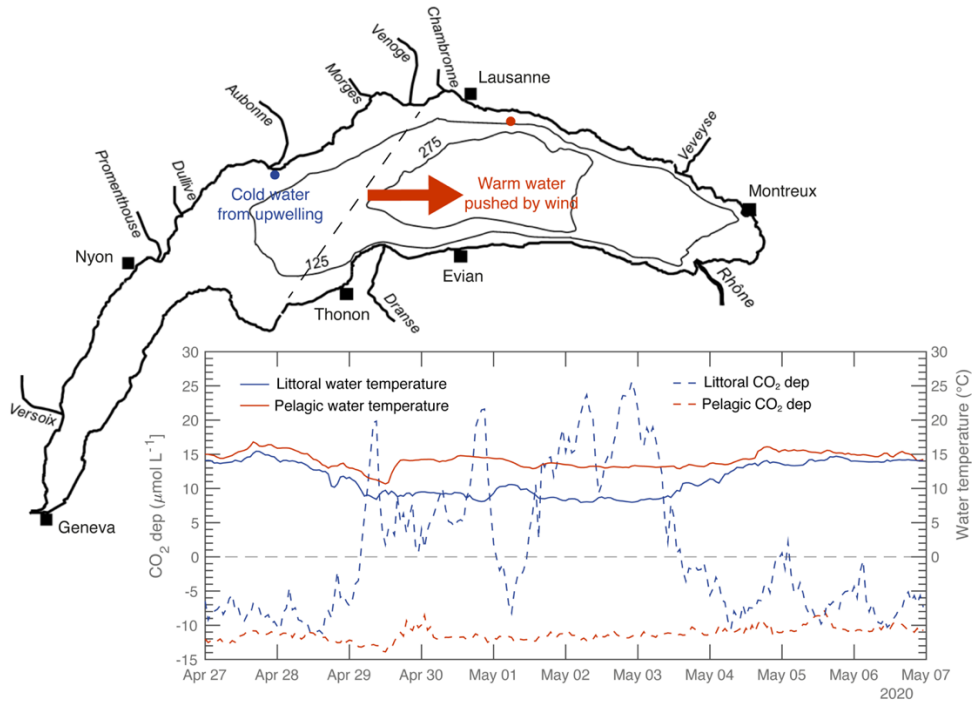

Fig. 5-3: Conceptual scheme of the seiche and upwelling after wind event occurring in spring when the stratification is weakly established **(top)**. Time series of ΔpCO_2 (or CO_2 dep; µmol L^{-1}) and water temperature (°C) in the littoral and pelagic sites **(down)**. These mechanisms produce a rise in CO_2 in the upwelling zone (littoral site), creating supersaturation conditions from April 29 to May 3 in the north-west zone while the concentration of CO_2 remains undersaturated where warm water is pushed into the east zone (pelagic site).

Chapter 3 demonstrated that high-frequency data of the main variables necessary for the computation of the CO_2 gas exchange were essential not to underestimate the annual flux balance. Moreover, the water pCO_2 remains the most challenging variable of the flux equation to acquire or model in space. We have shown sketches of the potential reconstruction of this data over time through new deep learning tools allowing it to be estimated with external forcing data after training and validation models. These innovative methods need further investigation to complete missing data during maintenance and even to be able to reconstruct long time series of pCO_2 to study changes related to climate and human pressure. Regarding the spatial resolution of water pCO_2, we believe that the 3D hydrodynamic models developed in recent years will be able to resolve this gap. We have seen that the surface CO_2 dynamics depend on the physical processes of mixing and water mass movement, which are linked to variations in water temperature. Finding a prediction method for pCO_2 passing through water temperature could allow a spatial representation that could improve the CO_2 gas exchange at the lake scale in coupling with the spatial *k* model. For example, we detected opposite ΔpCO_2 between the littoral and pelagic sites over a few days (April-May), coinciding with water temperature differences of more than 5°C (Fig. 5-3). This effect could be explained by forming a seiche and an upwelling creating this spatial heterogeneity. A wind event could produce a seiche which pushes the warm surface waters towards the east of the lake (pelagic site; Fig. 5-3 and 5-4), where the CO_2

concentration remains undersaturated. In contrast, an upwelling could be formed in the northwestern part of the lake (littoral site; Fig. 5-3 and 5-4), where the CO_2 concentration goes into supersaturation for a few days, producing opposite fluxes. Thus, the extraction of water temperature from a 3D hydrodynamic model (Meteolakes; Fig. 5-4) would allow us to study the link between water temperature and water pCO_2 to resolve spatial variability.

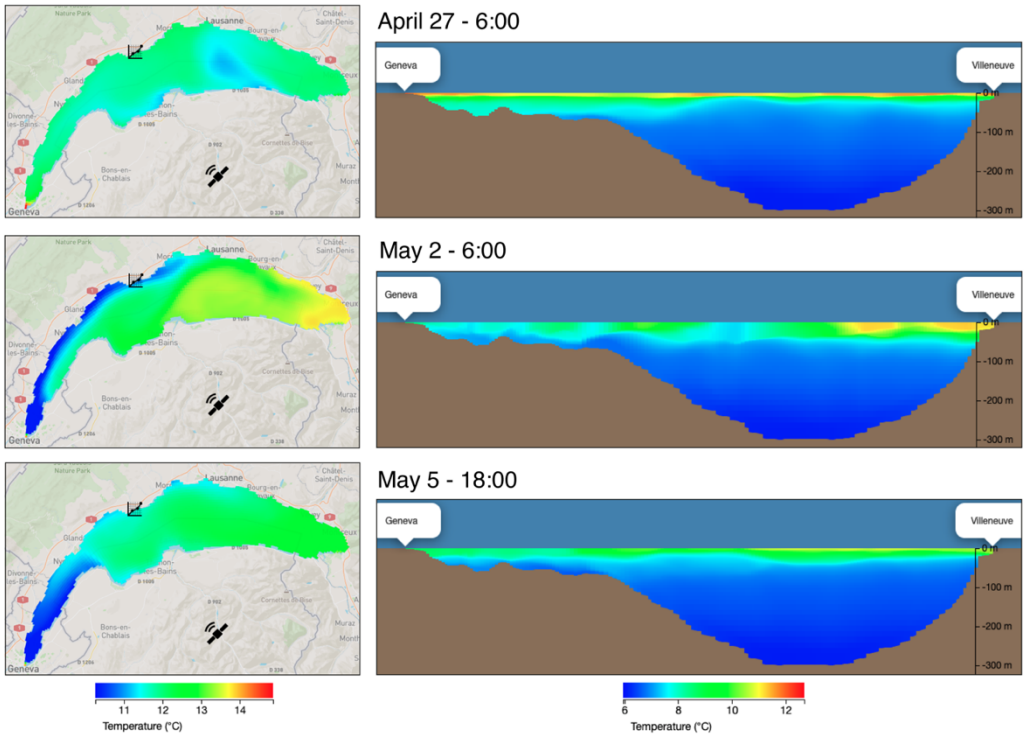

Fig. 5-4: 3D hydrodynamics model from Meteolakes (http://meteolakes.ch/#!/hydro/geneva). Spatial observation of water temperature is available on the Meteolakes website simulating the hydrodynamic of Lake Geneva.

Chapter 4 highlighted the alkalinity support to high GPP rates and focused on the first meter of the lake surface. However, GPP can have high rates, up to 10-15 m (Fernández et al., 2021). Future studies could integrate the methods used across the epilimnion and relate the metabolism to calcite precipitation rate estimates. Dr Escoffier is developing such research by linking daily precipitation rates with NEP, with convincing results. Moreover, the main shortcomings necessary to the carbon budget are those related to the sedimentation, dissolution, and mineralisation of calcite and organic matter and their burial and their return to the system, which have yet to be studied in detail.

Finally, the conceptual carbon cycle of a deep hardwater lake will require detailed quantification of each process (arrows; Fig. 5-1) to validate it and produce a complete carbon budget. The coupling of hydrodynamic and biogeochemical models (Simstrat and Aquatic Ecosystem Dynamics (AED)) carried out by Dr Many gives interesting intermediate results. Indeed, since a carbonate box model was implemented (which integrates the alkalinity-related processes), the model reproduces well the overall chain of processes along a year but still overestimates surface CO_2 during winter mixing. These shortcomings are likely due to problems in modelling lake bottom processes which have not yet been extensively investigated. However, once they are solved, this model

will allow sensitivity tests of each process and produce different scenarios concerning climate change and human impacts to prevent ecosystems' health and management.

5.4. References

Aho, K. S., Hosen, J. D., Logozzo, L. A., McGillis, W. R., & Raymond, P. A. (2021). Highest rates of gross primary productivity maintained despite CO2 depletion in a temperate river network. *Limnology and Oceanography Letters*, lol2.10195. https://doi.org/10.1002/lol2.10195

Bade, D. L., & Cole, J. J. (2006). Impact of chemically enhanced diffusion on dissolved inorganic carbon stable isotopes in a fertilized lake. *Journal of Geophysical Research*, *111*(C1), C01014. https://doi.org/10.1029/2004JC002684

Cole, J. J., Prairie, Y. T., Caraco, N. F., McDowell, W. H., Tranvik, L. J., Striegl, R. G., Duarte, C. M., Kortelainen, P., Downing, J. A., Middelburg, J. J., & Melack, J. (2007). Plumbing the Global Carbon Cycle: Integrating Inland Waters into the Terrestrial Carbon Budget. *Ecosystems*, *10*(1), 172–185. https://doi.org/10.1007/s10021-006-9013-8

Cole, J. J., & Caraco, N. F. (1998). Atmospheric exchange of carbon dioxide in a low-wind oligotrophic lake measured by the addition of SF_6. *Limnology*

Crusius, J., & Wanninkhof, R. (2003). Gas transfer velocities measured at low wind speed over a lake. *Limnology and Oceanography*, *48*(3), 1010–1017. https://doi.org/10.4319/lo.2003.48.3.1010

Engel, F., Farrell, K. J., McCullough, I. M., Scordo, F., Denfeld, B. A., Dugan, H. A., de Eyto, E., Hanson, P. C., McClure, R. P., Nõges, P., Nõges, T., Ryder, E., Weathers, K. C., & Weyhenmeyer, G. A. (2018). A lake classification concept for a more accurate global estimate of the dissolved inorganic carbon export from terrestrial ecosystems to inland waters. *The Science of Nature*, *105*(3–4). https://doi.org/10.1007/s00114-018-1547-z

Escoffier, N., P. Perolo, T. Lambert, J. Rüegg, D. Odermatt, T. Adatte, T. Vennemann, and M.-E. Perga. 2022. Whiting events in a large peri-alpine lake: Evidence of a catchment-scale process. J. Geophys. Res.: Biogeosci.

Fernández Castro, B., Chmiel, H. E., Minaudo, C., Krishna, S., Perolo, P., Rasconi, S., & Wüest, A. (2021). Primary and Net Ecosystem Production in a Large Lake Diagnosed from High-Resolution Oxygen Measurements. *Water Resources Research*, *57*(5). https://doi.org/10.1029/2020WR029283

Gaudard, A., Schwefel, R., Vinnå, L. R., Schmid, M., Wüest, A., & Bouffard, D. (2017). Optimizing the parameterization of deep mixing and internal seiches in one-dimensional hydrodynamic models: A case study with Simstrat v1.3. *Geoscientific Model Development*, *10*(9), 3411–3423. https://doi.org/10.5194/gmd-10-3411-2017

Gudasz, C., Bastviken, D., Steger, K., Premke, K., Sobek, S., & Tranvik, L. J. (2010). Temperature-controlled organic carbon mineralization in lake sediments. *Nature*, 466 (7305), 478–481. https://doi.org/10.1038/nature09186.

Hasselmann K., Barnett T. P., Bouws, E., Carlson, H, Cartwright D. E., Enke, K., Ewing, J. A., Gienapp, H., Hasselmann, D. E., Kruseman, P., Meerburg, A., Müller, P., Olbers, D. J., Richter, K., Sell, W., and Walden, H. (1973). Measurements of wind-wave growth and swell decay during the Joint North Sea Wave Project (JONSWAP), Dtsch. Hydrog. Z. Suppl. A, 8, 1–95.

Khan, H., Laas, A., Marcé, R., & Obrador, B. (2020). Major Effects of Alkalinity on the Relationship Between Metabolism and Dissolved Inorganic Carbon Dynamics in Lakes. *Ecosystems*, *23*(8), 1566–1580. https://doi.org/10.1007/s10021-020-00488-6

Kragh, T., & Sand-Jensen, K. (2018). Carbon limitation of lake productivity. *Proceedings of the Royal Society B: Biological Sciences*, *285*(1891), 20181415. https://doi.org/10.1098/rspb.2018.1415

MacIntyre, S., Jonsson, A., Jansson, M., Aberg, J., Turney, D. E., & Miller, S. D. (2010). Buoyancy flux, turbulence, and the gas transfer coefficient in a stratified lake: TURBULENCE AND GAS EVASION IN LAKES. *Geophysical Research Letters*, *37*(24), n/a-n/a. https://doi.org/10.1029/2010GL044164

Marcé, R., Obrador, B., Morguí, J.-A., Lluís Riera, J., López, P., & Armengol, J. (2015). Carbonate weathering as a driver of CO2 supersaturation in lakes. *Nature Geoscience*, *8*(2), 107–111. https://doi.org/10.1038/ngeo2341

Müller, B., Meyer, J. S., & Gächter, R. (2016). Alkalinity regulation in calcium carbonate-buffered lakes. *Limnology and Oceanography*, *61*(1), 341–352. https://doi.org/10.1002/lno.10213

Perolo, P., Fernández Castro, B., Escoffier, N., Lambert, T., Bouffard, D., & Perga, M.-E. (2021). Accounting for surface waves improves gas flux estimation at high wind speed in a large lake. *Earth System Dynamics*, *12*(4), 1169–1189. https://doi.org/10.5194/esd-12-1169-2021

Natchimuthu, S., Sundgren, I., Gålfalk, M., Klemedtsson, L., & Bastviken, D. (2017). Spatiotemporal variability of lake pCO $_2$ and CO $_2$ fluxes in a hemiboreal catchment: SPATIOTEMPORAL VARIABILITY OF LAKE CO $_2$. *Journal of Geophysical Research: Biogeosciences*, *122*(1), 30–49. https://doi.org/10.1002/2016JG003449

Perolo, P., Fernández Castro, B., Escoffier, N., Lambert, T., Bouffard, D., & Perga, M.-E. (2021). Accounting for surface waves improves gas flux estimation at high wind speed in a large lake. *Earth System Dynamics*, *12*(4), 1169–1189. https://doi.org/10.5194/esd-12-1169-2021

Read, J. S., Hamilton, D. P., Desai, A. R., Rose, K. C., MacIntyre, S., Lenters, J. D., Smyth, R. L., Hanson, P. C., Cole, J. J., Staehr, P. A., Rusak, J. A., Pierson, D. C., Brookes, J. D., Laas, A., & Wu, C. H. (2012). Lake-size dependency of wind shear and convection as controls on gas exchange. *Geophysical Research Letters*, *39*(9), n/a-n/a. https://doi.org/10.1029/2012GL051886

Reiss, R. S., Lemmin, U., Cimatoribus, A. A., & Barry, D. A. (2020). Wintertime Coastal Upwelling in Lake Geneva: An Efficient Transport Process for Deepwater Renewal in a Large, Deep Lake. *Journal of Geophysical Research: Oceans*, *125*(8). https://doi.org/10.1029/2020JC016095

Schwefel, R., Gaudard, A., Wüest, A., & Bouffard, D. (2016). Effects of climate change on deepwater oxygen and winter mixing in a deep lake (Lake Geneva): Comparing observational findings and modeling. *Water Resources Research*, *52*(11), 8811–8826. https://doi.org/10.1002/2016WR019194

Stets, E. G., Butman, D., McDonald, C. P., Stackpoole, S. M., DeGrandpre, M. D., & Striegl, R. G. (2017). Carbonate buffering and metabolic controls on carbon dioxide in rivers: Controls on CO2 in Rivers. *Global Biogeochemical Cycles*, *31*(4), 663–677. https://doi.org/10.1002/2016GB005578

Tedford, E. W., MacIntyre, S., Miller, S. D., & Czikowsky, M. J. (2014). Similarity scaling of turbulence in a temperate lake during fall cooling. *Journal of Geophysical Research: Oceans*, *119*(8), 4689–4713. https://doi.org/10.1002/2014JC010135

Umlauf, L., & Lemmin, U. (2005). Interbasin exchange and mixing in the hypolimnion of a large lake: The role of long internal waves. *Limnology and Oceanography*, *50*(5), 1601–1611. https://doi.org/10.4319/lo.2005.50.5.1601

Vachon, D., S. Sadro, M. J. Bogard, J. Lapierre, H. M. Baulch, J. A. Rusak, B. A. Denfeld, A. Laas, M. Klaus, J. Karlsson, G. A. Weyhenmeyer, and P. A. Giorgio. (2020). Paired O2–CO2 measurements provide emergent insights into aquatic ecosystem function. Limnol. Oceanogr. Lett. 5(4), 287–294, doi:10.1002/lol2.10135

Vachon, D., & Prairie, Y. T. (2013). The ecosystem size and shape dependence of gas transfer velocity versus wind speed relationships in lakes. *Canadian Journal of Fisheries and Aquatic Sciences*, *70*(12), 1757–1764. https://doi.org/10.1139/cjfas-2013-0241

Wanninkhof, R., & Knox, M. (1996). Chemical enhancement of CO2 exchange in natural waters. *Limnology and Oceanography*, *41*(4), 689–697. https://doi.org/10.4319/lo.1996.41.4.0689

Weyhenmeyer, G. A., Kosten, S., Wallin, M. B., Tranvik, L. J., Jeppesen, E., & Roland, F. (2015). Significant fraction of CO_2 emissions from boreal lakes derived from hydrologic inorganic carbon inputs. Nature Geoscience, 8(12), 933–936. https://doi.org/10.1038/ngeo2582

Chapter 6

Appendix

Personal achievement

Articles

Pascal Perolo, Nicolas Escoffier, Hannah Elisa Chmiel, Gaël Many, Damien Bouffard, and Marie-Elodie Perga. Submitted to L&O Letters. ***Alkalinity supports gross primary production in a hard water lake.***
Impact Factor: 7.87
Estimated contribution: Project design, data production, data analysis, and writing [90 %]

Pascal Perolo, Bieito Fernandez Castro, Nicolas Escoffier, Thibault Lambert, Damien Bouffard, and Marie-Elodie Perga. 2021. ***Accounting for surface waves improves gas flux estimation at high wind speed in a large lake.*** Earth System Dynamics, 12, 1169–1189.
Impact Factor: 5.54
Estimated contribution: Project design, data production, data analysis, and writing [90 %]

Pascal Perolo, Maarten Bakker, Chrystelle Gabbud, Gelare Moradi, Collin Rennie, and Stuart Lane. 2019. ***Subglacial sediment production and snout marginal ice uplift during the late ablation season.*** Earth Surface Processes and Landforms 44 (5), 1117–1136.
Impact Factor: 4.13
Estimated contribution: Project design, data production, data analysis, and writing [90 %]

Collaboration articles

Nicolas Escoffier, Pascal Perolo, Thibault Lambert, Thierry Adatte, Torsten Vennemann, and Marie-Elodie Perga. 2022. ***Whiting events in a large peri-alpine lake: Evidence of a catchment-scale process.*** JGR: Biogeosciences.
Impact Factor: 3.82
Estimated contribution: Sampling design and realization, ideas, and writing [15 %]

Thibault Lambert, Pascal Perolo, Nicolas Escoffier, and Marie-Elodie Perga, 2021. ***Enhanced bioavailability of dissolved organic matter (DOM) in human-disturbed streams in Alpine fluvial networks***. Biogeosciences.
Impact Factor: 4.29
Estimated contribution: Sampling design and realization, ideas, and writing [10 %]

Bieito Fernandez Castro, Hannah Elisa Chmiel, Camille Minaudo, Shubham Krishna, Pascal Perolo, Serena Rasconi, and Alfred Wüest. 2021. ***Primary and net ecosystem production in a large lake diagnosed from high-resolution oxygen measurements***. Water Resources Research 57 (5), e2020WR029283.
Impact Factor: 5.24
Estimated contribution: High frequency data production, writing [10 %]

Conferences

Swiss Geosciences Meeting November 2021 (Oral)

Is gross primary production carbon-limited at surface of Lake Geneva. Pascal Perolo, Hannah Elisa Chmiel, Nicolas Escoffier, Gaël Many, Damien Bouffard, and Marie-Elodie Perga.

ASLO Aquatic Sciences Meeting June 2021 (Oral)

Accounting for surface waves improves gas flux estimation at high wind speed in a large lake. Pascal Perolo, Bieito Fernandez Castro, Nicolas Escoffier, Thibault Lambert, Damien Bouffard, and Marie-Elodie Perga.

Primary Production and LéXPLORE Workshop January 2021 (Oral)

Surface waves contribute significantly to air-water gas exchange in a large lake. Pascal Perolo, Cintia Ramon Casanas, Nicolas Escoffier, Thibault Lambert, Damien Bouffard, and Marie-Elodie Perga.

American Geoscience Union – AGU Fall Meeting December 2020 (iPoster)

Surface waves contribute significantly to air-water gas exchange in a large lake. Pascal Perolo, Bieito Fernandez Castro, Nicolas Escoffier, Thibault Lambert, Damien Bouffard, and Marie-Elodie Perga. https://agu2020fallmeeting-agu.ipostersessions.com/Default.aspx?s=72-A9-04-9A-AE-97-6B-0B-8E-7C-E5-92-78-F8-C9-C7#stay

American Geoscience Union – AGU Fall Meeting December 2020 (iPoster)

Controls on whiting event triggering at the interface between Lake Geneva and the Rhône River. Nicolas Escoffier, Pascal Perolo, Thibault Lambert, Janine Rüegg, Daniel Odermatt, Thierry Adatte, Torsten W Vennemann, and Marie-Elodie Perga.

Sentinel Lakes Meeting November 2020 (Oral)

Lakes Bresses: Role of the watershed and effect of groundwater intrusion. Pascal Perolo, Raphaëlle Napoleoni, Damien Bouffard, and Marie-Elodie Perga.

Swiss Geosciences Meeting November 2020 (Poster)

Wave action for predicting air-water gas exchange in a large lake. Pascal Perolo, Bieito Fernandez Castro, Nicolas Escoffier, Thibault Lambert, Damien Bouffard, and Marie-Elodie Perga.

Primary Production and LéXPLORE Workshop November 2019 (Oral)

Variability of CO_2 at long term in Lake Geneva. Pascal Perolo, Cintia Ramon Casanas, Nicolas Escoffier, Thibault Lambert, Damien Bouffard, and Marie-Elodie Perga.

European Geosciences Union – EGU General Assembly April 2019 (Oral)

Spatiotemporal high-resolution data provide new insights on primary production in Lake Geneva (Switzerland). Hannah Elisa Chmiel, Camille Minaudo, Pascal Perolo, Shubham Krishna, Hugo Ulloa, Marie-Elodie Perga, and Alfred Wüest.

ELLS-IAGLR "Big Lakes – Small World" September 2018 (Poster)

Carbon cycle in Lake Geneva: Interannual variability of stocks. Pascal Perolo, Damien Bouffard, and Marie-Elodie Perga.

Data production

High mountain lakes: supervision of master's thesis (July-October 2021)

- High frequency measurements of DO, PAR, conductivity, water temperature and weather data
- Punctual water samplings (nitrate, phosphate, alkalinity, chlorophyl a, and sediment load) and multiparameter profiling in two lakes and one river.

LéXPLORE platform: pelagic area – 110 m (October 2018-August 2021)

- High frequency measurements of CO_2, DO, PAR, pH, conductivity, water temperature, weather data (in collaboration with Dr Hannah Chmiel and Dr Nicolas Escoffier)
- Implementation of a control and calibration of CO_2 sensors
- Punctual survey of gas exchange with automated (forced diffusion) CO_2 floating chamber during seven periods (June 2019, August 2019, October 2019, December 2019, February 2020, June-July 2020, and December 2020)

Buchillon antenna: littoral area – 4 m (August 2019-December 2020)

- CO_2, DO, pH, conductivity, and water temperature data (in collaboration with Dr Nicolas Escoffier)

Daily cycle on LéXPLORE platform (July 2020)

- Water sampling, profiling and first methane profile to LéXPLORE (in collaboration with Dr Thibault Lambert, Dr Nicolas Escoffier, and Professor Didier Jézéquel)

Lake Muzelle: high altitude lake, France (July 2020)

- Annual maintenance of sensors: water temperature, DO, conductivity, and PAR

Whiting event on Lake Geneva: two spatial field campaigns (June 2019)

- Whiting event survey, water sampling, profiling, logistic (in collaboration with Dr Nicolas Escoffier)

River inputs of Lake Geneva: spatial field campaign (November 2018)

- Whiting event survey, water sampling, profiling, logistic (in collaboration with Dr Thibault Lambert)

Haut Glacier d'Arolla and Borgne d'Arolla river: field campaign (July-August 2015)

- Lidar scans, suspended and bedload discharge in glacial river, sediment sampling (master thesis with Professor Stuart Lane)

Other studies

DATALAKES: Heterogeneous data platform for operational modelling and forecasting of Swiss lakes

- Team: Dr Damien Bouffard, Dr Artur Safin, Dr Jonas Sukys
- Pascal Perolo: integration of LéXPLORE data (CO_2 sensors) and Buchillon data (CO_2 sensors, DO sensors)

Hackathon: Sentinel lakes: High altitude lakes in France (February 2020 – 4 days)

- Lakes Bresses: Role of the watershed and the effect of groundwater intrusion. Pascal Perolo, Raphaëlle Napoleoni, Damien Bouffard and Marie-Elodie Perga.

Sediment cores in Lake Geneva and their methane flux (July 2020)

- Professor Didier Jézéquel: Vidy Bay, LéXPLORE platform, and deepest point of Lake Geneva (309 m)

Daily cycle and methane prospecting (July 2020)

- Dr Thibault Lambert: Investigating the role of microbial processing of phytoplankton derived aggregates on the production and fate of DOM in the lake.
- Dr Nicolas Escoffier: Daily dynamics of calcite precipitation/dissolution – When and where is it happening and is there a link with primary production and picoplankton?
- Professor Didier Jézéquel: sediment core and methane profiling to LéXPLORE.

Administrative tasks

Institute of Earth Surface Dynamics (IDYST) council (2020-2022)

One of the three representatives of PhD students

Participation in the meeting and voting (every 6 weeks)

Organization of the 2020 Doctoral Day on the theme of well-being and stress at work as well as the management of COVID-19

School council of the faculty of Geosciences and environment (2019-2022)

One of three representatives of administrative and technical staff or intermediary body of the faculty

Representative of the department of Environmental sciences

Participation in the meeting and voting (every 8 weeks)

Function as a Scientific Committee for bachelor and master programs

Decide on changes to these regulations

Teaching tasks

Master's thesis co-supervisor (UniL – FGSE, fall and spring semester 2021-2022)

Impacts of glacial sediment on proglacial lakes: physical and biogeochemical properties

Comparison of a glacier-fed lake and a non-glacier lake

Subject chosen by Lilian Hämmerli and financially supported by the Agassiz foundation

Bachelor coaching (UniL – FGSE, fall semester 2021)

Help students to construct their scientific research question as well as to organize the planning and structure of the bachelor's thesis

Field and laboratory methods (II): Alpine catchments (UniL – FGSE, spring semester 2021)

Water sampling, multiparameter profiling, mooring construction, high frequency data measurements, QA/QC

Aquatic ecosystems: Glaciers, rivers, and lakes (UniL – FGSE, spring semester 2019-2020-2021)

Practical work: How does climate change affect the thermal structure of lakes? Study case of Lake Geneva

Modelling and data analysis (SIMSTRAT and MATLAB use)

Bachelor presentation (UniL – FGSE, fall semester 2019-2020)

What is a doctoral thesis in our faculty?

Presentation of our research and our complementary activities

Bachelor excursion to LéXPLORE (UniL – FGSE, spring semester 2019)

Discover the platform and its use: water sampling, EXOsonde profile, plankton sampling

Certificates

Formamed: 1st aid in isolated environment (March 2020)

Motorboat license (October 2018)

PEST: Workshop Model Calibration Uncertainty Analysis Using PEST (September 2018)

Drone license: manual piloting and orthomozaic mapping – Ecole Suisse du drone (September-October 2017)

Referee subjects

AGU – Water Resources Research:	River, Geomorphology, and transport (1 review in 2021)
EGU – Earth System Dynamics:	Dynamics of the Earth System: interaction
PhD thesis:	Limnology and water carbon cycle